BABAR Analysis Document #436, Version 6.0
January 17, 2003

Measurement of $\Delta\Gamma/\Gamma$ and study of CPT and T violation using fully reconstructed CP and flavor eigenstates

Massimo Carpinelli, Francesco Forti, Marcello Giorgi, Fernando Martinez-Vidal[1],
Nicola Neri, Francesco Sandrelli

INFN-Sezione di Pisa and Università di Pisa, Italy

for the Mixing AWG

Abstract

The time and flavor structure of the decay of $B^0_d\bar{B}^0_d$ mesons is exploited to perform a measurement of the lifetime difference $\Delta\Gamma/\Gamma$ between the mass eigenstates. The analysis uses fully reconstructed B mesons into a flavor or CP (into charmonium) eigenstate and it is based on 56 fb^{-1} of data collected between 1999 and 2002 (Winter'02 data sample). The combined analysis of these samples offers also a way to perform a combined test of the CPT and T symmetries of the effective Hamiltonian of evolution of the B^0_d meson system, in an attempt to desintangle wether CP violation is due to T or CPT violation.

[1] Primary editor.

Contents

1 Introduction

Discrete symmetries play a fundamental role in our description of nature. The CPT theorem [1, 2], based on very general principles of relativistic quantum field theories, states that any order of the triple product of the discrete symmetries C, P and T represent an exact symmetry. The CPT symmetry has been tested in a variety of experiments [3], remaining to date the only combination of C, P, T that is observed as an exact symmetry in nature. However, precisely because the CPT theorem represents an essential pillar of our present description of nature, it is appropiate to improve such studies in the B meson neutral system where the the $B^0\bar{B}^0$ interferometry provides an exceptionally sensitive framework [4]. On the other hand, superstring theories are not local and therefore do not necessarily fulfill the conditions of the CPT theorem. CPT invariance has also been questioned in the context of quantum gravity [5]. With the indirect CP violation in the B^0_d system already well established [6], testing simultaneous and consistently the CP, T and CPT discrete symmetries of the effective Hamiltonian of evolution to disentangle whether the the CP violation is due to T or CPT violation (or both) is a natural step forward, and of great interest as outlined above. This is the ultimate goal of the analysis described here.

One of the main sources of possible competing contributions to the effects to be studied in this analysis are due to the difference in the decay widths of the B^0_d mesons, $\Delta\Gamma$, usually neglected because its smallness. In the Standard Model, the difference in the decay widths of the B^0_d mesons is CKM-suppressed with respect to that in the B^0_s system. A rough estimate leads to

$$\frac{\Delta\Gamma_d}{\Gamma_d} \sim \frac{\Delta\Gamma_s}{\Gamma_s} \times \lambda^2 \quad \approx \quad 0.5\% \tag{1}$$

where $\lambda = 0.225$ is the sine of the Cabibbo angle, and we have taken $\Delta\Gamma_s/\Gamma_s \approx 15\%$. In this analysis, $\Delta\Gamma/\Gamma$ effects are explicitely parameterized and extracted from the data, providing the first experimental measurement to date. However, as explored in [7], the measurement of $\Delta\Gamma/\Gamma$ is interesting by itself since it can provide constraints (or signal, if the measured value turns out to be larger than the theoretical expectations) on new physics processes.

To date there are no published direct measurements of $\Delta\Gamma/\Gamma$, and the CPT violation has been tested only with inclusive methods in $B^0\bar{B}^0$ mixing, which gives information about CPT violation only if $\Delta\Gamma/\Gamma \neq 0$. This analysis will improve the situation very significantly.

The outline of this document is as follows. In section 2 we summarize the formalism and derive the general time-dependent decay rates and likelihood function used in the analysis. Section 3 describes the decay modes, data and Monte Carlo samples. Section 4 provides some details about the resolution function treatment and tries to justify the motivation for the vertexing cuts applied. Section 5 describes the blinding strategy and in section 6 we describe the assumptions in the nominal fit. Sections 7 and 8 summarize the results of the fits and the consistency checks. Finally, section 9 is devoted to the evaluation of the systematic errors.

Many of the inputs and systematics in this analysis are common with the standard $\sin 2\beta$ analysis [8], so this document will concentrate on the aspects specific to the present analysis. In some cases we will summary some particular aspects common with the $\sin 2\beta$ analysis.

The calculation of the time-dependent decay rates follows the framework developped in reference [9]. This reference should be used in coordination with the present document for additional theoretical subtleties. The feasibility and reach studies, together with the validation of most aspects of the fitting procedure were documented in detail in [11].

2 Time-dependent decay rates and log-likelihood function

Starting from first principles we derive in this section the most general expression for the time-dependent decay rates in $\Upsilon(4S)$ decays as well as the final likelihood function including all the different experimental effects. In order to help our understanding of the main features of the PDF we also evaluate the time-dependence for different particular and simpler cases. For additional details about the formalism and the extraction of the decay rates, see reference [9].

2.1 Coherent B meson formalism

The neutral B meson system is a linear combination of the Schrödinger wave functions for the meson B^0 and its antimeson $\overline{B}^0$, $|\Psi\rangle = a|B^0\rangle + b|\overline{B}^0\rangle$. The time evolution of this combination is governed by the Schrödinger equation,

$$i\frac{\partial\Psi}{\partial t} = \tilde{H}\Psi \tag{2}$$

where $\tilde{H}$ is the 2×2 non-hermitian (probability is not conserved since the $B^0\overline{B}^0$ system decays) effective hamiltonian,

$$\tilde{H} = \tilde{M} - i\frac{\tilde{\Gamma}}{2} = \begin{pmatrix} M_{11} & M_{12} \\ M_{12}^* & M_{22} \end{pmatrix} - \frac{i}{2}\begin{pmatrix} \Gamma_{11} & \Gamma_{12} \\ \Gamma_{12}^* & \Gamma_{22} \end{pmatrix} \ . \tag{3}$$

$\tilde{M}$ and $\tilde{\Gamma}$ represent the mass (dispersive) and lifetime (absorptive) parts of the hamiltonian, both hermitian matrices[2].

The eigenvalues of (2) are

$$\lambda_\pm = \left(M - i\frac{\Gamma}{2}\right) \pm F' \tag{4}$$

where

$$F' = \sqrt{\left(M_{12} - i\frac{\Gamma_{12}}{2}\right)\left(M_{12}^* - i\frac{\Gamma_{12}^*}{2}\right) + \left(\delta M - i\frac{\delta\Gamma}{2}\right)^2} \tag{5}$$

$$M = \frac{M_{11}+M_{22}}{2} \quad , \qquad \Gamma = \frac{\Gamma_{11}+\Gamma_{22}}{2} \tag{6}$$

$$\delta M = \frac{M_{11}-M_{22}}{2} \quad , \qquad \delta\Gamma = \frac{\Gamma_{11}-\Gamma_{22}}{2} \ . \tag{7}$$

The corresponding eigenvectors are

[2] We use the notation H_{ij}, CP_{ij}, etc. to represent the matrix elements of the corresponding operators in the flavor basis, for instance $H_{12} \equiv \langle B^0|H|\overline{B}^0\rangle$.

$$
\begin{aligned}
\mid B_1\rangle &= \frac{1}{N_+}\left(p_+ \mid B^0\rangle + q_+ \mid \bar{B}^0\rangle\right) \\
\mid B_2\rangle &= \frac{1}{N_-}\left(p_- \mid B^0\rangle - q_- \mid \bar{B}^0\rangle\right)
\end{aligned} \tag{8}
$$

with $N_\pm^2 = \mid p_\pm \mid^2 + \mid q_\pm \mid^2$ and

$$
q_\pm = M_{12}^* - i\frac{\Gamma_{12}^*}{2} \tag{9}
$$

$$
p_\pm = \pm\left(\delta M - i\frac{\delta\Gamma}{2}\right) + F' \ . \tag{10}
$$

Inverting (8) one can writte the $\mid B^0\rangle$ and $\mid \bar{B}^0\rangle$ states in terms of the evolution eigenstates,

$$
\begin{aligned}
\mid B^0\rangle &= \frac{1}{p_+q_- + p_-q_+}\left(N_+q_- \mid B_1\rangle + N_-q_+ \mid B_2\rangle\right) \\
\mid \bar{B}^0\rangle &= \frac{1}{p_+q_- + p_-q_+}\left(N_+p_- \mid B_1\rangle - N_-p_+ \mid B_2\rangle\right) \ .
\end{aligned} \tag{11}
$$

Their time evolution is given by

$$
\begin{aligned}
\mid B^0(t)\rangle &= \frac{1}{p_+q_- + p_-q_+}\left(N_+q_-e^{-i\lambda_+t} \mid B_1\rangle + N_-q_+e^{-i\lambda_-t} \mid B_2\rangle\right) \\
\mid \bar{B}^0(t)\rangle &= \frac{1}{p_+q_- + p_-q_+}\left(N_+p_-e^{-i\lambda_+t} \mid B_1\rangle - N_-p_+e^{-i\lambda_-t} \mid B_2\rangle\right) \ .
\end{aligned} \tag{12}
$$

When we pay attention to the restrictions imposed by discrete symmetries on the effective Hamiltonian (3) we see that ($CP_{12} = \langle B^0 \mid CP \mid \bar{B}^0\rangle$ is the relative unphysical phase between $\mid B^0\rangle$ and $\mid \bar{B}^0\rangle$):

- CP conservation imposes $\mathrm{Im}(M_{12}CP_{12}^*) = \mathrm{Im}(\Gamma_{12}CP_{12}^*) = 0$ and $H_{11} = H_{22}$;
- CPT invariance requires $H_{11} = H_{22}$;
- T invariance imposes $\mathrm{Im}(M_{12}CP_{12}^*) = \mathrm{Im}(\Gamma_{12}CP_{12}^*) = 0$.

As a consequence, the complex parameter

$$
\Delta = 2\left(\delta M - i\frac{\delta\Gamma}{2}\right) \tag{13}
$$

parameterizes any CPT violation. If either CPT or CP invariance leads to $\delta M = \delta\Gamma = 0$, we have

$$
p \equiv p_+ = p_- = F \tag{14}
$$

$$F \equiv F' \;=\; \sqrt{\left(M_{12} - i\frac{\Gamma_{12}}{2}\right)\left(M_{12}^* - i\frac{\Gamma_{12}^*}{2}\right)} \tag{15}$$

$$q \equiv q_+ = q_- \;= M_{12}^* - i\tfrac{\Gamma_{12}^*}{2} \tag{16}$$

$$\frac{q}{p} = \sqrt{\frac{M_{12}^* - i\frac{\Gamma_{12}^*}{2}}{M_{12} - i\frac{\Gamma_{12}}{2}}} \tag{17}$$

$$\lambda_\pm \;=\; \left(M - i\frac{\Gamma}{2}\right) \pm F \;\; . \tag{18}$$

Let us note that, according to equation (8), the sign convention in the definition of q/p uses the heavier eigenstate. This convention is the same as used in [9], but opposite to that adopted in the BaBar Physics Book [10]. As another consequence, if CP is conserved then $q = p$.

If there are no absortive parts in the effective hamiltonian ($\Gamma_{12} = 0$), then q/p is a pure phase, $\frac{q}{p} = e^{-i\chi}$ and $\mid q/p \mid = 1$. If there are absortive parts but $\mid \Gamma_{12}/M_{12} \mid$ is small,

$$\mid q/p \mid^2 \;\approx\; 1 - \mathrm{Im}\left[\frac{\Gamma_{12}}{M_{12}}\right] \;\; . \tag{19}$$

From (12) and (8), the time evolution of a state that is initially a pure B^0 or $\overline{B}^0$ is ($\vec{p} = (p_+, p_-)$, $\vec{q} = (q_+, q_-)$)

$$\begin{aligned} \mid B^0(t)\rangle &= f_+(\vec{p},\vec{q};t) \mid B^0\rangle + f_-(\vec{p},\vec{q};t) \mid \overline{B}^0\rangle \\ \mid \overline{B}^0(t)\rangle &= f_-(\vec{q},\vec{p};t) \mid B^0\rangle + f_+(\vec{q},\vec{p};t) \mid \overline{B}^0\rangle \end{aligned} \tag{20}$$

where

$$f_+(\vec{p},\vec{q};t) \;=\; \frac{1}{p_+q_- + p_-q_+}\left(p_+q_-e^{-i\lambda_+t} + p_-q_+e^{-i\lambda_-t}\right) \tag{21}$$

$$f_-(\vec{p},\vec{q};t) \;=\; \frac{q_+q_-}{p_+q_- + p_-q_+}\left(e^{-i\lambda_+t} - e^{-i\lambda_-t}\right) \;\; . \tag{22}$$

With a little of algebra, equations (20) can be written in a more compact way as follows:

$$\begin{aligned} \mid B^0(t)\rangle &= [g_+(t) + zg_-(t)] \mid B^0\rangle + \frac{q}{p}\sqrt{1-z^2}\,g_-(t) \mid \overline{B}^0\rangle \\ \mid \overline{B}^0(t)\rangle &= \frac{p}{q}\sqrt{1-z^2}\,g_-(t) \mid B^0\rangle + [g_+(t) - zg_-(t)] \mid \overline{B}^0\rangle \end{aligned} \tag{23}$$

where

$$z \;=\; \frac{\delta M - i\frac{\delta\Gamma}{2}}{F'} \tag{24}$$

$$g_{\pm}(t) \;=\; \frac{1}{2}\left(e^{-i\lambda_+ t} \pm e^{-i\lambda_- t}\right) \;. \tag{25}$$

The masses (m_1, m_2) and widths (Γ_1, Γ_2) of the eigenstates $\mid B_1\rangle$ and $\mid B_2\rangle$ are related to the eigenvalues (λ_+, λ_-) as:

$$m_1 = \mathrm{Re}(\lambda_+) \;,\quad m_2 = \mathrm{Re}(\lambda_-) \quad ;\qquad \Gamma_1 = -2\mathrm{Im}(\lambda_+) \;,\quad \Gamma_2 = -2\mathrm{Im}(\lambda_-) \;. \tag{26}$$

The oscillation parameters can then be defined as

$$\Delta\lambda \;=\; \frac{\lambda_+ - \lambda_-}{2} = \frac{1}{2}\left(\Delta m + i\frac{\Delta\Gamma}{2}\right) = F' \tag{27}$$

with

$$\Delta m = m_1 - m_2 = \mathrm{Re}(\lambda_+ - \lambda_-) \quad ,\qquad \Delta\Gamma = -\Delta\gamma = \Gamma_2 - \Gamma_1 = -2\mathrm{Im}(\lambda_- - \lambda_+) \;. \tag{28}$$

Let us note that Δm is positive by definition and $\Delta\Gamma$ is expected to be positive within the Standard Model (as in the neutral kaon system). This $\Delta\Gamma$ sign convention is opposite to the one adopted in [10] and [9], but the same as in [22, 23]. When $\Delta\Gamma = 0$ we have $\delta\Gamma = 0$ and $\mid q/p \mid = 1$.

For later use it is convenient also to define

$$\lambda \;=\; \frac{\lambda_+ + \lambda_-}{2} = m - i\frac{\gamma}{2} = M - i\frac{\Gamma}{2} \tag{29}$$

with

$$m = \frac{m_1 + m_2}{2} = \frac{\mathrm{Re}(\lambda_+ + \lambda_-)}{2} \equiv M \quad ,\qquad \gamma = \frac{1}{\tau} = \frac{\Gamma_1 + \Gamma_2}{2} = -\mathrm{Im}(\lambda_+ + \lambda_-) \equiv \Gamma \;. \tag{30}$$

With these definitions, equations (5) and (24) can be rewritten, respectively, as

$$F' \;=\; \frac{1}{2}\left(\Delta m + i\frac{\Delta\Gamma}{2}\right) \tag{31}$$

and

$$z \;=\; 2\frac{\delta M - i\frac{\delta\Gamma}{2}}{\Delta m + i\frac{\Delta\Gamma}{2}} \;. \tag{32}$$

The complex-valued functions (25) in terms of the oscillation parameters are:

$$g_{\pm}(t) \;=\; \frac{1}{2}e^{-imt}e^{-t/2\tau}\left(e^{-i\Delta mt/2}e^{\Delta\Gamma t/4} \pm e^{i\Delta mt/2}e^{-\Delta\Gamma t/4}\right) \;. \tag{33}$$

In summary, we have four real parameters which carry information on the discrete symmetries of the effective Hamiltonian, according to the following list:

- $\mid q/p \mid \neq 1$ signals CP and T violation, with $\Delta\Gamma \neq 0$;

- $\arg q/p \neq 0$ indicates CP and T violation;
- $\delta M \neq 0$ (Rez $\neq 0$) means that CP and CPT violation exist;
- $\delta\Gamma \neq 0$ (Imz $\neq 0$) shows CP and CPT violation, with $\Delta\Gamma \neq 0$.

The fact that Rez is primarily connected to δM while Imz is to $\delta\Gamma$ makes Rez more interesting than Imz. Let us note that CPT or T violation requires CP violation, and CP violation implies T or CPT violation. As outlined in the introduction to this document, desintangle whether CP violation is due to T or CPT violation (or both) is one of the goals of this analysis.

So far we have considered the evolution of an isolated neutral B meson. Charge conjugation together with Bose statistics require that the $B^0\bar{B}^0$ state produced from the $\Upsilon(4S)$ decay is given in the eigenstate basis by

$$| \Upsilon\rangle = \frac{1}{\sqrt{2}} (| B_1\rangle | B_2\rangle - | B_2\rangle | B_1\rangle) \tag{34}$$

which evolves as

$$| \Upsilon(t_1,t_2)\rangle = \frac{1}{\sqrt{2}} \left(e^{-i\lambda_+ t_1} e^{-i\lambda_- t_2} | B_1\rangle | B_2\rangle - e^{-i\lambda_- t_1} e^{-i\lambda_+ t_2} | B_2\rangle | B_1\rangle \right) \ . \tag{35}$$

t_1 and t_2 are the proper times in the rest frames of the each B meson. If we make the change of variables

$$t = \frac{t_1+t_2}{2} \quad , \quad \Delta t = t_2 - t_1 \ , \tag{36}$$

equation (35) can be rewritten as

$$| \Upsilon(t,\Delta t)\rangle = \frac{1}{\sqrt{2}} e^{-i2\lambda t} \left(e^{i\Delta\lambda\Delta t} | B_1\rangle | B_2\rangle - e^{-i\Delta\lambda\Delta t} | B_2\rangle | B_1\rangle \right) \ . \tag{37}$$

If one of the B mesons decays to a final state f_1 at time t_1, the partially projected state reads

$$\langle f_1 | \Upsilon(t,\Delta t)\rangle = \frac{1}{\sqrt{2}} e^{-i2\lambda t} \left(e^{i\Delta\lambda\Delta t} \langle f_1 | B_1\rangle | B_2\rangle - e^{-i\Delta\lambda\Delta t} \langle f_1 | B_2\rangle | B_1\rangle \right) \ . \tag{38}$$

Definining $A_1 = \langle f_1 | B^0\rangle$ and $\overline{A}_1 = \langle f_1 | \bar{B}^0\rangle$, from equation (8) we can expand,

$$\begin{aligned} \langle f_1 | B_1\rangle &= \frac{1}{N_+} \left(p_+ A_1 + q_+ \overline{A}_1 \right) \\ \langle f_1 | B_2\rangle &= \frac{1}{N_-} \left(p_- A_1 - q_- \overline{A}_1 \right) \ . \end{aligned} \tag{39}$$

Using (39) and comparing with (12) for a single isolated B, the partially projected state (38) can be written as

$$\langle f_1 | \Upsilon(t_1,\Delta t)\rangle = \frac{1}{\sqrt{2}} e^{-i2\lambda t_1} \frac{p_+ q_- + p_- q_+}{N_+ N_-} \left(\overline{A}_1 | B^0(\Delta t)\rangle - A_1 | \bar{B}^0(\Delta t)\rangle \right) \ . \tag{40}$$

Let us note the change of variables from $(t,\Delta t)$ to $(t_1,\Delta t)$, since the overall exponential factor has a dependence with t_1.

If the other B meson decays to an state f_2 at time t_2 ($t_2 > t_1$, i.e. the collapse of the wave function occurs at t_1),

$$\langle f_1 f_2 \mid \Upsilon(t_1,\Delta t)\rangle \;=\; \frac{1}{\sqrt{2}} e^{-i2\lambda t_1} \frac{p_+q_- + p_-q_+}{N_+N_-} \left(\overline{A}_1 \langle f_2 \mid B^0(\Delta t)\rangle - A_1 \langle f_2 \mid \overline{B}^0(\Delta t)\rangle\right) \quad . \tag{41}$$

The normalization factor $\frac{p_+q_- + p_-q_+}{N_+N_-}$ is phase-convention independent and depends only on z, $\mid q/p \mid$ and pq (see [9] for explicit dependence). When $\Delta t < 0$, the collapse of the wave function happens at t_2 but the above formalism and expressions are still valid.

2.2 Time-dependent decay rates for coherent B mesons

In order to calculate the decay rates, it is convenient to express the time-dependence of the decay amplitudes in terms of the $g_\pm$ functions. Using (23) and defining $A_2 = \langle f_2 \mid B^0\rangle$ and $\overline{A}_2 = \langle f_2 \mid \overline{B}^0\rangle$,

$$\overline{A}_1 \langle f_2 \mid B^0(\Delta t)\rangle - A_1 \langle f_2 \mid \overline{B}^0(\Delta t)\rangle \;=\; a_+ g_+(\Delta t) + a_- g_-(\Delta t) \tag{42}$$

where

$$\begin{aligned} a_+ &= \bar{A}_1 A_2 - A_1 \bar{A}_2 \\ a_- &= z\left(\bar{A}_1 A_2 + A_1 \bar{A}_2\right) + \sqrt{1-z^2}\left(\frac{q}{p}\bar{A}_1\bar{A}_2 - \frac{p}{q}A_1A_2\right) \quad . \end{aligned} \tag{43}$$

From (41), (42) and (43), we obtain the corresponding decay rate,

$$\begin{aligned} \mid \langle f_1 f_2 \mid \Upsilon(t_1,\Delta t)\rangle \mid^2 \;=\; & \frac{1}{2} e^{-2t_1/\tau} \frac{\mid p_+q_- + p_-q_+ \mid^2}{\mid N_+N_- \mid^2} \times \\ & \left\{ \mid a_+ \mid^2 \mid g_+(\Delta t) \mid^2 + \mid a_- \mid^2 \mid g_-(\Delta t) \mid^2 + 2\mathrm{Re}\left[a_- a_+^* g_-(\Delta t) g_+^*(\Delta t)\right] \right\} \quad . \end{aligned} \tag{44}$$

We observe that the time dependence is described by two real-valued functions,

$$\mid g_\pm(\Delta t) \mid^2 \;=\; \frac{1}{2} e^{-\Delta t/\tau} \left[\cosh\left(\Delta\Gamma \Delta t/2\right) \pm \cos\left(\Delta m \Delta t\right)\right] \tag{45}$$

and the complex-valued function

$$g_+^*(\Delta t) g_-(\Delta t) \;=\; \frac{1}{2} e^{-\Delta t/\tau} \left[\sinh\left(\Delta\Gamma \Delta t/2\right) - i \sin\left(\Delta m \Delta t\right)\right] \quad . \tag{46}$$

If we replace (45) and (46) into (44),

$$
\begin{aligned}
|\langle f_1 f_2 \mid \Upsilon(t,\Delta t)\rangle|^2 &= \frac{1}{2}e^{-2t/\tau}\frac{|\, p_+q_- + p_-q_+ \,|^2}{|\, N_+N_- \,|^2}\times \\
&\left\{\frac{1}{2}c_+\cosh\left(\frac{\Delta\Gamma\Delta t}{2}\right)+\frac{1}{2}c_-\cos(\Delta m\Delta t)+\mathrm{Re}(s)\sinh\left(\frac{\Delta\Gamma\Delta t}{2}\right)+\mathrm{Im}(s)\sin(\Delta m\Delta t)\right\}
\end{aligned}
\tag{47}
$$

where

$$
c_\pm = |\, a_+ \,|^2 \pm |\, a_- \,|^2 \tag{48}
$$

$$
s = a_-a_+^* \ . \tag{49}
$$

Note the change of variables from $(t_1,\Delta t)$ back to $(t,\Delta t)$.

The coefficients $c_\pm$ and s can be written in terms of the base of parameters

$$
z\ , \quad u_\pm = \bar{A}_1A_2 \pm A_1\bar{A}_2\ , \quad m = \frac{q}{p}\bar{A}_1\bar{A}_2 - \frac{p}{q}A_1A_2 \tag{50}
$$

as follows:

$$
c_\pm = |\, u_- \,|^2 \pm \left[|\, z \,|^2|\, u_+ \,|^2 + |\, 1-z^2 \,||\, m \,|^2 + 2\mathrm{Re}\left(z^*\sqrt{1-z^2}u_+^*m\right)\right] \tag{51}
$$

$$
s = zu_+u_-^* + \sqrt{1-z^2}u_-^*m \ . \tag{52}
$$

As experimentally the information available for the time sum t of the meson evolution is quite poor compared to Δt, it is appropiate to work with an integrated probability,

$$
\begin{aligned}
h_{12}(\Delta t) \equiv |\langle f_1 f_2 \mid \Upsilon(\Delta t)\rangle|^2 &= \int_{|\Delta t|/2}^{+\infty} dt\, |\langle f_1 f_2 \mid \Upsilon(t,\Delta t)\rangle|^2 = \frac{\tau}{4}e^{-|\Delta t|/\tau}\frac{|\, p_+q_- + p_-q_+ \,|^2}{|\, N_+N_- \,|^2}\times \\
&\left\{\frac{1}{2}c_+\cosh\left(\frac{\Delta\Gamma\Delta t}{2}\right)+\frac{1}{2}c_-\cos(\Delta m\Delta t)+\mathrm{Re}(s)\sinh\left(\frac{\Delta\Gamma\Delta t}{2}\right)+\mathrm{Im}(s)\sin(\Delta m\Delta t)\right\} \ .
\end{aligned}
\tag{53}
$$

It is convenient to express the coefficients (51) and (52) in terms of the well-known convention independent parameter $\lambda = \frac{q}{p}\frac{\bar{A}}{A}$, where A and $\bar{A}$ are, respectively, the B^0 and $\bar{B}^0$ decay amplitudes into an arbitrary final state. Assuming that A_k and $\bar{A_k}$, with $k = 1,2$, are non-zero, we introduce the parameters

$$
\lambda_k = \frac{q}{p}\frac{\bar{A}_k}{A_k} = |\, q/p \,|\, r_k e^{i\theta_k} \tag{54}
$$

$$\bar{\lambda}_k \;=\; \frac{1}{\lambda_{\bar{k}}} = \frac{p}{q}\frac{A_{\bar{k}}}{A_{\bar{k}}} =\mid p/q \mid \bar{r}_k e^{i\bar{\theta}_k} \tag{55}$$

where

$$r_k \;=\; \mid \bar{A}_k \mid / \mid A_k \mid \tag{56}$$

$$\bar{r}_k = \frac{1}{r_{\bar{k}}} \;=\; \mid A_{\bar{k}} \mid / \mid \bar{A}_{\bar{k}} \mid \tag{57}$$

are the ratios of decay amplitudes of Doubly-CKM-Suppressed to favored processes, for $\mid f_k\rangle =\mid B^0\rangle$ and $\mid f_{\bar{k}}\rangle =\mid \bar{B}^0\rangle$ states, respectively. θ_k and $\bar{\theta}_k$ are the corresponding B^0 and $\bar{B}^0$ phases (overall phase of the ratio of decay amplitudes and the mixing phase). When there is one single process contributing to the favored and DCKM-supressed decays, $r_k = \bar{r}_k$. For $D^{(*)\pm}X^{\mp}$ final states, the amplitudes are expected to be dominated by the Standard Model $b \to c$ and $b \to u$ transitions for the favored and suppressed decays, respectively, as shown in figure 1. The expected relative amplitude of DCKM to favored decays can then be estimated to be $r_k = \bar{r}_k =\mid V^*_{ub}V_{cd} \mid\mid V^*_{cb}V_{ud} \mid\approx 0.02$, using the CKM matrix elements values from [23]. In this case we also have $\theta_k = -2\beta-\gamma-\delta_k$ and $\bar{\theta}_k = 2\beta+\gamma-\delta_k$, where 2β is the mixing (q/p) phase, γ the weak decay phase and δ_k the strong decay phase, which depends on the given final state. Semileptonic decays are free of DCKM-suppressed contributions.

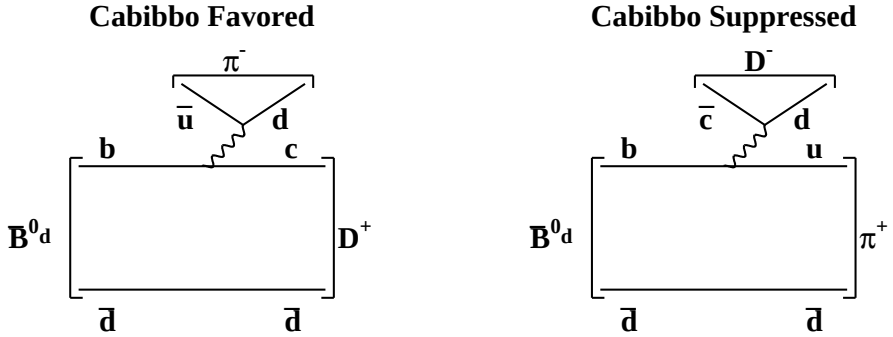

Figure 1: The CKM-allowed ($\sim \lambda^2$) and CKM-suppressed ($\sim \lambda^4$) diagrams for $B \to D^{(*\pm)}\pi^{\mp}/\rho^{\mp}/a_1^{\mp}$ decays. λ is the usual Wolfenstein paramater.

When $\mid f_k\rangle$ is a CP eigenstate ($k = CP$),

$$\lambda_{CP} \;=\; \frac{q}{p}\frac{\bar{A}_{CP}}{A_{CP}} =\mid q/p \mid r_{CP,CP}e^{i\theta_{CP}} \tag{58}$$

where

$$r_{CP,k} \;=\; \mid \bar{A}_{\bar{k}} \mid / \mid A_k \mid \tag{59}$$

parameterizes CP violation in decay ($k = 1,2,CP$). When there is one single process contributing, $r_{CP,k} = 1$. If the mechanisms contributing to the decay of CP eigenstates (f_{CP}) have the same weak phase for $\eta_{f_{CP}} = -1$ and $\eta_{f_{CP}} = +1$ modes,

$$\begin{aligned} \mathrm{Im}\lambda_{f_{CP}} &= -\eta_{f_{CP}}\mathrm{Im}\lambda_{CP} \\ \mathrm{Re}\lambda_{f_{CP}} &= \eta_{f_{CP}}\mathrm{Re}\lambda_{CP} \;. \end{aligned} \tag{60}$$

Let us note once more that the sign convention in the definition of q/p adopted in this document uses the heavier state, which is the same as used in [9]. The convention can be easily be changed to that used in the BaBar Physics Book [10] (lighter state) by replacing λ_k and $\bar{\lambda}_k$ by $-\lambda_k$ and $-\bar{\lambda}_k$, respectively. The latter is the convention used in the present analysis, although all the equations given in the document use the former.

In order to evaluate (51) and (52) having λ_k and $\bar{\lambda}_k$ well defined, we must distinguish the 4 different final state configurations ($|\, f_1 f_2\rangle$, $|\, f_1 \bar{f}_2\rangle$, $|\, \bar{f}_1 f_2\rangle$, $|\, \bar{f}_1 \bar{f}_2\rangle$). For each case we then must evaluate $u_\pm$ and m, and finally

$$|\, u_\pm \,|^2 \quad , \quad |\, m \,|^2 \quad , \quad u_\pm^* m \, , \quad u_+ u_-^* \, . \tag{61}$$

These factors are renormalized so that $|\, A_1 A_2 \,|^2 = 1$ (A_2 may be A_{CP}).

2.2.1 Case $|\, f_1 f_2\rangle$

$$\begin{aligned} u_\pm &= A_1 A_2 \frac{p}{q} (\lambda_1 \pm \lambda_2) \\ m &= A_1 A_2 \frac{p}{q} (\lambda_1 \lambda_2 - 1) \end{aligned} \tag{62}$$

$$\begin{aligned} |\, u_\pm \,|^2 &= |\, p/q \,|^2 \left\{ |\, \lambda_1 \,|^2 + |\, \lambda_2 \,|^2 \pm 2 \,|\, \lambda_1 \,||\, \lambda_2 \,|\, \mathrm{Re}\left(\lambda_1' \lambda_2'^*\right) \right\} \\ |\, m \,|^2 &= |\, p/q \,|^2 \left\{ 1 + |\, \lambda_1 \,|^2 |\, \lambda_2 \,|^2 - 2 \,|\, \lambda_1 \,||\, \lambda_2 \,|\, \mathrm{Re}\left(\lambda_1' \lambda_2'\right) \right\} \\ u_\pm^* m &= |\, p/q \,|^2 \left\{ |\, \lambda_1 \,|^2 |\, \lambda_2 \,|\, \lambda_2' - |\, \lambda_1 \,|\, \lambda_1'^* \pm |\, \lambda_2 \,|^2 |\, \lambda_1 \,|\, \lambda_1' \mp |\, \lambda_2 \,|\, \lambda_2'^* \right\} \\ u_+ u_-^* &= |\, p/q \,|^2 \left\{ |\, \lambda_1 \,|^2 - |\, \lambda_2 \,|^2 + 2i \,|\, \lambda_1 \,||\, \lambda_2 \,|\, \mathrm{Im}\left(\lambda_2' \lambda_1'^*\right) \right\} \end{aligned} \tag{63}$$

where

$$\lambda_k' = \frac{\lambda_k}{|\, \lambda_k \,|} \equiv e^{i\theta_k} \quad , \quad \bar{\lambda}_k' = \frac{\bar{\lambda}_k}{|\, \lambda_k \,|} \equiv e^{i\bar{\theta}_k} \tag{64}$$

and

$$|\, \lambda_k \,| = |\, q/p \,|\, r_k \quad , \quad |\, \bar{\lambda}_k \,| = |\, p/q \,|\, \bar{r}_k \tag{65}$$

for flavor eigenstates ($k = 1, 2$), and

$$|\, \lambda_{CP} \,| \;=\; |\, q/p \,|\, r_{CP,CP} \tag{66}$$

for CP eigenstates.

2.2.2 Case $|\, \bar{f}_1 f_2\rangle$

$$\begin{aligned} u_\pm &= \bar{A}_{\bar{1}} A_2 \left(1 \pm \bar{\lambda}_1 \lambda_2\right) \\ m &= \bar{A}_{\bar{1}} A_2 \left(\lambda_2 - \bar{\lambda}_1\right) \end{aligned} \tag{67}$$

$$
\begin{aligned}
|\,u_\pm\,|^2 &= r_{CP,1}^2\left\{1+|\,\bar{\lambda}_1\,|^2|\,\lambda_2\,|^2 \pm 2\,|\,\bar{\lambda}_1\,||\,\lambda_2\,|\,\mathrm{Re}\left(\bar{\lambda}_1'\lambda_2'\right)\right\}\\
|\,m\,|^2 &= r_{CP,1}^2\left\{|\,\lambda_2\,|^2+|\,\bar{\lambda}_1\,|^2-2\,|\,\lambda_2\,||\,\bar{\lambda}_1\,|\,\mathrm{Re}\left(\lambda_2'\bar{\lambda}_1'^*\right)\right\}\\
u_\pm^* m &= r_{CP,1}^2\left\{|\,\lambda_2\,|\,\lambda_2'-|\,\bar{\lambda}_1\,|\,\bar{\lambda}_1'\pm|\,\lambda_2\,|^2|\,\bar{\lambda}_1\,|\,\bar{\lambda}_1'^*\mp|\,\bar{\lambda}_1\,|^2|\,\lambda_2\,|\,\lambda_2'^*\right\}\\
u_+u_-^* &= r_{CP,1}^2\left\{1-|\,\bar{\lambda}_1\,|^2|\,\lambda_2\,|^2+2i\,|\,\bar{\lambda}_1\,||\,\lambda_2\,|\,\mathrm{Im}\left(\bar{\lambda}_1'\lambda_2'\right)\right\}
\end{aligned}
\tag{68}
$$

2.2.3 Case $|\,f_1\bar{f}_2\rangle$

$$
\begin{aligned}
u_\pm &= A_1\bar{A}_{\bar{2}}\left(\lambda_1\bar{\lambda}_2\pm 1\right)\\
m &= A_1\bar{A}_{\bar{2}}\left(\lambda_1-\bar{\lambda}_2\right)
\end{aligned}
\tag{69}
$$

$$
\begin{aligned}
|\,u_\pm\,|^2 &= r_{CP,2}^2\left\{1+|\,\lambda_1\,|^2|\,\bar{\lambda}_2\,|^2 \pm 2\,|\,\lambda_1\,||\,\bar{\lambda}_2\,|\,\mathrm{Re}\left(\lambda_1'\bar{\lambda}_2'\right)\right\}\\
|\,m\,|^2 &= r_{CP,2}^2\left\{|\,\lambda_1\,|^2+|\,\bar{\lambda}_2\,|^2-2\,|\,\lambda_1\,||\,\bar{\lambda}_2\,|\,\mathrm{Re}\left(\lambda_1'\bar{\lambda}_2'^*\right)\right\}\\
u_\pm^* m &= r_{CP,2}^2\left\{|\,\lambda_1\,|^2|\,\bar{\lambda}_2\,|\,\bar{\lambda}_2'^*-|\,\bar{\lambda}_2\,||\,\lambda_1\,|\,\lambda_1'^*\pm|\,\lambda_1\,|\,\lambda_1'\mp|\,\bar{\lambda}_2\,|\,\bar{\lambda}_2'\right\}\\
u_+u_-^* &= r_{CP,2}^2\left\{|\,\lambda_1\,|^2|\,\bar{\lambda}_2\,|^2-1+2i\,|\,\lambda_1\,||\,\bar{\lambda}_2\,|\,\mathrm{Im}\left(\lambda_1'^*\bar{\lambda}_2'^*\right)\right\}
\end{aligned}
\tag{70}
$$

2.2.4 Case $|\,\bar{f}_1\bar{f}_2\rangle$

$$
\begin{aligned}
u_\pm &= \bar{A}_{\bar{1}}\bar{A}_{\bar{2}}\frac{q}{p}\left(\bar{\lambda}_2\pm\bar{\lambda}_1\right)\\
m &= \bar{A}_{\bar{1}}\bar{A}_{\bar{2}}\frac{q}{p}\left(1-\bar{\lambda}_1\bar{\lambda}_2\right)
\end{aligned}
\tag{71}
$$

$$
\begin{aligned}
|\,u_\pm\,|^2 &= r_{CP,1}^2r_{CP,2}^2\,|\,q/p\,|^2\left\{|\,\bar{\lambda}_2\,|^2+|\,\bar{\lambda}_1\,|^2 \pm 2\,|\,\bar{\lambda}_1\,||\,\bar{\lambda}_2\,|\,\mathrm{Re}\left(\bar{\lambda}_1'\bar{\lambda}_2'^*\right)\right\}\\
|\,m\,|^2 &= r_{CP,1}^2r_{CP,2}^2\,|\,q/p\,|^2\left\{1+|\,\bar{\lambda}_1\,|^2|\,\bar{\lambda}_2\,|^2-2\,|\,\bar{\lambda}_1\,||\,\bar{\lambda}_2\,|\,\mathrm{Re}\left(\bar{\lambda}_1'\bar{\lambda}_2'\right)\right\}\\
u_\pm^* m &= r_{CP,1}^2r_{CP,2}^2\,|\,q/p\,|^2\left\{|\,\bar{\lambda}_2\,|^2\,\bar{\lambda}_2'^*-|\,\bar{\lambda}_2\,|^2|\,\bar{\lambda}_1\,|\,\lambda_1'\pm|\,\bar{\lambda}_1\,|\,\lambda_1'^*\mp|\,\bar{\lambda}_1\,|^2|\,\bar{\lambda}_2\,|\,\bar{\lambda}_2'\right\}\\
u_+u_-^* &= r_{CP,1}^2r_{CP,2}^2\,|\,q/p\,|^2\left\{|\,\bar{\lambda}_2\,|^2-|\,\bar{\lambda}_1\,|^2+2i\,|\,\bar{\lambda}_2\,||\,\bar{\lambda}_1\,|\,\mathrm{Im}\left(\bar{\lambda}_1'\bar{\lambda}_2'^*\right)\right\}
\end{aligned}
\tag{72}
$$

2.2.5 Parameter counting

From the above expressions we determine the parameters that contribute to the coefficients $c_\pm$, $\mathrm{Re}(s)$ and $\mathrm{Im}(s)$, for the most general case, assuming that a single final state contributes to $|\,f_1\rangle$, $|\,f_{\bar{1}}\rangle$, $|\,f_2\rangle$ and $|\,f_{\bar{2}}\rangle$. In the following we identify $|\,f_1\rangle$ as the state used for B tagging ($k=1\equiv tag$), and $|\,f_2\rangle$ the reconstructed final state, flavor ($k=2\equiv flav$) or CP ($k=CP$):

- $|\,A_1A_2\,|^2$ is a global normalization factor, therefore irrelevant for any time-dependent analysis;

- $r_{CP,k}$ can be used to parameterize CP violation in decay (3 parameters):
  - $r_{CP,1}$, for tagging side,
  - $r_{CP,2}$, for reconstructed side, flavor sample,
  - $r_{CP,CP}$, for reconstructed side, CP sample;
- Rez and Imz, the CPT/CP violation parameters (2 parameters);
- $\mid q/p \mid$, the T/CP violation parameter (1 parameter);
- r_k and $\bar{r_k}$ are the ratios of the magnitudes of decay amplitudes of DCKM to favored processes, for B^0 and $\bar{B}^0$ (4 parameters):
  - r_1,$\bar{r_1}$, for tagging side,
  - r_2,$\bar{r_2}$, for reconstructed side, flavor sample;
- θ_k and $\bar{\theta}_k$ are the overall B^0 and $\bar{B}^0$ phases of the ratio of decay amplitudes and the mixing phase (5 parameters):
  - θ_1,$\bar{\theta}_1$, for tagging side,
  - θ_2,$\bar{\theta}_2$, for reconstructed side, flavor sample,
  - θ_{CP}, for reconstructed side, CP sample.

When we consider a combined analysis of the flavor and CP eigenstates, we have a total of 6 different final state configurations: 4 for flavor eigenstates ($B^0_{flav}B^0_{tag}$, $\bar{B}^0_{flav}B^0_{tag}$, $\bar{B}^0_{flav}B^0_{tag}$, $\bar{B}^0_{flav}\bar{B}^0_{tag}$) and 2 for CP eigenstates (B^0_{tag}, $\bar{B}^0_{tag}$). For each specific final state configuration the number of independent coefficients in the decay rate is, up to a sign ambiguity, 2. This can be seen as follows (see [9] for details). From (48) and (49) it can be shown that the coefficients $c_\pm$ and s satisfy the constraint

$$c_+^2 - c_-^2 \;=\; 4\left(\mathrm{Re}(s)^2 + \mathrm{Im}(s)^2\right) \;. \tag{73}$$

Since c_+ is always positive we can re-parameterize the decay rate (53) in terms of the coefficients of the sinh, cos and sin terms relative to the cosh term:

$$\begin{aligned} \mid \langle f_1 f_2 \mid \Upsilon(\Delta t)\rangle \mid^2 \;\propto\; & \frac{\tau}{4} e^{-|\Delta t|/\tau}\left\{\cosh\left(\frac{\Delta\Gamma\Delta t}{2}\right) + C_{12}\cos(\Delta m\Delta t) + \right. \\ & \left. \sigma_{12}\sqrt{1-C_{12}^2-S_{12}^2}\sinh\left(\frac{\Delta\Gamma\Delta t}{2}\right) + S_{12}\sin(\Delta m\Delta t)\right\} \end{aligned} \tag{74}$$

where

$$C_{12} \;=\; \frac{\mid a_+ \mid^2 - \mid a_- \mid^2}{\mid a_+ \mid^2 + \mid a_- \mid^2} \tag{75}$$

$$S_{12} \;=\; 2\frac{\mathrm{Im}(a_+^* a_-)}{\mid a_+ \mid^2 + \mid a_- \mid^2} \;. \tag{76}$$

The parameter σ_{12} can only take the values ± 1 since equation (73) fixes only the magnitude of the sinh coefficient, but not its sign. This gives the 2 independent coefficients per configurations, resulting in a total of 12 independent observations. The basic problem now is that the total number of parameters above is 15, so we require additional assumptions:

- $r_{CP,1}$, $r_{CP,2}$ and $r_{CP,CP}$ can be assumed to be 1;
- r_1 and r_2 can be assumed to be equal to $\bar{r_1}$ and $\bar{r_2}$, respectively, and assume to be known (≈ 0.02 according to the CKM matrix elements [23]).

With these (reasonable) assumptions we reduce in 6 parameters, which gives, in principle, enough observations to extract all the other parameters. In practice, to avoid problems derived from fits collapsing to the borders of the physical region and an underevaluation of the statistical errors, the sines and cosines of the phases θ_1, $\bar{\theta}_1$, θ_2, $\bar{\theta}_2$, θ_{CP} should be extracted instead of the phases themselves, increasing from 9 to 14 the number of parameters. Sign ambiguities and small sensitivity to some of these parameters require additional assumptions, as discussed in the following.

2.2.6 Simplified expressions

In order to help our understanding of the main features of the time dependence, it is useful to evaluate the previous equations for several special cases. In some cases the coefficients $c_\pm$, $\mathrm{Re}(s)$ and $\mathrm{Im}(s)$ will be also given to first order in the CPT parameter z:

$$\begin{aligned} c_\pm &= |\, u_- \,|^2 \pm \left[|\, m \,|^2 + 2\mathrm{Re}(z^* u_+^* m) \right] \\ s &= z u_+ u_-^* + u_-^* m \,. \end{aligned} \tag{77}$$

Perfect tagging states

In the case when the flavor final states (reconstructed side in flavor events and tagging B) are perfect tagging states (λ_k and $\bar{\lambda}_k$, $k = 1, 2$, are zero), the coefficients simplify to those given in tables 1 and 2, for flavor and CP eigenstates respectively. The same coefficients to first order in the CPT parameter z are given in tables 3 and 4.

Coefficient	$\mid f_1 f_2 \rangle$	$\mid \bar{f_1} f_2 \rangle$	$\mid f_1 \rangle \mid \bar{f_2} \rangle$	$\mid \bar{f_1} \rangle \mid \bar{f_2} \rangle$
$c_\pm$	$\pm \mid q/p \mid^{-2} \mid 1 - z^2 \mid$	$r_{CP,1}^2 \left(1 \pm \mid z \mid^2\right)$	$r_{CP,2}^2 \left(1 \pm \mid z \mid^2\right)$	$\pm r_{CP,1}^2 r_{CP,2}^2 \mid q/p \mid^2 \mid 1 - z^2 \mid$
s	0	$r_{CP,1}^2 z$	$-r_{CP,2}^2 z$	0

Table 1: Coefficients of the time-dependent decay rate for flavor eigenstates (perfect tagging states).

Coefficient	$\mid f_1 f_{CP} \rangle$
$c_\pm$	$\mid q/p \mid^{-2} \left\{ \mid \lambda_{CP} \mid^2 \pm \mid z \mid^2 \mid \lambda_{CP} \mid^2 \pm \mid 1 - z^2 \mid \mp 2 \mid \lambda_{CP} \mid \mathrm{Re}\left(z^* \sqrt{1 - z^2} \lambda_{CP}'^* \right) \right\}$
s	$\mid q/p \mid^{-2} \left\{ - \mid \lambda_{CP} \mid^2 z + \mid \lambda_{CP} \mid \sqrt{1 - z^2} \lambda_{CP}'^* \right\}$
	$\mid \bar{f_1} f_{CP} \rangle$
$c_\pm$	$r_{CP,1}^2 \left\{ 1 \pm \mid z \mid^2 \pm \mid 1 - z^2 \mid\mid \lambda_{CP} \mid^2 \pm 2 \mid \lambda_{CP} \mid \mathrm{Re}\left(z^* \sqrt{1 - z^2} \lambda_{CP}' \right) \right\}$
s	$r_{CP,1}^2 \left(z + \mid \lambda_{CP} \mid \sqrt{1 - z^2} \lambda_{CP}' \right)$

Table 2: Coefficients of the time-dependent decay rate for CP eigenstates (perfect tagging states).

After a close inspection of tables 1, 2, 3 and 4, we observe that the coefficients $c_\pm$ and s remain unchanged under a simultaneous sign change of $\Delta\Gamma$, Rez and $\mathrm{Re}\lambda_{CP}'$. This discrete ambiguity is resolved if we take $\mathrm{Re}\lambda_{CP}' = +\sqrt{1 - (\mathrm{Im}\lambda_{CP}')^2}$ and then consider as physical parameters $\Delta\Gamma \times sign(\mathrm{Re}\lambda_{CP}')$ and $\mathrm{Rez}\mathrm{Re}\lambda_{CP}'$ instead

Coefficient	$\mid f_1 f_2\rangle$	$\mid f_1^- f_2\rangle$	$\mid f_1\rangle \mid f_2^-\rangle$	$\mid f_1^-\rangle \mid f_2^-\rangle$
$c_\pm$	$\pm \mid q/p \mid^{-2}$	$r^2_{CP,1}$	$r^2_{CP,2}$	$\pm r^2_{CP,1} r^2_{CP,2} \mid q/p \mid^2$
s	0	$r^2_{CP,1} z$	$-r^2_{CP,2} z$	0

Table 3: Coefficients of the time-dependent decay rate for flavor eigenstates (perfect tagging states), to first order in the CPT parameter z.

Coefficient	$\mid f_1 f_{CP}\rangle$
$c_\pm$	$\mid q/p \mid^{-2} \{\mid \lambda_{CP} \mid^2 \pm 1 \mp 2 \mid \lambda_{CP} \mid [\mathrm{RezRe}\lambda'_{CP} - \mathrm{ImzIm}\lambda'_{CP}]\}$
s	$\mid q/p \mid^{-2} \{- \mid \lambda_{CP} \mid^2 z + \mid \lambda_{CP} \mid \lambda'^*_{CP}\}$
	$\mid f_1^- f_{CP}\rangle$
$c_\pm$	$r^2_{CP,1} \{1 \pm \mid \lambda_{CP} \mid^2 \pm 2 \mid \lambda_{CP} \mid [\mathrm{RezRe}\lambda'_{CP} + \mathrm{ImzIm}\lambda'_{CP}]\}$
s	$r^2_{CP,1} (z + \mid \lambda_{CP} \mid \lambda'_{CP})$

Table 4: Coefficients of the time-dependent decay rate for CP eigenstates (perfect tagging states), to first order in the CPT parameter z.

of $\Delta\Gamma$ and Rez, respectively. We take the product $\mathrm{RezRe}\lambda'_{CP}$ rather than $\mathrm{Rez} \times sign(\mathrm{Re}\lambda'_{CP})$ because the CPT asymmetries turn out to be proportional to $\mathrm{RezRe}\lambda'_{CP}$ [11, 13]. Therefore, the choice of independent physics parameters that model CPT/CP, CP/T and mixing is:

$$\boxed{\mathrm{Rez}\frac{\mathrm{Re}\lambda_{CP}}{|\lambda_{CP}|} \ , \ \mathrm{Imz} \ , \ \frac{\mathrm{Im}\lambda_{CP}}{|\lambda_{CP}|} \ , \ |\, q/p \,| \ , \ \Delta\Gamma/\Gamma \times sign(\mathrm{Re}\lambda_{CP}) \ , \ \Delta m \ , \ \tau \, .}$$

The previous tables also provide very useful information about where the sensitivity to the different parameters comes from:

- the $\Delta\Gamma$ dependence for flavor eigenstates appears to be at second order in $\Delta\Gamma$ (from the cosh term) while it is to first order for CP eigenstates (sinh term). This implies that the precision on $\Delta\Gamma/\Gamma$ from CP events scales as $1/\sqrt{N}$ (N is here the number of events), constant as a function of $\Delta\Gamma/\Gamma$, while for flavor eigenstates the statistical error scales as $1/N^{1/4}$ for small values of $\Delta\Gamma/\Gamma$, while for large values it goes as $1/\sqrt{N}1/\Delta\Gamma$ [15]. Clearly, for small values of $\Delta\Gamma$ and in the presence of CP violation, even though the CP eigenstate sample is about 10 times smaller than the flavor eigenstate sample, it largely dominates the determination of $\Delta\Gamma$. Another consequence of the different $\Delta\Gamma$ dependence for flavor and CP states is the fact that the PDF for flavor events is symmetric with respect to $\Delta\Gamma$=0, so only CP events allow to extract information about the $\Delta\Gamma$ sign, up to the discrete ambiguity from $\mathrm{Re}\lambda_{CP}$;
- the dependence with Rez (even in Δt) is suppressed by terms linear in $\Delta\Gamma$ for flavor eigenstates. This implies, again, that for small values of $\Delta\Gamma$ and in the presence of CP violation, the CP eigenstate sample largely dominates the determination of Rez;
- the dependence with $\mathrm{Im}\lambda_{CP}$ (CP eigenstates) appears to be odd in Δt, and therefore can be resolved from the even dependence with Rez;
- the determination of $\mid q/p \mid$, Imz and Δm is dominated by the high statistics flavor sample due to the absence of suppression factors.

Overall, the combined use of flavor and CP samples provides maximal sensitivity to all the physics parameters, with small correlations, since they are determined either from different samples, either from different Δt

dependencies. All these features were checked numerically using toy Monte Carlo [11].

Flavor eigenstates with $\lambda_2, \bar{\lambda}_2 \neq 0$, $\lambda_1 = \bar{\lambda}_1 = 0$, $z = 0$, $\Delta\Gamma = 0$ and $\mid q/p \mid = 1$

When $\lambda_1 = \bar{\lambda}_1 = 0$, $z = 0$, $\Delta\Gamma = 0$ and $\mid q/p \mid = 1$, we have, for flavor eigenstates

	$\mid f_1 f_2 \rangle$	$\mid f_1 \bar{f}_2 \rangle$	$\mid f_1 \rangle \mid \bar{f}_2 \rangle$	$\mid \bar{f}_1 \rangle \mid \bar{f}_2 \rangle$
$c_\pm$	$\mid \lambda_2 \mid^2 \pm 1$	$r_{CP,1}^2 \left(1 \pm \mid \lambda_2 \mid^2\right)$	$r_{CP,2}^2 \left(1 \pm \mid \bar{\lambda}_2 \mid^2\right)$	$r_{CP,1}^2 r_{CP,2}^2 \left(\mid \bar{\lambda}_2 \mid^2 \pm 1\right)$
$\mathrm{Im}(s)$	$-\mid \lambda_2 \mid \mathrm{Im}\lambda_2'$	$r_{CP,1}^2 \mid \lambda_2 \mid \mathrm{Im}\lambda_2'$	$r_{CP,2}^2 \mid \bar{\lambda}_2 \mid \mathrm{Im}\lambda_2'$	$-r_{CP,1}^2 r_{CP,2}^2 \mid \bar{\lambda}_2 \mid \mathrm{Im}\lambda_2'$

and for CP eigenstates

	$\mid f_1 f_{CP} \rangle$	$\mid \bar{f}_1 f_{CP} \rangle$
$c_\pm$	$\mid \lambda_{CP} \mid^2 \pm 1$	$r_{CP,1}^2 \left(1 \pm \mid \lambda_{CP} \mid^2\right)$
$\mathrm{Im}(s)$	$-\mid \lambda_{CP} \mid \mathrm{Im}\lambda_{CP}'$	$r_{CP,1}^2 \mid \lambda_{CP} \mid \mathrm{Im}\lambda_{CP}'$

where $\mathrm{Im}\lambda_2' = -\sin(2\beta+\gamma+\delta)$, $\mathrm{Im}\bar{\lambda}_2' = \sin(2\beta+\gamma-\delta)$ and $\mathrm{Im}\lambda_{CP}' = -\sin(2\beta+\delta)$, δ being the strong phase. For $B^0 \to J/\psi K^0$ decays, $\mathrm{Im}\lambda_{CP}' = -\eta_{CP}\sin(2\beta)$. We recover here the usual expressions used in the $\sin(2\beta)$, $\sin(2\alpha)$ and $\sin(2\beta+\gamma)$ analyses.

Flavor eigenstates with $\lambda_1, \bar{\lambda}_1 \neq 0$ and $\lambda_2 = \bar{\lambda}_2 = 0$

This corresponds to the case when the fully reconstructed B mesons are perfect tagging states (i.e. from semileptonic decays) but the tagging B's are not:

- Case $\mid f_1 f_2 \rangle$

$$\begin{aligned} \mid u_\pm \mid^2 &= \mid p/q \mid^2 \mid \lambda_1 \mid^2 \\ \mid m \mid^2 &= \mid p/q \mid^2 \\ u_\pm^* m &= -\mid p/q \mid^2 \mid \lambda_1 \mid \lambda_1'^* \\ u_+ u_-^* &= \mid p/q \mid^2 \mid \lambda_1 \mid^2 \end{aligned}$$

To first order in z,

$$\begin{aligned} c_\pm &= \mid p/q \mid^2 \left\{ \mid \lambda_1 \mid^2 \pm 1 \mp 2\mathrm{Re}z \mid \lambda_1 \mid \mathrm{Re}\lambda_1' \pm 2\mathrm{Im}z \mid \lambda_1 \mid \mathrm{Im}\lambda_1' \right\} \\ \mathrm{Re}(s) &= \mid p/q \mid^2 \left\{ \mid \lambda_1 \mid^2 \mathrm{Re}z - \mid \lambda_1 \mid \mathrm{Re}\lambda_1' \right\} \\ \mathrm{Im}(s) &= \mid p/q \mid^2 \left\{ \mid \lambda_1 \mid^2 \mathrm{Im}z + \mid \lambda_1 \mid \mathrm{Im}\lambda_1' \right\} \end{aligned}$$

- Case $\mid \bar{f}_1 f_2 \rangle$

$$\begin{aligned} \mid u_\pm \mid^2 &= r_{CP,1}^2 \\ \mid m \mid^2 &= r_{CP,1}^2 \mid \bar{\lambda}_1 \mid^2 \\ u_\pm^* m &= -r_{CP,1}^2 \mid \bar{\lambda}_1 \mid \bar{\lambda}_1' \\ u_+ u_-^* &= r_{CP,1}^2 \end{aligned}$$

To first order in z,

$$
\begin{aligned}
c_{\pm} &= r^2_{CP,1}\left\{1\pm \mid \bar{\lambda}_1 \mid^2 \mp 2\mathrm{Re}z \mid \bar{\lambda}_1 \mid \mathrm{Re}\bar{\lambda}'_1 \mp 2\mathrm{Im}z \mid \bar{\lambda}_1 \mid \mathrm{Im}\bar{\lambda}'_1\right\} \\
\mathrm{Re}(s) &= r^2_{CP,1}\left\{\mathrm{Re}z- \mid \bar{\lambda}_1 \mid \mathrm{Re}\bar{\lambda}'_1\right\} \\
\mathrm{Im}(s) &= r^2_{CP,1}\left\{\mathrm{Im}z- \mid \bar{\lambda}_1 \mid \mathrm{Im}\bar{\lambda}'_1\right\}
\end{aligned}
$$

- Case $\mid f_1 \bar{f}_2\rangle$

$$
\begin{aligned}
\mid u_{\pm} \mid^2 &= r^2_{CP,2} \\
\mid m \mid^2 &= r^2_{CP,2} \mid \lambda_1 \mid^2 \\
u^*_{\pm} m &= \pm r^2_{CP,2} \mid \lambda_1 \mid \lambda'_1 \\
u_+ u^*_- &= -r^2_{CP,2}
\end{aligned}
$$

To first order in z,

$$
\begin{aligned}
c_{\pm} &= r^2_{CP,2}\left\{1\pm \mid \lambda_1 \mid^2 \pm 2\mathrm{Re}z \mid \lambda_1 \mid \mathrm{Re}\lambda'_1 \pm 2\mathrm{Im}z \mid \lambda_1 \mid \mathrm{Re}\lambda'_1\right\} \\
\mathrm{Re}(s) &= r^2_{CP,2}\left\{-\mathrm{Re}z- \mid \lambda_1 \mid \mathrm{Re}\lambda'_1\right\} \\
\mathrm{Im}(s) &= r^2_{CP,2}\left\{-\mathrm{Im}z- \mid \lambda_1 \mid \mathrm{Im}\lambda'_1\right\}
\end{aligned}
$$

- Case $\mid \bar{f}_1 \bar{f}_2\rangle$

$$
\begin{aligned}
\mid u_{\pm} \mid^2 &= r^2_{CP,1} r^2_{CP,2} \mid q/p \mid^2 \mid \bar{\lambda}_1 \mid^2 \\
\mid m \mid^2 &= r^2_{CP,1} r^2_{CP,2} \mid q/p \mid^2 \\
u^*_{\pm} m &= \pm r^2_{CP,1} r^2_{CP,2} \mid q/p \mid^2 \mid \bar{\lambda}_1 \mid \bar{\lambda}'^*_1 \\
u_+ u^*_- &= -r^2_{CP,1} r^2_{CP,2} \mid q/p \mid^2 \mid \bar{\lambda}_1 \mid^2
\end{aligned}
$$

To first order in z,

$$
\begin{aligned}
c_{\pm} &= r^2_{CP,1} r^2_{CP,2} \mid q/p \mid^2 \left\{\mid \bar{\lambda}_1 \mid^2 \pm 1 \pm 2\mathrm{Re}z \mid \bar{\lambda}_1 \mid \mathrm{Re}\bar{\lambda}'_1 \mp 2\mathrm{Im}z \mid \bar{\lambda}_1 \mid \mathrm{Im}\bar{\lambda}'_1\right\} \\
\mathrm{Re}(s) &= -r^2_{CP,1} r^2_{CP,2} \mid q/p \mid^2 \left\{\mid \bar{\lambda}_1 \mid^2 \mathrm{Re}z+ \mid \bar{\lambda}_1 \mid \mathrm{Re}(\bar{\lambda}'_1)\right\} \\
\mathrm{Im}(s) &= -r^2_{CP,1} r^2_{CP,2} \mid q/p \mid^2 \left\{\mid \bar{\lambda}_1 \mid^2 \mathrm{Im}z- \mid \bar{\lambda}_1 \mid \mathrm{Im}\lambda'_1\right\}
\end{aligned}
$$

From these expressions we observe that DCKM decays in the tagging side induce a sign ambiguity similar to that described previously, but now involving $\mathrm{Re}\lambda'_1$ ($\mathrm{Re}\bar{\lambda}'_1$) instead of $\mathrm{Re}\lambda'_{CP}$, for $B^0(\bar{B}^0)$ tags. It can also be seen that the parameter Rez always appears either multiplied by or added to a term proportional to $\mathrm{Re}\lambda'_1$ ($\mathrm{Re}\bar{\lambda}'_1$). Similarly, Imz is always accompanied by a term proportional to $\mathrm{Im}\lambda'_1$ ($\mathrm{Im}\bar{\lambda}'_1$). This implies that Rez(Imz) will be mainly affected by (correlated with) the DCKM real(imaginary) parts. The dominant dependence with λ'_1 and $\bar{\lambda}'_1$ is in all cases linear in $\mid \lambda_1 \mid$ and $\mid \bar{\lambda}_1 \mid$. A similar analysis for $\lambda_1, \bar{\lambda}_1 \neq 0$, $\lambda_2 = \bar{\lambda}_2 = 0$ reveals the same features for the reconstructed B (flavor sample). In this case, however, given that the flavor eigenstate sample is analyzed in combination with the CP sample, it is expected the DCKM effects to be smaller, as will be discussed later.

CP eigenstates ($\lambda_2 = \lambda_{CP}$) with $\lambda_1, \bar{\lambda}_1 \neq 0$

This corresponds to the most general case for fully reconstructed CP eigenstates:

- Case $|\, f_1 f_{CP}\rangle$

$$\begin{aligned}
|\, u_\pm \,|^2 &= |\, p/q \,|^2 \left\{ |\, \lambda_1 \,|^2 + |\, \lambda_{CP} \,|^2 \pm 2\, |\, \lambda_1 \,||\, \lambda_{CP} \,|\, \mathrm{Re}\left(\lambda_1' \lambda_{CP}'^*\right) \right\} \\
|\, m \,|^2 &= |\, p/q \,|^2 \left\{ 1 + |\, \lambda_1 \,|^2 |\, \lambda_{CP} \,|^2 - 2\, |\, \lambda_1 \,||\, \lambda_{CP} \,|\, \mathrm{Re}\left(\lambda_1' \lambda_{CP}'\right) \right\} \\
u_\pm^* m &= |\, p/q \,|^2 \left\{ |\, \lambda_1 \,|^2 |\, \lambda_{CP} \,|\, \lambda_{CP}' - |\, \lambda_1 \,|\, \lambda_1'^* \pm |\, \lambda_{CP} \,|^2 |\, \lambda_1 \,|\, \lambda_1' \mp |\, \lambda_{CP} \,|\, \lambda_{CP}'^* \right\} \\
u_+ u_-^* &= |\, p/q \,|^2 \left\{ |\, \lambda_1 \,|^2 - |\, \lambda_{CP} \,|^2 + 2i\, |\, \lambda_1 \,||\, \lambda_{CP} \,|\, \mathrm{Im}\left(\lambda_{CP}' \lambda_1'^*\right) \right\}
\end{aligned} \tag{78}$$

- Case $|\, f_1^- f_{CP}\rangle$

$$\begin{aligned}
|\, u_\pm \,|^2 &= r_{CP,1}^2 \left\{ 1 + |\, \bar{\lambda}_1 \,|^2 |\, \lambda_{CP} \,|^2 \pm 2\, |\, \bar{\lambda}_1 \,||\, \lambda_{CP} \,|\, \mathrm{Re}\left(\bar{\lambda}_1' \lambda_{CP}'\right) \right\} \\
|\, m \,|^2 &= r_{CP,1}^2 \left\{ |\, \lambda_{CP} \,|^2 + |\, \bar{\lambda}_1 \,|^2 - 2\, |\, \lambda_{CP} \,||\, \bar{\lambda}_1 \,|\, \mathrm{Re}\left(\lambda_{CP}' \bar{\lambda}_1'^*\right) \right\} \\
u_\pm^* m &= r_{CP,1}^2 \left\{ |\, \lambda_{CP} \,|\, \lambda_{CP}' - |\, \bar{\lambda}_1 \,|\, \bar{\lambda}_1' \pm |\, \lambda_{CP} \,|^2 |\, \bar{\lambda}_1 \,|\, \bar{\lambda}_1'^* \mp |\, \bar{\lambda}_1 \,|^2 |\, \lambda_{CP} \,|\, \lambda_{CP}'^* \right\} \\
u_+ u_-^* &= r_{CP,1}^2 \left\{ 1 - |\, \bar{\lambda}_1 \,|^2 |\, \lambda_{CP} \,|^2 + 2i\, |\, \bar{\lambda}_1 \,||\, \lambda_{CP} \,|\, \mathrm{Im}\left(\bar{\lambda}_1' \lambda_{CP}'\right) \right\}
\end{aligned} \tag{79}$$

Substituting equations (78) and (79) into (77), it can easily be seen that the coefficients $c_\pm$ and s remain unchanged under the simultaneous sign change of $\Delta\Gamma$, Rez, $\mathrm{Re}\lambda_{CP}'$, $\mathrm{Re}\lambda_1'$ and $\mathrm{Re}\bar{\lambda}_1'$. The ambiguity can be resolved if we take $\mathrm{Re}\lambda_{CP}' = +\sqrt{1 - (\mathrm{Im}\lambda_{CP}')^2}$ and the consider as physical parameters $\Delta\Gamma sign(\mathrm{Re}\lambda_{CP}')$ and $\mathrm{Rez}\mathrm{Re}\lambda_{CP}'$ instead of $\Delta\Gamma$ and Rez, respectively. This solves mathametically the complete ambiguity. In practice, due to the poor resolution on $\mathrm{Re}\lambda_1'$ and $\mathrm{Re}\bar{\lambda}_1'$ we may need to fix these parameters. The dependence with λ_1' and $\bar{\lambda}_1'$ is, for all terms, linear in $|\, \lambda_1 \,|$ and $|\, \bar{\lambda}_1 \,|$. Finally, let us note that the dependence of $\mathrm{Im}\lambda_{CP}'$ with $\mathrm{Im}\lambda_1'$ is to first order in Δm, while with $\mathrm{Re}\lambda_1'$ is to second order in Δm as well as in $\Delta\Gamma$.

Flavor eigenstates with $\lambda_2, \bar{\lambda}_2 \neq 0$ and $\lambda_1, \bar{\lambda}_1 \neq 0$

This corresponds to the most general case for fully reconstructed flavor eigenstates. For our purposes here, it is enough to analyze the case $|\, f_1 f_2\rangle$, given by equation (63):

$$\begin{aligned}
|\, u_\pm \,|^2 &= |\, p/q \,|^2 \left\{ |\, \lambda_1 \,|^2 + |\, \lambda_2 \,|^2 \pm 2\, |\, \lambda_1 \,||\, \lambda_2 \,|\, \mathrm{Re}\left(\lambda_1' \lambda_2'^*\right) \right\} \\
|\, m \,|^2 &= |\, p/q \,|^2 \left\{ 1 + |\, \lambda_1 \,|^2 |\, \lambda_2 \,|^2 - 2\, |\, \lambda_1 \,||\, \lambda_2 \,|\, \mathrm{Re}\left(\lambda_1' \lambda_2'\right) \right\} \\
u_\pm^* m &= |\, p/q \,|^2 \left\{ |\, \lambda_1 \,|^2 |\, \lambda_2 \,|\, \lambda_2' - |\, \lambda_1 \,|\, \lambda_1'^* \pm |\, \lambda_2 \,|^2 |\, \lambda_1 \,|\, \lambda_1' \mp |\, \lambda_2 \,|\, \lambda_2'^* \right\} \\
u_+ u_-^* &= |\, p/q \,|^2 \left\{ |\, \lambda_1 \,|^2 - |\, \lambda_2 \,|^2 + 2i\, |\, \lambda_1 \,||\, \lambda_2 \,|\, \mathrm{Im}\left(\lambda_2' \lambda_1'^*\right) \right\}
\end{aligned}$$

We observe again the sign ambiguity, now involving $\mathrm{Re}\lambda_2'$ ($\mathrm{Re}\bar{\lambda}_2'$) instead of $\mathrm{Re}\lambda_{CP}'$, for $B^0(\bar{B}^0)$. Mathematically the ambiguity is already resolved once we have solved it for CP eigenstates (assuming a combined analysis of the flavor and CP eigenstates). In practice, as before, due to the poor resolution on $\mathrm{Re}\lambda_{1/2}'$ and $\mathrm{Re}\bar{\lambda}_{1/2}'$ we may need to fix these parameters. Let us note that in this case the dependence with $\lambda_{1/2}'$ and $\bar{\lambda}_{1/2}'$ is linear in $|\, \lambda_{1/2} \,|$ and $|\, \bar{\lambda}_{1/2} \,|$ only for the $u_\pm^* m$ term, while it is quadratic for the rest.

2.3 $\{|q/p|,\lambda,z\}$ vs $\{\varepsilon,\delta\}$ formalisms

Alternative formalisms can be used to describe flavor and CP mixing [12, 9]. One of these alternative choices is a phase-convention independent formalism similar to that used in kaon system phenomenology [13] ($\{\varepsilon,\delta\}$). To first order in the CPT parameter Δ -the same as defined in equation 13-, the parameters ε and δ parameterize CP/T and CP/CPT violation, and are defined as [13, 11]:

$$\varepsilon = \frac{\mathrm{Im}(\Gamma_{12}CP^*_{12}) + 2i\mathrm{Im}(M_{12}CP^*_{12})}{2\mathrm{Re}(M_{12}CP^*_{12}) - i\mathrm{Re}(\Gamma_{12}CP^*_{12}) + 2F'} \tag{80}$$

$$\delta = \frac{2\Delta}{2\mathrm{Re}(M_{12}CP^*_{12}) - i\mathrm{Re}(\Gamma_{12}CP^*_{12}) + 2F'} \tag{81}$$

where $CP_{12} = \langle B^0 \,|\, CP \,|\, \bar{B}^0\rangle = e^{-i\alpha}$ is the unphysical relative phase between $|\,B^0\rangle$ and $|\,\bar{B}^0\rangle$. The main difference with respect to the standard $\{|q/p|,\lambda,z\}$ formalism is that it relies on the base of CP eigenstates, rather than flavor eigenstates. This is then used to make the formalism phase-convention independent without the need of introducing a specific decay process to unambiguosly define the unphysical relative phase between B^0 and $\bar{B}^0$. This requires, however, of a CP-conserving decay into a definite CP final state. If the decay does not fall into a CP-conserving direction (i.e there is CP violation in the decay and/or not perfect tagging states), corrections are needed in order to define the CP tag appropiately [13]. These corrections are in practice not simple to introduce, limiting the application of the formalism.

After some algebra one can obtain, to first order in CPT and assuming CP conserving decays and perfect tagging states, the relations connecting the two formalisms [11]:

$$\frac{\delta}{1-\varepsilon^2} = z \tag{82}$$

and

$$\frac{q}{p}e^{i\alpha} = \frac{1-\varepsilon}{1+\varepsilon}\,. \tag{83}$$

From (82) and (83) and taking first order in Reε we found the following relations:

$$\frac{2\mathrm{Re}\varepsilon}{1+|\,\varepsilon\,|^2} \equiv \frac{1-|\,q/p\,|^2}{1+|\,q/p\,|^2} \tag{84}$$

$$\frac{\mathrm{Im}\varepsilon}{1+|\,\varepsilon\,|^2} \equiv -\frac{1}{2}\frac{\mathrm{Im}\lambda_{CP}}{|\,\lambda_{CP}\,|} \tag{85}$$

$$\frac{1-|\,\varepsilon\,|^2}{1+|\,\varepsilon\,|^2} \equiv \frac{\mathrm{Re}\lambda_{CP}}{|\,\lambda_{CP}\,|} \tag{86}$$

$$\frac{\mathrm{Re}\delta}{1+\mid\varepsilon\mid^2}\frac{1-\mid\varepsilon\mid^2}{1+\mid\varepsilon\mid^2} \equiv \mathrm{Re}z\frac{\mathrm{Re}\lambda_{CP}}{\mid\lambda_{CP}\mid} \tag{87}$$

$$\frac{\mathrm{Im}\delta}{1+\mid\varepsilon\mid^2} \equiv \mathrm{Im}z \tag{88}$$

2.4 Mistag fractions, $B^0\bar{B}^0$ differences in tagging and reconstruction efficiencies and direct CP violation in tagging and flavor eigenstates

The time-dependent decay rates given in equation (53) have to be corrected by the fraction w^α of events with wrongly assigned flavor in tagging category α, the *mistag fraction*. On the other hand, differences in reconstruction and tagging efficiencies for B^0 and $\bar{B}^0$ can induce biases in the decay time distributions due to the presence of even terms in Δt (odd terms do not contribute). Let us define first the quantities used to parameterize all these effects (we use the same definitions as in [8]).

$w^\alpha_{B^0}$ is defined as the fraction of true B^0 but are incorrectly tagged as $\bar{B}^0$ for tagging category α, and similarly for $w^\alpha_{\bar{B}^0}$. As the mistag fraction can be different for B^0 and $\bar{B}^0$ due to differences in the material interactions (especially for kaons), it is convenient to define

$$w^\alpha = \frac{w^\alpha_{B^0} + w^\alpha_{\bar{B}^0}}{2} \tag{89}$$

and

$$\Delta w^\alpha = w^\alpha_{B^0} - w^\alpha_{\bar{B}^0} \tag{90}$$

which give, respectively, the mean value and the difference of the mistag fractions for B^0 and $\bar{B}^0$. With these definitions,

$$w^\alpha_{B^0} = w^\alpha + \Delta w^\alpha/2 \tag{91}$$

and

$$w^\alpha_{\bar{B}^0} = w^\alpha - \Delta w^\alpha/2 \ . \tag{92}$$

Let us define now

$$\mu^\alpha = \frac{t_1^\alpha - t_1^\alpha}{t_1^\alpha + t_1^\alpha} \tag{93}$$

and

$$\nu = \frac{t_2 - t_2^-}{t_2 + t_2^-} \tag{94}$$

where $t^{\alpha}_{1/\bar{1}}$ is the tagging efficiency for $B^0/\bar{B}^0$ and tagging category α. Similarly $t_{2/\bar{2}}$ is the reconstruction efficiency for $B^0/\bar{B}^0$. If we call T^{α} and R the average tagging and reconstruction efficiencies ($T^{\alpha} = \frac{t^{\alpha}_1 + t^{\bar{\alpha}}_1}{2}$ and $R = \frac{t_2 + t_{\bar{2}}}{2}$), we have

$$t^{\alpha}_1 = T^{\alpha}(1+\mu^{\alpha}) \quad , \quad t^{\bar{\alpha}}_1 = T^{\alpha}(1-\mu^{\alpha}) \tag{95}$$

and

$$t_2 = R(1+\nu) \quad , \quad t_{\bar{2}} = R(1-\nu) \ . \tag{96}$$

The corrected expressions read, for flavor eigenstates (B_{flav}):

$$h^{\alpha}_{k_1 k_2}(\Delta t) \ = \ t_{k_2}\left\{ t^{\alpha}_{k_1}(1-w^{\alpha}_{k_1}) h_{k_1 k_2}(\Delta t) + t^{\bar{\alpha}}_{k_1} w^{\alpha}_{k_1} h_{\bar{k}_1 k_2}(\Delta t) \right\} \tag{97}$$

and for CP eigenstates (B_{CP}):

$$h^{\alpha}_{k_1 k_2}(\Delta t) \ = \ t^{\alpha}_{k_1}(1-w^{\alpha}_{k_1}) h_{k_1 k_2}(\Delta t) + t^{\bar{\alpha}}_{k_1} w^{\alpha}_{k_1} h_{\bar{k}_1 k_2}(\Delta t) \tag{98}$$

where $k_1 = 1, \bar{1}$ and $k_2 = 2, \bar{2}, CP$. The difference among equations (97) and (98) is because $\eta_{f_{CP}} = -1$ (B_{CP-}) and $\eta_{f_{CP}} = +1$ (B_{CP+}) states are normalized separately, while B^0_{flav} and $\overline{B}^0_{flav}$ are normalized together.

CP violation in the decay of B tagging states and flavor eigenstates was explicitely included in equation (53) and terms (63), (68), (70) and (72). Alternatively, it can be included in equations (97) and (98) with the replacement $t^{\alpha}_1 \to t^{\alpha}_1 r^2_{CP,1}$ and $t_{\bar{2}} \to t_{\bar{2}} r^2_{CP,2}$ (t_1 and t_2 remain unchanged). Equations (93) and (94) should then be rewritten as

$$\mu^{\alpha} \ = \ \frac{t^{\alpha}_1 - t^{\bar{\alpha}}_1 r^2_{CP,1}}{t^{\alpha}_1 + t^{\bar{\alpha}}_1 r^2_{CP,1}} \tag{99}$$

and

$$\nu \ = \ \frac{t_2 - t_{\bar{2}} r^2_{CP,2}}{t_2 + t_{\bar{2}} r^2_{CP,2}} \ . \tag{100}$$

From these expressions we see that the net effect of any possible CP violation in the decay of B tagging states and/or flavor eigenstates cannot be distinguished from a charge asymmetry of the detector response.

2.5 Δt resolution function

The introduction of the resolution effects requires the convolution of equations (97) and (98) with the resolution function $\mathcal{R}(\Delta t - \Delta t', \sigma_{\Delta t}; \vec{q}_{\alpha})$:

$$h^{\alpha,resol}_{k_1 k_2}(\Delta t, \sigma_{\Delta t}) \ = \ \int_{-\infty}^{+\infty} \mathcal{R}(\Delta t - \Delta t', \sigma_{\Delta t}; \vec{q}_{\alpha}) h^{\alpha}_{k_1 k_2}(\Delta t') d\Delta t' \ . \tag{101}$$

The problem can be reduced to the convolution of a set of basis functions,

$$\frac{1}{2\tau}\exp\left(\mp\tau_{eff}\Delta t'\right)\exp\left(i\Delta m\Delta t'\right) \tag{102}$$

with (125), where

$$\tau_{eff} = \frac{2\tau}{2\mp\tau\Delta\Gamma} = \frac{\tau}{1\mp\Delta\Gamma/2\Gamma} \tag{103}$$

and $\tau = 1/\Gamma$. The $-(+)$ sign applies for $\Delta t' > 0$ ($\Delta t' < 0$). The normalization of (101) over a finite domain $(\Delta t_1, \Delta t_2)$ can then be calculated from the integral

$$H^{\alpha,resol}_{k_1k_2}(\sigma_{\Delta t}) \;=\; \int_{\Delta t_1}^{\Delta t_2} h^{\alpha,resol}_{k_1k_2}(\Delta t,\sigma_{\Delta t})d\Delta t \;\; . \tag{104}$$

All the integrals (101) and their normalizations (104) can be calculated analytically, and expressed in terms of complex exponentials and the complementary complex error function [16]. The integration limits Δt_1 and Δt_2 can be the acceptance cuts on Δt (finite normalization) or infinity (asymptotic normalization). Asymptotic normalization is used by default in this analysis. The specific resolution models used in this analysis are discussed in section 4.

2.6 Background treatment

In the presence of backgrounds, the PDF has to be extended to include a term for each significant background source. The backgrounds for B_{flav} and $B_{CPK^0_S} \equiv B_{CP-}$ states are small and mostly combinatoric. They are estimated from the beam-energy substituted mass (m_{ES}) sideband, assuming a single Gaussian distribution for the signal and an Argus parameterization for the background. From unbinned maximum likelihood fits to the m_{ES} spectrum, an event-by-event signal probability, $p^{\alpha}_{sig}(m_{ES})$, for each tagging category α, is calculated. The corrected general PDF can then be written as

$$\begin{aligned} h^{\alpha,obs}_{k_1k_2}(\Delta t,\sigma_{\Delta t}) \;=\; & (1-f^{\alpha}_{peak})\,p^{\alpha}_{sig}(m_{ES})\,h^{\alpha,resol,sig}_{k_1k_2}(\Delta t,\sigma_{\Delta t}) + \\ & f^{\alpha}_{peak}\,p^{\alpha}_{sig}(m_{ES})\,h^{\alpha,resol,peak}_{k_1k_2}(\Delta t,\sigma_{\Delta t}) + \\ & \left\{1-p^{\alpha}_{sig}(m_{ES})\right\}\sum_{\beta} f^{\alpha}_{\beta}\,h^{\alpha,resol,\beta}_{k_1k_2}(\Delta t,\sigma_{\Delta t}) \end{aligned} \tag{105}$$

where f^{α}_{β} and f^{α}_{peak} are the combinatorial and peaking background component fractions for the given sample. It is verified that

$$\sum_{\beta} f^{\alpha}_{\beta} \;=\; 1 \;\; . \tag{106}$$

The signal probability is calculated separately for each tagging category.

For each individual signal and background component, $j = sig, peak, \beta$, and tagging category α, the distributions (105) are normalized so that:

$$\sum_{k_1=1,\bar{1}} H_{k_1k_2}^{\alpha,resol,j}(\sigma_{\Delta t})d\Delta t \;=\; 1\;,\quad \forall\; j,\alpha \tag{107}$$

for B_{CP} events, and

$$\sum_{k_2=2,\bar{2}}\sum_{k_1=1,\bar{1}} H_{k_1k_2}^{\alpha,resol,j}(\sigma_{\Delta t})d\Delta t \;=\; 1\;,\quad \forall\; j,\alpha \tag{108}$$

for B_{flav} events.

For the $B^0 \to J/\psi K_L^0$ channel ($B_{CPK_L^0} \equiv B_{CP+}$ sample) the background level is significantly higher with significant non-combinatorial component, therefore requiring an special treatment [18]. The data are used to determine the relative amount of signal, background from $B \to J/\psi X$ events and events from a misreconstructed $J/\psi \to \ell\ell$ candidate. The Monte Carlo simulation is then used to evaluate the channels that contribute to the $B \to J/\psi X$ background. All this information is used to determine the composition of the $B^0 \to J/\psi K_L^0$ sample from a fit to the ΔE spectrum after flavor tagging. Moreover, some of the decay modes in the inclusive J/ψ background have an expected CP structure. The PDF can then be formulated as

$$\begin{aligned} h_{k_1k_2}^{\alpha,obs}(\Delta t,\sigma_{\Delta t}) \;=\;& f_{sig}^{\alpha}(\Delta E)h_{k_1k_2}^{\alpha,resol,sig}(\Delta t,\sigma_{\Delta t}) + \\ & \sum_{j=J/\psi\;X} f_j^{\alpha}(\Delta E)h_{k_1k_2}^{\alpha,resol,j}(\Delta t,\sigma_{\Delta t}) + \\ & f_{non-J/\psi}^{\alpha}(\Delta E)\left[f_{prompt}^{\alpha}h_{k_1k_2}^{\alpha.resol,prompt}(\Delta t,\sigma_{\Delta t}) + f_{non-prompt}^{\alpha}h_{k_1k_2}^{\alpha,resol,non-prompt}(\Delta t,\sigma_{\Delta t})\right] \end{aligned} \tag{109}$$

where

$$f_{prompt}^{\alpha} + f_{non-prompt}^{\alpha} \;=\; 1 \tag{110}$$

and

$$f_{sig}^{\alpha}(\Delta E) + \sum_{j=J/\psi\;X} f_j^{\alpha}(\Delta E) + f_{non-J/\psi}^{\alpha}(\Delta E) \;=\; 1\,. \tag{111}$$

2.7 The log-likelihood function

The log-likelihood function for tagging category α is finally defined as

$$\begin{aligned}
\ln \mathcal{L}_\alpha \;=\; & \sum_i^{N^\alpha_{B^0_{tag}B_{CP-}}} \ln h^{\alpha,obs}_{B^0_{tag}B_{CP-}}(\Delta t_i,\sigma_{\Delta t,i}) + \sum_i^{N^\alpha_{\overline{B}^0_{tag}B_{CP-}}} \ln h^{\alpha,obs}_{\overline{B}^0_{tag}B_{CP-}}(\Delta t_i,\sigma_{\Delta t,i}) + \\
& \sum_i^{N^\alpha_{B^0_{tag}B_{CP+}}} \ln h^{\alpha,obs}_{B^0_{tag}B_{CP+}}(\Delta t_i,\sigma_{\Delta t,i}) + \sum_i^{N^\alpha_{\overline{B}^0_{tag}B_{CP+}}} \ln h^{\alpha,obs}_{\overline{B}^0_{tag}B_{CP+}}(\Delta t_i,\sigma_{\Delta t,i}) + \\
& \sum_i^{N^\alpha_{B^0_{tag}B^0_{flav}}} \ln h^{\alpha,obs}_{B^0_{tag}B^0_{flav}}(\Delta t_i,\sigma_{\Delta t,i}) + \sum_i^{N^\alpha_{\overline{B}^0_{tag}\overline{B}^0_{flav}}} \ln h^{\alpha,obs}_{\overline{B}^0_{tag}\overline{B}^0_{flav}}(\Delta t_i,\sigma_{\Delta t,i}) + \\
& \sum_i^{N^\alpha_{B^0_{tag}\overline{B}^0_{flav}}} \ln h^{\alpha,obs}_{B^0_{tag}\overline{B}^0_{flav}}(\Delta t_i,\sigma_{\Delta t,i}) + \sum_i^{N^\alpha_{\overline{B}^0_{tag}B^0_{flav}}} \ln h^{\alpha,obs}_{\overline{B}^0_{tag}B^0_{flav}}(\Delta t_i,\sigma_{\Delta t,i})
\end{aligned} \tag{112}$$

where $N^\alpha_{k_1k_2}$ is the total number of k_2 events tagged as k_1 in tagging category α. The global likelihood function for all tagging categories is then calculated as

$$\ln \mathcal{L} = \sum_\alpha \ln \mathcal{L}_\alpha \; . \tag{113}$$

ν, μ^α and T^α, given in equations (99), (100) and (95), respectively, can be calculated from time integrated flavor transition rates following the prescription documented in [14]. It has been generalized to account for non-zero $\Delta\Gamma$ values, CP violation in mixing and CPT violation (see appendix B):

$$\nu \;=\; \frac{1}{2}\frac{(z+x)(c+d)-(w+y)(a+b)}{(a+b)(c+d)} \tag{114}$$

$$\mu^\alpha \;=\; \frac{x(1-\nu)(c+d)-y(1+\nu)(a+b)}{y(1+\nu)(a-b)-x(1-\nu)(c-d)} \tag{115}$$

$$T^\alpha \;=\; \frac{1}{1-(\nu)^2}\frac{x(c-d)(1-\nu)-y(a-b)(1+\nu)}{2(bc-da)} \tag{116}$$

where

$$a = H_{B^0_{tag}B^0_{flav}} \;,\;\; b = H_{\overline{B}^0_{tag}B^0_{flav}} \;,\;\; c = H_{B^0_{tag}\overline{B}^0_{flav}} \;,\;\; d = H_{\overline{B}^0_{tag}\overline{B}^0_{flav}}$$

are the time integrated theoretical rates (with $r_{CP,1} = r_{CP,2} = 1$), i.e. the result of integrating over $-\infty < \Delta t < +\infty$ equation (53) with coefficients from (63), (68), (70) and (72), for B_{flav} events; and

$$x = H^\alpha_{any\ tag B^0_{flav}} \;,\;\; y = H^\alpha_{any\ tag \overline{B}^0_{flav}} \;,\;\; z = H^\alpha_{no\ tag B^0_{flav}} \;,\;\; w = H^\alpha_{no\ tag \overline{B}^0_{flav}}$$

are the measured rates of tagged events in category α for B^0_{flav} (x) and $\overline{B}^0_{flav}$ (y) processes, and the total measured rates of B^0_{flav} and $\overline{B}^0_{flav}$ except those tagged in category α (z,w). Let us note that following the discussion at the end of section 2.4, possible direct CP violation effects (together with the detector charge asymmetries)

are already included in the B counting, so that the PDF for the final fit should have $r_{CP,1} = r_{CP,2} = 1$. In addition to the dependence with the number of $B^0/\overline{B}^0$/mixed/unmixed events, the extraction of ν, μ^α and T^α relies on estimates of the parameters which are going to be extracted from the time dependent analysis, independently of mistags and Δt resolution [14]. The terms with odd Δt dependence do not contribute.This is critical for the extraction of $\mid q/p \mid$, since this parameter is anticorrelated with the detector asymmetries (ν and μ^α) [11]. In order to introduce the time integrated constraint given by equations (114) and (115), an extended maximum likelihood was constructed to incorporate the Poisson uncertainties from the B counting. The modified likelihood function reads

$$\ln \mathcal{L}_{Extended} = \ln \mathcal{L} + \Delta \ln \mathcal{L} \tag{117}$$

where $\ln \mathcal{L}$ was defined in equation (113) and

$$\begin{aligned} \Delta \ln \mathcal{L} &= \sum_\alpha \Delta \ln \mathcal{L}_\alpha \qquad (118) \\ &- \ln N_{B^0_{flav},notag}! + N_{B^0_{flav},notag} \ln \eta_{B^0_{flav},notag} - \eta_{B^0_{flav},notag} \\ &- \ln N_{\overline{B}^0_{flav},notag}! + N_{\overline{B}^0_{flav},notag} \ln \eta_{\overline{B}^0_{flav},notag} - \eta_{\overline{B}^0_{flav},notag} \qquad (119) \end{aligned}$$

and

$$\begin{aligned} \Delta \ln \mathcal{L}_\alpha &= - \ln N^\alpha_{B^0_{flav},tag}! + N^\alpha_{B^0_{flav},tag} \ln \eta^\alpha_{B^0_{flav},tag} - \eta^\alpha_{B^0_{flav},tag} \\ &- \ln N^\alpha_{\overline{B}^0_{flav},tag}! + N^\alpha_{\overline{B}^0_{flav},tag} \ln \eta^\alpha_{\overline{B}^0_{flav},tag} - \eta^\alpha_{\overline{B}^0_{flav},tag} \end{aligned} \tag{120}$$

$N^\alpha_{B^0_{flav}(\overline{B}^0_{flav}),tag}$ is the number of B_{flav} events reconstructed as $B^0(\bar{B}^0)$ and tagged in category α, and $N_{B^0_{flav}(\overline{B}^0_{flav}),notag}$ is the total number of untagged B_{flav} events and reconstructed as $B^0(\bar{B}^0)$. $\eta^\alpha_{B^0_{flav}(\overline{B}^0_{flav}),tag}$ and $\eta_{B^0_{flav}(\overline{B}^0_{flav}),notag}$ denote the corresponding expected numbers of events. ν and μ^α are finally calculated at each step of the minimization procedure using the values of the expected number of events and the physical parameters from the previous iteration. This method can be applied by counting the number of signal events (estimated from m_{ES} fits). This methods accounts for the correlations induced by the reuse of events in the evaluation of ν and μ^α: for each tagging category it is used the number of tagged events in that category together with the remaining events (events tagged by other categories plus the untagged events).

For combinatorial background components, where typically we assume Δm=0, $\Delta\Gamma/\Gamma$=0, $\mid q/p \mid$=1 and $z = 0$, there is no need to apply this method, and the parameters ν and μ^α can be fixed to the estimates obtained previously to the fit using events from the sideband region (see section 6). The method has been validated with extensive toy Monte Carlo studies, as documented in [11]. With this technique we are able to to desintangle physics and detector asymmetries, at the cost of a reasonable increase in the statistical error on $\mid q/p \mid$ ($\approx 30\%$), while all the other physics parameters remain basically unchanged.

An standalone fitting program, called `cptNagFit`, has been developped to find the solution of (117) and the errors on the fitted parameters. The program has been interfaced to the NAG library [28] and the MINUIT package [29]. All the numerical and minimization routines are based on the NAG library, and the error estimation relies on the HESSE and MINOS methods of MINUIT. This simultaneous interfacing allows direct comparison and cross-checking of the fitting results using two completely different libraries. As described in section 8, the `cptNagFit` fitting program has been cross-checked performing standard $\sin 2\beta$ fits with the widely used `RootFitTools` package [16].

2.8 Discussion about Doubly-CKM-Suppressed effects

The numerical sensitivity of the CPT/T/CPT/oscillation parameters to DCKM effects in the tagging and reconstructed (flavor sample) sides was investigated using toy Monte Carlo[3], as described in detail in appendix A.1. The studies confirmed the main features described in section 2.2.6. First, Rez is mainly correlated with the DCKM real parts, while Imz and to a less extend $\mathrm{Im}\lambda'_{CP}$ are mainly correlated with DCKM imaginary parts. Second, the sensitivity to the DCKM real parts is poor ($\frac{\mathrm{Re}\lambda_{tag}}{|\lambda_{tag}|}$ and $\frac{\mathrm{Re}\bar{\lambda}_{tag}}{|\lambda_{tag}|}$) or none ($\frac{\mathrm{Re}\lambda_{flav}}{|\lambda_{flav}|}$ and $\frac{\mathrm{Re}\bar{\lambda}_{flav}}{|\lambda_{flav}|}$). The poor sensitivities together with the discrete ambiguities involved will require to fix (e.g. to zero) these parameters. Third, DCKM effects on Δm and $\Delta\Gamma$ are small since most of the impact is absorbed by the coefficients of the time dependence. Four, the tagging side gives the largest contribution (assuming a single channel contributing to the sample, see discussion below). This is expected in a combined analysis of flavor and CP eigenstates since the tagging side effects are common to all samples, while the CP sample would contribute to reduce dependencies from the reconstructed side of the flavor sample. In the extreme case of parameters dominated by the CP sample (e.g. Rez, $\mathrm{Im}\lambda'_{CP}$) we expect the effects from the reconstructed side of the flavor sample to be very small or negligible, as seen in the toy Monte Carlo studies (as well as in the final systematics from this source). From these studies we concluded that the optimal trade-off between statistical precision and systematic uncertainties induced by DCKM decays requires the introduction of new fit parameters (to be added to the 6 CPT/T/CP/oscillation parameters), the sines of the DCKM phases, 2 for the tagging side (common to all samples) and 2 for the reconstructed side (flavor sample). Using toy Monte Carlo, it was verified (for different DCKM phase configurations) that this fitting configuration provides unbiassed estimates for all the parameters, and the Gaussian errors reported by the fit give a good estimation of the statistical reach, within 10%.

Supposse now that we identify f_2 accurately, but we have a probability w_1 of misidentifying f_1 as $f_{\bar{1}}$, and a probability $\bar{w}_1$ of misidentifying $f_{\bar{1}}$ as f_1. From equation (41), the time-dependent decay rate can be written as

$$\begin{aligned}
|\langle f_1 f_2 \mid \Upsilon(t_1,\Delta t)\rangle|^2 \;=\; & \frac{1}{2}e^{-2t_1/\tau}\frac{|\,p_+q_- + p_-q_+\,|^2}{|\,N_+N_-\,|^2}\Big\{|\langle f_2 \mid B^0(\Delta t)\rangle|^2\left[(1-w_1)\,|\,\bar{A}_1\,|^2 + \bar{w}_1\,|\,\bar{A}_{\bar{1}}\,|^2\right] + \\
& |\langle f_2 \mid \bar{B}^0(\Delta t)\rangle|^2\left[(1-w_1)\,|\,A_1\,|^2 + \bar{w}_1\,|\,A_{\bar{1}}\,|^2\right] - \\
& 2\mathrm{Re}\left[\langle f_2 \mid B^0(\Delta t)\rangle\langle f_2 \mid \bar{B}^0(\Delta t)\rangle^*\left((1-w_1)\bar{A}_1A_1^* + \bar{w}_1\bar{A}_{\bar{1}}A_{\bar{1}}^*\right)\right]\Big\} \quad . \qquad (121)
\end{aligned}$$

with the following relations being satisfied:

$$\begin{aligned}
|\,\bar{A}_1\,|^2 &= r_1^2\,|\,A_1\,|^2 \\
|\,\bar{A}_{\bar{1}}\,|^2 &= r_{CP,1}^2\,|\,A_1\,|^2 \\
|\,A_{\bar{1}}\,|^2 &= \bar{r}_1^2 r_{CP,1}^2\,|\,A_1\,|^2 \\
\bar{A}_1A_1^* &= r_1 e^{i\phi_1}\,|\,A_1\,|^2 \\
\bar{A}_{\bar{1}}A_{\bar{1}}^* &= \bar{r}_1 r_{CP,1}^2 e^{-i\bar{\phi}_1}\,|\,A_1\,|^2 \quad . \qquad (122)
\end{aligned}$$

$\phi_1(\bar{\phi}_1)$ is the relative phase of $\bar{A}_1(A_{\bar{1}})$ with respect to $A_1(\bar{A}_{\bar{1}})$. From equations (121) and (122) it can easily be seen that a change in r_1 and $\bar{r}_1$ can be completely absorbed in a redefinition of w_1, $\bar{w}_1$, $\mathrm{Re}(e^{i\phi_1})$, $\mathrm{Im}(e^{i\phi_1})$, $\mathrm{Re}(e^{-i\bar{\phi}_1})$ and $\mathrm{Im}(e^{-i\bar{\phi}_1})$. The dependence with r_1 and $\bar{r}_1$ is quadratic for the former and linear for the latter. Of course, if the real and imaginary parts are either fixed or constrained to be within the physical region this is anymore true since the complete absortion of the effect requires the simultaneous change of all the above quantities. If

[3] All the feasibility, reach and validation studies when DCKM effects are neglected were described in detail in [11].

for example (our case) $\mathrm{Re}(e^{i\phi_1})$ and $\mathrm{Re}(e^{-i\bar{\phi}_1})$ are fixed to zero, the systematics from their variation from -1 to $+1$ will scale linearly with the largest possible value assumed for r_1 and $\bar{r_1}$, while the uncertainty from r_1 and $\bar{r_1}$ in the sine terms will be absorbed in a redefinition of the fitted value of $\mathrm{Im}(e^{i\phi_1})$ and $\mathrm{Im}(e^{-i\bar{\phi}_1})$. This feature was verified using toy Monte Carlo, as described in appendix A.2.

So far we assumed that the final states f_1 and f_2 receive contributions from a single channel. In practice, the B sample used for B tagging and the flavor eigenstate sample are an admixture of different channels. When we consider semi-inclusive measurements that do not distinguish between different final states, the decay rate distribution has to be expressed as

$$|\langle f_1 f_2 \mid \Upsilon(\Delta t)\rangle|^2 \quad \propto \quad \sum_j \omega_j \,|\langle f_{1,j} f_{2,j} \mid \Upsilon(\Delta t)\rangle|^2 \tag{123}$$

where the set of final states has been denoted by $\{f_1 f_2\}_j$. ω_j are the weights for each final state, and include relative normalization factors and experimental efficiencies. The decay rate distribution can be written in the form of equation (53) with the following substitutions:

$$\begin{aligned}
|u_\pm|^2 &\rightarrow \sum_j \omega_j \,|u_{\pm,}|^2 \\
|m|^2 &\rightarrow \sum_j \omega_j \,|m_j|^2 \\
u_\pm^* m &\rightarrow \sum_j \omega_j u_{\pm,j}^* m_j \\
u_+ u_-^* &\rightarrow \sum_j \omega_j u_{+,j} u_{-,j}^*
\end{aligned}$$

It is therefore expected that multiple channels would result in an effective single channel which overall effect would be a weigthed average of each individual channel. As a consequence, the effects from more than one channel should always be smaller than the worse possible single channel. This was confirmed by a toy Monte Carlo study, described in appendix A.3. This proves that the DCKM systematics extracted under the single channel assumptio will be conservative.

3 Decay modes, data and Monte Carlo samples

The decay modes considered for the analysis are:

$B_{CPK_S^0}$ **sample:** $B^0 \rightarrow J/\psi K_S^0(\pi^+\pi^-$ and $\pi^0\pi^0)$, $B^0 \rightarrow \psi(2S)K_S^0(\pi^+\pi^-)$, $\chi_{c1}\, K_S^0(\pi^+\pi^-)$;
$J/\psi \rightarrow e^+e^-, \mu^+\mu^-$; $\psi(2S) \rightarrow e^+e^-, \mu^+\mu^-, J/\psi\pi^+\pi^-$; $\chi_{c1} \rightarrow J/\psi\gamma$;

$B_{CPK_L^0}$ **sample:** $B^0 \rightarrow J/\psi K_L^0$;

B_{flav} **sample:** $B^0 \rightarrow \mathrm{D}^{(*)}\pi(\rho, \mathrm{a}_1)$ and $B^0 \rightarrow J/\psi K^{*0}$. Charmed mesons are reconstructed in the following modes: $\mathrm{D}^{*-} \rightarrow \overline{\mathrm{D}}^0\pi^-$ with $\overline{\mathrm{D}}^0 \rightarrow \mathrm{K}^+\pi^-, \mathrm{K}^+\pi^-\pi^0, \mathrm{K}^+\pi^+\pi^-\pi^-, \mathrm{K}_S^0\pi^+\pi^-$; $\mathrm{D}^- \rightarrow \mathrm{K}^+\pi^-\pi^-, \mathrm{K}_S^0\pi^-$; $\rho^- \rightarrow \pi^-\pi^0$, $a_1 \rightarrow \pi^+\pi^-\pi^+$, $K^{*0} \rightarrow K^+\pi^-$.

Fig.	Mode		$\sigma\, m_{ES}$ (MeV)	m_{ES} Yield (ΔE for $J/\psi K_L^0$)	Purity (%)
2	$D^*\pi$		2.57 ± 0.05	5076 ± 90	92
	$D^*\rho$		2.91 ± 0.08	3190 ± 84	84
	$D^* a_1$		2.57 ± 0.08	2371 ± 75	78
3	$D\pi$		2.49 ± 0.05	5596 ± 111	81
	$D\rho$		2.85 ± 0.08	3230 ± 92	76
	Da_1		2.43 ± 0.10	1780 ± 73	65
4	$J/\psi K^{*0}$	e^+e^-	2.74 ± 0.10	1016 ± 38	95
	$(K^\pm\pi^\mp)$	$\mu^+\mu^-$	2.58 ± 0.10	931 ± 35	96
	all B_{flav}		2.63 ± 0.03	23192 ± 225	82
5	$J/\psi K_S^0$	e^+e^-	2.68 ± 0.16	470 ± 27	94
	$(\pi^+\pi^-)$	$\mu^+\mu^-$	2.63 ± 0.13	529 ± 25	98
6	$J/\psi K_S^0$	e^+e^-	3.1 ± 0.5	83 ± 14	84
	$(\pi^0\pi^0)$	$\mu^+\mu^-$	3.2 ± 0.4	100 ± 14	89
7	$\psi(2S)K_S^0$	e^+e^-	3.0 ± 0.5	80 ± 14	85
		$\mu^+\mu^-$	2.4 ± 0.3	82 ± 11	94
8	$\chi_{c1}K_S^0$	e^+e^-	3.5 ± 0.7	42 ± 8	95
		$\mu^+\mu^-$	2.3 ± 0.5	40 ± 8	93
	all $B_{CPK_S^0}$		2.73 ± 0.09	1426 ± 47	94
9	$J/\psi K_L^0$(EMC)	e^+e^-	—	154 ± 15	54 ± 3
		$\mu^+\mu^-$	—	174 ± 17	49 ± 3
10	$J/\psi K_L^0$(IFR)	e^+e^-	—	160 ± 15	70 ± 4
		$\mu^+\mu^-$	—	163 ± 16	65 ± 4

Table 5: Event yields, signal resolutions, and signal purities for the B_{flav} and B_{CP} decay modes, from 56 fb^{-1} of data (Winter'02 data sample). Results are shown separately for $J/\psi \to e^+e^-$ and $J/\psi \to \mu^+\mu^-$ channels. The errors on these quantities are the statistical errors from the distribution. The m_{ES} results, yields and purities were determined from a fit to a Gaussian plus Argus background in a 3σ ΔE window (the purity was estimated for the region $m_{ES} > 5.27$ GeV/c^2), as shown in figures 2 to 10.

Each of these samples is separated by tagging category, with a total of 4 tagging categories: the default tagger used here is the Elba Tagger [19], while the Moriond Tagger [20] will be used as cross-check.

The selection cuts for all the modes are the same as those used in [8, 18, 21]. The data sample corresponds to an integrated luminosity of approximately 56 fb^{-1}. Table 5 summarizes the event yields on the full data sample for all the B_{flav} and charmonium modes. In each case, the $\sigma(m_{ES})$, yield and purity (estimated as the signal fraction for events with $m_{ES} > 5.27$ GeV for modes other than $J/\psi K_L^0$ and $|\,\Delta E\,| < 10$ MeV for $J/\psi K_L^0$) are given separately for each mode, and in the case of charmonium modes it is given for *ee* and $\mu\mu$. Figures 2, 3, 4, 5, 6, 7 and 8, show the unbinned maximum likelihood fit used to extract the yields and purities given in table 5. The fits are performed to the beam-energy substituted mass, $m_{ES} = \sqrt{E^{*2} - p^{*2}}$, using a Gaussian plus Argus background shape. The $J/\psi K_L^0$ channel is handled differently, using the variable $\Delta E = E^*_{J/\psi} + E^*_{K_L^0} - E_{beam}$. See [18] for details. The fit results to the ΔE distributions are shown in figures 9 and 10.

Two different Monte Carlo samples are used: an standard sample, the same as used in [8, 18], and a dedicated one. The values of the physics parameters used in the generation of the two samples are shown in table 6. Each sample contains B_{flav}, $B_{CPK_S^0}$ and $B_{CPK_L^0}$ decay modes. The standard sample itself has two

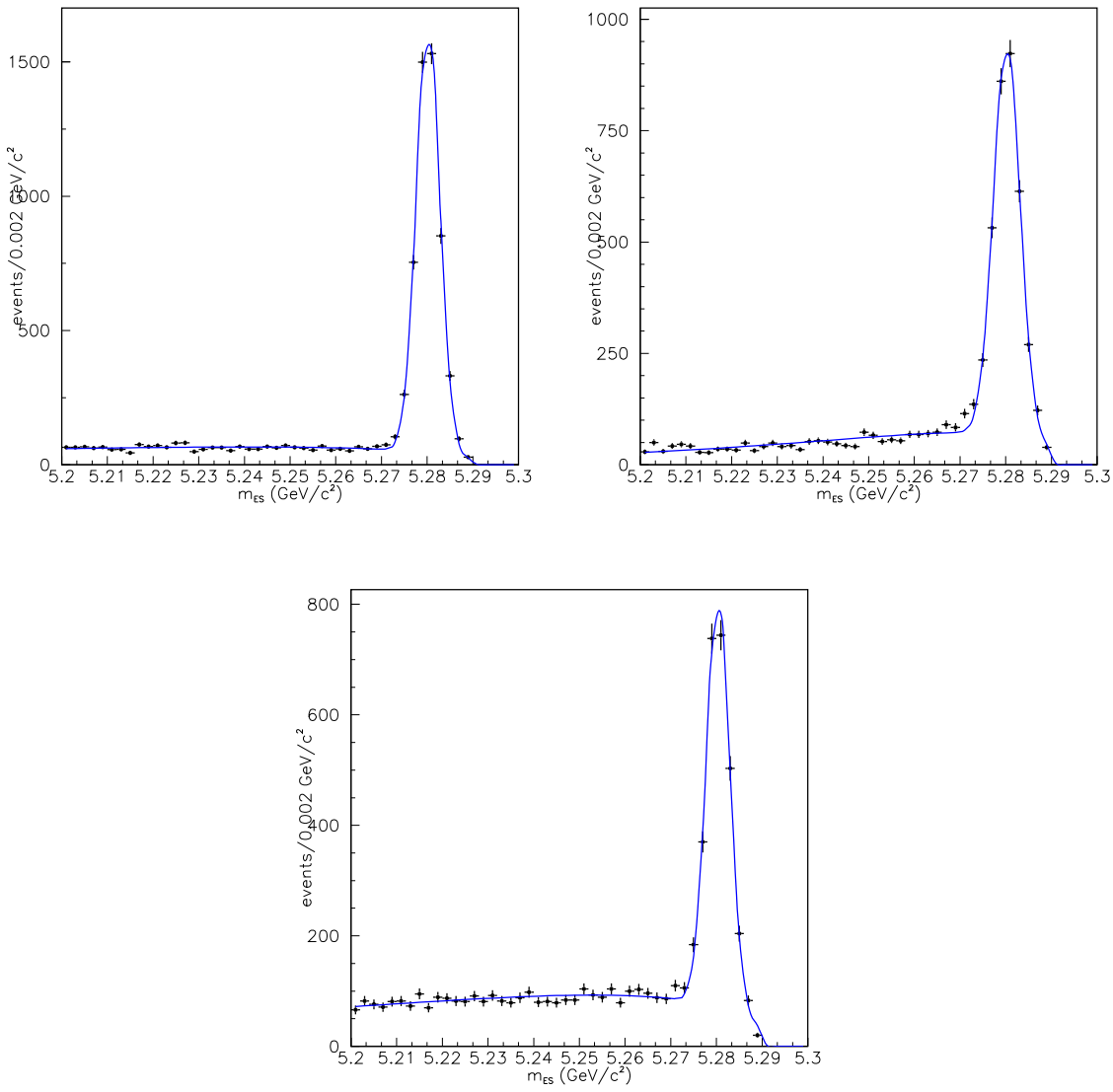

Figure 2: Fits to the m_{ES} distributions in the $B^0 \to \mathrm{D}^*\pi$ (top/left), $B^0 \to \mathrm{D}^*\rho$ (top/right) and $B^0 \to \mathrm{D}^* a_1$ (bottom) channels. Vertexing cuts have not been applied.

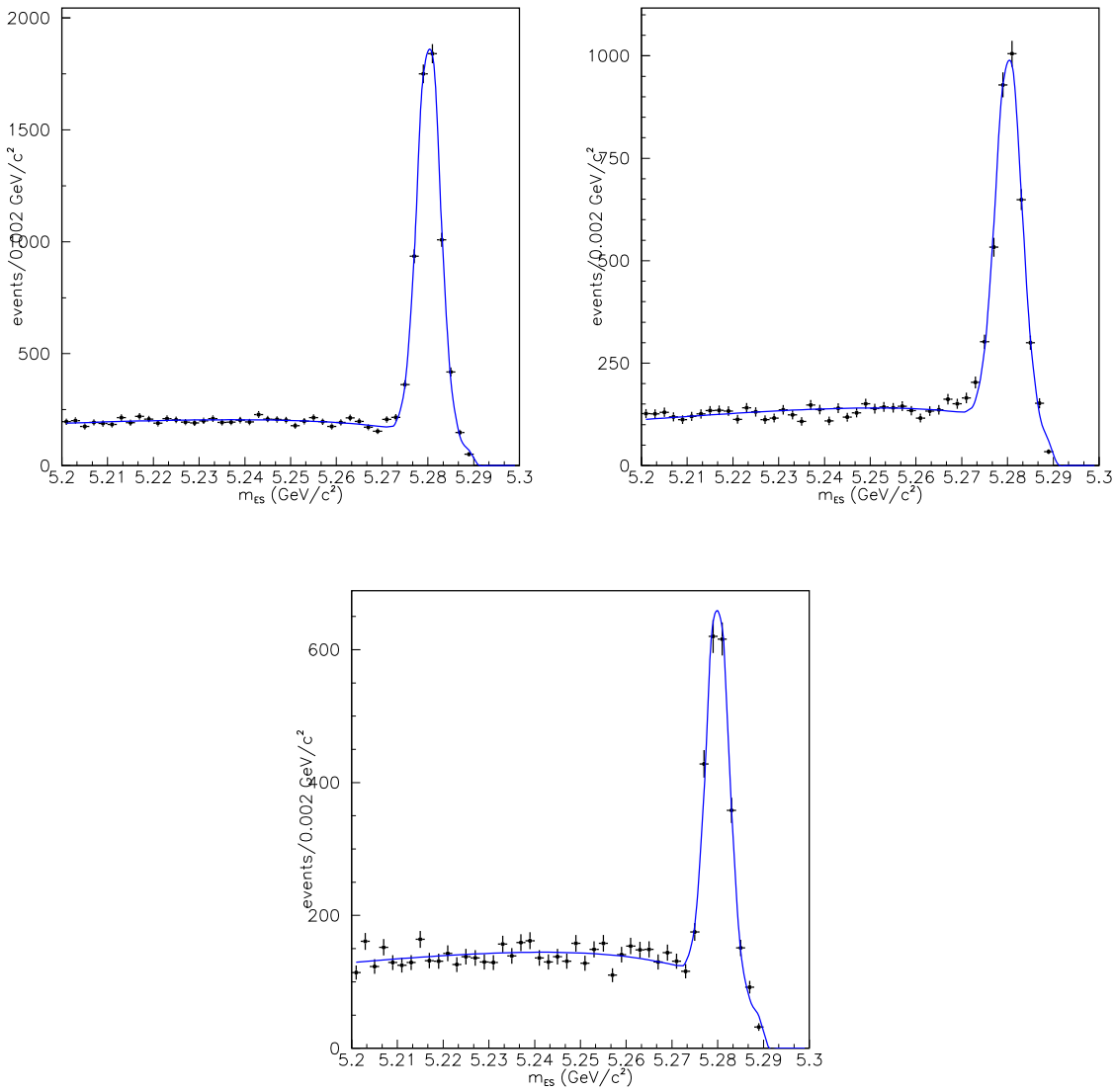

Figure 3: Fits to the m_{ES} distributions in the $B^0 \to D\pi$ (top/left), $B^0 \to D\rho$ (top/right) and $B^0 \to Da_1$ (bottom) channels. Vertexing cuts have not been applied.

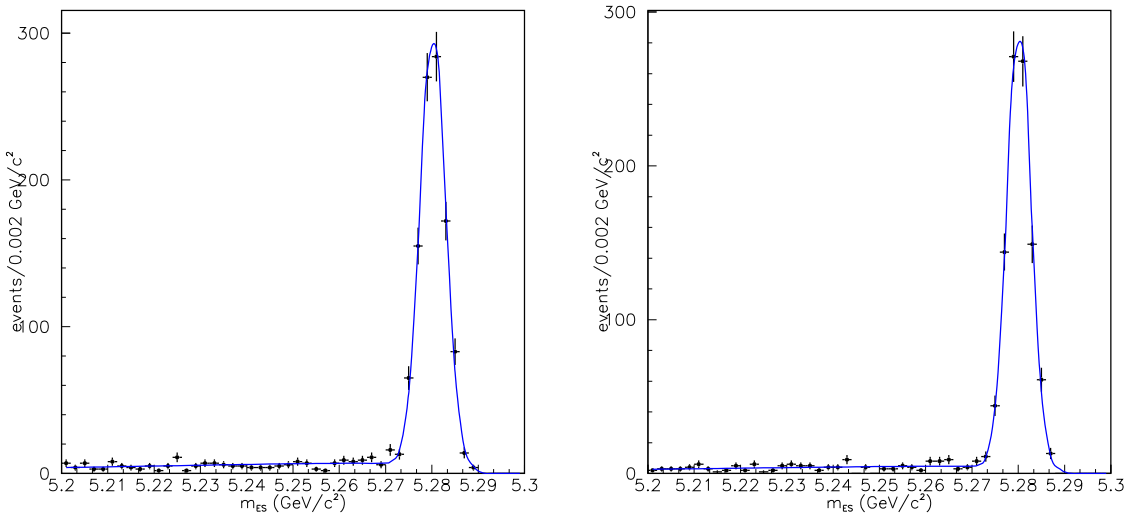

Figure 4: Fits to the m_{ES} distributions in the $B^0 \to J/\psi K^*$ ($K^{\pm}\pi^{\mp}$) channel for the $J/\psi \to e^+e^-$ (left) and $J/\psi \to \mu^+\mu^-$ (right) modes. Vertexing cuts have not been applied.

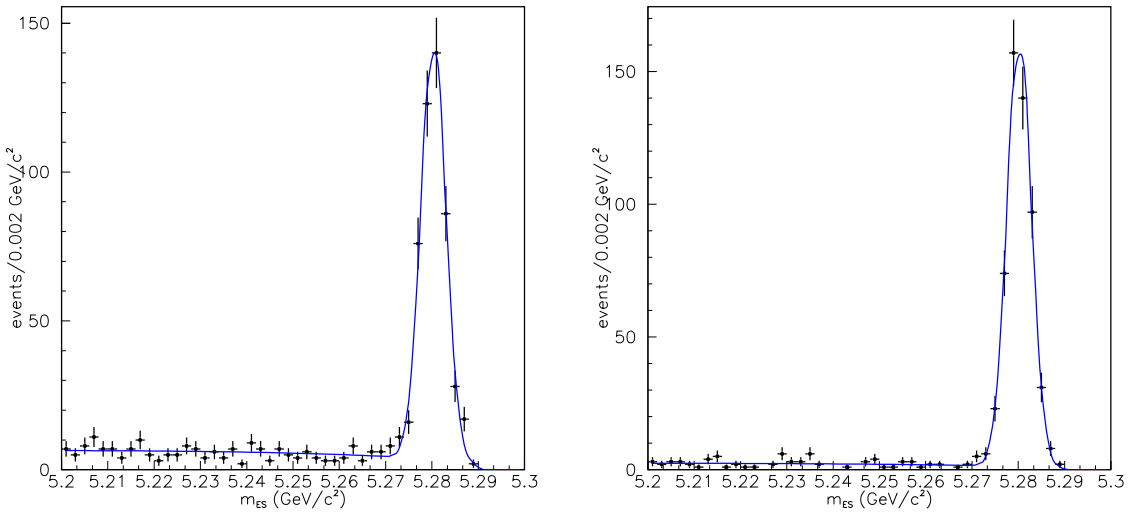

Figure 5: Fits to the m_{ES} distributions in the $B^0 \to J/\psi K^0_S$ ($\pi^+\pi^-$) channel for the $J/\psi \to e^+e^-$ (left) and $J/\psi \to \mu^+\mu^-$ (right) modes. Vertexing cuts have not been applied.

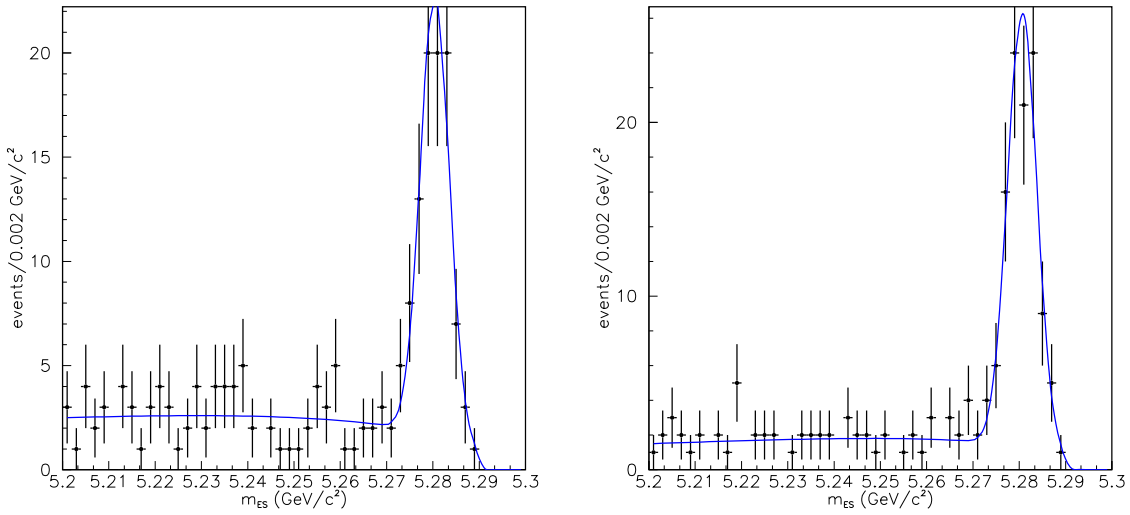

Figure 6: Fits to the m_{ES} distributions in the $B^0 \to J/\psi K_S^0$ ($\pi^0\pi^0$) channel for the $J/\psi \to e^+e^-$ (left) and $J/\psi \to \mu^+\mu^-$ (right) modes. Vertexing cuts have not been applied.

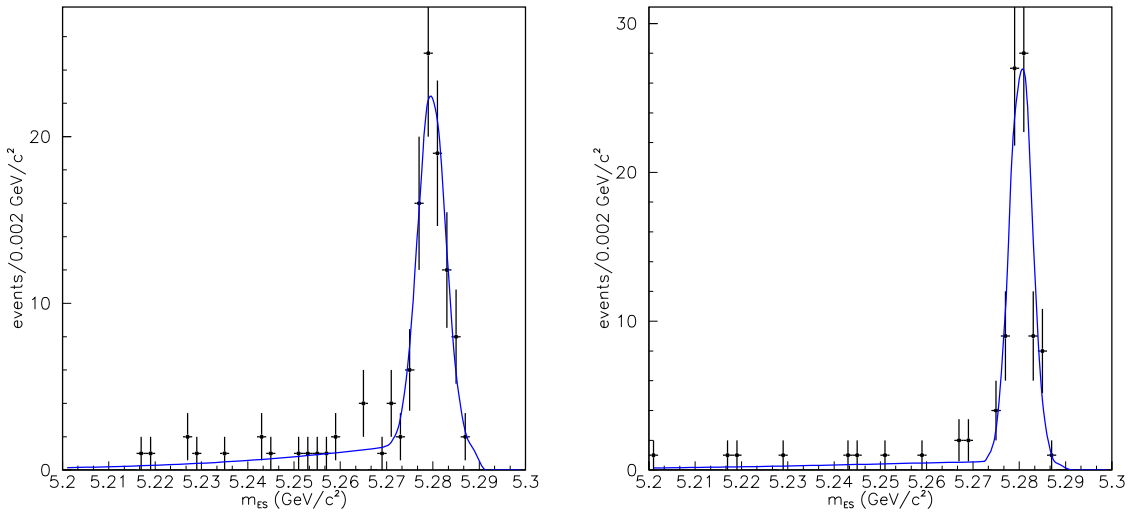

Figure 7: Fits to the m_{ES} distributions in the $B^0 \to \psi(2S)K_S^0$ channel for the $J/\psi \to e^+e^-$ (left) and $J/\psi \to \mu^+\mu^-$ (right) modes. Vertexing cuts have not been applied.

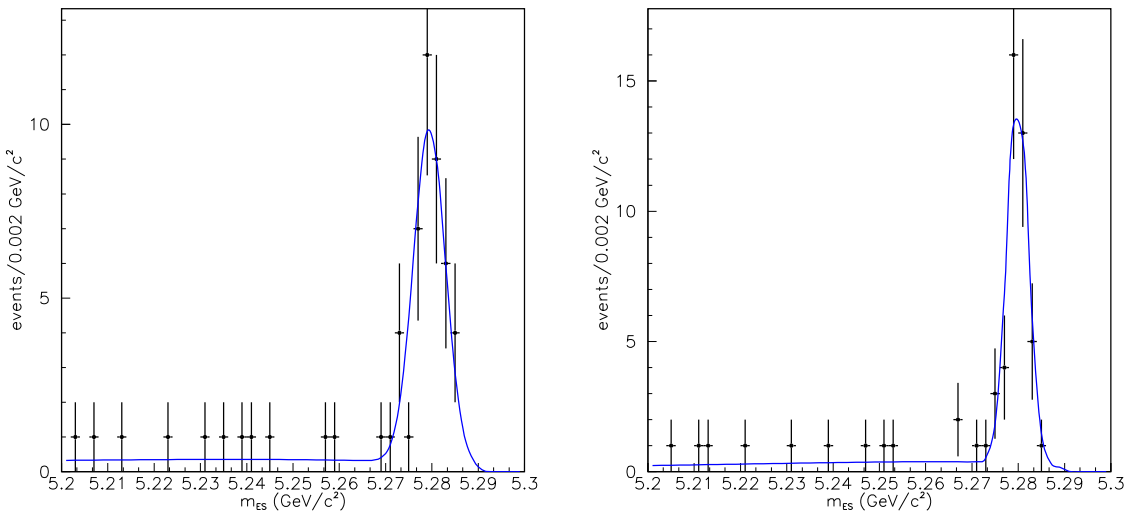

Figure 8: Fits to the m_{ES} distributions in the $B^0 \to \chi_{c1} K^0_S$ channel for the $J/\psi \to e^+e^-$ (left) and $J/\psi \to \mu^+\mu^-$ (right) modes. Vertexing cuts have not been applied.

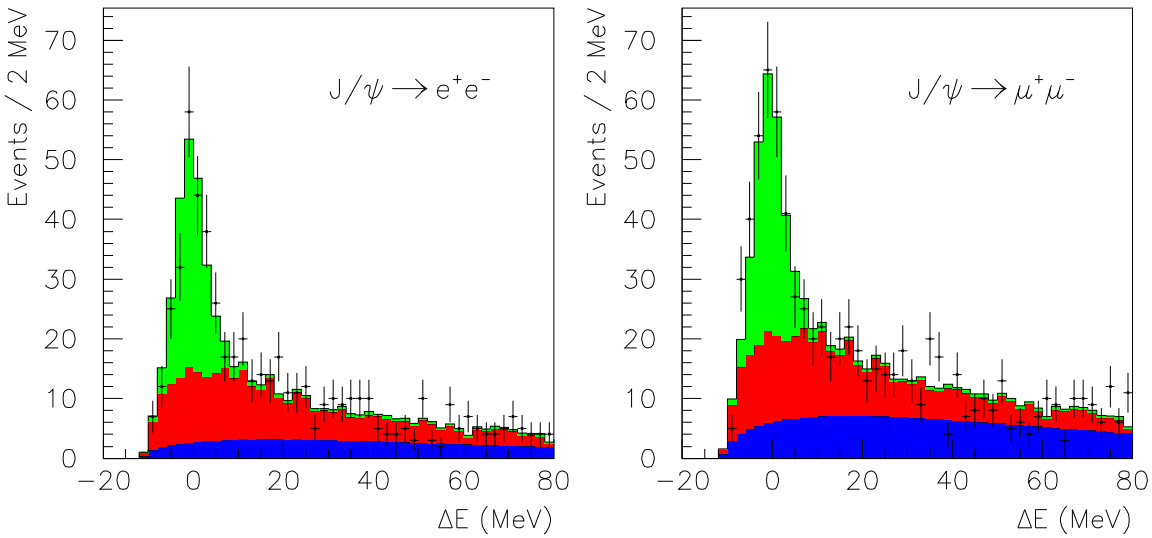

Figure 9: Fits to the ΔE distribution in the $B^0 \to J/\psi K^0_L$ channel for K^0_L detected in the Emc. Vertexing cuts have not been applied. The red (blue) histogram is the fitted inclusive J/ψ (fake J/ψ) background contribution.

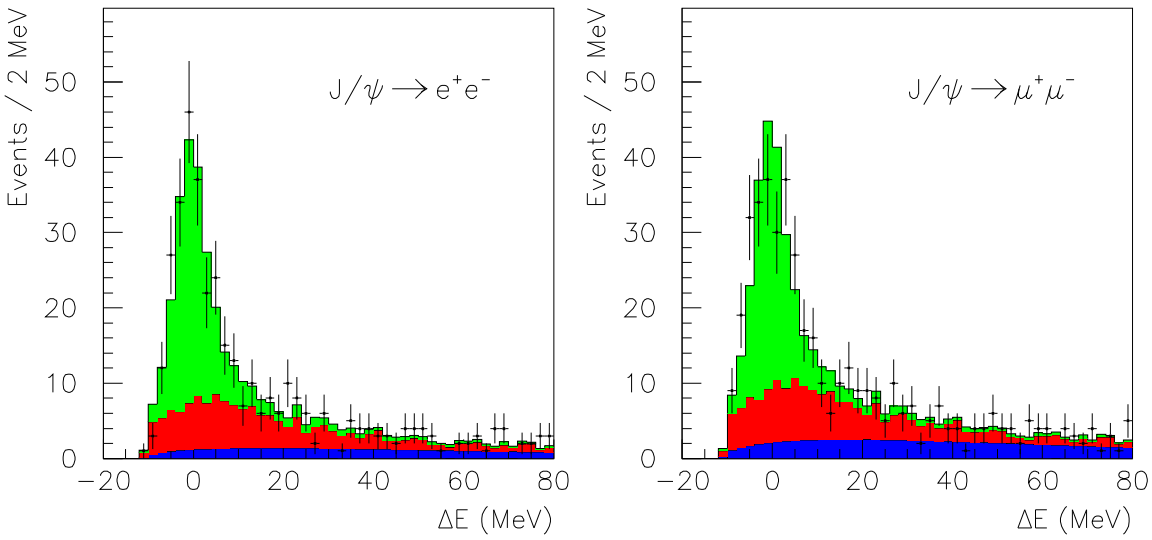

Figure 10: Fits to the ΔE distribution in the $B^0 \to J/\psi K_L^0$ channel for K_L^0 detected in the IFR. Vertexing cuts have not been applied. The red (blue) histogram is the fitted inclusive J/ψ (fake J/ψ) background contribution.

Parameter	Standard Monte Carlo (exclusive and inclusive)	Dedicated Monte Carlo (exclusive)
$\Delta\Gamma/\Gamma$	0.00	0.20
$\mid q/p \mid$	1.00	1.04
$\frac{\mathrm{Im}\lambda_{CP}}{\mid\lambda_{CP}\mid}$	0.70	0.70
Δm	0.472	0.472
$\frac{\mathrm{Re}\lambda_{CP}}{\mid\lambda_{CP}\mid}$ Rez	0.00	0.00
Imz	0.00	0.00

Table 6: Physics parameter values of the standard and dedicated Monte Carlo samples.

subsamples, one with exclusive charmonium decays and the other with inclusive decays. The dedicated sample has only exclusive charmonium decays. The statistics of reconstructed B mesons (before vertexing cuts and tagging) are given in table 7, for each mode and sample separately. It must be noted that the relative statistics among the samples as we have in the data was not kept here.

`ASCII` files input to the fits are taken from:

`/nfs/farm/babar/AWG2/sin2b/data_run2/BReco/ASCII/anal-12a/`

`/nfs/farm/babar/AWG2/sin2b/mc_run2/BReco/ASCII/anal-12a/`

`/nfs/farm/babar/AWG2/sin2b/data_run2/Charmonium/ASCII/anal-12a/`

`/farm/babar/AWG2/sin2b/mc_run2/Charmonium/ASCII/anal-12a/`

`/nfs/farm/babar/AWG2/sin2b/mc_run2/Charmonium/ASCII/alignment/`

`/nfs/farm/babar/AWG2/sin2b/mc_run2/BReco/ASCII/anal-12a-MCalign/`

Sample	Standard Monte Carlo	Dedicated Monte Carlo
B^0 cocktail	57080	85048
exclusive $B^0 \to J/\psi K_S^0$	41433	12858
exclusive $B^0 \to \psi(2S) K_S^0$	5186	5248
exclusive $B^0 \to \chi_{c1} K_S^0$	5357	5050
exclusive $B^0 \to J/\psi K_L^0$	20814	5431
inclusive $B^0 \to J/\psi K_S^0(\pi^+\pi^-)$	3190	
inclusive $B^0 \to J/\psi K_S^0(\pi^0\pi^0)$	763	
inclusive $B^0 \to \psi(2S) K_S^0$	326	
inclusive $B^0 \to \chi_{c1} K_S^0$	305	
inclusive $B^0 \to J/\psi K_L^0$	5452	

Table 7: Standard and dedicated Monte Carlo statistics (after reconstruction and before vertexing cuts and tagging). The values of the physics parameters for each generation were shown in table 6. For the $J/\psi K_L^0$ mode the statistics is given for the ΔE interval $[-20, 80]$ MeV.

at SLAC, and

`/net/fcbabar02/space/local2/sandrel/cptWinter02Productions/newMC/`

in Pisa.

4 Resolution function and vertexing cuts

The decay time difference Δt between the two decaying B mesons is calculated from the z positions of the reconstructed vertices, using the *average* τ_B *approximation* [24], which uses the measured $\Upsilon(4S)$ boost (determined on a run-by-run basis) as well as the polar angle of the reconstructed B, therefore accounting for the boost of the B mesons with respect to the $\Upsilon(4S)$. The standard *BABAR* algorithm, `BtaSelFit`, with default configuration (beam constraints) is used for the Δz reconstruction [24]. Only events satisfying that $|\Delta t| < 20$ ps and $\sigma_{\Delta t} < 1.4$ ps are accepted, the same as using in the hadronic mixing analysis [21]. The nominal fit (section 6) does not include in the normalization of the PDF the Δt cut. The fit including the limited Δt range will be done as well and used to estimate a systematic uncertainty due to this assumption. Fits in different Δt and $\sigma_{\Delta t}$ ranges will be performed as well as cross-check.

The Δt resolution is modelled using two different parameterizations [26].

The first approach, called thereafter *GG model*, asumes three Gaussians [21]. The *core* component tries to describe well measured vertices, meanwhile the *tail* part accounts for poorly measured decay times. Finally, there is a small fraction of *outliers* (a few per mille) where Δt is badly reconstructed, partly due to mistakes in the track reconstruction, partly to tracks from secondary decays (long living particles and hard scatters). As the reconstructed Δt error provides a good (approximate) representation of the resolution for the core (tail) Gaussian, it is used to weight the events on a event-by-event basis, rather than to use a global resolution, therefore increasing the sensitivity of the analysis to well measured events. As the error is still not a perfect representation of the resolution (especially for the tail component) we allow for two global scale factors. On the contrary, the event-by-event Δt error is not a good representation of the resolution for the outliers component, and in this case a global and fixed (8 ps) resolution is used instead. In addition to the increase of the sensitivity, the weighting of the events according to the reconstructed Δt error largely eliminates small differences in resolution between the different classes of events entering in the analysis. Very small residual effects due to

differences in the scale factors can then be considered as part of the systematic uncertainties. Figure 11 shows the distributions of the per-event error on Δt for the B_{flav} and $B_{CPK^0_S}$ data samples, for signal ($m_{ES} > 5.27$ GeV) and sideband ($5.2 < m_{ES} < 5.27$ GeV) region events. The curves correspond to the unbinned maximum likelihood fit to a Crystall Ball shape. The results of these fits are the basis to define the probability density function used to generate realistic Δt error distributions in toy Monte Carlo studies, but they do not enter in the definition of the likelihood function.

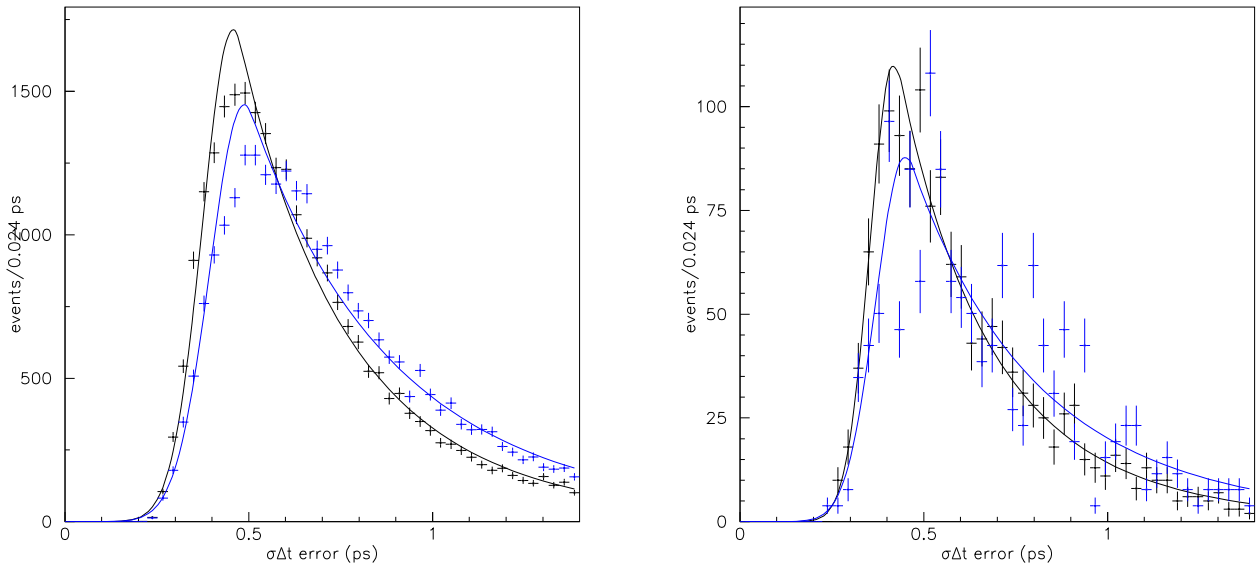

(a) (b)

Figure 11: Event-by-event error on Δt for the (a) B_{flav} and (b) $B_{CPK^0_S}$ data samples, for for signal ($m_{ES} > 5.27$ GeV, black) and sideband ($5.2 < m_{ES} < 5.27$ GeV, blue) region events. The sideband statistics has been normalized to the same number of signal events. The curves currespond to the fit to a Crystall Ball shape.

Although the vertex reconstruction algorithm minimizes biases due to the secondary charm decays and V^0's in the tagging side, the z_{TAG} position is on average biased towards positive z values, resulting in a negative shift in Δt. This effect is accounted in the resolution function by introducing a shift in the central value of the core and tail Gaussians. Due to the different B decay channels populating the different tagging categories, the average bias is category dependent. It was found that introducing a different bias in each tagging category for the core component but having a common tail bias provides the optimal trade-off between systematic effects and number of different parameters in the resolution [21].

The second parameterization, called *GExp*, uses one Gaussian with variable width and zero bias plus the same Gaussian convoluted with an exponential which effective lifetime is intended to describe the charm bias [26]. Similarly to the *GG* model, the reconstructed Δt error is used to weight the events, and different effective lifetimes and fractions of the exponential part are assumed for each tagging category, in order to take into account the different B decay channels populating each tagging category. The outlier component in this model is assumed the same as in the *GG* parameterization.

In summary, for an event with reconstructed $(\Delta t, \sigma_{\Delta t})$, the *GG* resolution function for tagging category α reads

$$\begin{aligned}\mathcal{R}(\Delta t-\Delta t',\sigma_{\Delta t};\vec{q}_\alpha) &= (1-f_{tail}-f_{outlier})h_G(\Delta t-\Delta t';\delta^\alpha_{core},S_{core}\sigma_{\Delta t})+\\ &\quad f_{tail}h_G(\Delta t-\Delta t';\delta_{tail},S_{tail}\sigma_{\Delta t})+\\ &\quad f_{outlier}h_G(\Delta t-\Delta t',;\delta_{outlier},\sigma_{outlier})\end{aligned} \tag{124}$$

where

$$h_G(t;\delta,\sigma) = \frac{1}{\sqrt{2\pi}\sigma}\exp(-(t-\delta)^2/(2\sigma^2)) \ . \tag{125}$$

The equivalent *GExp* resolution function for tagging category α reads

$$\begin{aligned}\mathcal{R}(\Delta t-\Delta t',\sigma_{\Delta t};\vec{q}_\alpha) &= (1-f^\alpha_{Exp}-f_{outlier})h_G(\Delta t-\Delta t';\delta=0,S\sigma_{\Delta t})+\\ &\quad f^\alpha_{Exp}\frac{1}{2\sigma_{\Delta t}\tau^\alpha_r}\left[\exp\left(\frac{S^2}{2(\tau^\alpha_r)^2}+\frac{\Delta t-\Delta t'}{\sigma_{\Delta t}\tau^\alpha_r}\right)erfc\left(\frac{S}{\sqrt{2}\tau^\alpha_r}+\frac{\Delta t-\Delta t'}{\sqrt{2}S\sigma_{\Delta t}}\right)\right]+\\ &\quad f_{outlier}h_G(\Delta t-\Delta t',;\delta_{outlier},\sigma_{outlier})\end{aligned} \tag{126}$$

The complete signal resolution function for all tagging categories is therefore represented by 11 parameters in the *GG* model,

$$\vec{q}=\left\{S_{core},\delta^{leptons}_{core},\delta^{kaons}_{core},\delta^{NT1}_{core},\delta^{NT2}_{core},f_{tail},\delta_{tail},S_{tail},f_{outlier},\delta_{outlier},\sigma_{outlier}\right\} \tag{127}$$

and 12 in the *GExp* parameterization,

$$\vec{q}=\left\{S,\tau^{leptons}_r,\tau^{kaons}_r,\tau^{NT1}_r,\tau^{NT2}_r,f^{leptons}_{Exp},f^{kaons}_{Exp},f^{NT1}_{Exp},f^{NT2}_{Exp},f_{outlier},\delta_{outlier},\sigma_{outlier}\right\} \ . \tag{128}$$

$\sigma_{outlier}$ and $\delta_{outlier}$ are fixed, respectively, to 8 and 0 ps.

In the *GG* model all offsets δ^α_{core} and δ_{tail} are modeled to be proportional to the reconstructed error $\sigma_{\Delta t}$, since it was found that events with high $\sigma_{\Delta t}$ tend to have high Δt residual [31]. Figure 12, extracted from [21], shows the dependence of the mean (and RMS) of the Monte Carlo Δt residual in bins of the reconstructed $\sigma_{\Delta t}$. It can be seen that the linear scaling is a good approximation for $\sigma_{\Delta t} < 1.4$ ps. Above this value the observed dependence diverges from the linear model, although the statistics there is small. The *GExp* model accounts implicitely for this observed correlation [31].

The reconstructed event-by-event Δt error ($\sigma_{\Delta t}$) is used to weight the events in the fitting procedure [11]. It is therefore important to make sure that there are no significant correlations among this variable and the variables parameterizing the tagging performance, w^α (average mistag) and Δw^α ($B^0\bar{B}^0$ mistag difference), and if there are, then model them properly. As shown in figure 13(top), there is an almost perfect linear correlation between the mean wrong tag fraction, w^α, and the Δt error, especially for the `Kaon` tagging category, being much weaker or negligible for the other categories. We then model the wrong tag fraction according to the following model:

$$w^\alpha = w^\alpha_0 + w^\alpha_{slope}\sigma_{\Delta t} \ . \tag{129}$$

As it can be seen in figure 13(top), for kaons this linear model applies better for $\sigma_{\Delta t} < 1.4$ ps. Detailed studies to explain the mechanism of this observed correlation can be found in [30]. The difference of the mistag fractions for B^0 and $\bar{B}^0$, Δw^α, is well constant over the full $\sigma_{\Delta t}$ range, for all tagging categories, as shown in figure 13(bottom).

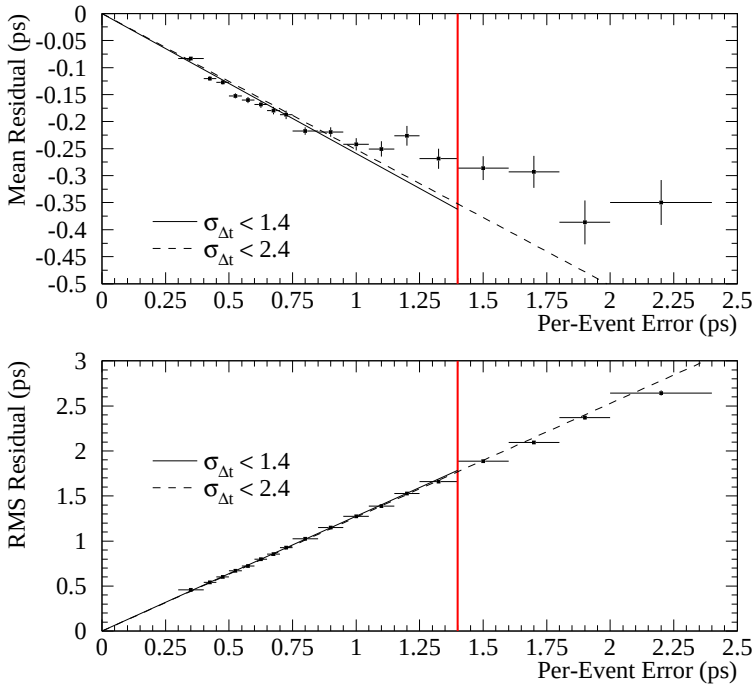

Figure 12: Mean and width of the MC Δt residual in bins of the per-event error $\sigma_{\Delta t}$. Fits are shown to a line constrained to pass through the origin for $\sigma_{\Delta t} < 1.4$ and $\sigma_{\Delta t} < 2.4$ ps.

5 Blinding

Tables 8 summarizes the blinding strings, as well as the central values and RMS of the blinding for each parameter and fit configuration. Δm and τ_B (when τ_B is free) were unblided between version 2.0 and version 3.0 of this note. Common blinding strings for Analysis 1 and Analysis 2, as well as for B_{CP}, $B_{CPK_S^0}$ only and $B_{CPK_L^0}$ only fits, are used. The time distributions and asymmetries are hidden.

Parameter	Central value	RMS	Blinding String
$\Delta\Gamma/\Gamma$	0.00	0.50	Here we blind the width difference
$\mid q/p \mid$	1.00	0.04	Here we blind absqoverp
$\frac{\mathrm{Im}\lambda_{CP}}{\mid\lambda_{CP}\mid}$	0.60	0.20	Here we blind imagLambda
$\frac{\mathrm{Re}\lambda_{CP}}{\mid\lambda_{CP}\mid}$Rez	0.00	0.50	Here we blind realZ
Imz	0.00	0.50	Here we blind imagZ

Table 8: Central values, RMS and strings of the blinding strategy.

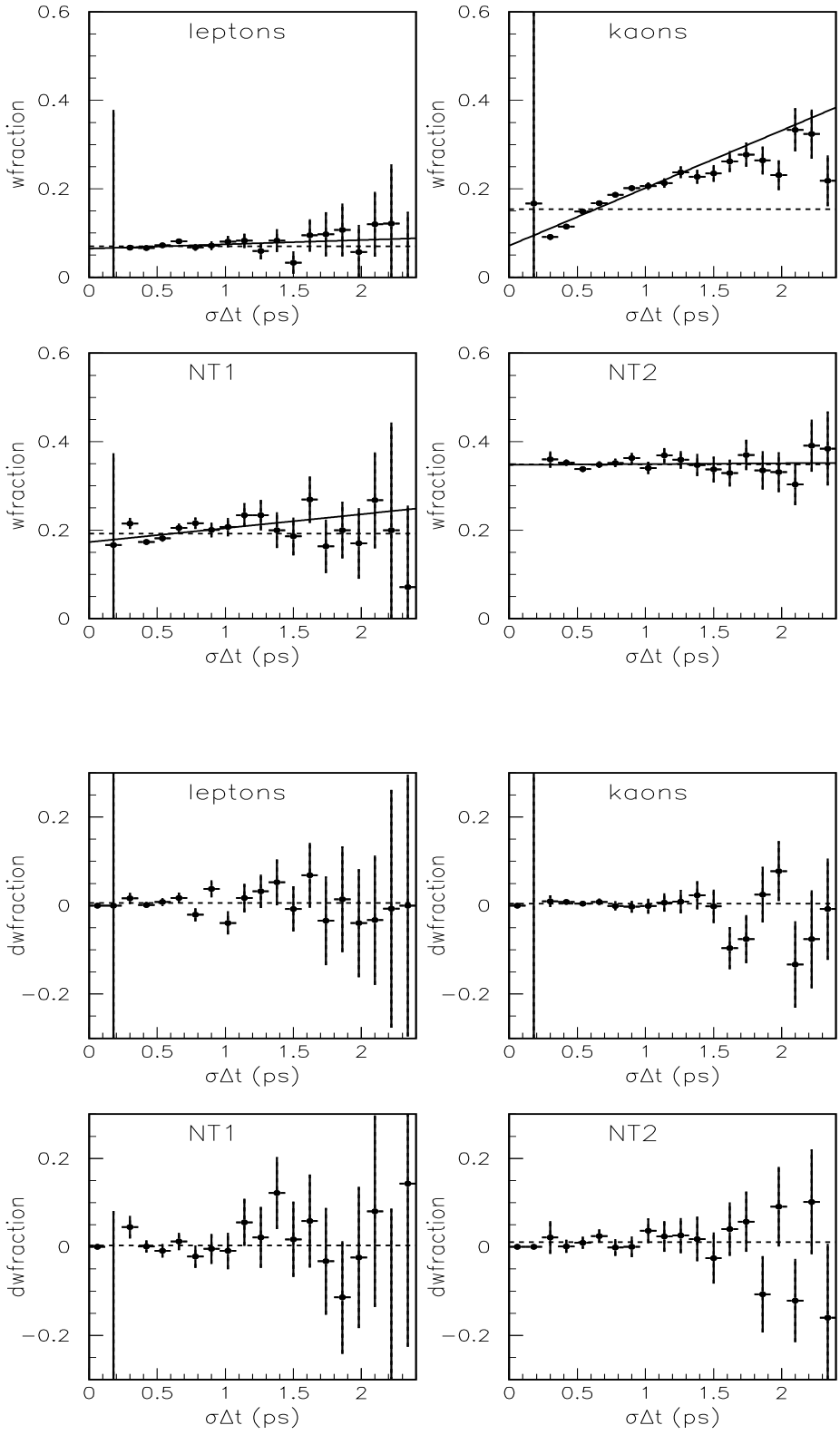

Figure 13: (Top) Mistag fraction from Monte Carlo in bins of per-event error $\sigma_{\Delta t}$, for each tagging category. (Bottom) $B^0\overline{B}^0$ mistag fraction differences from Monte Carlo in bins of per-event error $\sigma_{\Delta t}$, for each tagging category. The straight lines are the result of a simple binned fit to the points (with slope and origin free).

6 Description of the nominal fit

The complete log-likelihood function used in this analysis was described in detail in section 2. The assumptions made in the nominal fit are the following:

- Two configurations (Analyses):

  Analysis 1: fit for $\Delta\Gamma/\Gamma \times sign(\frac{\mathrm{Re}\lambda_{CP}}{|\lambda_{CP}|})$, Δm, $\mid q/p \mid$ and $\frac{\mathrm{Im}\lambda_{CP}}{|\lambda_{CP}|}$ (4 parameters); Thus this analysis assumes CPT conservation.

  Analysis 2: fit for $\Delta\Gamma/\Gamma \times sign(\frac{\mathrm{Re}\lambda_{CP}}{|\lambda_{CP}|})$, Δm, $\mid q/p \mid$, $\frac{\mathrm{Im}\lambda_{CP}}{|\lambda_{CP}|}$, $\mathrm{Rez}\frac{\mathrm{Re}\lambda_{CP}}{|\lambda_{CP}|}$ and Imz (6 parameters).

  τ will be kept as fixed parameter. Although all the parameters (except τ) are left free in the nominal fit (as required in order to have a theoretically consistent scenario), only measurements of $\Delta\Gamma/\Gamma \times sign(\frac{\mathrm{Re}\lambda_{CP}}{|\lambda_{CP}|})$, $\mathrm{Rez}\frac{\mathrm{Re}\lambda_{CP}}{|\lambda_{CP}|}$, Imz and $\mid q/p \mid$ will be provided. Δm and $\frac{\mathrm{Im}\lambda_{CP}}{|\lambda_{CP}|}$ will be used as cross-checks. Fits with τ free will also be performed as cross-check. $\frac{\mathrm{Re}\lambda_{CP}}{|\lambda_{CP}|}$ is extracted as $\frac{\mathrm{Re}\lambda_{CP}}{|\lambda_{CP}|} = +\sqrt{1-\left(\frac{\mathrm{Im}\lambda_{CP}}{|\lambda_{CP}|}\right)^2}$, so it is constrained to be within the physical region, i.e. $1-\left(\frac{\mathrm{Im}\lambda_{CP}}{|\lambda_{CP}|}\right)^2 \geq 0$;

- assume that the mechanisms contributing to the decay of CP eigenstates have the same weak phase for $\eta_{f_{CP}} = -1$ and $\eta_{f_{CP}} = +1$ modes;

- assume a single effective channel in the tagging and flavor eigenstate B sides and fit for the imaginary parts of the corresponding doubly-CKM-suppressed phases: $\frac{\mathrm{Im}\lambda_{tag}}{|\lambda_{tag}|}$, $\frac{\mathrm{Im}\bar{\lambda}_{tag}}{|\lambda_{tag}|}$, $\frac{\mathrm{Im}\lambda_{flav}}{|\lambda_{flav}|}$, $\frac{\mathrm{Im}\bar{\lambda}_{flav}}{|\lambda_{flav}|}$ (4 parameters). The real parts are all fixed to zero. The ratios of the decay amplitudes of DCKM to favored processes, r_{tag} and r_{flav} are also fixed to the value discussed in section 7.1.4. The corresponding ratios for $\bar{B}^0$, $\bar{r}_{tag}$ and $\bar{r}_{flav}$, are assumed to be the same as for B^0;

- a total of 9(11) parameters are used to describe the signal resolution function with the GG($GExp$) model:

  GG**:** scale factors of the core and tails components, S_{core} and S_{tail}; tagging category dependent core bias, δ^{α}_{core}; common tail bias, δ_{tail}; fraction of tail and outlier Gaussians, f_{tail} and $f_{outlier}$; the width and bias of the outlier Gaussian were fixed to 8 ps and 0 respectively. This is the model used for the central value;

  $GExp$**:** scale factor of the Gaussian, S, tagging category dependent effective lifetime (τ^{α}_{r}) and exponential component fraction (f^{α}_{Exp}); the width and bias of the outlier Gaussian were fixed to 8 ps and 0 respectively. This model is used as cross-check and to estimate a systematic uncertainty due to the resolution model parameterization;

- a total of 12 parameters are used to describe the signal mistags: for each tagging category, the average mistag fraction (origin, w^{α}_{0}, and slope w^{α}_{slope}) and the $B^0\bar{B}^0$ differences, Δw^{α};

- 3 background components are assumed for the B_{flav} sample (16 parameters):

  – a prompt (zero lifetime) and non-prompt (non-vanishing and free lifetime -1 parameter-) components, with their own effective wrong tag fraction (w^{α}_{slope} and Δw^{α} fixed to zero) (8 parameters) and a common resolution function, described as a common single Gaussian distribution with a scale factor S_{backg} and a bias δ_{backg} (GG model) or a common single unbiassed Gaussian with a scale factor S_{backg} plus the same Gaussian convoluted with an exponential function with effective lifetime

$\tau_{r,backg}$ (*GExp* model), and an outlier fraction $f_{backg,outlier}$ (3 parameters); the width of the outlier component is taken to be fixed at 8 ps with zero bias; the relative $f^{\alpha}_{prompt,B_{flav}}$ fraction of prompt background for each tagging category are also considered as free parameters (4 parameters);

  - a peaking contribution, which resolution function is the same as that of the signal, with B^+ fixed lifetime to the PDG2000 value (1.653 ± 0.028) [22]; the peaking background fraction is fixed;
  - no oscillatory/CPT/CP/T structure is assumed for the non-prompt combinatorial background component. Checks will be performed to evaluate possible systematic uncertainties;

- 3 background components are assumed for the $B_{CPK^0_S}$ sample (2 parameters):

  - prompt, non-prompt and peaking background, where the peaking background fraction is also fixed, and a common (averaged over tagging categories) prompt fraction is assumed (1 parameter). The wrong tag fraction parameters, lifetime and resolution function of the peaking background component is assumed to be the same as those of the signal. The lifetime of the non-prompt background is left free (1 parameter) and assumed the same for all tagging categories. No CPT/T/CP/oscillation structure in the background is assumed. Finally, the resolution function parameters of the prompt and non-prompt components are assumed the same as those of the prompt and non-prompt background components of the B_{flav} sample;

- the background treatment in the $B_{CPK^0_L}$ sample is performed as outlined in section 2 and described in detail in [18], with only one difference. While in [18] the resolution function parameters of the non-J/ψ background are extracted from an external fit to the J/ψ dilepton mass sideband, here we assume them to be same as for the prompt and non-prompt background components of the B_{flav} sample, similarly as it is done for the $B_{CPK^0_S}$ sample. Only the fraction of prompt component and the lifetime of the non-prompt one are fixed to the values extracted from the external fit. As in [18], due to different background composition, the $B_{CPK^0_L}$ sample is splitted according to the K^0_L type (IFR and EMC) and J/ψ channel (e^-e^- and $\mu^+\mu^-$). See section 7.1.5 for more details;

- the signal $B^0\bar{B}^0$ differences in reconstruction and tagging efficiencies, ν and μ^{α}, are extracted simultaneously together with the other parameters using the extended likelihood described in section 2. The method uses signal B_{flav} events as extracted from standard m_{ES} fits. This method translates any systematics due to detector charge asymmetries into an additional contribution to the statistical error. For the prompt and non-prompt background components (for all samples, B_{flav}, $B_{CPK^0_S}$ and $B_{CPK^0_L}$), the values assumed for ν and μ^{α} are those extracted from the B_{flav} sideband sample, $5.2 < m_{ES} < 5.27$ GeV/c^2. As for these background components we assume Δm=0, $\Delta\Gamma/\Gamma$=0, $\mid q/p \mid$=1 and $z = 0$, the extended likelihood method turns out to be equivalent to fix ν and μ^{α} to the values extracted previously to the fit;

- assume direct CP conservation, for both B_{flav} and B_{CP} samples;

- the parameters of the signal probablity obtained from the m_{ES} fits are taken as fixed (B_{flav} and $B_{CPK^0_S}$ samples).

The total number of parameters is therefore:

Analysis 1: 57 with *GG* model, 59 with *GExp*;

Analysis 2: 59 with *GG* model, 61 with *GExp*.

In both cases, 10 parameters are those from the B counting entering in the extended likelihood term (those used to extract the detector asymmetries).

Results in the $\{\varepsilon, \delta\}$ formalism will be also provided to first order in Reε and δ, using the relations given in section 2.3.

7 Results

7.1 Fit inputs

7.1.1 Mistag fractions for charged B's

The mistag of charged B mesons are extracted from a maximum likelihood fit to the B^+ sample alone. The decay modes, $\sigma(m_{ES})$, yield and purity are shown in table 9. The lifetime of B^+ mesons is left free. All the other oscillation/CPT/T/CP and DCKM parameters were assumed to be zero (except $\mid q/p \mid$=1). The fitting strategy is similar as same as for the B_{flav} sample (excluding the $B_{CPK^0_S}$ and $B_{CPK^0_L}$ samples). The peaking background component due to B^0 decays is assumed to be $(2.0 \pm 1.5)\%$ [26]. The mistags for the peaking background are assumed the same as for the signal (no corrections are assumed here due to the known differences of mistags for neutral and charged B mesons since would propagate to our measurements at second or third order, as will be shown in section 9.8). The charge asymmetries for signal and prompt and non-prompt background components are fixed to the values extracted previously to the fit (tables 10,11), using signal and sideband events.

Mode	σ m_{ES} (MeV)	m_{ES} Yield	Purity (%)
$\overline{\mathrm{D}}^{*0}\pi^+$	2.94 ± 0.06	5451 ± 103	88
$\overline{\mathrm{D}}^{0}\pi^+$	2.54 ± 0.03	14013 ± 173	83

Table 9: Event yields, signal resolutions, and signal purities for the B^+ decay modes, from 56 fb^{-1} of data (Winter'02 data sample), before vertexing cuts. The errors on these quantities are the statistical errors from the distribution. The m_{ES} results, yields and purities were determined from a fit to a Gaussian plus Argus background in a 3σ ΔE window (the purity was estimated for the region $m_{ES} > 5.27$ GeV/c^2).

Sample	ν^α
B^+ signal	0.013 ± 0.011
B^+ sideband	0.010 ± 0.012

Table 10: Measured ν^α values ($B^0\bar{B}^0$ difference in reconstruction efficiency) from the B^+ data sample. UPDATED.

Sample	Lepton	Kaon	NT1	NT2
B^+ signal	-0.017 ± 0.028	0.015 ± 0.013	0.037 ± 0.038	0.018 ± 0.028
B^+ sideband	0.081 ± 0.091	-0.008 ± 0.016	0.023 ± 0.051	0.019 ± 0.027

Table 11: Measured μ^α values ($B^0\bar{B}^0$ difference in tagging efficiency) from the B^+ data sample. UPDATED.

The results of the fit with the *GG* and *GExp* resolution models are shown in tables 12 and 13, respectively. The lifetime is unblinded. Figure 14 shows the normalized residuals (defined as the difference between the data and the fit projection onto the Δt axis divided by the error), separately for each tagging category and for B^- and B^+ events.

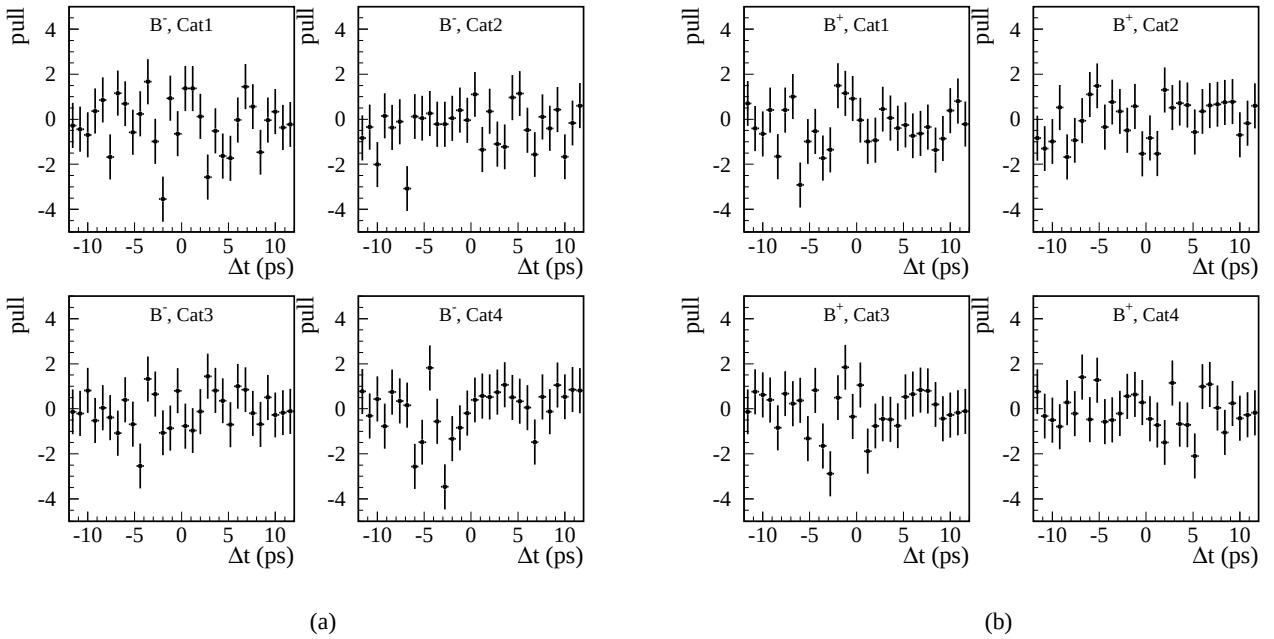

Figure 14: Normalized residuals of the Δt projections of the nominal fit to the charged B data for (a) B^- and (b) B^+ events, for the different tagging categories (*GG* model).

7.1.2 m_{ES} fit results

An event-by-event signal probability, $p^{\alpha}_{sig}(m_{ES})$, for the B_{flav} and $B_{CPK^0_S}$ samples is estimated from unbinned maximum likelihood fits to the m_{ES} spectra, assuming a Gaussian plus an Argus background shape, in a 3σ ΔE window. The m_{ES} fits are performed separately for each tagging category, for both, the B_{flav} and $B_{CPK^0_S}$ samples. The results of these fits are shown in figures 15 and 16, for the B_{flav} and $B_{CPK^0_S}$ samples, respectively. The parameters describing the signal probability obtained from these fits are fixed in the final likelihood fit.

7.1.3 Peaking background for B_{flav} and $B_{CPK^0_S}$ samples

The amount of charged B background that peaks in the m_{ES} B_{flav} distribution was estimated by using generic Monte Carlo. In addition, a cocktail Monte Carlo sample of charged B's containing the main sources of the background in the generic Monte Carlo was also generated and used [21]. The signal events from all reconstructed modes are removed from the Monte Carlo and a fit is performed to the remaining distribution including a Gaussian term plus an Argus background. The f^{α}_{peak} fraction was finally estimated to be $(1.5 \pm 0.6)\%$ [21]. In the case of the $B_{CPK^0_S}$ sample, the inclusive J/ψ Monte Carlo was used [8], and the amount

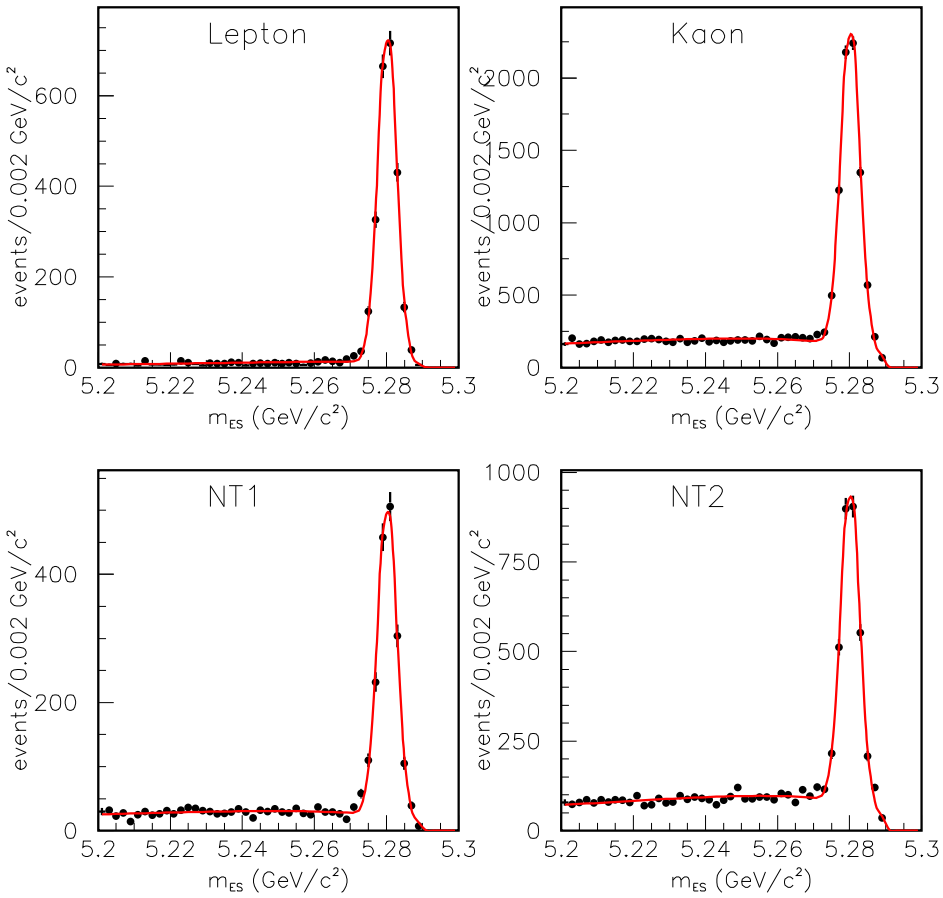

Figure 15: m_{ES} fits to each tagging category for the B_{flav} sample, after vertex cuts.

of peaking background was estimated similarly, but now for each channel separately. Only tagged events are considered. The averaged f^{α}_{peak} value was found $(1.5 \pm 1.0)\%$ [8].

7.1.4 Doubly-CKM-Suppressed decays

The expected relative amplitude of DCKM to favored decays, r_k and $\bar{r}_k$ ($k = tag, flav$), was fixed to 0.02, as our best estimate assuming that the amplitudes are dominated by the Standard Model $b \to c$ and $b \to u$ transitions, $| V^*_{ub} V_{cd} | | V^*_{cb} V_{ud} |$, for the favored and suppressed decays, respectively (figure 1), using the CKM matrix elements values from [23]. We assumed the same value for tagging and reconstructed B sides. In the case of the `Lepton` tagging category, largely dominated by semileptonic decays (more than 95%) the value of of r_{tag} and $\bar{r}_{tag}$ were assumed to be 0 instead.

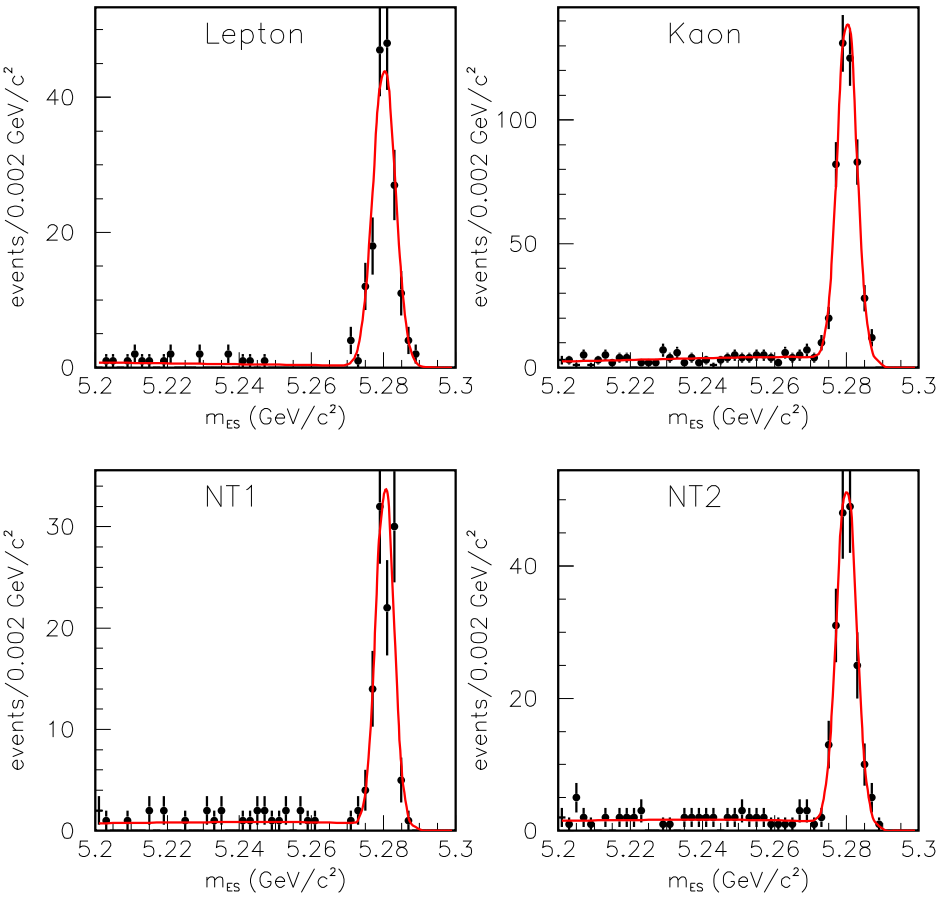

Figure 16: m_{ES} fits to each tagging category for the $B_{CPK_S^0}$ sample, after vertex cuts.

7.1.5 $B^0 \to J/\psi K_L^0$ background parameters

Fit inputs to the $B_{CPK_L^0}$ sample are basically the same as those in [18]. More than 90% of the events that pass the K_L^0 selection cuts contain a real J/ψ [18]. Table 14 lists the signal and total inclusive J/ψ fractions, broken down by the top seven decay modes of the J/ψ, and the K_L^0 reconstruction type, for events that pass the selection cuts, in a window $|\Delta E| < 10$ MeV. The effective η_{CP} is also shown.

Events from the J/ψ dilepton invariant mass sideband are used to determine the properties of the non-J/ψ background. From a comparison of the flavor tagging efficiency in the data sideband with those of the B_{flav} data it is found that the lepton category tagging efficiency in the data sideband does not agree very well with those of the B_{flav} data (and inclusive J/ψ Monte Carlo). This is consequence of the loosening of the PID requirement on the muons in the $J/\psi \to \mu\mu$ selection [18]. A a result of this difference, the sample composition has been splitted by flavor tag, allowing for the lepton-tagged events to be treated separately from other tagged events. The fractions for the three non-lepton tag categories are therefore the same.

A binned likelihood fit to the ΔE spectrum in the data is used to determine the relative amounts of signal,

inclusive J/ψ background and non-J/ψ background. In these fits, the signal and inclusive-J/ψ distributions are obtained from inclusive J/ψ Monte Carlo, while the non-J/ψ distribution is obtained from the J/ψ dilepton mass sideband. The fit is performed separately for each K_L^0 reconstruction type (EMC and IFR), due to differences in purity and background composition. Due to the lowered PID requirements in the $J/\psi \to \mu\mu$ selection, the sample is further splitted into lepton type. The $J/\psi \to ee$ and $J/\psi \to \mu\mu$ fits are performed simultaneously by constraining the ratio of $J/\psi K_L^0$ events to inclusive J/ψ events in $J/\psi \to ee$ and $J/\psi \to \mu\mu$ to be within the precision of the Monte Carlo. The different inclusive J/ψ backgrounds from Monte Carlo are then renormalized to the J/ψ background fraction extracted from the data. The fractions are adjusted for lepton-tagged and non-lepton tagged events in order to adecuate for the observed differences in flavor tagging efficiencies in the J/ψ sideband events relative to the B_{flav} and inclusive J/ψ Monte Carlo (see [18] for details). The sample omposition fractions finally obtained with the procedure in the data are given in table 15.

The variable ΔE is used on an event-by-event basis to discriminate between signal and background. As the J/ψ lepton type is not expected to influence the ΔE shape, the PDFs were used without regard to lepton type. The ΔE PDFs where used separately for EMC and IFR K_L^0 type, and they were grouped for $J/\psi K_L^0$ (signal), $J/\psi K_S^0$ background, $J/\psi\ X$ background (excluding $J/\psi K_S^0$) and non-J/ψ. The ΔE PDF's are taken from the fits contained in the hbook file:

`/nfs/farm/babar/AWG/sin2b/data_run2_winter02/Charmonium/klong-input/de-pdfs-winter-2002-v1.hbook.`

According to the studies reported in [18], the different decay modes contributing to the $J/\psi K_L^0$ mode are statistically consistent with having the same mistag fractions as in the B_{flav} sample. In this analysis, the resolution function of the signal and inclusive-J/ψ background was assumed to be same as for the B_{flav} sample. The resolution function for the non-J/ψ component (combinatoric in nature) was assumed the same as the prompt and non-prompt background components of the B_{flav} and $B_{CPK_S^0}$ samples. As the relative fraction of prompt to non-prompt component and the effective lifetime of the non-prompt in the non-J/ψ background are not necessarily the same as in the B_{flav} and $B_{CPK_S^0}$ samples, an external fit to the J/ψ dileptopn mass sideband was performed, and then were fixed in the nominal fit. The external fit used a *GG* resolution model, and the mistag fraction was assume to be 0.5, and the scale of the tail Guassian, S_{tail}, was fixed to 3.0. The results are reported in table 16. The fixed prompt fraction and effective lifetime were finally, respectively, 0.59 ± 0.12 and 1.7 ± 0.3.

7.1.6 Direct CP violation

The nominal fit includes in the PDF (via the parameters ν^α and μ^α) any possible violation of CP in the decay of tagging and flavor states. In the case of CP eigenstates we assume CP conservation in the decay ($r_{CP,CP}$=1). A systematic error will be assigned due to this source by varying $r_{CP,CP}$ by $\pm 10\%$.

Parameter	B^+ fit results (*GG* model)
τ	1.632 ± 0.033
S_{core}	1.246 ± 0.075
δ_{core}^{lepton}	-0.252 ± 0.086
δ_{core}^{kaon}	-0.261 ± 0.047
δ_{core}^{NT1}	-0.25 ± 0.11
δ_{core}^{NT2}	-0.253 ± 0.078
f_{tail}	$(0.8 \pm 1.8) \cdot 10^{-2}$
S_{tail}	7.0 ± 4.4
δ_{tail}	-0.4 ± 4.1
$f_{outlier}$	$(0.2 \pm 1.6) \cdot 10^{-3}$
w_0^{lepton}	$(4.8 \pm 1.4) \cdot 10^{-2}$
w_0^{kaon}	$(3.9 \pm 1.3) \cdot 10^{-2}$
w_0^{NT1}	$(9.4 \pm 3.1) \cdot 10^{-2}$
w_0^{NT2}	0.318 ± 0.030
w_{slope}^{lepton}	$(-1.1 \pm 2.5) \cdot 10^{-2}$
w_{slope}^{kaon}	0.139 ± 0.022
w_{slope}^{NT1}	0.170 ± 0.057
w_{slope}^{NT2}	$(5.0 \pm 4.7) \cdot 10^{-2}$
Δw^{lepton}	$(5.8 \pm 9.3) \cdot 10^{-3}$
Δw^{kaon}	$(1.2 \pm 8.4) \cdot 10^{-3}$
Δw^{NT1}	$(2.7 \pm 2.3) \cdot 10^{-2}$
Δw^{NT2}	$(-1.8 \pm 2.1) \cdot 10^{-2}$

Parameter	B^+ fit results (*GG* model)
$f_{prompt,B_{flav}}^{lepton}$	0.241 ± 0.081
$f_{prompt,B_{flav}}^{kaon}$	0.680 ± 0.024
$f_{prompt,B_{flav}}^{NT1}$	0.725 ± 0.036
$f_{prompt,B_{flav}}^{NT2}$	0.753 ± 0.026
S_{back}	1.400 ± 0.024
δ_{back}	$(-4.0 \pm 1.9) \cdot 10^{-2}$
$f_{back,outlier}$	$(1.09 \pm 0.23) \cdot 10^{-2}$
$w_{0,prompt}^{lepton}$	0.26 ± 0.12
$w_{0,prompt}^{kaon}$	0.1636 ± 0.0097
$w_{0,prompt}^{NT1}$	0.281 ± 0.028
$w_{0,prompt}^{NT2}$	0.399 ± 0.016
$w_{0,non-prompt}^{lepton}$	0.128 ± 0.038
$w_{0,non-prompt}^{kaon}$	0.231 ± 0.019
$w_{0,non-prompt}^{NT1}$	0.430 ± 0.062
$w_{0,non-prompt}^{NT2}$	0.392 ± 0.042
$\tau_{non-prompt}$	1.361 ± 0.068

Table 12: Fit results for B^+ data (*GG* resolution model). The lifetime is unblinded.

Parameter	B^+ fit results (*GExp* model)
τ	1.634 ± 0.021
S	1.167 ± 0.084
τ_r^{lepton}	0.248 ± 0.084
τ_r^{kaon}	0.67 ± 0.36
τ_r^{NT1}	0.70 ± 0.55
τ_r^{NT2}	$5.0000^* \pm 0.0073$
f_{Exp}^{lepton}	$1.00000^* \pm 0.00094$
f_{Exp}^{kaon}	0.41 ± 0.22
f_{Exp}^{NT1}	0.37 ± 0.30
f_{Exp}^{NT2}	$(4.6 \pm 1.5) \cdot 10^{-2}$
$f_{outlier}$	$(0.0^* \pm 5.2) \cdot 10^{-5}$
w_0^{lepton}	$(4.8 \pm 1.4) \cdot 10^{-2}$
w_0^{kaon}	$(3.9 \pm 1.3) \cdot 10^{-2}$
w_0^{NT1}	$(9.4 \pm 3.1) \cdot 10^{-2}$
w_0^{NT2}	0.318 ± 0.029
w_{slope}^{lepton}	$(-1.1 \pm 2.5) \cdot 10^{-2}$
w_{slope}^{kaon}	0.139 ± 0.022
w_{slope}^{NT1}	0.171 ± 0.055
w_{slope}^{NT2}	$(5.0 \pm 4.6) \cdot 10^{-2}$
Δw^{lepton}	$(5.8 \pm 9.3) \cdot 10^{-3}$
Δw^{kaon}	$(1.3 \pm 8.4) \cdot 10^{-3}$
Δw^{NT1}	$(2.7 \pm 2.3) \cdot 10^{-2}$
Δw^{NT2}	$(-1.8 \pm 2.1) \cdot 10^{-2}$

Parameter	B^+ fit results (*GExp* model)
$f_{prompt,B_{flav}}^{lepton}$	0.245 ± 0.079
$f_{prompt,B_{flav}}^{kaon}$	0.680 ± 0.024
$f_{prompt,B_{flav}}^{NT1}$	0.726 ± 0.036
$f_{prompt,B_{flav}}^{NT2}$	0.753 ± 0.026
S_{back}	1.400 ± 0.024
$\tau_{r,back}$	-1.4 ± 4.8
$f_{back,outlier}$	$(1.06 \pm 0.23) \cdot 10^{-2}$
$w_{0,prompt}^{lepton}$	0.26 ± 0.11
$w_{0,prompt}^{kaon}$	0.1635 ± 0.0097
$w_{0,prompt}^{NT1}$	0.281 ± 0.027
$w_{0,prompt}^{NT2}$	0.399 ± 0.016
$w_{0,non-prompt}^{lepton}$	0.128 ± 0.038
$w_{0,non-prompt}^{kaon}$	0.231 ± 0.019
$w_{0,non-prompt}^{NT1}$	0.430 ± 0.062
$w_{0,non-prompt}^{NT2}$	0.392 ± 0.041
$\tau_{non-prompt}$	1.365 ± 0.068

Table 13: Fit results for B^+ data (*GExp* resolution model). * at limit. The lifetime is unblinded.

K_L type	EMC	IFR	η_{CP}
$J/\psi K_L$	0.622	0.732	+1
$J/\psi K^{*0}$	0.077	0.064	-0.68
$J/\psi K^{*+}$	0.109	0.114	0
$J/\psi K_s$	0.031	0.009	-1
$J/\psi K_L \pi^0$	0.004	0.002	0
$J/\psi K_L \pi^+$	0.004	0.007	0
$\chi_c K_L$	0.011	0.015	+1
$J/\psi X$ other	0.142	0.150	0
$non-J/\psi$	0	0	0.21

Table 14: Sample composition fractions for $J/\psi K_L$ inclusive charmonium Monte Carlo.

K_L type	EMC				IFR			
Tag type	Lepton		non-Lepton		Lepton		non-Lepton	
J/ψ mode	ee	$\mu\mu$	ee	$\mu\mu$	ee	$\mu\mu$	ee	$\mu\mu$
$J/\psi K_L$	0.5701	0.5294	0.5367	0.4747	0.6988	0.6679	0.6788	0.6336
$J/\psi K^{*0}$	0.0824	0.0847	0.0776	0.0760	0.0661	0.0701	0.0642	0.0665
$J/\psi K^{*+}$	0.1141	0.1174	0.1075	0.1052	0.1216	0.1290	0.1182	0.1224
$J/\psi K_s$	0.0335	0.0345	0.0315	0.0309	0.0085	0.0090	0.0083	0.0086
$J/\psi K_L\pi^0$	0.0035	0.0036	0.0033	0.0032	0.0025	0.0027	0.0024	0.0025
$J/\psi K_L\pi^+$	0.0031	0.0032	0.0030	0.0029	0.0080	0.0085	0.0078	0.0081
$\chi_c K_L$	0.0122	0.0126	0.0115	0.0113	0.0165	0.0175	0.0160	0.0166
$J/\psi X$ other	0.1466	0.1507	0.1380	0.1352	0.0616	0.0653	0.0598	0.0619
non-J/ψ	0.0345	0.0640	0.0909	0.1607	0.0164	0.0301	0.0445	0.0799

Table 15: Sample composition fractions for $J/\psi K_L$ data.

Parameter	Fit result
S_{core}	1.45 ± 0.15
δ_{core}	0.04 ± 0.15
f_{tail}	0.03 ± 0.11
S_{tail}	3.0
δ_{tail}	-2 ± 6
$f_{outlier}$	0.0000 ± 0.0002
$f_{prompt,B_{CPK_L^0}}$	0.59 ± 0.12
$\tau_{non-prompt,B_{CPK_L^0}}$	1.7 ± 0.3

Table 16: Results from the external unbinned likelihood fit of the J/ψ dilepton mass sideband data, used to extract the fraction of prompt to non-prompt background and the effective lifetime for the non-J/ψ $J/\psi K_L^0$ background component.

7.2 Analysis 1 results

Tables 17 and 18 report the fitted parameters for Analysis 1, for the *GG* and *GExp* resolution models, respectively (combined fit, B_{flav}+$B_{CPK^0_S}$+$B_{CPK^0_L}$). Tables 19 and 20 give the correlations among the 4 physics parameters, again for *GG* and *GExp*.

Parameter	B^0 fit results (*GG* model)
Δm	0.5220 ± 0.0098
$\Delta\Gamma/\Gamma$	$(-0.8 \pm 4.9) \cdot 10^{-2}$
$\mid q/p \mid$	0.946 ± 0.018
$\frac{\mathrm{Im}\lambda_{CP}}{\lvert\lambda_{CP}\rvert}$	0.612 ± 0.085
S_{core}	1.240 ± 0.058
δ^{lepton}_{core}	$(0.6 \pm 8.2) \cdot 10^{-2}$
δ^{kaon}_{core}	-0.303 ± 0.058
δ^{NT1}_{core}	-0.216 ± 0.092
δ^{NT2}_{core}	-0.264 ± 0.075
f_{tail}	$(3.9 \pm 1.8) \cdot 10^{-2}$
S_{tail}	4.4 ± 1.6
δ_{tail}	-2.7 ± 1.3
$f_{outlier}$	$(1.5 \pm 2.0) \cdot 10^{-3}$
w^{lepton}_0	$(9.3 \pm 2.4) \cdot 10^{-2}$
w^{kaon}_0	$(7.1 \pm 2.0) \cdot 10^{-2}$
w^{NT1}_0	0.183 ± 0.043
w^{NT2}_0	0.362 ± 0.038
w^{lepton}_{slope}	$(-3.4 \pm 4.3) \cdot 10^{-2}$
w^{kaon}_{slope}	0.166 ± 0.033
w^{NT1}_{slope}	$(4.3 \pm 7.3) \cdot 10^{-2}$
w^{NT2}_{slope}	$(1.3 \pm 5.6) \cdot 10^{-2}$
Δw^{lepton}	$(2.2 \pm 1.6) \cdot 10^{-2}$
Δw^{kaon}	$(-1.2 \pm 1.2) \cdot 10^{-2}$
Δw^{NT1}	$(1.8 \pm 2.4) \cdot 10^{-2}$
Δw^{NT2}	$(-3.4 \pm 1.9) \cdot 10^{-2}$

Parameter	B^0 fit results (*GG* model)
$\frac{\mathrm{Im}\lambda_{flav}}{\lvert\lambda_{flav}\rvert}$	0.7 ± 1.2
$\frac{\mathrm{Im}\lambda_{flav}}{\lvert\lambda_{flav}\rvert}$	0.5 ± 1.2
$\frac{\mathrm{Im}\lambda_{tag}}{\lvert\lambda_{tag}\rvert}$	0.5 ± 1.3
$\frac{\mathrm{Im}\lambda_{tag}}{\lvert\lambda_{tag}\rvert}$	0.5 ± 1.3
$f^{lepton}_{prompt,B_{flav}}$	0.383 ± 0.067
$f^{kaon}_{prompt,B_{flav}}$	0.643 ± 0.024
$f^{NT1}_{prompt,B_{flav}}$	0.615 ± 0.038
$f^{NT2}_{prompt,B_{flav}}$	0.701 ± 0.025
S_{back}	1.389 ± 0.023
δ_{back}	$(-3.8 \pm 1.7) \cdot 10^{-2}$
$f_{back,outlier}$	$(1.18 \pm 0.21) \cdot 10^{-2}$
$w^{lepton}_{0,prompt}$	0.143 ± 0.080
$w^{kaon}_{0,prompt}$	0.250 ± 0.011
$w^{NT1}_{0,prompt}$	0.339 ± 0.030
$w^{NT2}_{0,prompt}$	0.449 ± 0.015
$w^{lepton}_{0,non-prompt}$	0.399 ± 0.055
$w^{kaon}_{0,non-prompt}$	0.387 ± 0.020
$w^{NT1}_{0,non-prompt}$	0.448 ± 0.045
$w^{NT2}_{0,non-prompt}$	0.460 ± 0.032
$\tau_{non-prompt}$	1.319 ± 0.056
$f_{prompt,B_{CPK^0_S}}$	0.632 ± 0.070
$\tau_{non-prompt,B_{CPK^0_S}}$	2.30 ± 0.45

Table 17: Analysis 1 results, *GG* resolution model.

7.3 Analysis 2 results

Similarly, tables 21 and 22 report the fitted parameters from Analysis 2, for the *GG* and *GExp* resolution models, respectively (combined fit, B_{flav}+$B_{CPK^0_S}$+$B_{CPK^0_L}$). Tables 23 and 24 give the correlations among the 6 physics parameters, again for *GG* and *GExp*.

The normalized residuals, defined as the difference between the data and the fit projection (nominal fit to all samples together) onto the Δt axis divided by the error, for the B_{flav}, $B_{CPK^0_S}$ and $B_{CPK^0_L}$ samples and the different tagging categories are shown in figures 17, 18 and 19. The time distributions themselves are hidden.

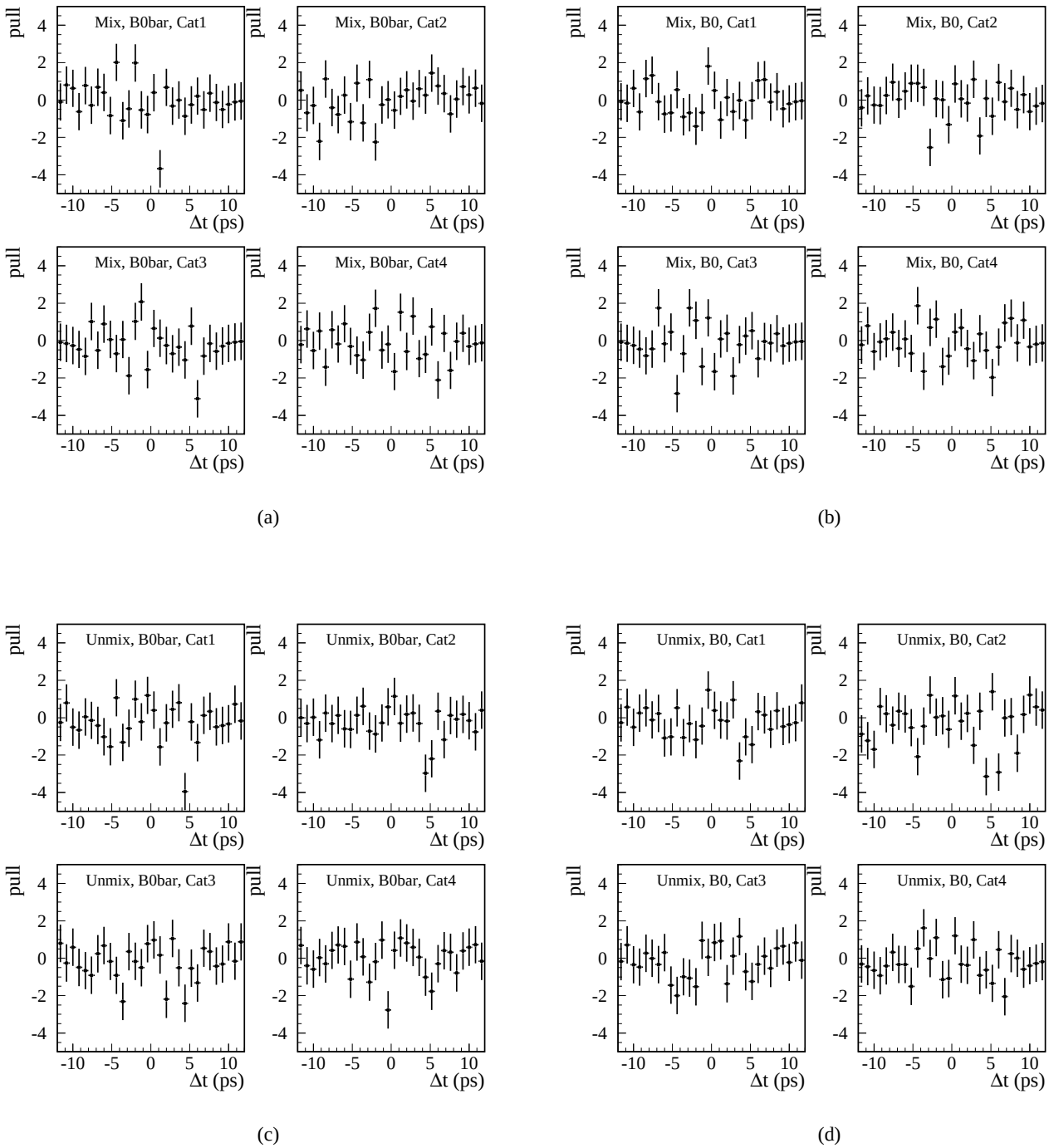

Figure 17: Normalized residuals of the Δt projections of the nominal fit (Analysis 2) for the B_{flav} sample: (a) mixed $\bar{B}^0$ tagged, (b) mixed B^0 tagged, (c) unmixed $\bar{B}^0$ tagged and (d) unmixed B^0 tagged (*GG* model), for each tagging category.

Parameter	B^0 fit results (*GExp* model)
Δm	0.5195 ± 0.0097
$\Delta\Gamma/\Gamma$	$(-0.3 \pm 5.3) \cdot 10^{-2}$
$\mid q/p \mid$	0.946 ± 0.018
$\frac{\mathrm{Im}\lambda_{CP}}{\mid\lambda_{CP}\mid}$	0.614 ± 0.085
S	1.138 ± 0.052
τ_r^{lepton}	3.6 ± 1.2
τ_r^{kaon}	1.30 ± 0.23
τ_r^{NT1}	3.9 ± 1.1
τ_r^{NT2}	1.68 ± 0.39
f_{Exp}^{lepton}	$(4.6 \pm 2.5) \cdot 10^{-2}$
f_{Exp}^{kaon}	0.291 ± 0.059
f_{Exp}^{NT1}	$(6.5 \pm 3.2) \cdot 10^{-2}$
f_{Exp}^{NT2}	0.219 ± 0.063
$f_{outlier}$	$(1.8 \pm 1.3) \cdot 10^{-3}$
w_0^{lepton}	$(9.2 \pm 2.4) \cdot 10^{-2}$
w_0^{kaon}	$(7.3 \pm 2.0) \cdot 10^{-2}$
w_0^{NT1}	0.182 ± 0.043
w_0^{NT2}	0.363 ± 0.037
w_{slope}^{lepton}	$(-2.8 \pm 4.3) \cdot 10^{-2}$
w_{slope}^{kaon}	0.165 ± 0.033
w_{slope}^{NT1}	$(4.0 \pm 7.2) \cdot 10^{-2}$
w_{slope}^{NT2}	$(1.1 \pm 5.6) \cdot 10^{-2}$
Δw^{lepton}	$(2.1 \pm 1.6) \cdot 10^{-2}$
Δw^{kaon}	$(-1.2 \pm 1.2) \cdot 10^{-2}$
Δw^{NT1}	$(1.8 \pm 2.4) \cdot 10^{-2}$
Δw^{NT2}	$(-3.4 \pm 1.9) \cdot 10^{-2}$

Parameter	B^0 fit results (*GExp* model)
$\frac{\mathrm{Im}\lambda_{flav}}{\mid\lambda_{flav}\mid}$	0.4 ± 1.2
$\frac{\mathrm{Im}\lambda_{flav}}{\mid\lambda_{flav}\mid}$	0.1 ± 1.2
$\frac{\mathrm{Im}\lambda_{tag}}{\mid\lambda_{tag}\mid}$	0.2 ± 1.3
$\frac{\mathrm{Im}\lambda_{tag}}{\mid\lambda_{tag}\mid}$	0.1 ± 1.3
$f_{prompt,B_{flav}}^{lepton}$	0.379 ± 0.071
$f_{prompt,B_{flav}}^{kaon}$	0.665 ± 0.026
$f_{prompt,B_{flav}}^{NT1}$	0.632 ± 0.040
$f_{prompt,B_{flav}}^{NT2}$	0.728 ± 0.026
S_{back}	1.377 ± 0.023
$\tau_{r,back}$	2.42 ± 0.41
$f_{back,outlier}$	$(9.9 \pm 2.0) \cdot 10^{-3}$
$w_{0,prompt}^{lepton}$	0.142 ± 0.084
$w_{0,prompt}^{kaon}$	0.250 ± 0.012
$w_{0,prompt}^{NT1}$	0.340 ± 0.030
$w_{0,prompt}^{NT2}$	0.450 ± 0.015
$w_{0,non-prompt}^{lepton}$	0.397 ± 0.056
$w_{0,non-prompt}^{kaon}$	0.397 ± 0.022
$w_{0,non-prompt}^{NT1}$	0.454 ± 0.049
$w_{0,non-prompt}^{NT2}$	0.460 ± 0.036
$\tau_{non-prompt}$	1.278 ± 0.060
$f_{prompt,B_{CPK_S^0}}$	0.657 ± 0.072
$\tau_{non-prompt,B_{CPK_S^0}}$	2.31 ± 0.49

Table 18: Analysis 1 results, *GExp* resolution model.

	$\Delta\Gamma/\Gamma$	$\mid q/p \mid$	$\frac{\mathrm{Im}\lambda_{CP}}{\mid\lambda_{CP}\mid}$
Δm	-2.3%	-1.1%	-5.7%
$\Delta\Gamma/\Gamma$		9.4%	-1.9%
$\mid q/p \mid$			-0.9%

Table 19: Correlations among the 4 physics parameters, Analysis 1, *GG* resolution model.

	$\Delta\Gamma/\Gamma$	$\mid q/p \mid$	$\frac{\mathrm{Im}\lambda_{CP}}{\mid\lambda_{CP}\mid}$
Δm	-2.1%	-1.5%	-6.1%
$\Delta\Gamma/\Gamma$		10.2%	-0.7%
$\mid q/p \mid$			-1.0%

Table 20: Correlations among the 4 physics parameters, Analysis 1, *GExp* resolution model.

7.4 Asymmetric (MINOS) errors

The statistical errors shown in all the previous tables are those obtained assuming that all the parameters are Gaussian. Deviations from an ideal Gaussian behaviour are expected from toy Monte Carlo studies. It is therefore important to provide the asymmetric error estimates (MINOS). They can be found in tables 26, for the two analyses. The only significantly asymmetric error was found for Rez$\frac{\mathrm{Re}\lambda_{CP}}{\mid\lambda_{CP}\mid}$.

Parameter	B^0 fit results (*GG* model)
Δm	0.523 ± 0.010
$\Delta\Gamma/\Gamma$	$(-2.1 \pm 4.8) \cdot 10^{-2}$
$\mid q/p \mid$	0.945 ± 0.018
$\frac{\mathrm{Im}\lambda_{CP}}{\mid\lambda_{CP}\mid}$	0.620 ± 0.083
$\frac{\mathrm{Re}\lambda_{CP}}{\mid\lambda_{CP}\mid}\mathrm{Re}z$	$(-6.4 \pm 4.6) \cdot 10^{-2}$
$\mathrm{Im}z$	-0.918 ± 0.034
S_{core}	1.241 ± 0.059
δ_{core}^{lepton}	$(0.4 \pm 8.4) \cdot 10^{-2}$
δ_{core}^{kaon}	-0.302 ± 0.060
δ_{core}^{NT1}	-0.215 ± 0.093
δ_{core}^{NT2}	-0.263 ± 0.077
f_{tail}	$(3.8 \pm 1.8) \cdot 10^{-2}$
S_{tail}	4.3 ± 1.7
δ_{tail}	-2.7 ± 1.4
$f_{outlier}$	$(1.5 \pm 2.0) \cdot 10^{-3}$
w_0^{lepton}	$(9.3 \pm 2.4) \cdot 10^{-2}$
w_0^{kaon}	$(7.1 \pm 2.0) \cdot 10^{-2}$
w_0^{NT1}	0.184 ± 0.043
w_0^{NT2}	0.362 ± 0.037
w_{slope}^{lepton}	$(-3.5 \pm 4.3) \cdot 10^{-2}$
w_{slope}^{kaon}	0.167 ± 0.033
w_{slope}^{NT1}	$(4.2 \pm 7.3) \cdot 10^{-2}$
w_{slope}^{NT2}	$(1.3 \pm 5.6) \cdot 10^{-2}$
Δw^{lepton}	$(2.1 \pm 1.6) \cdot 10^{-2}$
Δw^{kaon}	$(-1.3 \pm 1.2) \cdot 10^{-2}$
Δw^{NT1}	$(1.7 \pm 2.4) \cdot 10^{-2}$
Δw^{NT2}	$(-3.5 \pm 1.9) \cdot 10^{-2}$

Parameter	B^0 fit results (*GG* model)
$\frac{\mathrm{Im}\lambda_{flav}}{\mid\lambda_{flav}\mid}$	1.7 ± 1.4
$\frac{\mathrm{Im}\lambda_{flav}}{\mid\lambda_{flav}\mid}$	-0.7 ± 1.4
$\frac{\mathrm{Im}\lambda_{tag}}{\mid\lambda_{tag}\mid}$	1.7 ± 1.5
$\frac{\mathrm{Im}\lambda_{tag}}{\mid\lambda_{tag}\mid}$	-0.8 ± 1.6
$f_{prompt,B_{flav}}^{lepton}$	0.384 ± 0.067
$f_{prompt,B_{flav}}^{kaon}$	0.643 ± 0.024
$f_{prompt,B_{flav}}^{NT1}$	0.615 ± 0.038
$f_{prompt,B_{flav}}^{NT2}$	0.701 ± 0.025
S_{back}	1.389 ± 0.023
δ_{back}	$(-3.8 \pm 1.7) \cdot 10^{-2}$
$f_{back,outlier}$	$(1.18 \pm 0.21) \cdot 10^{-2}$
$w_{0,prompt}^{lepton}$	0.143 ± 0.080
$w_{0,prompt}^{kaon}$	0.250 ± 0.011
$w_{0,prompt}^{NT1}$	0.339 ± 0.030
$w_{0,prompt}^{NT2}$	0.449 ± 0.015
$w_{0,non-prompt}^{lepton}$	0.399 ± 0.055
$w_{0,non-prompt}^{kaon}$	0.388 ± 0.020
$w_{0,non-prompt}^{NT1}$	0.448 ± 0.045
$w_{0,non-prompt}^{NT2}$	0.461 ± 0.032
$\tau_{non-prompt}$	1.319 ± 0.057
$f_{prompt,B_{CPK_S^0}}$	0.632 ± 0.070
$\tau_{non-prompt,B_{CPK_S^0}}$	2.30 ± 0.45

Table 21: Analysis 2 results, *GG* resolution model.

Parameter	B^0 fit results (*GExp* model)
Δm	0.521 ± 0.010
$\Delta\Gamma/\Gamma$	$(-2.0 \pm 5.1) \cdot 10^{-2}$
$\mid q/p \mid$	0.944 ± 0.018
$\frac{\mathrm{Im}\lambda_{CP}}{\mid\lambda_{CP}\mid}$	0.622 ± 0.082
$\frac{\mathrm{Re}\lambda_{CP}}{\mid\lambda_{CP}\mid}\mathrm{Rez}$	$(-5.7 \pm 4.6) \cdot 10^{-2}$
Imz	-0.919 ± 0.034
S	1.138 ± 0.052
τ_r^{lepton}	3.6 ± 1.2
τ_r^{kaon}	1.29 ± 0.22
τ_r^{NT1}	3.9 ± 1.1
τ_r^{NT2}	1.68 ± 0.39
f_{Exp}^{lepton}	$(4.6 \pm 2.5) \cdot 10^{-2}$
f_{Exp}^{kaon}	0.293 ± 0.059
f_{Exp}^{NT1}	$(6.4 \pm 3.2) \cdot 10^{-2}$
f_{Exp}^{NT2}	0.219 ± 0.064
$f_{outlier}$	$(1.8 \pm 1.3) \cdot 10^{-3}$
w_0^{lepton}	$(9.2 \pm 2.4) \cdot 10^{-2}$
w_0^{kaon}	$(7.3 \pm 2.0) \cdot 10^{-2}$
w_0^{NT1}	0.183 ± 0.043
w_0^{NT2}	0.363 ± 0.037
w_{slope}^{lepton}	$(-2.9 \pm 4.3) \cdot 10^{-2}$
w_{slope}^{kaon}	0.166 ± 0.033
w_{slope}^{NT1}	$(3.9 \pm 7.2) \cdot 10^{-2}$
w_{slope}^{NT2}	$(1.1 \pm 5.6) \cdot 10^{-2}$
Δw^{lepton}	$(2.0 \pm 1.6) \cdot 10^{-2}$
Δw^{kaon}	$(-1.2 \pm 1.2) \cdot 10^{-2}$
Δw^{NT1}	$(1.8 \pm 2.4) \cdot 10^{-2}$
Δw^{NT2}	$(-3.4 \pm 1.9) \cdot 10^{-2}$

Parameter	B^0 fit results (*GExp* model)
$\frac{\mathrm{Im}\lambda_{flav}}{\mid\lambda_{flav}\mid}$	1.4 ± 1.4
$\frac{\mathrm{Im}\lambda_{flav}}{\mid\lambda_{flav}\mid}$	-1.0 ± 1.4
$\frac{\mathrm{Im}\lambda_{tag}}{\mid\lambda_{tag}\mid}$	1.4 ± 1.5
$\frac{\mathrm{Im}\lambda_{tag}}{\mid\lambda_{tag}\mid}$	-1.1 ± 1.5
$f_{prompt,B_{flav}}^{lepton}$	0.379 ± 0.071
$f_{prompt,B_{flav}}^{kaon}$	0.665 ± 0.026
$f_{prompt,B_{flav}}^{NT1}$	0.632 ± 0.040
$f_{prompt,B_{flav}}^{NT2}$	0.728 ± 0.026
S_{back}	1.378 ± 0.023
$\tau_{r,back}$	2.42 ± 0.41
$f_{back,outlier}$	$(9.9 \pm 2.0) \cdot 10^{-3}$
$w_{0,prompt}^{lepton}$	0.143 ± 0.084
$w_{0,prompt}^{kaon}$	0.250 ± 0.012
$w_{0,prompt}^{NT1}$	0.340 ± 0.030
$w_{0,prompt}^{NT2}$	0.450 ± 0.015
$w_{0,non-prompt}^{lepton}$	0.397 ± 0.056
$w_{0,non-prompt}^{kaon}$	0.397 ± 0.022
$w_{0,non-prompt}^{NT1}$	0.454 ± 0.049
$w_{0,non-prompt}^{NT2}$	0.460 ± 0.036
$\tau_{non-prompt}$	1.278 ± 0.060
$f_{prompt,B_{CPK_S^0}}$	0.657 ± 0.072
$\tau_{non-prompt,B_{CPK_S^0}}$	2.31 ± 0.49

Table 22: Analysis 2 results, *GExp* resolution model.

	$\Delta\Gamma/\Gamma$	$\mid q/p \mid$	$\frac{\mathrm{Im}\lambda_{CP}}{\mid\lambda_{CP}\mid}$	$\frac{\mathrm{Re}\lambda_{CP}}{\mid\lambda_{CP}\mid}$Rez	Imz
Δm	-6.7%	-2.1%	-6.3%	23.9%	-3.2%
$\Delta\Gamma/\Gamma$		9.8%	-3.6%	-20.4%	-7.2%
$\mid q/p \mid$			0.3%	-4.7%	-1.2%
$\frac{\mathrm{Im}\lambda_{CP}}{\mid\lambda_{CP}\mid}$				-16.8%	14.3%
$\frac{\mathrm{Re}\lambda_{CP}}{\mid\lambda_{CP}\mid}$Rez					-3.4%

Table 23: Correlations among the 6 physics parameters, Analysis 2, *GG* resolution model.

	$\Delta\Gamma/\Gamma$	$\mid q/p \mid$	$\frac{\mathrm{Im}\lambda_{CP}}{\mid\lambda_{CP}\mid}$	$\frac{\mathrm{Re}\lambda_{CP}}{\mid\lambda_{CP}\mid}$Rez	Imz
Δm	-6.9%	-2.8%	-6.0%	26.6%	-2.1%
$\Delta\Gamma/\Gamma$		10.9%	-4.3%	-23.1%	-9.8%
$\mid q/p \mid$			0.1%	-5.2%	-2.1%
$\frac{\mathrm{Im}\lambda_{CP}}{\mid\lambda_{CP}\mid}$				-16.5%	14.5%
$\frac{\mathrm{Re}\lambda_{CP}}{\mid\lambda_{CP}\mid}$Rez					-2.4%

Table 24: Correlations among the 6 physics parameters, Analysis 2, *GExp* resolution model.

	$\Delta\Gamma/\Gamma$	$\mid q/p \mid$	$\frac{\mathrm{Im}\lambda_{CP}}{\mid\lambda_{CP}\mid}$	$\frac{\mathrm{Re}\lambda_{CP}}{\mid\lambda_{CP}\mid}$Rez	Imz	$\frac{\mathrm{Im}\lambda_{flav}}{\mid\lambda_{flav}\mid}$	$\frac{\mathrm{Im}\bar{\lambda}_{flav}}{\mid\bar{\lambda}_{flav}\mid}$	$\frac{\mathrm{Im}\lambda_{tag}}{\mid\lambda_{tag}\mid}$	$\frac{\mathrm{Im}\bar{\lambda}_{tag}}{\mid\bar{\lambda}_{tag}\mid}$
Δm	-6.7%	-2.1%	-6.3%	23.9%	-3.2%	-3.6%	0.3%	-2.1%	3.7%
$\Delta\Gamma/\Gamma$		9.8%	-3.6%	-20.4%	-7.2%	-0.0%	-2.4%	-0.3%	-1.8%
$\mid q/p \mid$			0.3%	-4.7%	-1.2%	0.9%	0.5%	0.2%	1.3%
$\frac{\mathrm{Im}\lambda_{CP}}{\mid\lambda_{CP}\mid}$				-16.8%	14.3%	10.2%	-4.7%	10.9%	-3.5%
$\frac{\mathrm{Re}\lambda_{CP}}{\mid\lambda_{CP}\mid}$Rez					-3.4%	-3.8%	1.3%	-3.2%	2.0%
Imz						50.1%	-53.2%	53.1%	-55.5%
$\frac{\mathrm{Im}\lambda_{flav}}{\mid\lambda_{flav}\mid}$							8.8%	74.3%	15.8%
$\frac{\mathrm{Im}\bar{\lambda}_{flav}}{\mid\bar{\lambda}_{flav}\mid}$								15.0%	77.0%
$\frac{\mathrm{Im}\lambda_{tag}}{\mid\lambda_{tag}\mid}$									24.5%

Table 25: Correlations among the physics parameters and DCSD phases, Analysis 2, *GG* resolution model.

7.5 $B^0\bar{B}^0$ differences in reconstruction and tagging efficiencies

The $B^0\bar{B}^0$ asymmetries in reconstruction (ν^α) and tagging (μ^α) efficiencies for signal and sideband events obtained in the two analyses are shown in tables 27 and 28 (sideband values are independent of which analysis we are running). The difference in the signal region values for the two analyses are so small that there are no differences when rounding to the most significant digits. It can be seen that the detector asymmetries are compatible within zero.

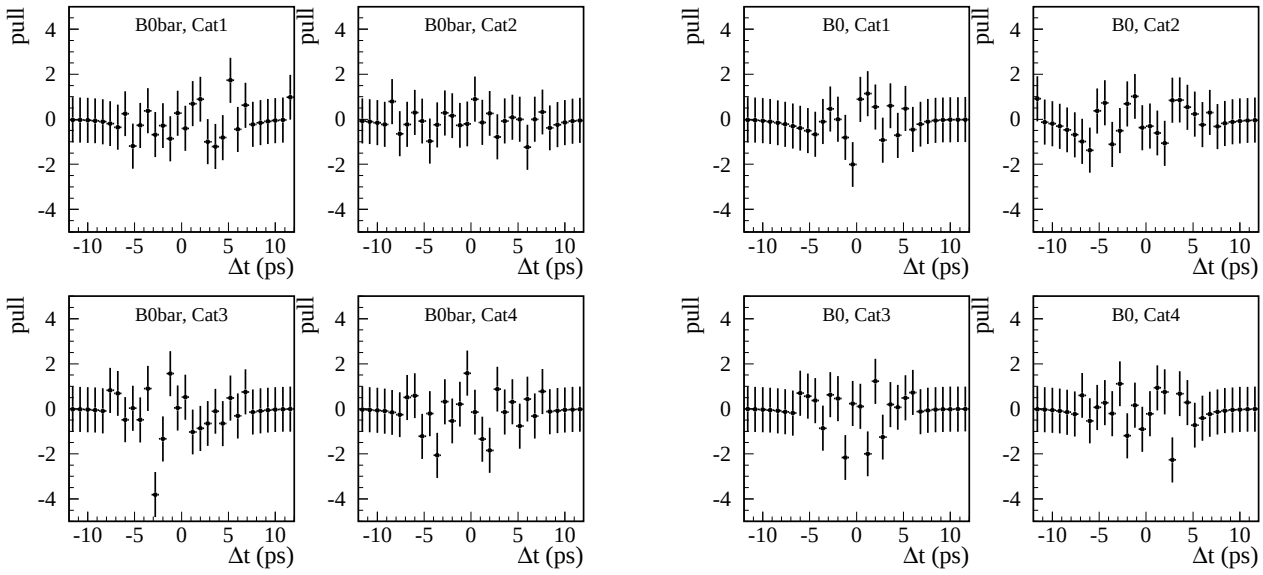

(a) (b)

Figure 18: Normalized residuals of the Δt projections of the nominal fit (Analysis 2) for the $B_{CPK^0_S}$ sample: (a) $\overline{B}^0$ tagged, (b) B^0 tagged (*GG* model), for each tagging category.

Parameter	Analysis 1 *GG*	Analysis 2 *GG*
Δm	$0.5220^{+0.0098}_{-0.0098}$	$0.523^{+0.017}_{-0.010}$
$\Delta\Gamma/\Gamma$	$-0.008^{+0.048}_{-0.049}$	$-0.021^{+0.048}_{-0.047}$
$\mid q/p \mid$	$0.946^{+0.018}_{-0.018}$	$0.945^{+0.018}_{-0.018}$
$\frac{\mathrm{Im}\lambda_{CP}}{\mid\lambda_{CP}\mid}$	$0.612^{+0.085}_{-0.086}$	$0.620^{+0.081}_{-0.084}$
$\frac{\mathrm{Re}\lambda_{CP}}{\mid\lambda_{CP}\mid}\mathrm{Re}z$	—	$-0.064^{+0.074}_{-0.047}$
$\mathrm{Im}z$	—	$-0.918^{+0.034}_{-0.034}$

Table 26: Results with asymmetric errors from Analysis 1 and 2 data fits, *GG* model.

7.6 Goodness-of-fit and expected errors

The estimation of the goodness-of-fit has been done using toy Monte Carlo. The toy Monte Carlo generator used for this study was described in detail in reference [11]. The following effects where included in the simulation:

- m_{ES} and ΔE distributions for each sample and tagging category;

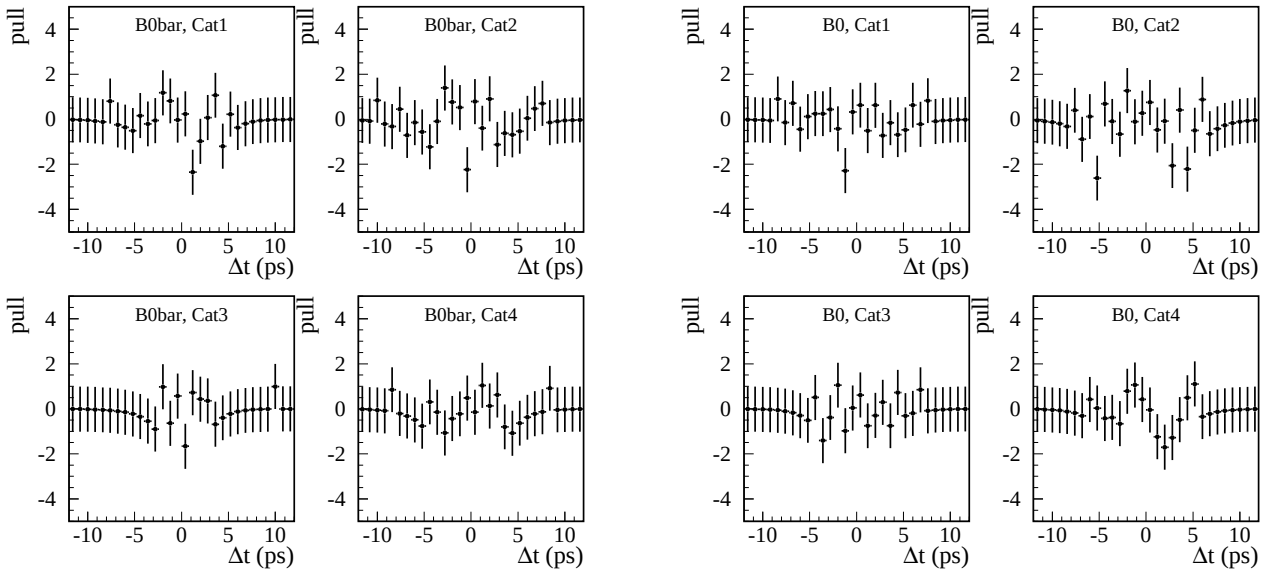

(a) (b)

Figure 19: Normalized residuals of the Δt projections of the nominal fit (Analysis 2) for the $B_{CPK_L^0}$ sample: (a) $\overline{B}^0$ tagged, (b) B^0 tagged (*GG* model), for each tagging category.

Sample	`Lepton`	non `Lepton`
B^0 signal	-0.009 ± 0.010	-0.008 ± 0.010
B^0 sideband	0.005 ± 0.010	0.005 ± 0.010

Table 27: Measured ν^α values ($B^0\overline{B}^0$ difference in reconstruction efficiency) from the B_{flav} data sample, for Analysis 1 and 2.

- for each sample, two $\sigma_{\Delta t}$ distributions were genenerated using the Crystall Ball parameters extracted from the data fits to signal and sideband events (section 4). For B_{flav} and $B_{CPK_S^0}$ events, the signal region distribution was used for signal and peaking background, while the sideband distribution was used for combinatorial backgrounds (prompt and non-prompt). For signal and inclusive $J/\psi X$ background in the $B_{CPK_L^0}$ sample the same distribution as for signal $B_{CPK_S^0}$ events was generated, while for non-J/ψ backgrounds we used the parent distribution of the $B_{CPK_S^0}$ sideband events;
- Δt distribution (truth+smeared) for signal and background components (prompt, non-prompt, peaking and specific channels for the $J/\psi K_L^0$ mode), for each tagging category;
- mistag rates, $B^0\overline{B}^0$ differences in reconstruction and tagging efficiencies and linear correlation between the average mistag fractions and $\sigma_{\Delta t}$;

The experiments use the same statistics and configuration as the nominal fit. All the generated parameters were tunned to those in the data. The generated values of the physics parameters obtained in the data fit are internally unblinded by the generation code. Only converged fits are accepted.

Sample	Lepton	Kaon	NT1	NT2
B^0 signal	0.050 ± 0.045	-0.019 ± 0.022	0.006 ± 0.056	0.007 ± 0.040
B^0 sideband	-0.010 ± 0.076	-0.010 ± 0.014	0.022 ± 0.044	-0.019 ± 0.023

Table 28: Measured μ^{α} values ($B^0\bar{B}^0$ difference in tagging efficiency) from the B_{flav} data sample, for Analysis 1 and 2.

x

Comparing the likelihood distribution coming from the experiments with the value obtained in the nominal data fit (see figure 20), the goodness-of-fit of the data is evaluated to be 51% for Analysis 1 and 49% for Analysis 2.

The errors on the physical parameters (Gaussians) coming from the toy Monte Carlo fits are compared with the RMS of the residual distribution and the errors (Gaussians and asymmetric) extracted from the nominal data fit (see figures 21, 22, 23 and 24). In the same figure are shown the residual distributions from the same experiments. These figures deserve several remarks. First, Gaussian errors give a good estimate of the resolution as extracted from the RMS of the residual distributions, within 10%. In addition, there is an overall good agreement between the Gaussian and asymetric errors. Second, there is indication that the error from the data sample tends to be slightly better than the prediction from the Monte Carlo, but still within the expected range. This effect was extensively investigated a no problem was found, so we concluded that we were lucky with the current data sample. Third, the biases from the residual distributions are in all cases very small compared with the current statistical precision. The larger between the bias and its error will be assigned as systematic error due to the fitting procedure (see section 9.13).

The correlation coefficients and the scatter distributions among all the CPT/T/CP/oscillation and DCKM parameters coming from the toy Monte Carlo fits are also compared with the values extracted from the nominal data fit in figures 25-28 and 30-34, respectively. In all cases the data values fall into the expected range.

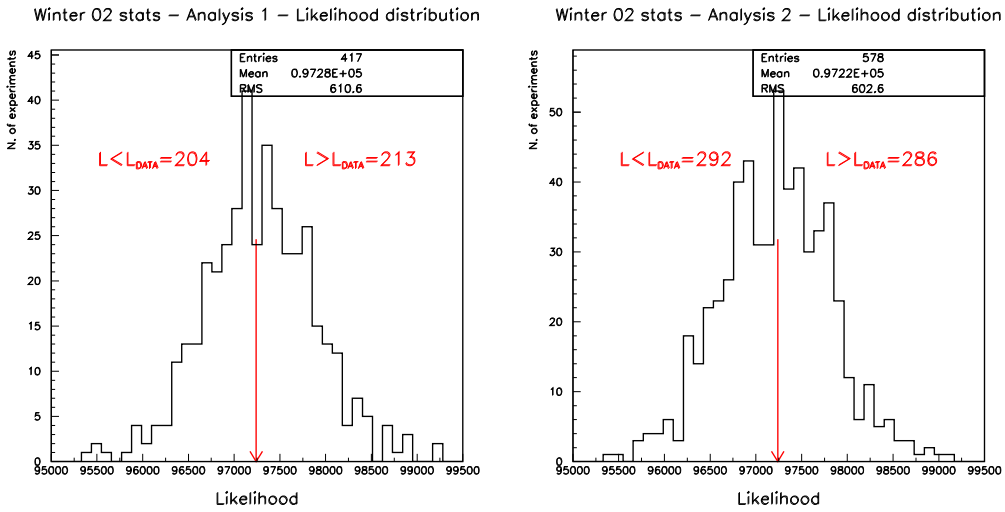

Figure 20: Likelihood distribution from toy Monte Carlo experiments (Analysis 1 and 2). The arrow shows the value obtained from the nominal data fit. The number of experiments with likelihood value smaller and greater than the data is quoted. The probability that the toy Monte Carlo experiments are less likely (larger negative log-likelihood) than the data is evaluated to be 51% for analysis 1 and 49% for analysis 2.

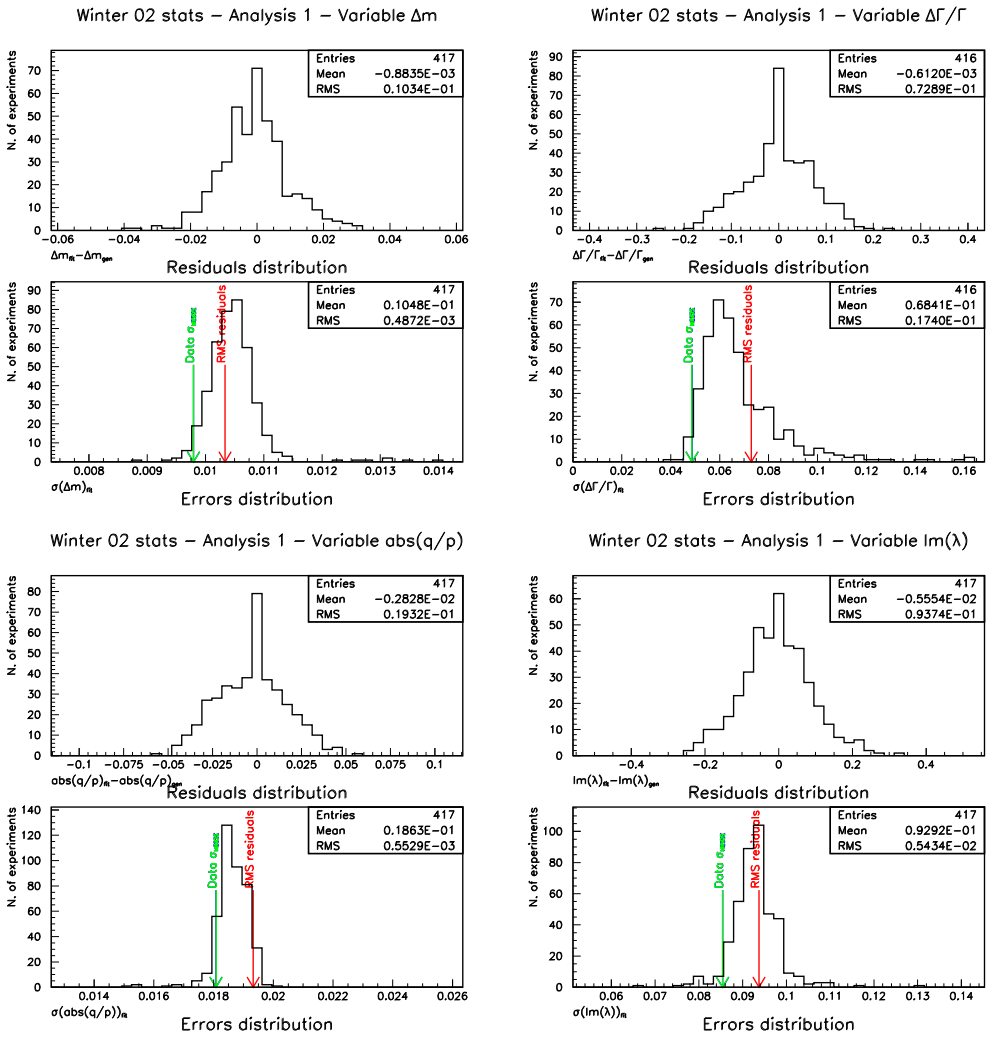

Figure 21: The residual and Gaussian error distributions for the oscillation/CPT/T/CP parameters coming from the Analysis 1 of toy Monte Carlo experiments. In the error distribution indicated are the RMS of the residual distribution (red arrow) and the values of the Gaussian error (blue arrow) and quadratic average of the asymmetric errors (green arrow) extracted from the data fit.

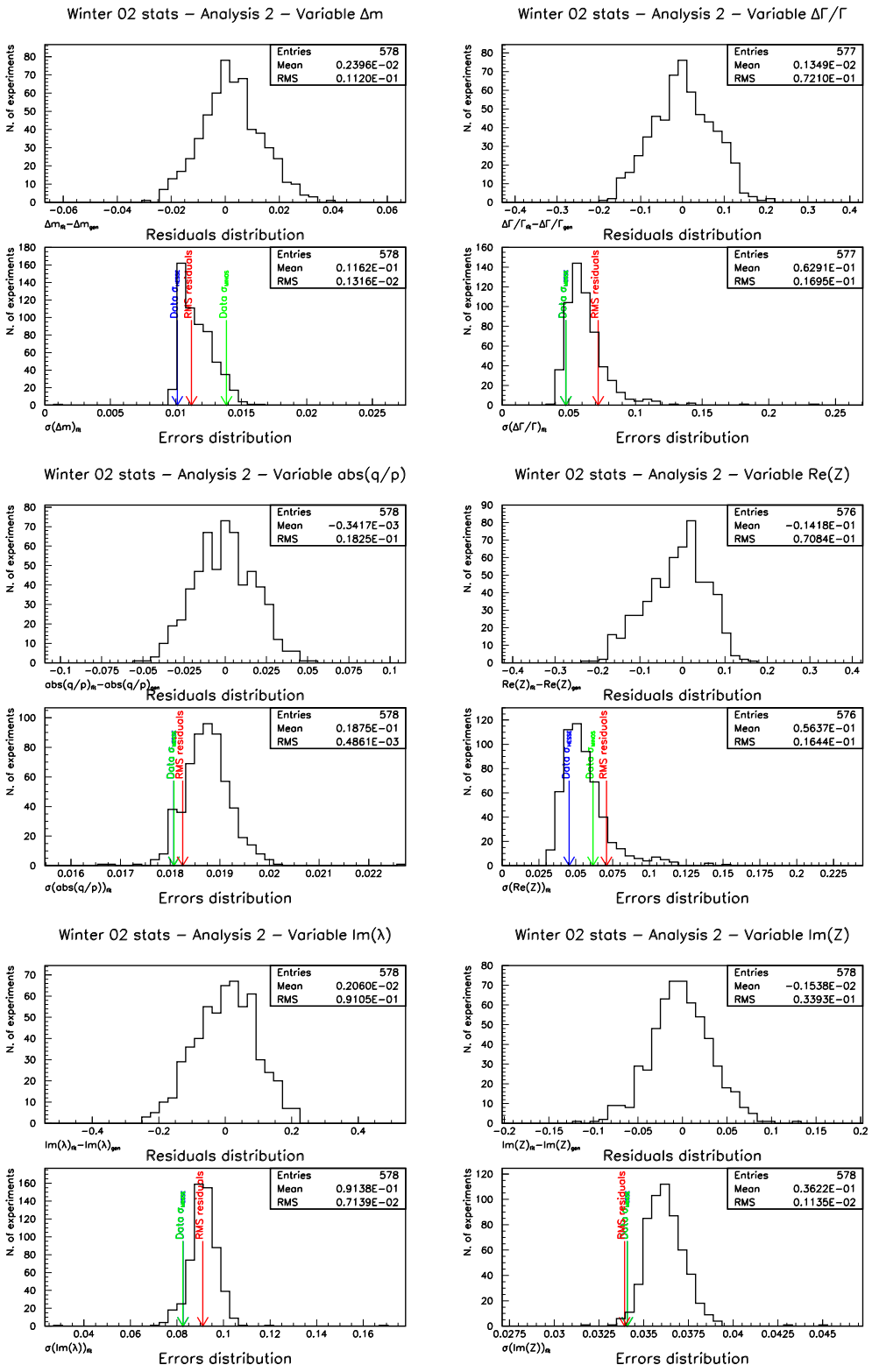

Figure 22: The residual and Gaussian error distributions for the oscillation/CPT/T/CP parameters coming from the Analysis 2 of toy Monte Carlo experiments. In the error distribution indicated are the RMS of the residual distribution (red arrow) and the values of the Gaussian error (blue arrow) and quadratic average of the asymmetric errors (green arrow) extracted from the data fit.

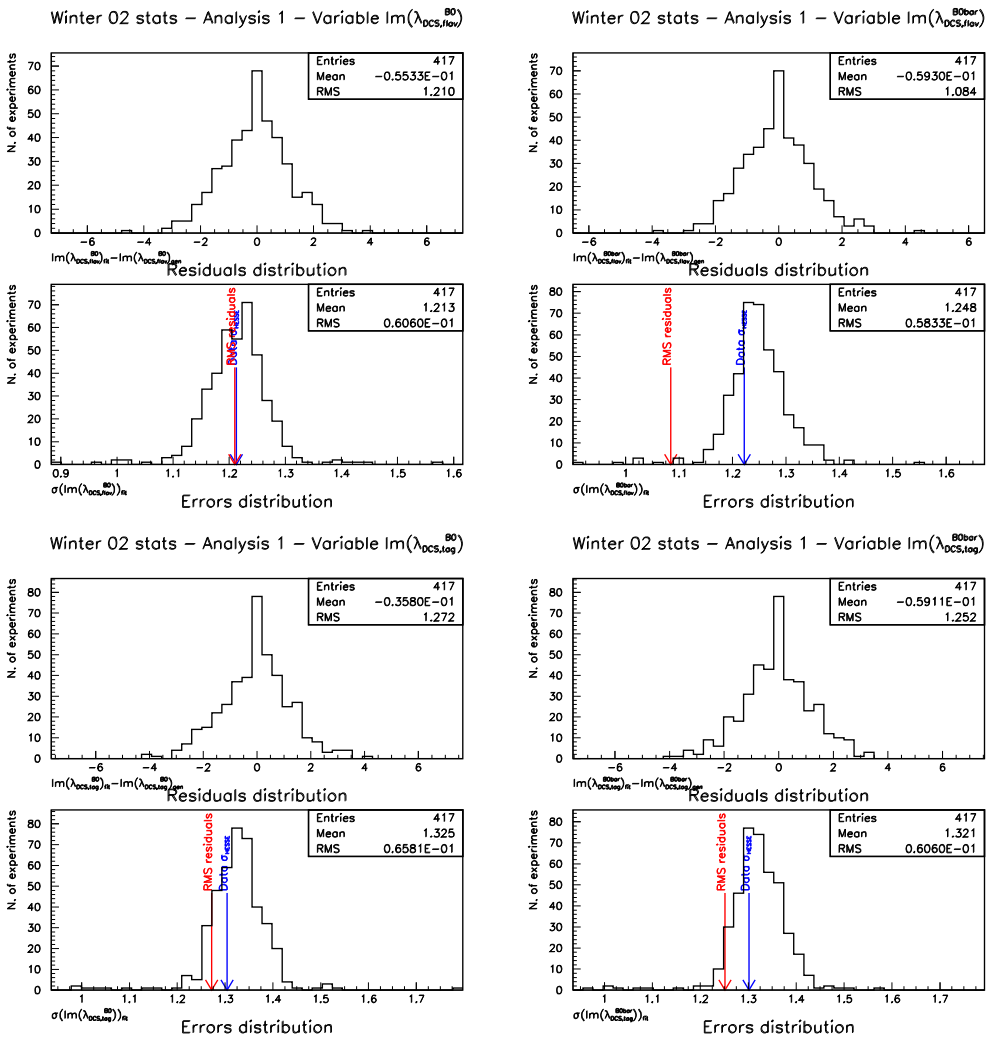

Figure 23: The residual and Gaussian error distributions for the DCKM free parameters coming from the Analysis 1 of toy Monte Carlo experiments. In the error distribution indicated are the RMS of the residual distribution (red arrow) and the value of the Gaussian error (blue arrow).

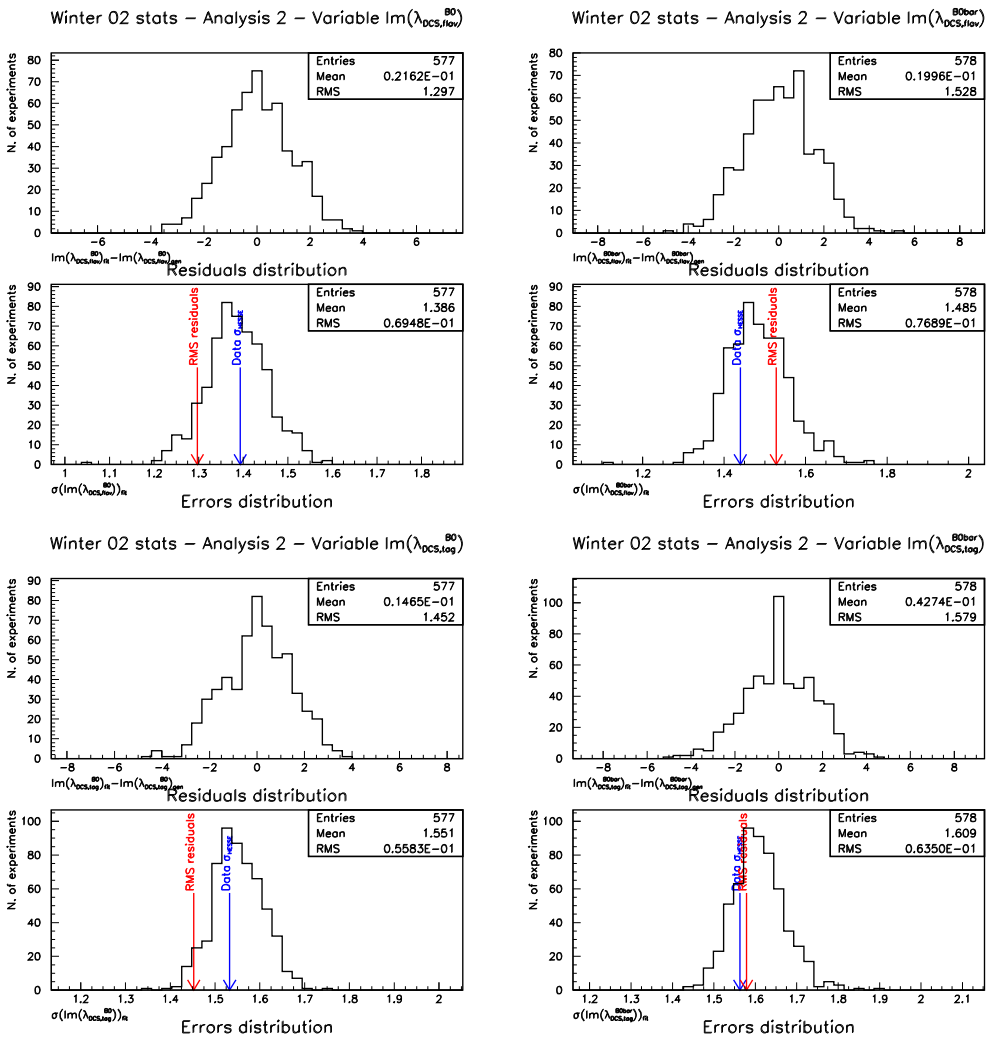

Figure 24: The residual and Gaussian error distributions for the DCKM free parameters coming from the Analysis 2 of toy Monte Carlo experiments. In the error distribution indicated are the RMS of the residual distribution (red arrow) and the value of the Gaussian error (blue arrow).

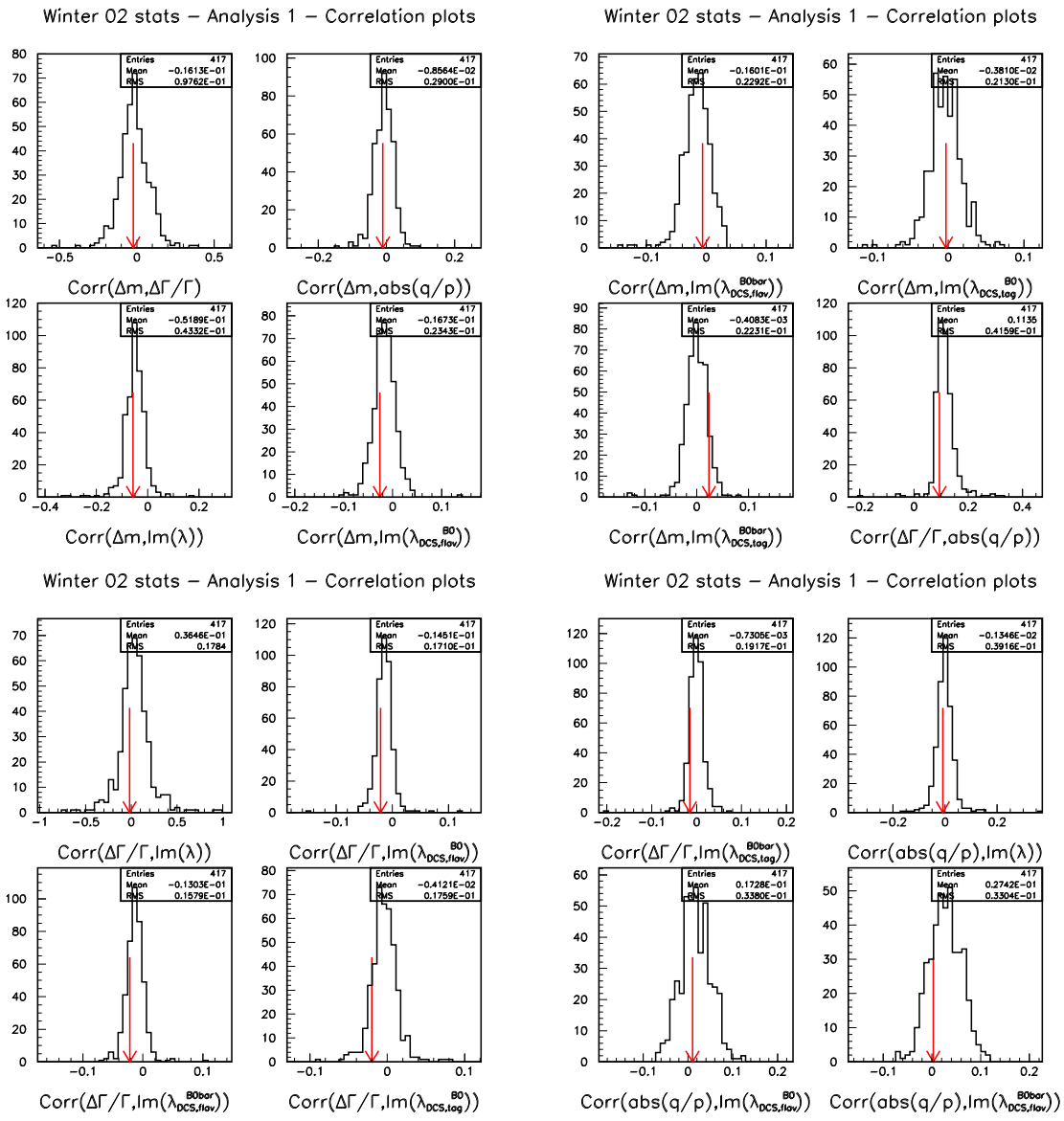

Figure 25: Distribution of the correlation coefficients among the physical and DCKM parameters coming from the Analysis 1 of toy Monte Carlo experiments. The values corresponding to the nominal data fit (red arrow) are indicated.

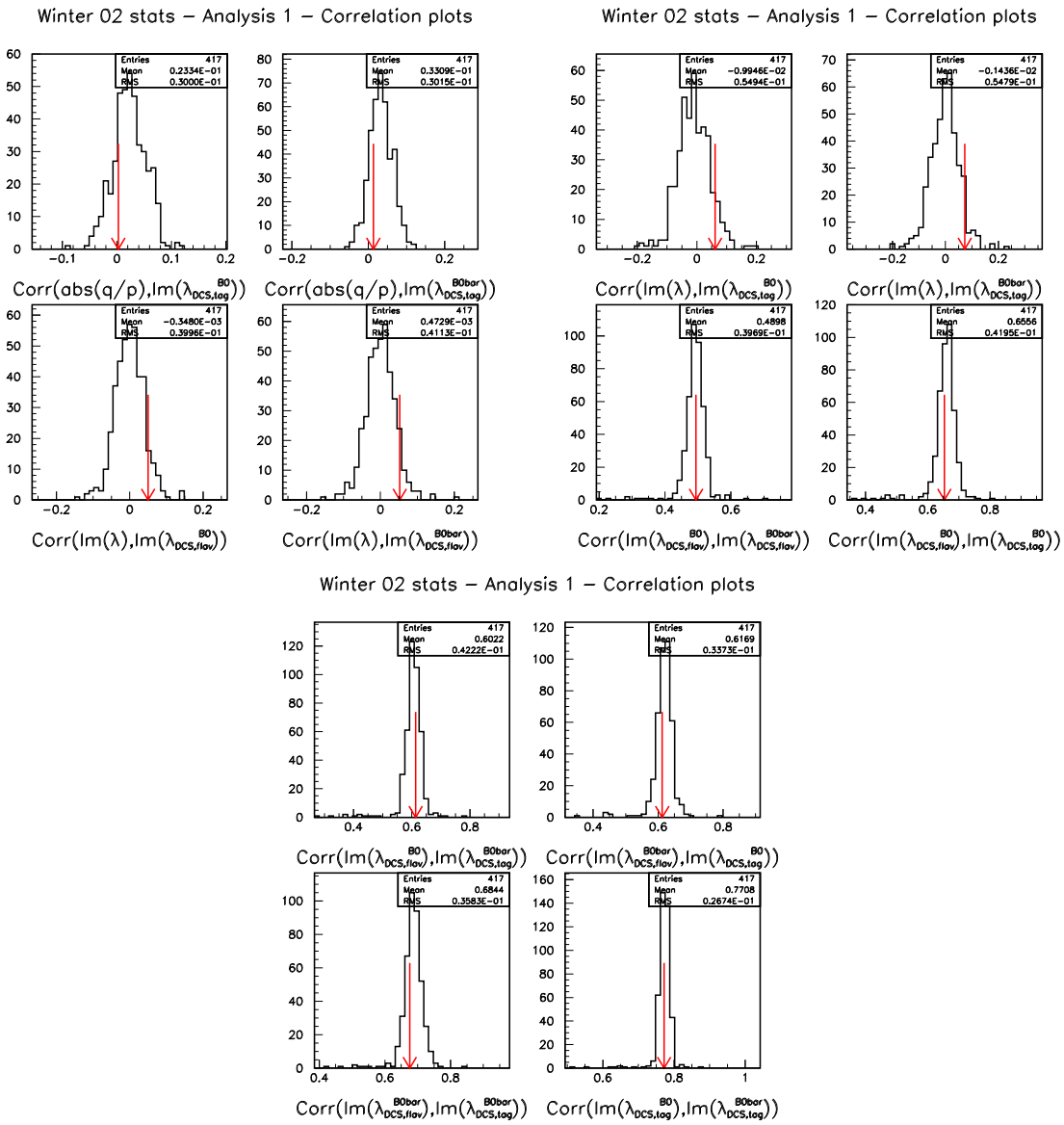

Figure 26: Distribution of the correlation coefficients among the physical and DCKM parameters coming from the Analysis 1 of toy Monte Carlo experiments. The values corresponding to the nominal data fit (red arrow) are indicated (con't).

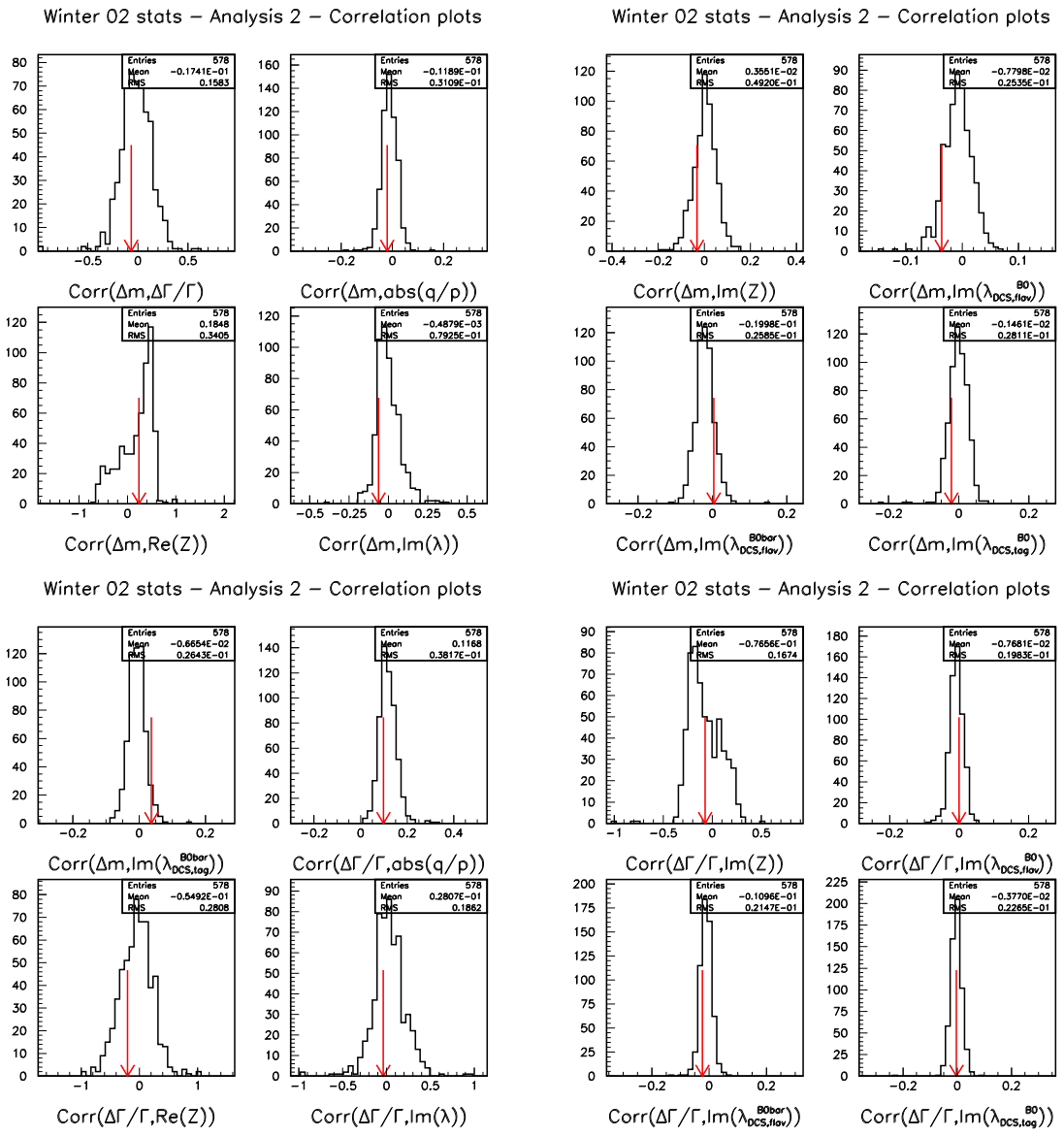

Figure 27: Distribution of the correlation coefficients among the physical and DCKM parameters coming from the Analysis 2 of toy Monte Carlo experiments. The values corresponding to the nominal data fit (red arrow) are indicated.

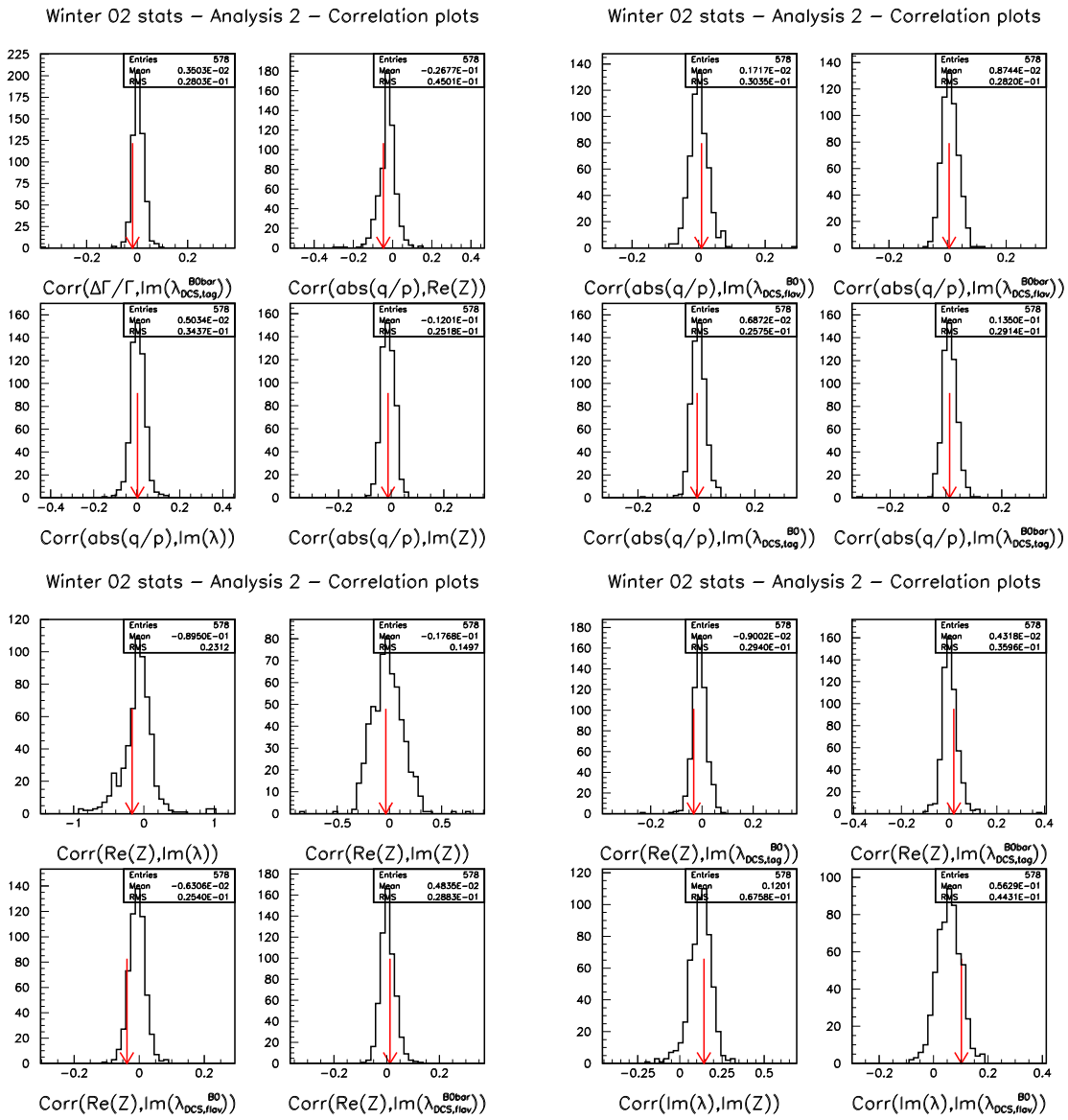

Figure 28: Distribution of the correlation coefficients among the physical and DCKM parameters coming from the Analysis 2 of toy Monte Carlo experiments. The values corresponding to the nominal data fit (red arrow) are indicated (con't).

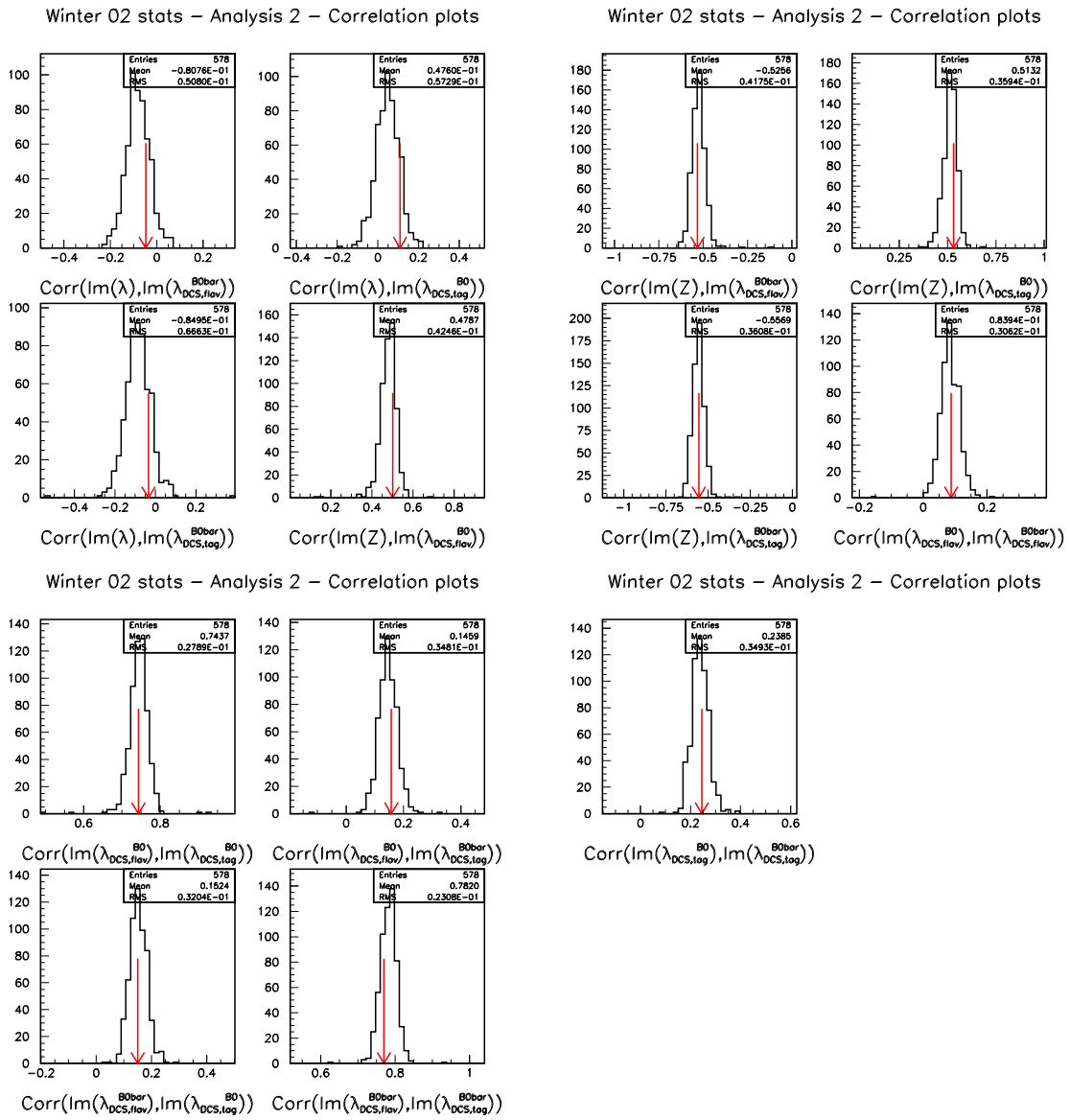

Figure 29: Distribution of the correlation coefficients among the physical and DCKM parameters coming from the Analysis 2 of toy Monte Carlo experiments. The values corresponding to the nominal data fit (red arrow) are indicated (con't).

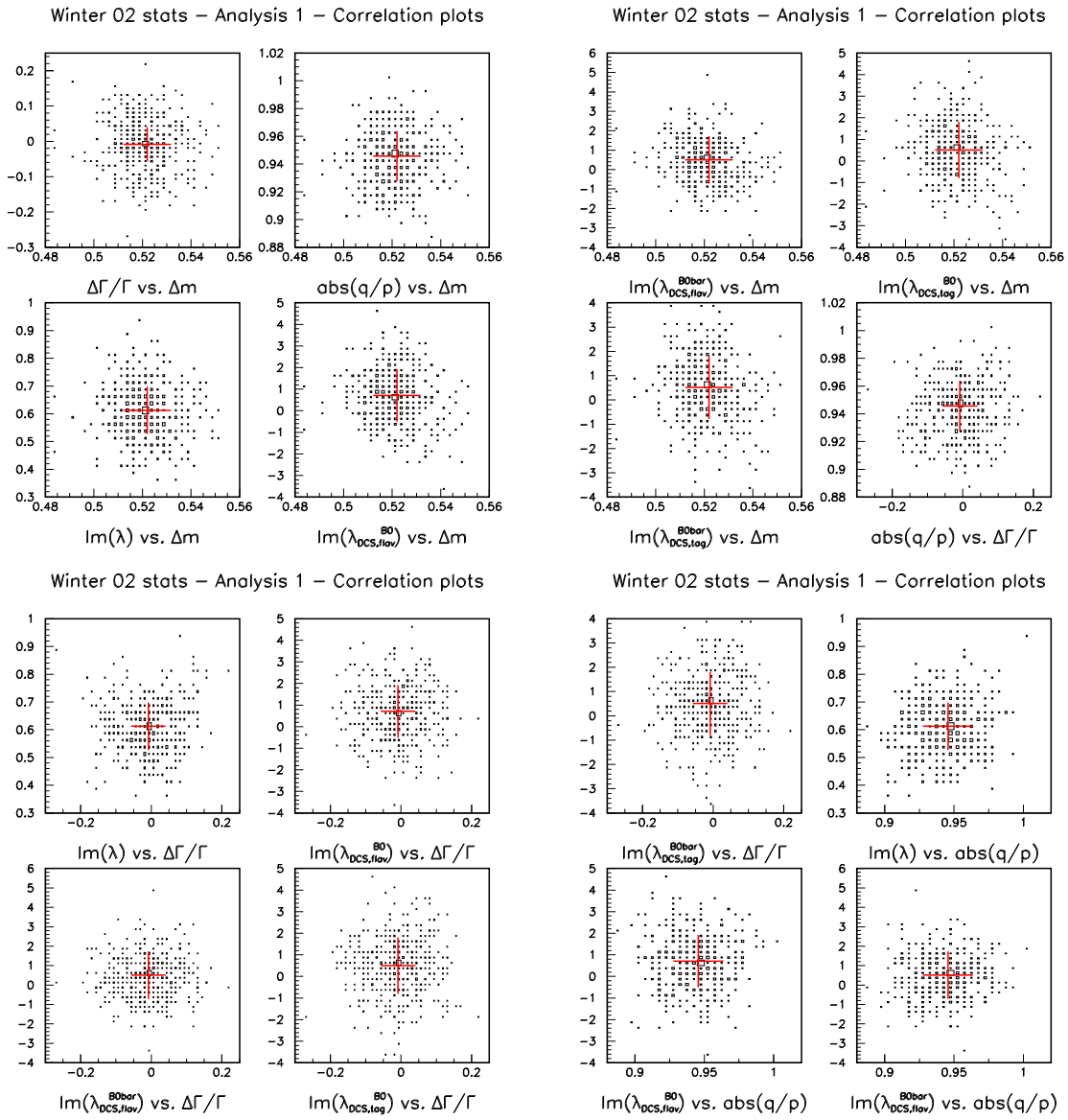

Figure 30: Scatter distributions among the physical and DCKM parameters coming from the Analysis 1 of toy Monte Carlo experiments. The values corresponding to the nominal data fit (red arrow) are indicated.

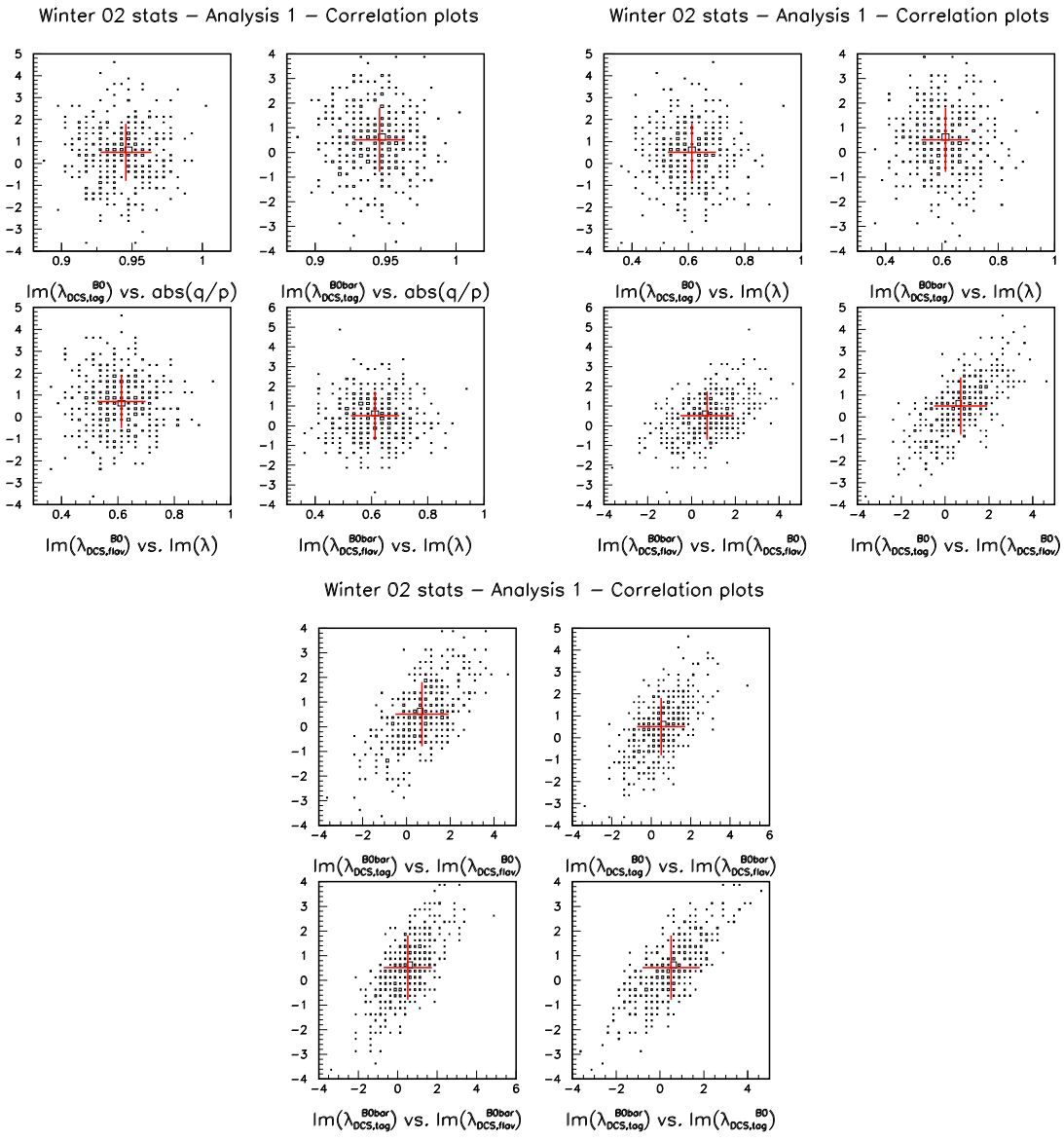

Figure 31: Scatter distributions among the physical and DCKM parameters coming from the Analysis 1 of toy Monte Carlo experiments. The values corresponding to the nominal data fit (red arrow) are indicated (con't).

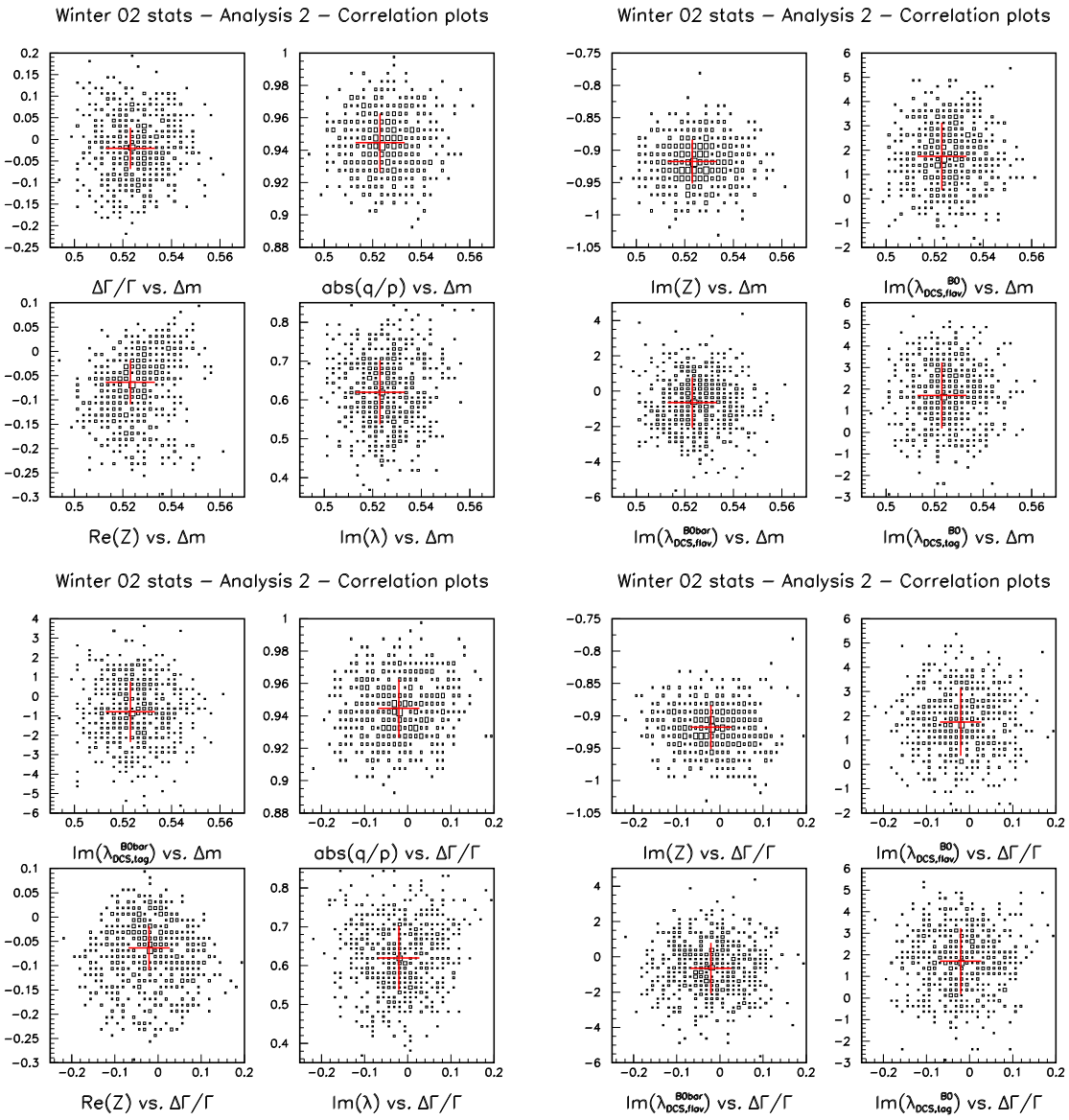

Figure 32: Scatter distributions among the physical and DCKM parameters coming from the Analysis 2 of toy Monte Carlo experiments. The values corresponding to the nominal data fit (red arrow) are indicated.

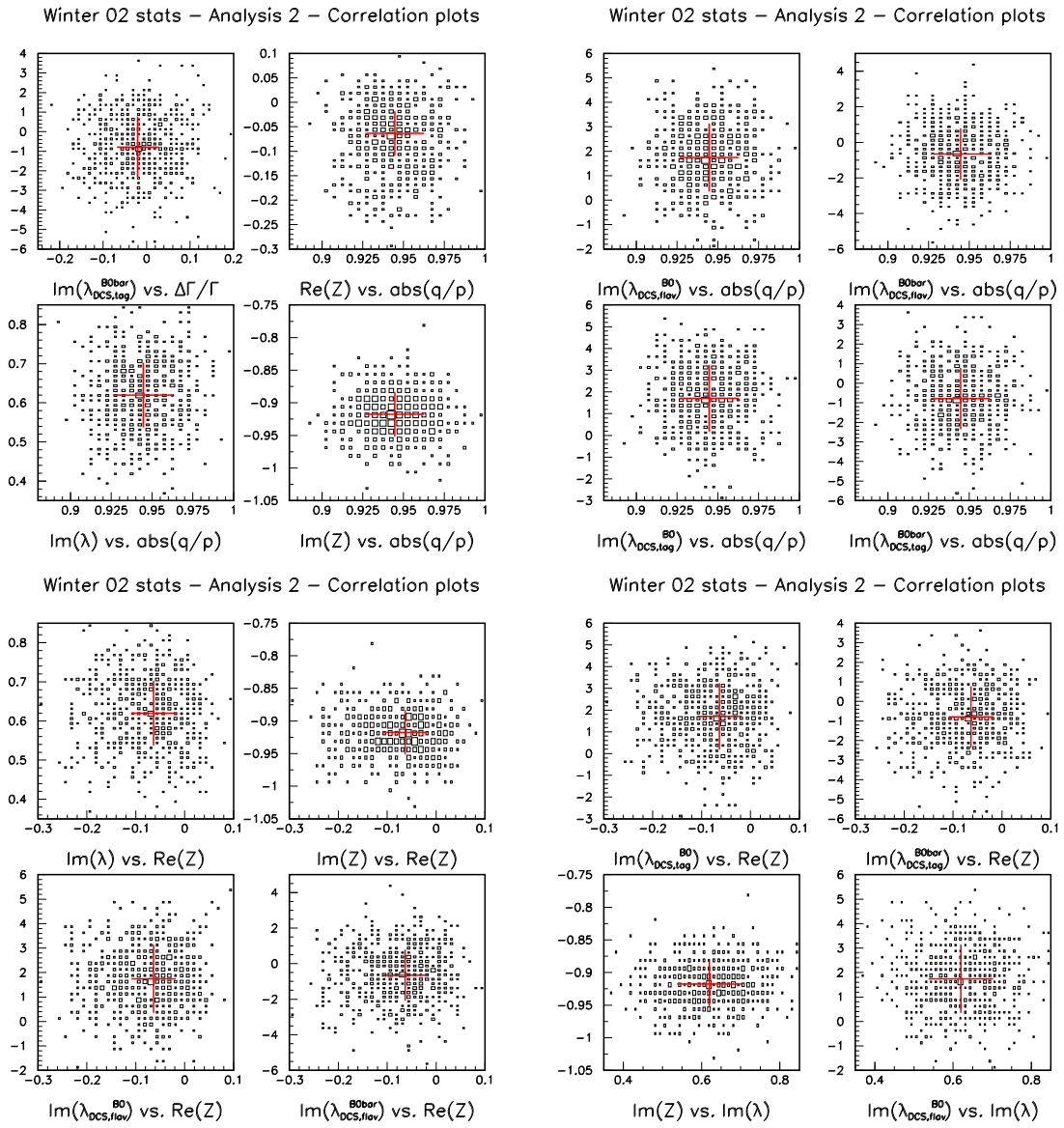

Figure 33: Scatter distributions among the physical and DCKM parameters coming from the Analysis 2 of toy Monte Carlo experiments. The values corresponding to the nominal data fit (red arrow) are indicated (con't).

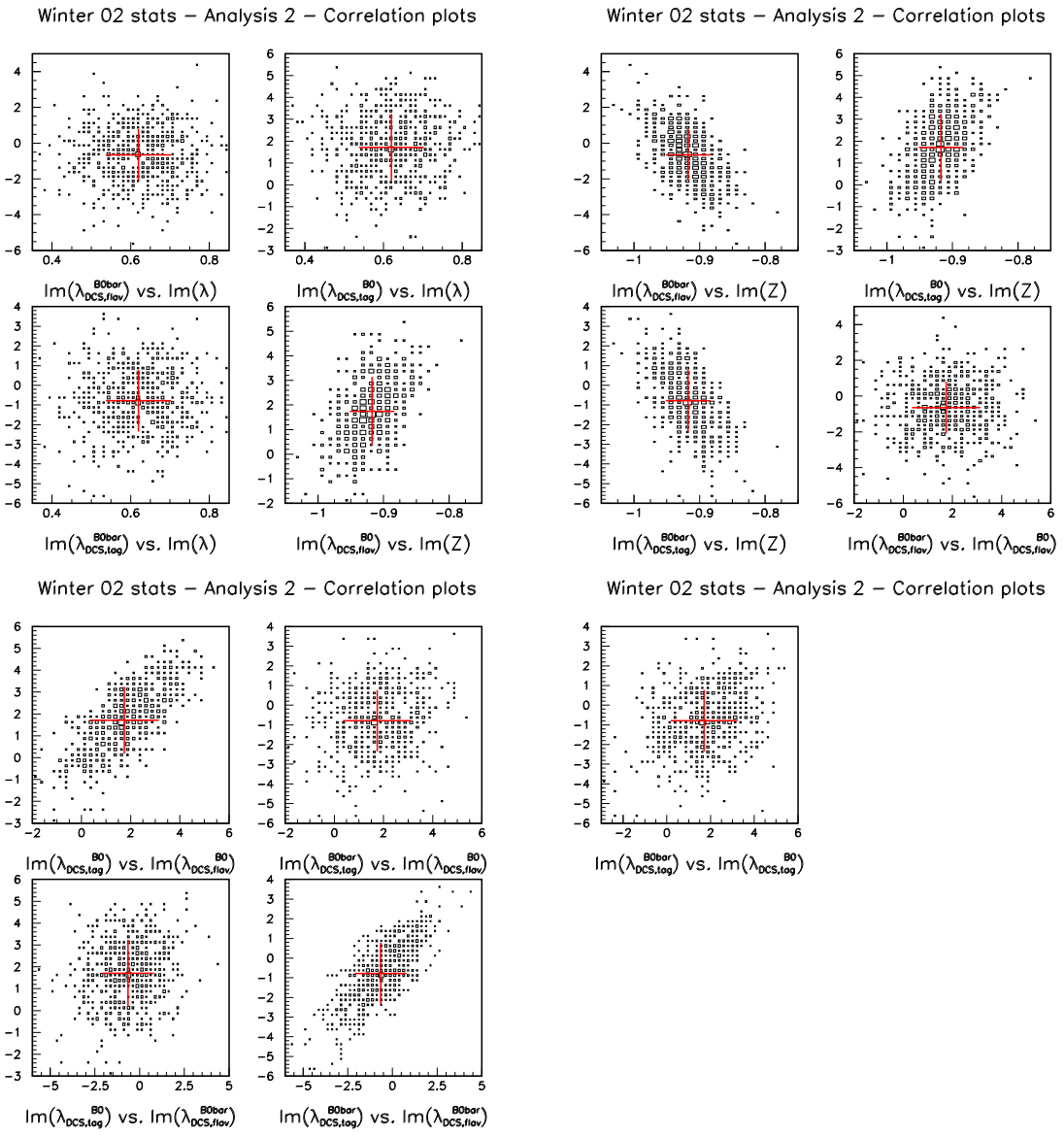

Figure 34: Scatter distributions among the physical and DCKM parameters coming from the Analysis 2 of toy Monte Carlo experiments. The values corresponding to the nominal data fit (red arrow) are indicated (con't).

7.7 Unblind results

Here we will include the results after unblinding (tables, time distributions and asymmetries).

8 Cross-checks

We have performed several checks, on both data and Monte Carlo, of the consistency of the measurements. They are reported in the following subsections.

8.1 Average B^0 lifetime results

In the nominal fit the average B^0 lifetime is fixed to the PDG2000 [22] value, $\tau_B = 1.548 \pm 0.034$. The fit on data was redone but now fitting also for τ_B. The results for Analysis 1 and Analysis 2, compared to the nominal fits, are shown in tables 29 and 30, for the `GG` resolution model. The corresponding results for the `GExp` model are in tables 31 and 32. τ_B is unblinded.

Parameter	Nominal fit	τ_B free
τ	—	1.515 ± 0.022
Δm	0.5220 ± 0.0098	0.528 ± 0.011
$\Delta\Gamma/\Gamma$	$(-0.8 \pm 4.9) \cdot 10^{-2}$	$(-0.4 \pm 5.5) \cdot 10^{-2}$
$\mid q/p \mid$	0.946 ± 0.018	0.946 ± 0.018
$\frac{\mathrm{Im}\lambda_{CP}}{\mid\lambda_{CP}\mid}$	0.612 ± 0.085	0.619 ± 0.086

Table 29: Analysis 1 results with the B^0 lifetime free. For comparison, nominal fit results are reported as well. *GG* resolution model.

Parameter	Nominal fit	τ_B free
τ	—	1.517 ± 0.022
Δm	0.523 ± 0.010	0.528 ± 0.011
$\Delta\Gamma/\Gamma$	$(-2.1 \pm 4.8) \cdot 10^{-2}$	$(-1.7 \pm 5.4) \cdot 10^{-2}$
$\mid q/p \mid$	0.945 ± 0.018	0.945 ± 0.018
$\frac{\mathrm{Im}\lambda_{CP}}{\mid\lambda_{CP}\mid}$	0.620 ± 0.083	0.626 ± 0.083
$\frac{\mathrm{Re}\lambda_{CP}}{\mid\lambda_{CP}\mid}\mathrm{Re}z$	$(-6.4 \pm 4.6) \cdot 10^{-2}$	$(-7.3 \pm 4.4) \cdot 10^{-2}$
$\mathrm{Im}z$	-0.918 ± 0.034	-0.917 ± 0.035

Table 30: Analysis 2 results with the B^0 lifetime free. For comparison, nominal fit results are reported as well. *GG* model resolution model.

8.2 $B_{CPK^0_S}$ and $B_{CPK^0_L}$ separately

We performed the nominal fit separately for the $B_{CPK^0_S}$ and $B_{CPK^0_L}$ samples only. Results are summarized in tables 33 and 34, and they are compared to the nominal fits, for Analysis 1 and 2 respectively.

Parameter	Nominal fit	τ_B free
τ	—	1.528 ± 0.020
Δm	0.5195 ± 0.0097	0.523 ± 0.010
$\Delta\Gamma/\Gamma$	$(-0.3 \pm 5.3) \cdot 10^{-2}$	$(0.2 \pm 5.8) \cdot 10^{-2}$
$\mid q/p \mid$	0.946 ± 0.018	0.946 ± 0.018
$\frac{\mathrm{Im}\lambda_{CP}}{\lvert\lambda_{CP}\rvert}$	0.614 ± 0.085	0.618 ± 0.085

Table 31: Analysis 1 results with the B^0 lifetime free. For comparison, the fits with the lifetime fixed are reported as well. *GExp* resolution model.

Parameter	Nominal fit	τ_B free
τ	—	1.530 ± 0.020
Δm	0.521 ± 0.010	0.524 ± 0.011
$\Delta\Gamma/\Gamma$	$(-2.0 \pm 5.1) \cdot 10^{-2}$	$(-1.7 \pm 5.6) \cdot 10^{-2}$
$\mid q/p \mid$	0.944 ± 0.018	0.945 ± 0.018
$\frac{\mathrm{Im}\lambda_{CP}}{\lvert\lambda_{CP}\rvert}$	0.622 ± 0.082	0.626 ± 0.082
$\frac{\mathrm{Re}\lambda_{CP}}{\lvert\lambda_{CP}\rvert}\mathrm{Re}z$	$(-5.7 \pm 4.6) \cdot 10^{-2}$	$(-6.3 \pm 4.6) \cdot 10^{-2}$
$\mathrm{Im}z$	-0.919 ± 0.034	-0.919 ± 0.034

Table 32: Analysis 2 results with the B^0 lifetime free. For comparison, the fits with the lifetime fixed are reported as well. *GExp* resolution model.

Parameter	all CP (nominal)	$B_{CPK^0_S}$ sample	$B_{CPK^0_L}$ sample
Δm	0.5220 ± 0.0098	0.5219 ± 0.0098	0.5238 ± 0.0098
$\Delta\Gamma/\Gamma$	$(-0.8 \pm 4.9) \cdot 10^{-2}$	$(-0.7 \pm 5.3) \cdot 10^{-2}$	$(-2.1 \pm 7.4) \cdot 10^{-2}$
$\mid q/p \mid$	0.946 ± 0.018	0.949 ± 0.018	0.946 ± 0.019
$\frac{\mathrm{Im}\lambda_{CP}}{\lvert\lambda_{CP}\rvert}$	0.612 ± 0.085	0.615 ± 0.096	0.59 ± 0.19

Table 33: Comparison of analysis 1 nominal fit, with the full CP, $B_{CPK^0_S}$ and $B_{CPK^0_L}$ samples. The blinding string of the results is the same for all the columns.

Parameter	all CP (nominal)	$B_{CPK^0_S}$ sample	$B_{CPK^0_L}$ sample
Δm	0.523 ± 0.010	0.5220 ± 0.0100	0.524 ± 0.010
$\Delta\Gamma/\Gamma$	$(-2.1 \pm 4.8) \cdot 10^{-2}$	$(-1.8 \pm 5.5) \cdot 10^{-2}$	$(-3.0 \pm 6.9) \cdot 10^{-2}$
$\mid q/p \mid$	0.945 ± 0.018	0.948 ± 0.018	0.946 ± 0.019
$\frac{\mathrm{Im}\lambda_{CP}}{\lvert\lambda_{CP}\rvert}$	0.620 ± 0.083	0.645 ± 0.091	0.51 ± 0.20
$\frac{\mathrm{Re}\lambda_{CP}}{\lvert\lambda_{CP}\rvert}\mathrm{Re}z$	$(-6.4 \pm 4.6) \cdot 10^{-2}$	$(-8.6 \pm 4.9) \cdot 10^{-2}$	$(-6.8 \pm 6.8) \cdot 10^{-2}$
$\mathrm{Im}z$	-0.918 ± 0.034	-0.910 ± 0.035	-0.912 ± 0.036

Table 34: Comparison of analysis 2 nominal fit, with the full CP, $B_{CPK^0_S}$ and $B_{CPK^0_L}$ samples. The blinding string of the results is the same for all the columns.

Analysis 1 fits with $\Delta\Gamma/\Gamma$ and $\mid q/p \mid$ fixed to 0 and 1 ($\sin 2\beta$ only fits), respectively, were also performed, for all B_{CP} modes together as well as for $B_{CPK^0_S}$ and $B_{CPK^0_L}$ separately. The results can be found in table 35. The

Δm and $\frac{\mathrm{Im}\lambda_{CP}}{|\lambda_{CP}|}$ results should be compared to those of table 33. Let us remark that the fact that the blinding is in this case the same as for the Analysis 1 and 2 fits but this does not unblind the actual fitted values of the other parameters since the correlation among these parameters is small.

Parameter	$\sin 2\beta$ full CP sample	$\sin 2\beta$ $B_{CPK_S^0}$ sample	$\sin 2\beta$ $B_{CPK_L^0}$ sample
Δm	0.5220 ± 0.0098	0.5219 ± 0.0098	0.5238 ± 0.0098
$\frac{\mathrm{Im}\lambda_{CP}}{\lvert\lambda_{CP}\rvert}$	0.613 ± 0.085	0.616 ± 0.096	0.59 ± 0.19

Table 35: Comparison of $\sin 2\beta$ only fits (analysis 1 with $\Delta\Gamma/\Gamma$ and $\mid q/p \mid$ fixed to 0 and 1), using the full CP, $B_{CPK_S^0}$ and $B_{CPK_L^0}$ samples. $\frac{\mathrm{Im}\lambda_{CP}}{|\lambda_{CP}|}$ results are here blinded.

8.3 $B^0\bar{B}^0$ shape only fit

The normalization of the PDF (section 2) is performed for all mixed/unmixed/$B^0/\bar{B}^0$ events together, but separately for the B_{flav}, $B_{CPK_S^0}$ and $B_{CPK_L^0}$ samples. As a cross-check, the fit was also performed normalizing separately for B^0 and $\bar{B}^0$ events. Taking out this constraint implies to perform a fit to the $B^0\bar{B}^0$ Δt shape only fit, being therefore insensitive to the total number of B^0, $\bar{B}^0$ events. The results are reported in table 36, for Analysis 1 and Analysis 2 respectively (to be compared with tables 17 and 21). Let us note the larger statistical error on $\mathrm{Re}z\frac{\mathrm{Re}\lambda_{CP}}{|\lambda_{CP}|}$ and $\mid q/p \mid$. The results are compatible within the statistical differences.

8.4 Results per tagging category

The fit has also been performed for each tagging category separately. In these fits the resolution function and mistags are extracted as in the nominal fit but now the physics parameters are allowed to be different for each tagging category. However, allowing 6 independent physics parameters for each category increase very significantly the total number of parameters, reducing the robustness and stability of the fit. To overcome this problem, Δm and $\frac{\mathrm{Im}\lambda_{CP}}{|\lambda_{CP}|}$ were fitted for all tagging categories together (as in the nominal fit), and only $\Delta\Gamma/\Gamma$, $\mid q/p \mid$, Rez and Imz were allowed to float for each category. The results from this check are shown in table 37, for Analysis 1 and Analysis 2 respectively. In the case of Analysis 2 they are also shown separately for $B_{CPK_S^0}$ and $B_{CPK_L^0}$. The results are in all cases compatible within statistics.

Parameter	Analysis 1	Analysis 2
Δm	0.5220 ± 0.0098	0.5215 ± 0.0098
$\Delta\Gamma/\Gamma$	$(-0.8 \pm 4.9) \cdot 10^{-2}$	$(-0.9 \pm 5.1) \cdot 10^{-2}$
$\mid q/p \mid$	0.938 ± 0.024	0.938 ± 0.024
$\frac{\mathrm{Im}\lambda_{CP}}{\lvert\lambda_{CP}\rvert}$	0.610 ± 0.085	0.626 ± 0.083
$\frac{\mathrm{Re}\lambda_{CP}}{\lvert\lambda_{CP}\rvert}\mathrm{Re}z$	—	-0.110 ± 0.054
$\mathrm{Im}z$	—	-0.916 ± 0.034

Table 36: Only shape fits. See text for explanation. These results must be compared to those of tables 17 and 21.

Parameter	Analysis 1	Analysis 2 all CP	Analysis 2 $B_{CPK^0_S}$ sample	Analysis 2 $B_{CPK^0_L}$ sample
Δm	0.5208 ± 0.0098	0.522 ± 0.010	0.5213 ± 0.0100	0.524 ± 0.010
$\Delta\Gamma/\Gamma(\texttt{Lepton})$	0.163 ± 0.079	0.154 ± 0.082	0.140 ± 0.091	0.14 ± 0.11
$\Delta\Gamma/\Gamma(\texttt{Kaon})$	$(-0.6 \pm 7.0) \cdot 10^{-2}$	$(-2.8 \pm 7.4) \cdot 10^{-2}$	$(-4.2 \pm 9.0) \cdot 10^{-2}$	-0.00 ± 0.12
$\Delta\Gamma/\Gamma(\texttt{NT1})$	-0.15 ± 0.10	-0.14 ± 0.11	-0.10 ± 0.12	-0.07 ± 0.16
$\Delta\Gamma/\Gamma(\texttt{NT2})$	-0.07 ± 0.10	$(-7.2 \pm 9.9) \cdot 10^{-2}$	-0.05 ± 0.12	-0.11 ± 0.12
$\mid q/p \mid (\texttt{Lepton})$	0.969 ± 0.029	0.971 ± 0.029	0.974 ± 0.030	0.969 ± 0.030
$\mid q/p \mid (\texttt{Kaon})$	0.956 ± 0.022	0.953 ± 0.021	0.956 ± 0.022	0.956 ± 0.022
$\mid q/p \mid (\texttt{NT1})$	0.920 ± 0.040	0.920 ± 0.040	0.924 ± 0.040	0.920 ± 0.040
$\mid q/p \mid (\texttt{NT2})$	0.920 ± 0.033	0.917 ± 0.033	0.918 ± 0.034	0.921 ± 0.033
$\frac{\mathrm{Im}\lambda_{CP}}{\lvert\lambda_{CP}\rvert}$	0.592 ± 0.082	0.617 ± 0.079	0.650 ± 0.086	0.44 ± 0.20
$\frac{\mathrm{Re}\lambda_{CP}}{\lvert\lambda_{CP}\rvert}\mathrm{Rez}(\texttt{Lepton})$	—	$(-6.6 \pm 6.5) \cdot 10^{-2}$	$(-7.3 \pm 6.5) \cdot 10^{-2}$	$(-8.4 \pm 9.8) \cdot 10^{-2}$
$\frac{\mathrm{Re}\lambda_{CP}}{\lvert\lambda_{CP}\rvert}\mathrm{Rez}(\texttt{Kaon})$	—	$(-7.8 \pm 7.1) \cdot 10^{-2}$	$(-9.5 \pm 7.8) \cdot 10^{-2}$	-0.07 ± 0.12
$\frac{\mathrm{Re}\lambda_{CP}}{\lvert\lambda_{CP}\rvert}\mathrm{Rez}(\texttt{NT1})$	—	-0.09 ± 0.12	-0.14 ± 0.13	-0.02 ± 0.18
$\frac{\mathrm{Re}\lambda_{CP}}{\lvert\lambda_{CP}\rvert}\mathrm{Rez}(\texttt{NT2})$	—	-0.04 ± 0.15	-0.05 ± 0.17	-0.06 ± 0.19
$\mathrm{Imz}(\texttt{Lepton})$	—	-0.940 ± 0.038	-0.929 ± 0.039	-0.931 ± 0.040
$\mathrm{Imz}(\texttt{Kaon})$	—	-0.846 ± 0.056	-0.834 ± 0.058	-0.836 ± 0.058
$\mathrm{Imz}(\texttt{NT1})$	—	-0.910 ± 0.068	-0.906 ± 0.070	-0.900 ± 0.069
$\mathrm{Imz}(\texttt{NT2})$	—	-0.825 ± 0.066	-0.818 ± 0.069	-0.814 ± 0.070

Table 37: Results per tagging category. GG resolution model was used.

8.5 Δt and $\sigma_{\Delta t}$ cuts variation

Likelihood fits were performed for different values of the Δt and $\sigma_{\Delta t}$ cuts. The chosen Δt cut values were $5, 10, 15, 20$ ps (20 is the nominal one). The set of cuts taken for $\sigma_{\Delta t}$ were $0.6, 1.0, 1.4, 1.8, 2.2$ ps (1.4 is the nominal). In the first case, finite normalization, according to equation (104), was used instead of the asymptotic one used in the nominal fit. The stability of the results compared to the nominal cuts is shown in figures 35 and 36.

8.6 Results from standard full Monte Carlo

The nominal fits were performed on the high statistics standard Monte Carlo (exclusive and inclusive charmonium), described in section 3. The fit results corresponding to Analysis 2 are given in tables 38 and 39, for the *GG* and *GExp* resolution models. Table 40 summarizes the Analysis 2 results (restricted to physical parameters) obtained from the exclusive and inclusive charmonium samples, all B_{CP} or $B_{CPK^0_S}$ and $B_{CPK^0_L}$ only separately. The B_{flav} peaking background in these fits was assumed to be 0. The $B_{CPK^0_S}$ peaking background in the exclusive sample was taken also 0, and 1.5% in the inclusive one. The non-J/ψ background components in the $J/\psi K^0_L$ sample were taken 0. The fit projections (global fit with all samples) onto the Δt axis and the corresponding normalized residuals (defined as the difference between the data and the fit projection), for each standard Monte Carlo (inclusive charmonium) sample abd tagging category separately are shown in figures 37, 38 (B_{flav}), 39 ($B_{CPK^0_S}$) and 40 ($B_{CPK^0_L}$). Let us note that for this check we did not keep the relative fractions of B_{flav}, $B_{CPK^0_S}$ and $B_{CPK^0_L}$ events as observed in the data but we just put together the maximum available standard Monte Carlo statistics.

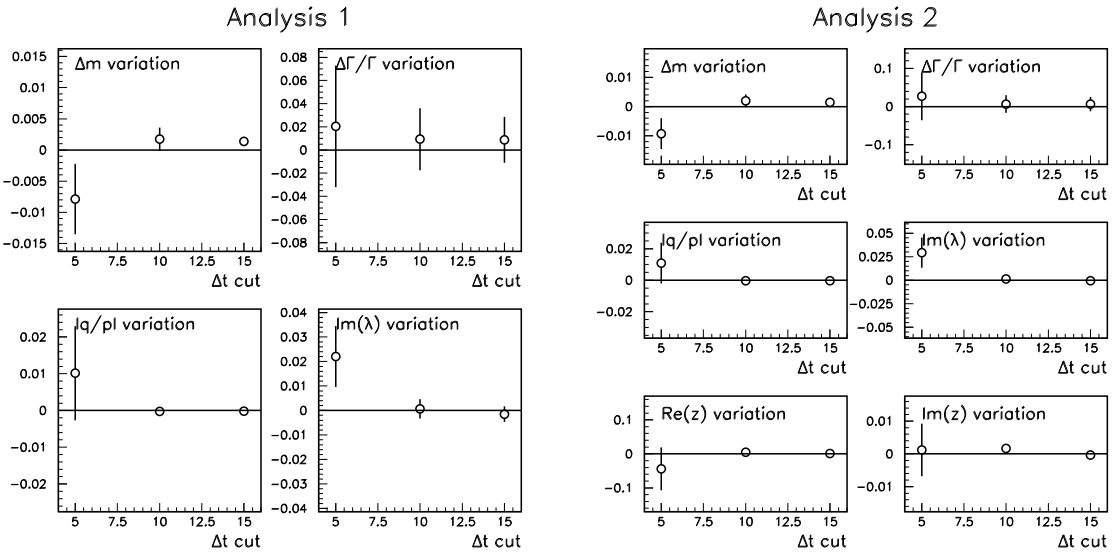

Figure 35: Stability of the fitted physical parameters from Analysis 1 and 2 against the Δt cut. The variation with respect to the nominal configuration is shown.

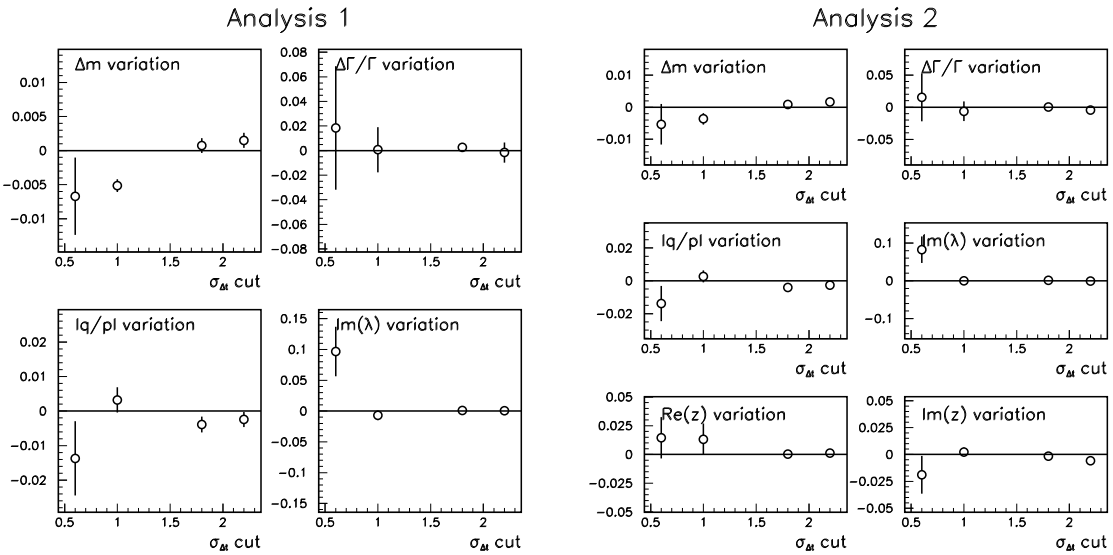

Figure 36: Stability of the fitted physical parameters from Analysis 1 and 2 against the $\sigma_{\Delta t}$ cut. The variation with respect to the nominal configuration is shown.

Parameter	excl. charmonium	incl. charmonium all CP
Δm	0.4792 ± 0.0051	0.4785 ± 0.0061
$\Delta\Gamma/\Gamma$	$(-1.7 \pm 1.3) \cdot 10^{-2}$	$(3.6 \pm 3.0) \cdot 10^{-2}$
$\mid q/p \mid$	1.007 ± 0.010	1.009 ± 0.012
$\frac{\mathrm{Im}\lambda_{CP}}{\mid\lambda_{CP}\mid}$	0.715 ± 0.017	0.679 ± 0.048
$\frac{\mathrm{Re}\lambda_{CP}}{\mid\lambda_{CP}\mid}$ Rez	$(-0.4 \pm 1.4) \cdot 10^{-2}$	$(-0.1 \pm 3.4) \cdot 10^{-2}$
Imz	$(-0.3 \pm 1.7) \cdot 10^{-2}$	$(-0.8 \pm 2.1) \cdot 10^{-2}$
$\frac{\mathrm{Im}\lambda_{flav}}{\mid\lambda_{flav}\mid}$	-0.51 ± 0.69	-0.81 ± 0.82
$\frac{\mathrm{Im}\lambda_{flav}}{\mid\lambda_{flav}\mid}$	-0.12 ± 0.71	-0.29 ± 0.87
$\frac{\mathrm{Im}\lambda_{tag}}{\mid\lambda_{tag}\mid}$	-0.19 ± 0.63	-0.24 ± 0.91
$\frac{\mathrm{Im}\lambda_{tag}}{\mid\lambda_{tag}\mid}$	-0.22 ± 0.64	-0.28 ± 0.95
S_{core}	1.308 ± 0.027	1.309 ± 0.041
δ_{core}^{lepton}	-0.152 ± 0.031	-0.152 ± 0.044
δ_{core}^{kaon}	-0.323 ± 0.019	-0.358 ± 0.026
δ_{core}^{NT1}	-0.166 ± 0.040	-0.233 ± 0.055
δ_{core}^{NT2}	-0.272 ± 0.028	-0.322 ± 0.039
f_{tail}	$(1.98 \pm 0.62) \cdot 10^{-2}$	$(2.1 \pm 1.3) \cdot 10^{-2}$
S_{tail}	6.4 ± 1.0	5.3 ± 1.4
δ_{tail}	-1.43 ± 0.57	-1.51 ± 0.84
$f_{outlier}$	$(1.83 \pm 0.87) \cdot 10^{-3}$	$(2.3 \pm 1.1) \cdot 10^{-3}$
w_0^{lepton}	$(5.9 \pm 1.3) \cdot 10^{-2}$	$(5.7 \pm 1.4) \cdot 10^{-2}$
w_0^{kaon}	$(5.4 \pm 1.1) \cdot 10^{-2}$	$(6.1 \pm 1.2) \cdot 10^{-2}$
w_0^{NT1}	0.169 ± 0.022	0.156 ± 0.024
w_0^{NT2}	0.352 ± 0.020	0.365 ± 0.022
w_{slope}^{lepton}	$(0.7 \pm 2.4) \cdot 10^{-2}$	$(1.3 \pm 2.6) \cdot 10^{-2}$
w_{slope}^{kaon}	0.181 ± 0.018	0.167 ± 0.019
w_{slope}^{NT1}	$(3.8 \pm 3.7) \cdot 10^{-2}$	$(7.2 \pm 4.1) \cdot 10^{-2}$
w_{slope}^{NT2}	$(0.3 \pm 3.0) \cdot 10^{-2}$	$(-1.2 \pm 3.3) \cdot 10^{-2}$
Δw^{lepton}	$(4.6 \pm 8.5) \cdot 10^{-3}$	$(1.7 \pm 9.3) \cdot 10^{-3}$
Δw^{kaon}	$(-2.20 \pm 0.59) \cdot 10^{-2}$	$(-2.08 \pm 0.69) \cdot 10^{-2}$
Δw^{NT1}	$(1.3 \pm 1.2) \cdot 10^{-2}$	$(1.8 \pm 1.5) \cdot 10^{-2}$
Δw^{NT2}	$(-2.84 \pm 0.86) \cdot 10^{-2}$	$(-3.7 \pm 1.2) \cdot 10^{-2}$
$f_{prompt,B_{flav}}^{lepton}$	0.40 ± 0.12	0.40 ± 0.11
$f_{prompt,B_{flav}}^{kaon}$	0.327 ± 0.059	0.326 ± 0.058
$f_{prompt,B_{flav}}^{NT1}$	0.33 ± 0.12	0.33 ± 0.12
$f_{prompt,B_{flav}}^{NT2}$	0.333 ± 0.090	0.334 ± 0.089
S_{back}	1.76 ± 0.12	1.76 ± 0.11
δ_{back}	-0.104 ± 0.062	$(-9.6 \pm 6.1) \cdot 10^{-2}$
$f_{back,outlier}$	$(6.3 \pm 5.6) \cdot 10^{-3}$	$(6.3 \pm 5.6) \cdot 10^{-3}$
$w_{0,prompt}^{lepton}$	$(0.0 \pm 5.3) \cdot 10^{-4}$	$(0.0 \pm 5.3) \cdot 10^{-4}$
$w_{0,prompt}^{kaon}$	$(0.0 \pm 4.5) \cdot 10^{-4}$	$(0.0 \pm 4.6) \cdot 10^{-4}$
$w_{0,prompt}^{NT1}$	0.09 ± 0.15	0.08 ± 0.15
$w_{0,prompt}^{NT2}$	0.17 ± 0.12	0.17 ± 0.12
$w_{0,non-prompt}^{lepton}$	0.288 ± 0.069	0.287 ± 0.069
$w_{0,non-prompt}^{kaon}$	0.422 ± 0.040	0.423 ± 0.040
$w_{0,non-prompt}^{NT1}$	0.420 ± 0.083	0.418 ± 0.083
$w_{0,non-prompt}^{NT2}$	0.496 ± 0.057	0.495 ± 0.057
$\tau_{non-prompt}$	1.568 ± 0.096	1.573 ± 0.096
$f_{prompt,B_{CPK_S^0}}$	0.200 ± 0.094	0.31 ± 0.13
$\tau_{non-prompt,B_{CPK_S^0}}$	2.60 ± 0.31	1.92 ± 0.29

Table 38: Analysis 2 results, *GG* resolution model for the standard full Monte Carlo sample (exclusive and inclusive charmonium).

Parameter	excl. charmonium	incl. charmonium
Δm	0.4789 ± 0.0051	0.4773 ± 0.0062
$\Delta\Gamma/\Gamma$	$(-1.3 \pm 1.3) \cdot 10^{-2}$	$(4.3 \pm 3.2) \cdot 10^{-2}$
$\mid q/p \mid$	1.0066 ± 0.0100	1.009 ± 0.012
$\frac{\mathrm{Im}\lambda_{CP}}{\mid\lambda_{CP}\mid}$	0.713 ± 0.017	0.679 ± 0.048
$\frac{\mathrm{Re}\lambda_{CP}}{\mid\lambda_{CP}\mid}\mathrm{Rez}$	$(-0.2 \pm 1.4) \cdot 10^{-2}$	$(0.1 \pm 3.6) \cdot 10^{-2}$
Imz	$(-0.8 \pm 1.7) \cdot 10^{-2}$	$(-0.9 \pm 2.0) \cdot 10^{-2}$
$\frac{\mathrm{Im}\lambda_{flav}}{\mid\lambda_{flav}\mid}$	-0.77 ± 0.68	-0.87 ± 0.82
$\frac{\mathrm{Im}\lambda_{flav}}{\mid\lambda_{flav}\mid}$	-0.20 ± 0.71	-0.32 ± 0.86
$\frac{\mathrm{Im}\lambda_{tag}}{\mid\lambda_{tag}\mid}$	-0.26 ± 0.63	-0.12 ± 0.91
$\frac{\mathrm{Im}\lambda_{tag}}{\mid\lambda_{tag}\mid}$	-0.15 ± 0.64	-0.12 ± 0.95
S	1.213 ± 0.028	1.219 ± 0.043
τ_r^{lepton}	1.06 ± 0.38	0.62 ± 0.68
τ_r^{kaon}	1.18 ± 0.14	1.14 ± 0.17
τ_r^{NT1}	0.83 ± 0.54	0.82 ± 0.50
τ_r^{NT2}	0.58 ± 0.22	0.37 ± 0.25
f_{Exp}^{lepton}	0.166 ± 0.069	0.27 ± 0.31
f_{Exp}^{kaon}	0.306 ± 0.038	0.350 ± 0.055
f_{Exp}^{NT1}	0.22 ± 0.15	0.31 ± 0.20
f_{Exp}^{NT2}	0.50 ± 0.19	0.91 ± 0.62
$f_{outlier}$	$(4.87 \pm 0.76) \cdot 10^{-3}$	$(4.17 \pm 0.99) \cdot 10^{-3}$
w_0^{lepton}	$(6.0 \pm 1.3) \cdot 10^{-2}$	$(5.6 \pm 1.4) \cdot 10^{-2}$
w_0^{kaon}	$(5.6 \pm 1.1) \cdot 10^{-2}$	$(6.2 \pm 1.2) \cdot 10^{-2}$
w_0^{NT1}	0.169 ± 0.022	0.155 ± 0.024
w_0^{NT2}	0.352 ± 0.020	0.364 ± 0.022
w_{slope}^{lepton}	$(0.9 \pm 2.4) \cdot 10^{-2}$	$(1.7 \pm 2.6) \cdot 10^{-2}$
w_{slope}^{kaon}	0.176 ± 0.018	0.166 ± 0.019
w_{slope}^{NT1}	$(4.1 \pm 3.7) \cdot 10^{-2}$	$(7.6 \pm 4.1) \cdot 10^{-2}$
w_{slope}^{NT2}	$(0.6 \pm 3.0) \cdot 10^{-2}$	$(-0.9 \pm 3.3) \cdot 10^{-2}$
Δw^{lepton}	$(4.4 \pm 8.5) \cdot 10^{-3}$	$(1.6 \pm 9.3) \cdot 10^{-3}$
Δw^{kaon}	$(-2.19 \pm 0.59) \cdot 10^{-2}$	$(-2.09 \pm 0.70) \cdot 10^{-2}$
Δw^{NT1}	$(1.3 \pm 1.2) \cdot 10^{-2}$	$(1.8 \pm 1.5) \cdot 10^{-2}$
Δw^{NT2}	$(-2.82 \pm 0.86) \cdot 10^{-2}$	$(-3.7 \pm 1.2) \cdot 10^{-2}$
$f_{prompt,B_{flav}}^{lepton}$	0.38 ± 0.12	0.38 ± 0.12
$f_{prompt,B_{flav}}^{kaon}$	0.321 ± 0.059	0.326 ± 0.057
$f_{prompt,B_{flav}}^{NT1}$	0.32 ± 0.12	0.33 ± 0.12
$f_{prompt,B_{flav}}^{NT2}$	0.325 ± 0.093	0.326 ± 0.091
S_{back}	1.73 ± 0.12	1.73 ± 0.11
$\tau_{r,back}$	5.0000 ± 0.0085	5.000 ± 0.010
$f_{back,outlier}$	$(0.0 \pm 1.1) \cdot 10^{-4}$	$(0.0 \pm 1.1) \cdot 10^{-4}$
$w_{0,prompt}^{lepton}$	$(0.0 \pm 5.2) \cdot 10^{-4}$	$(0.0 \pm 5.3) \cdot 10^{-4}$
$w_{0,prompt}^{kaon}$	$(0.0 \pm 4.3) \cdot 10^{-4}$	$(0.0 \pm 4.5) \cdot 10^{-4}$
$w_{0,prompt}^{NT1}$	0.08 ± 0.17	0.08 ± 0.16
$w_{0,prompt}^{NT2}$	0.17 ± 0.12	0.17 ± 0.12
$w_{0,non-prompt}^{lepton}$	0.276 ± 0.068	0.275 ± 0.067
$w_{0,non-prompt}^{kaon}$	0.419 ± 0.040	0.423 ± 0.039
$w_{0,non-prompt}^{NT1}$	0.421 ± 0.085	0.422 ± 0.085
$w_{0,non-prompt}^{NT2}$	0.493 ± 0.059	0.492 ± 0.058
$\tau_{non-prompt}$	1.521 ± 0.085	1.539 ± 0.085
$f_{prompt,B_{CPK_S^0}}$	0.191 ± 0.096	0.31 ± 0.13
$\tau_{non-prompt,B_{CPK_S^0}}$	2.52 ± 0.31	1.91 ± 0.28

Table 39: Analysis 2 results, *GExp* resolution model for the standard full Monte Carlo sample (exclusive and inclusive charmonium).

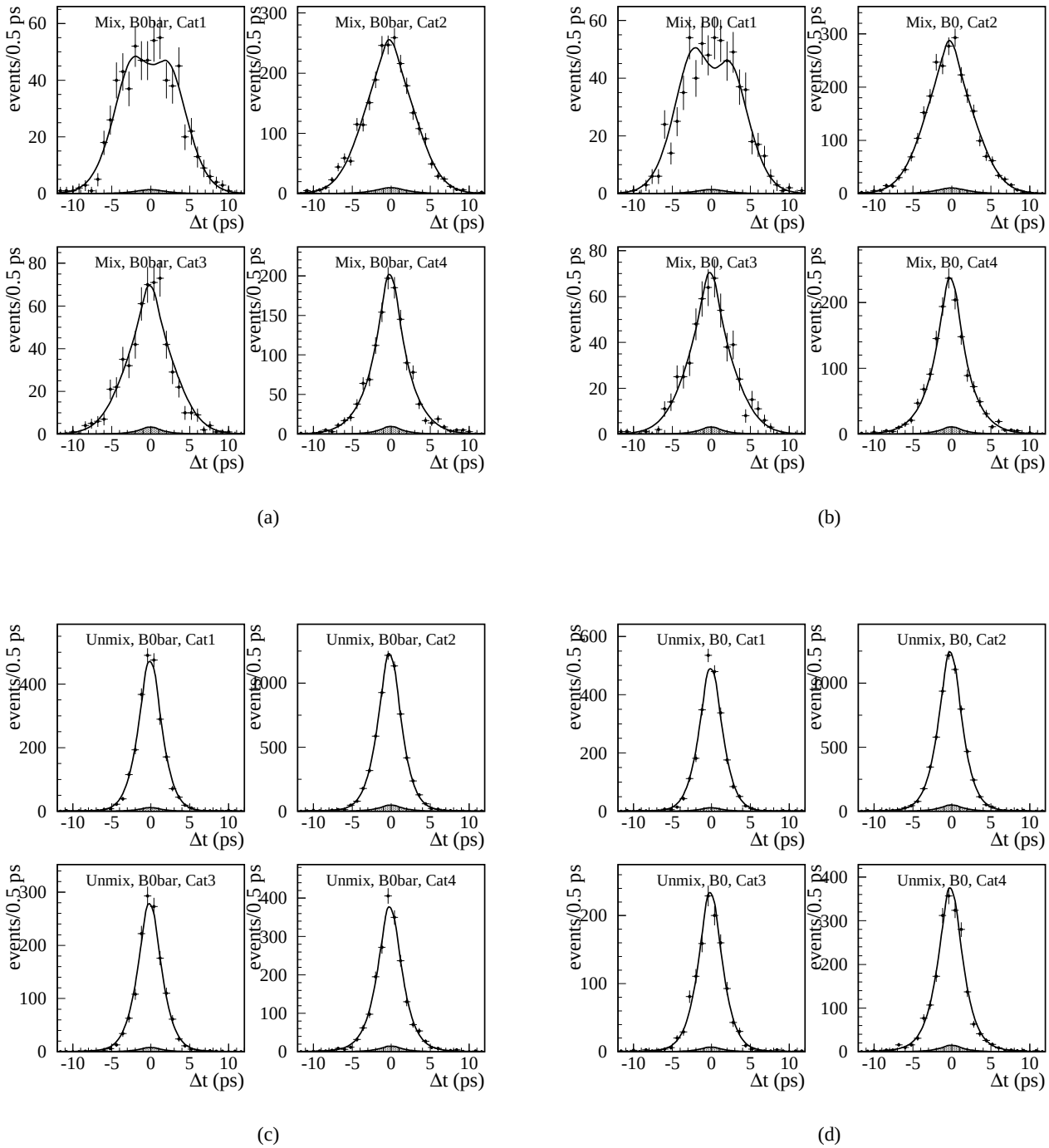

Figure 37: Δt projections of the nominal fit (Analysis 2) for the B_{flav} standard Monte Carlo sample: (a) mixed $\bar{B}^0$ tagged, (b) mixed B^0 tagged, (c) unmixed $\bar{B}^0$ tagged and (d) unmixed B^0 tagged (GG model), for each tagging category.

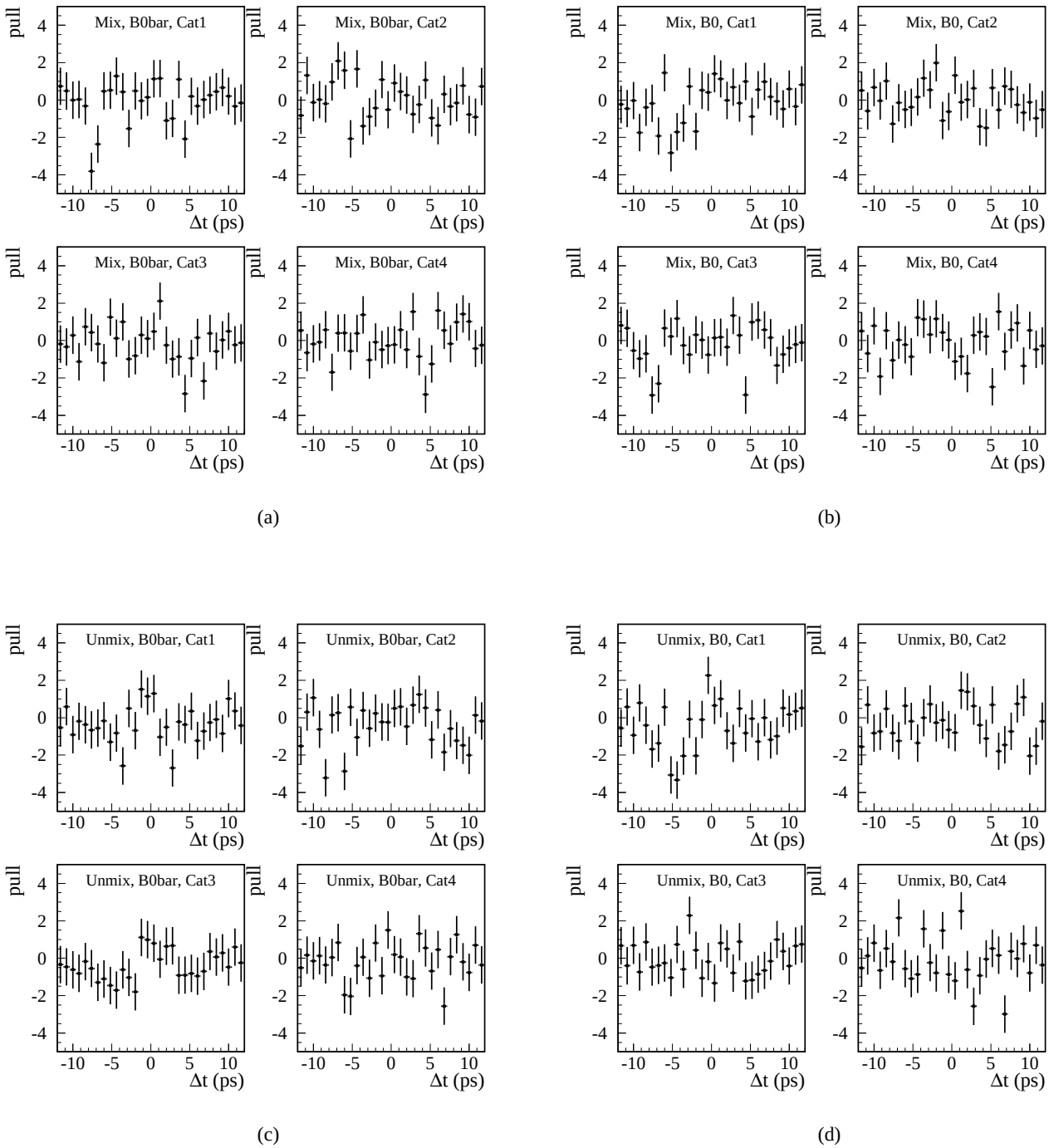

Figure 38: Normalized residuals of the Δt projections of the nominal fit (Analysis 2) for the B_{flav} standard Monte Carlo sample: (a) mixed $\bar{B}^0$ tagged, (b) mixed B^0 tagged, (c) unmixed $\bar{B}^0$ tagged and (d) unmixed B^0 tagged (*GG* model), for each tagging category.

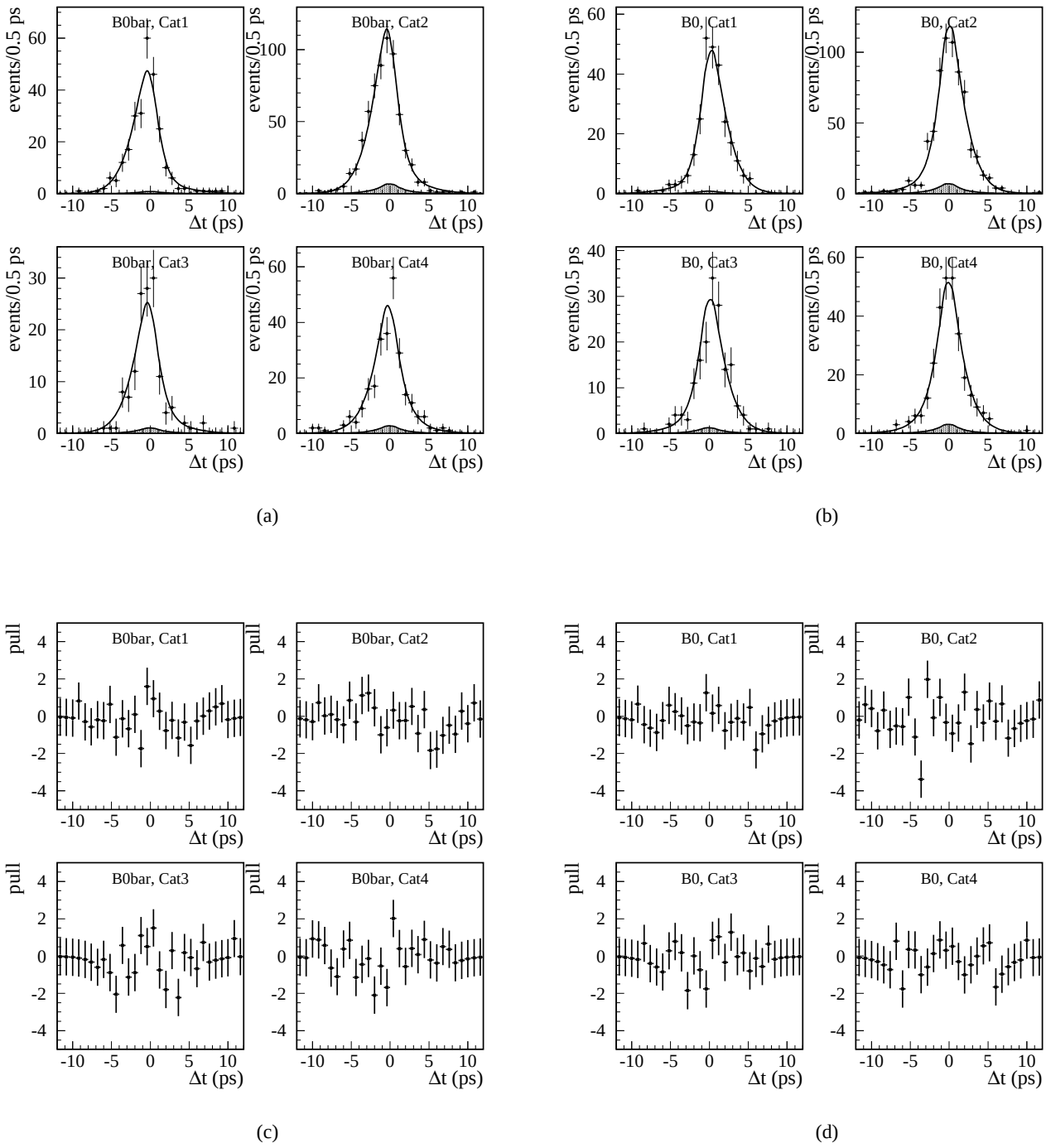

Figure 39: Δt projections and normalized residuals of the nominal fit (Analysis 2) for the $B_{CPK^0_S}$ standard inclusive Monte Carlo sample: (a)(c) $\bar{B}^0$ tagged, (b)(d) B^0 tagged (*GG* model), for each tagging category.

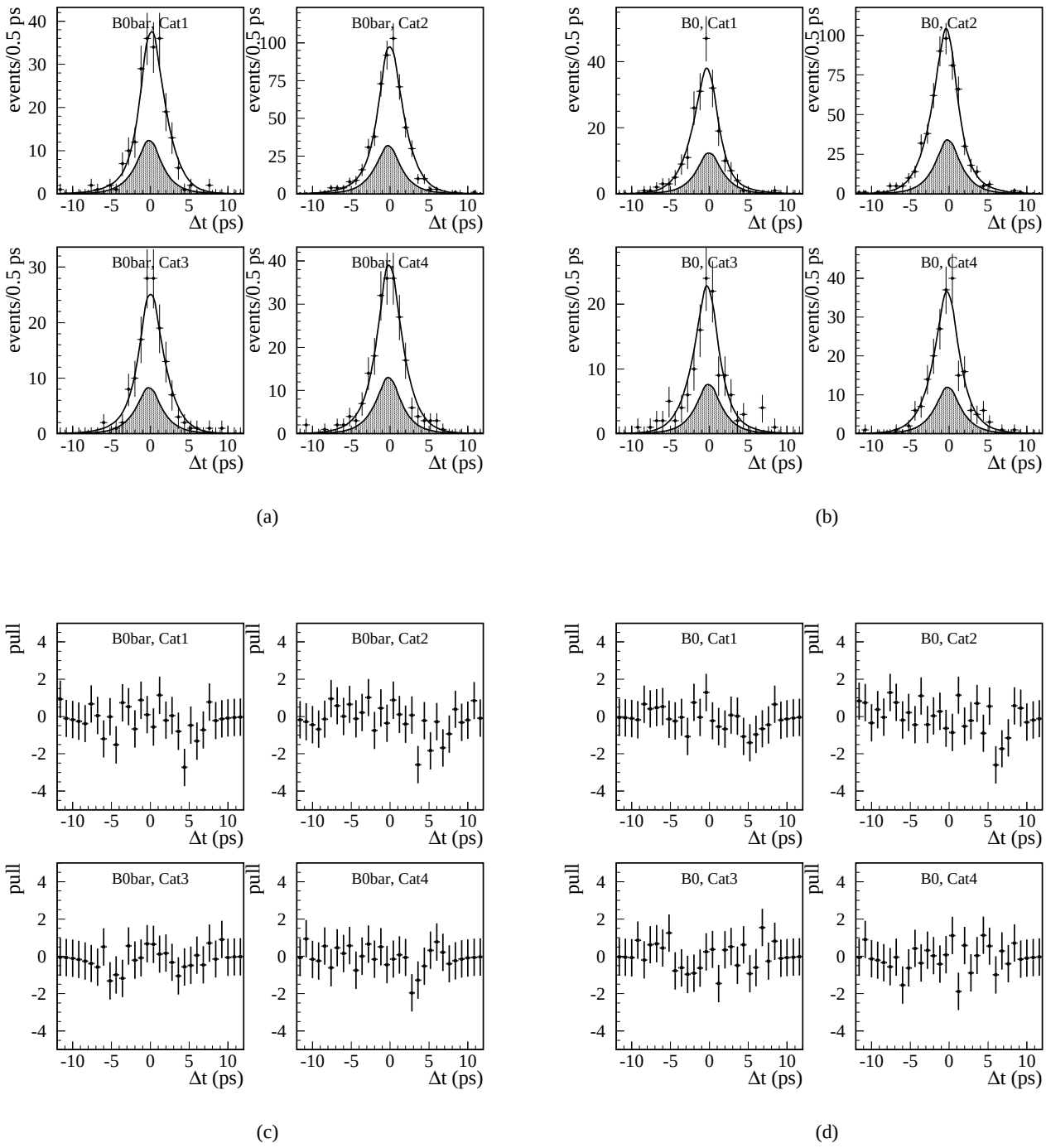

Figure 40: Δt projections and normalized residuals of the nominal fit (Analysis 2) for the $B_{CPK^0_L}$ standard inclusive Monte Carlo sample: (a)(c) $\overline{B}^0$ tagged, (b)(d) B^0 tagged (*GG* model), for each tagging category.

Parameter	excl. charmonium	incl. charmonium all CP	incl. charmonium $B_{CPK_S^0}$	incl. charmonium $B_{CPK_L^0}$
Δm	0.4792 ± 0.0051	0.4785 ± 0.0061	0.4789 ± 0.0061	0.4791 ± 0.0065
$\Delta\Gamma/\Gamma$	$(-1.7 \pm 1.3) \cdot 10^{-2}$	$(3.6 \pm 3.0) \cdot 10^{-2}$	$(-1.2 \pm 3.5) \cdot 10^{-2}$	$(9.7 \pm 3.8) \cdot 10^{-2}$
$\mid q/p \mid$	1.007 ± 0.010	1.009 ± 0.012	1.014 ± 0.012	1.009 ± 0.012
$\frac{\mathrm{Im}\lambda_{CP}}{\mid\lambda_{CP}\mid}$	0.715 ± 0.017	0.679 ± 0.048	0.703 ± 0.057	0.614 ± 0.090
$\frac{\mathrm{Re}\lambda_{CP}}{\mid\lambda_{CP}\mid}\mathrm{Re}z$	$(-0.4 \pm 1.4) \cdot 10^{-2}$	$(-0.1 \pm 3.4) \cdot 10^{-2}$	$(-1.0 \pm 3.8) \cdot 10^{-2}$	$(3.9 \pm 4.0) \cdot 10^{-2}$
$\mathrm{Im}z$	$(-0.3 \pm 1.7) \cdot 10^{-2}$	$(-0.8 \pm 2.1) \cdot 10^{-2}$	$(0.0 \pm 2.2) \cdot 10^{-2}$	$(-1.4 \pm 2.3) \cdot 10^{-2}$

Table 40: Analysis 2 results, limited to physics parameters, *GG* resolution model for the standard full Monte Carlo sample, with exclusive, inclusive charmonium with both CP samples, $B_{CPK_S^0}$ and $B_{CPK_L^0}$ samples.

8.7 Asymmetries from standard full standard Monte Carlo

All possible CPT/CP/T asymmetries for the standard Monte Carlo (inclusive charmonium) sample have been constructed, for each tagging category separately and for all categories together (see reference [11] -which follows the discussion in [13]- for details):

- the mixing asymmetry (figure 41),

$$A_{Mixing}(\Delta t) \equiv \frac{N_{\overline{B}^0_{tag}B^0_{flav}}(\Delta t) + N_{B^0_{tag}\overline{B}^0_{flav}}(\Delta t) - N_{B^0_{tag}B^0_{flav}}(\Delta t) - N_{\overline{B}^0_{tag}\overline{B}^0_{flav}}(\Delta t)}{N_{\overline{B}^0_{tag}B^0_{flav}}(\Delta t) + N_{B^0_{tag}\overline{B}^0_{flav}}(\Delta t) + N_{B^0_{tag}B^0_{flav}}(\Delta t) + N_{\overline{B}^0_{tag}\overline{B}^0_{flav}}(\Delta t)} \tag{130}$$

  proportional to $\frac{\cos(\Delta m \Delta t)}{\cosh(\Delta\Gamma\Delta t/2)}$;

- the T flavor asymmetry (Kabir asymmetry) (figure 42),

$$A_{T,flav}(\Delta t) \equiv \frac{N_{B^0_{tag}B^0_{flav}}(\Delta t) - N_{\overline{B}^0_{tag}\overline{B}^0_{flav}}(\Delta t)}{N_{B^0_{tag}B^0_{flav}}(\Delta t) + N_{\overline{B}^0_{tag}\overline{B}^0_{flav}}(\Delta t)} \tag{131}$$

  primarily proportional to $2\frac{1-|q/p|^2}{1+|q/p|^2}$ and independent of Δt. In the limit $\Delta\Gamma = 0$ this asymmetry vanishes;

- the CPT flavor asymmetry (figure 43),

$$A_{CPT,flav}(\Delta t) \equiv \frac{N_{\overline{B}^0_{tag}B^0_{flav}}(\Delta t) - N_{B^0_{tag}\overline{B}^0_{flav}}(\Delta t)}{N_{\overline{B}^0_{tag}B^0_{flav}}(\Delta t) + N_{B^0_{tag}\overline{B}^0_{flav}}(\Delta t)} \tag{132}$$

  primarily proportional to $2\frac{\mathrm{Re}z\sinh(\Delta\Gamma\Delta t/2)+\mathrm{Im}z\sin(\Delta m\Delta t)}{\cosh(\Delta\Gamma\Delta t/2)+\cos(\Delta m\Delta t)}$, so it vanishes for $\Delta\Gamma$=0 since it is linear in both $\Delta\Gamma$ and z;

- the CP asymmetries (figures 44 and 45),

$$\begin{aligned} A_{CP,B_{CPK_S^0}}(\Delta t) &\equiv \frac{N_{B^0_{tag}B_{CPK_S^0}}(\Delta t) - N_{\overline{B}^0_{tag}B_{CPK_S^0}}(\Delta t)}{N_{B^0_{tag}B_{CPK_S^0}}(\Delta t) + N_{\overline{B}^0_{tag}B_{CPK_S^0}}(\Delta t)} \\ A_{CP,B_{CPK_L^0}}(\Delta t) &\equiv \frac{N_{B^0_{tag}B_{CPK_L^0}}(\Delta t) - N_{\overline{B}^0_{tag}B_{CPK_L^0}}(\Delta t)}{N_{B^0_{tag}B_{CPK_L^0}}(\Delta t) + N_{\overline{B}^0_{tag}B_{CPK_L^0}}(\Delta t)} \end{aligned} \tag{133}$$

which has contributions from CP/T-violating (odd Δt dependence) and CP/CPT-violating (even Δt dependence) terms, independent of $\Delta\Gamma$. The asymmetry also containts correction terms which are proportional to $\Delta\Gamma$, but cannot introduce fake effects since those terms are at the same time proportional to CP/T and CP/CPT-violating terms;

- the non-genuine[4] T asymmetries (Δt asymmetries) (figures 46, 47, 48 and 49),

$$\begin{aligned}
A_{\Delta t,B_{CPK_S^0},\bar{B}^0}(\Delta t) &\equiv \frac{N_{\overline{B}^0_{tag}B_{CPK_S^0}}(\Delta t)-N_{\overline{B}^0_{tag}B_{CPK_S^0}}(-\Delta t)}{N_{\overline{B}^0_{tag}B_{CPK_S^0}}(\Delta t)+N_{\overline{B}^0_{tag}B_{CPK_S^0}}(-\Delta t)}\\
A_{\Delta t,B_{CPK_S^0},B^0}(\Delta t) &\equiv \frac{N_{B^0_{tag}B_{CPK_S^0}}(\Delta t)-N_{B^0_{tag}B_{CPK_S^0}}(-\Delta t)}{N_{B^0_{tag}B_{CPK_S^0}}(\Delta t)+N_{B^0_{tag}B_{CPK_S^0}}(-\Delta t)}\\
A_{\Delta t,B_{CPK_L^0},\bar{B}^0}(\Delta t) &\equiv \frac{N_{\overline{B}^0_{tag}B_{CPK_L^0}}(\Delta t)-N_{\overline{B}^0_{tag}B_{CPK_L^0}}(-\Delta t)}{N_{\overline{B}^0_{tag}B_{CPK_L^0}}(\Delta t)+N_{\overline{B}^0_{tag}B_{CPK_L^0}}(-\Delta t)}\\
A_{\Delta t,B_{CPK_L^0},B^0}(\Delta t) &\equiv \frac{N_{B^0_{tag}B_{CPK_L^0}}(\Delta t)-N_{B^0_{tag}B_{CPK_L^0}}(\Delta t)}{N_{B^0_{tag}B_{CPK_L^0}}(\Delta t)+N_{B^0_{tag}B_{CPK_L^0}}(-\Delta t)}
\end{aligned} \tag{134}$$

which has contributions from CP/T and CP/CPT violating terms as well as $\Delta\Gamma$ terms which do not depend on CP/T and CP/CPT violating parameters and therefore are a potencial source of fake effects. In the limit $\Delta\Gamma$=0 this asymmetry equals to the genuine T asymmetry;

- the genuine T asymmetry (figure 50),

$$A_T(\Delta t) \equiv \frac{N_{B^0_{tag}B_{CPK_S^0}}(\Delta t)-N_{\overline{B}^0_{tag}B_{CPK_L^0}}(-\Delta t)}{N_{B^0_{tag}B_{CPK_S^0}}(\Delta t)+N_{\overline{B}^0_{tag}B_{CPK_L^0}}(-\Delta t)} \tag{135}$$

which includes CP/T and CP/CPT violating terms. $\Delta\Gamma$ correction terms are also proportional to CP/T and CP/CPT violating parameters so $\Delta\Gamma \neq 0$ cannot introduce fake effects. In the limit $\Delta\Gamma = 0$ the asymmetry is primarily proportional to CP/T violation (odd in Δt);

- the non-genuine CPT asymmetries (CPΔt asymmetries) (figures 51 and 52),

$$\begin{aligned}
A_{CP\Delta t,B_{CPK_S^0}}(\Delta t) &\equiv \frac{N_{B^0_{tag}B_{CPK_S^0}}(\Delta t)-N_{\overline{B}^0_{tag}B_{CPK_S^0}}(-\Delta t)}{N_{B^0_{tag}B_{CPK_S^0}}(\Delta t)+N_{\overline{B}^0_{tag}B_{CPK_S^0}}(-\Delta t)}\\
A_{CP\Delta t,B_{CPK_L^0}}(\Delta t) &\equiv \frac{N_{B^0_{tag}B_{CPK_L^0}}(\Delta t)-N_{\overline{B}^0_{tag}B_{CPK_L^0}}(-\Delta t)}{N_{B^0_{tag}B_{CPK_L^0}}(\Delta t)+N_{\overline{B}^0_{tag}B_{CPK_L^0}}(-\Delta t)}
\end{aligned} \tag{136}$$

which has, similarly to the non-genuine T asymmetries, contributions from CP/T and CP/CPT violating terms as well as $\Delta\Gamma$ terms which do not depend on CP/T and CP/CPT parameters, and therefore are a potencial source of fake effects. In the limit $\Delta\Gamma$=0 this asymmetry equals to the genuine CPT asymmetry;

[4] By non-genuine asymmetries we mean asymmetries which do not involve processes conected by any fundamental discrete symmetry but that in the limit $\Delta\Gamma$=0 they turn out to be equivalent to the genuine case, i.e. the asymmetries defined with the processes related by that fundamental symmetry [13].

- the genuine CPT asymmetries (figures 53 and 54),

$$
\begin{aligned}
A_{CPT,B^0}(\Delta t) &\equiv \frac{N_{B^0_{tag}B_{CPK^0_S}}(\Delta t) - N_{B^0_{tag}B_{CPK^0_L}}(-\Delta t)}{N_{B^0_{tag}B_{CPK^0_S}}(\Delta t) + N_{B^0_{tag}B_{CPK^0_L}}(-\Delta t)} \\
A_{CPT,\bar{B}^0}(\Delta t) &\equiv \frac{N_{\overline{B}^0_{tag}B_{CPK^0_S}}(\Delta t) - N_{\overline{B}^0_{tag}B_{CPK^0_L}}(-\Delta t)}{N_{\overline{B}^0_{tag}B_{CPK^0_S}}(\Delta t) + N_{\overline{B}^0_{tag}B_{CPK^0_L}}(-\Delta t)}
\end{aligned}
\tag{137}
$$

  which also contains CP/T and CP/CPT violation terms but is primarily even in Δt and mainly proportional to Rez. To leading order, this asymmetry has no $\Delta\Gamma$ terms. A non-vanishing value of Rez will genuinely manifest in this asymmetry.

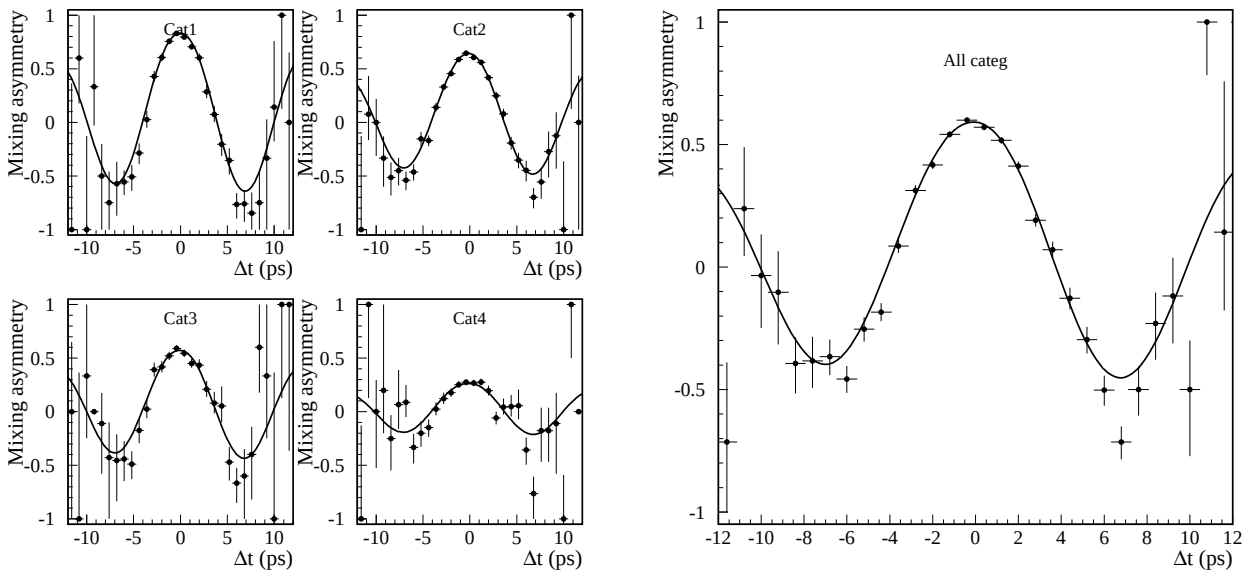

Figure 41: The mixing asymmetry $A_{Mixing}(\Delta t)$ as defined in equation (130) for each tagging category (left) and all categories together (right), for standard Monte Carlo (inclusive charmonium).

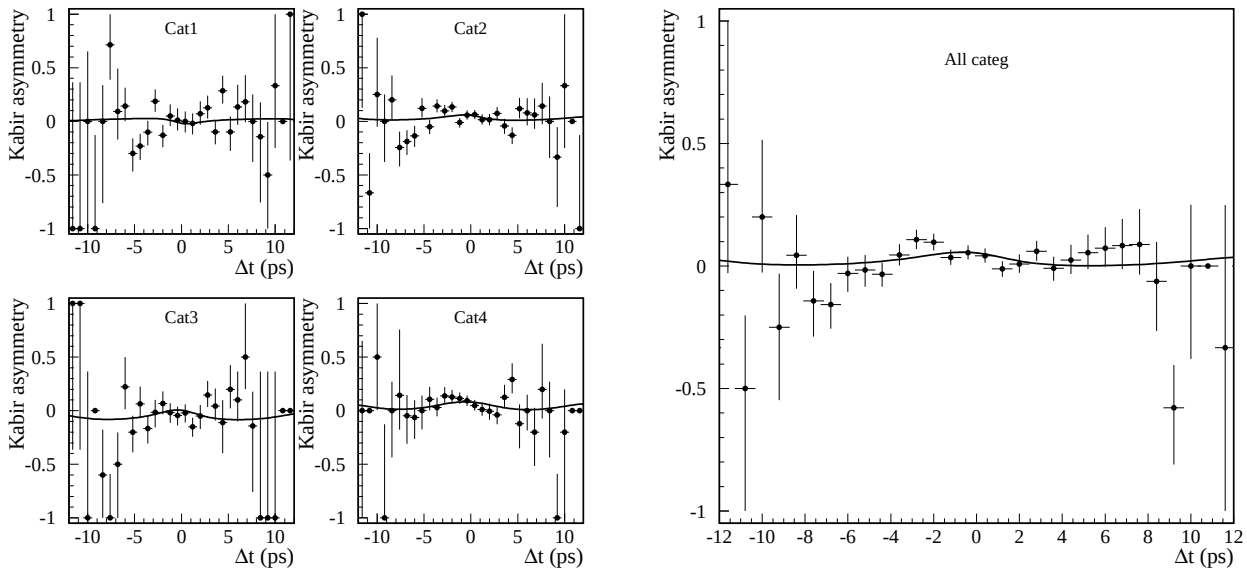

Figure 42: Kabir asymmetry $A_{T,flav}(\Delta t)$ as defined in equation (131) for each tagging category (left) and all categories together (right), for standard Monte Carlo (inclusive charmonium).

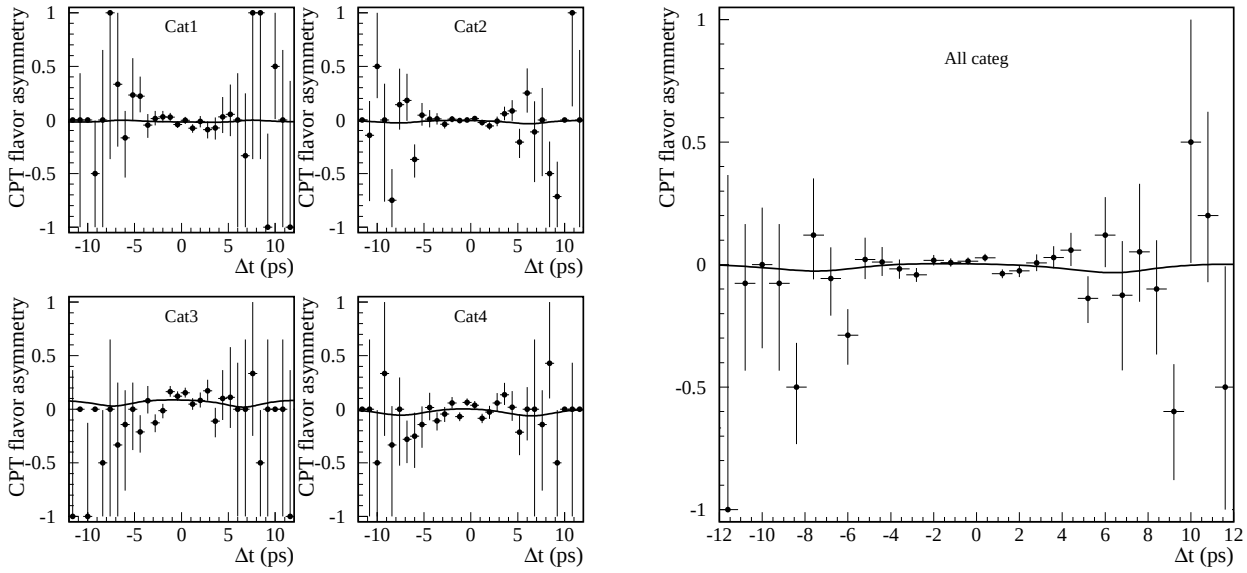

Figure 43: The CPT flavor asymmetry $A_{CPT,flav}(\Delta t)$ as defined in equation (132) for each tagging category (left) and all categories together (right), for standard Monte Carlo (inclusive charmonium).

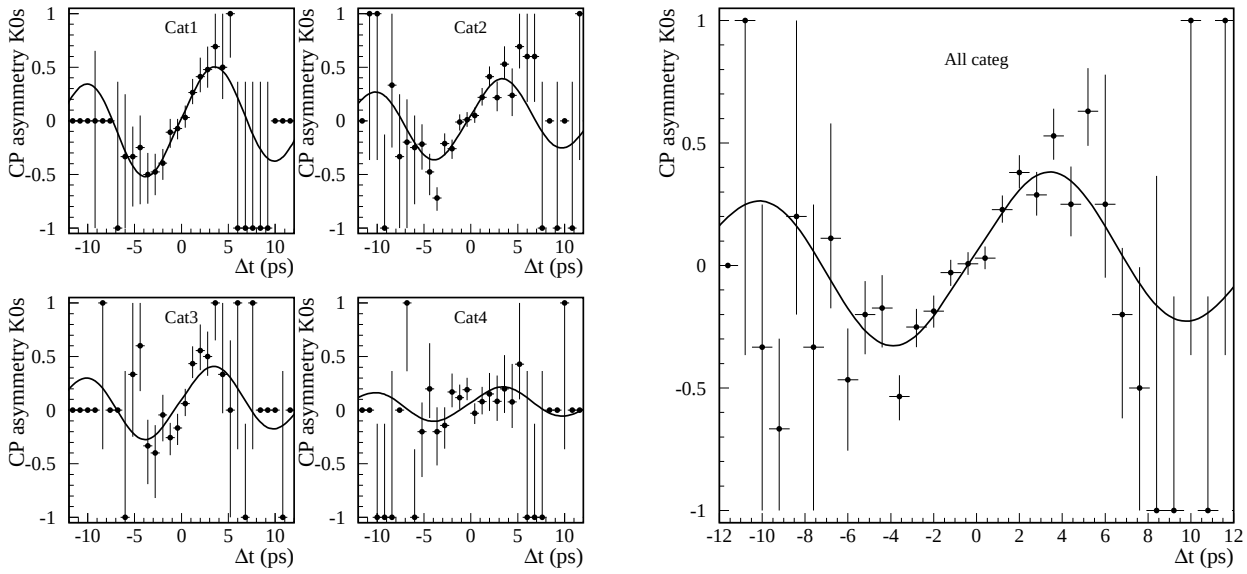

Figure 44: The CP asymmetry $A_{CP,B_{CPK^0_S}}(\Delta t)$ as defined in equation (133) for each tagging category (left) and all categories together (right), for standard Monte Carlo (inclusive charmonium).

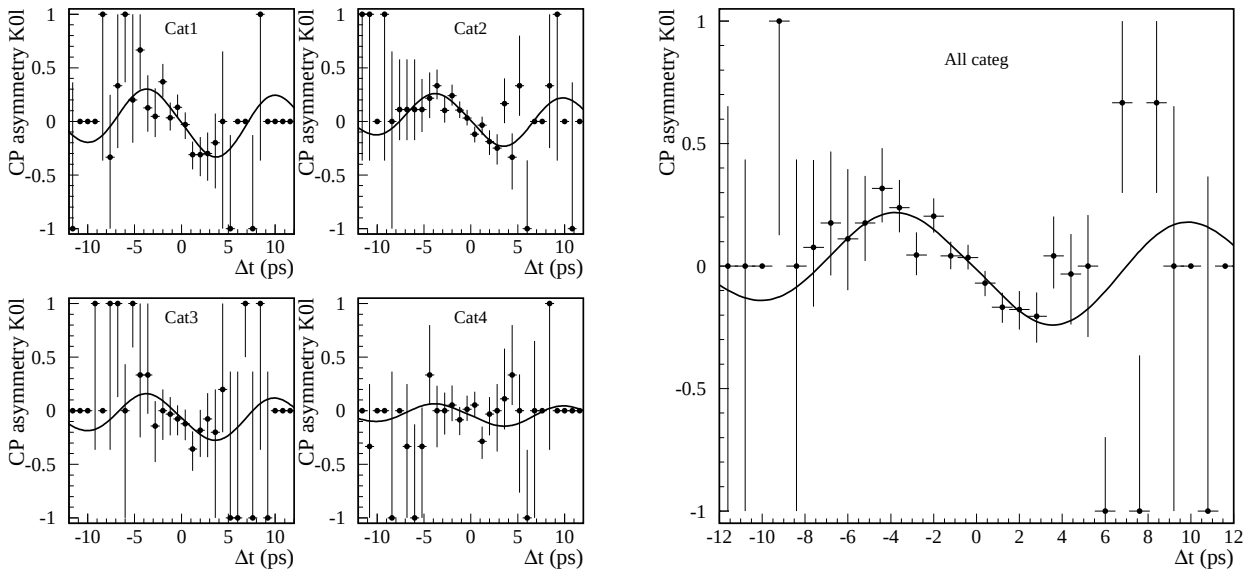

Figure 45: The CP asymmetry $A_{CP,B_{CPK^0_L}}(\Delta t)$ as defined in equation (133) for each tagging category (left) and all categories together (right), for standard Monte Carlo (inclusive charmonium).

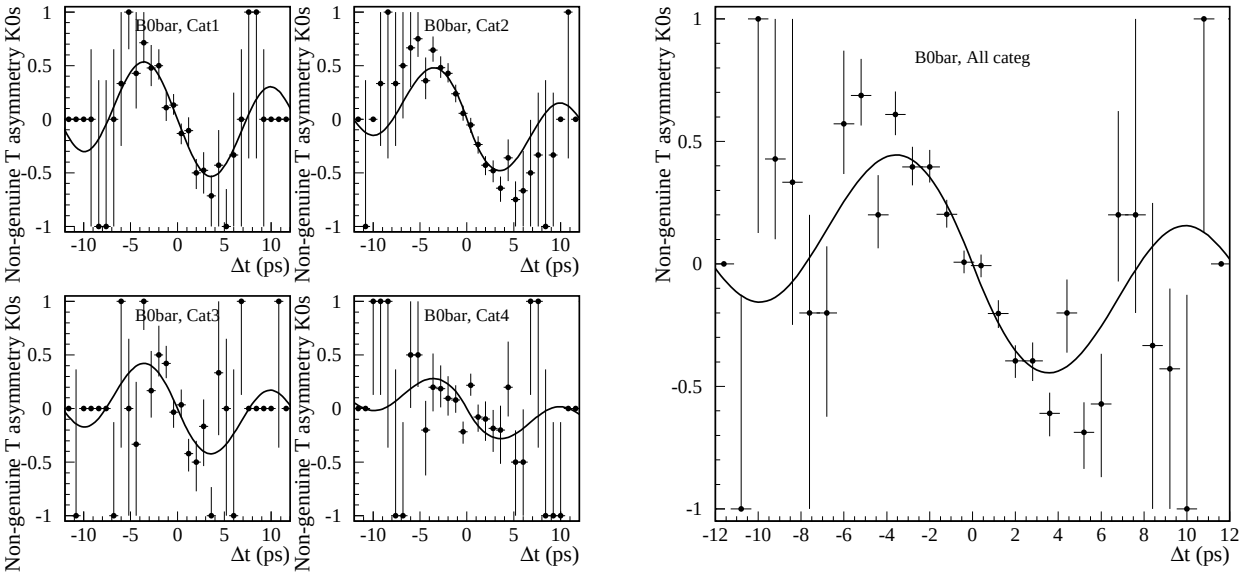

Figure 46: The non-genuine T asymmetry $A_{\Delta t, B_{CPK^0_S}, \bar{B}^0}(\Delta t)$ as defined in equation (134) for each tagging category (left) and all categories together (right), for standard Monte Carlo (inclusive charmonium).

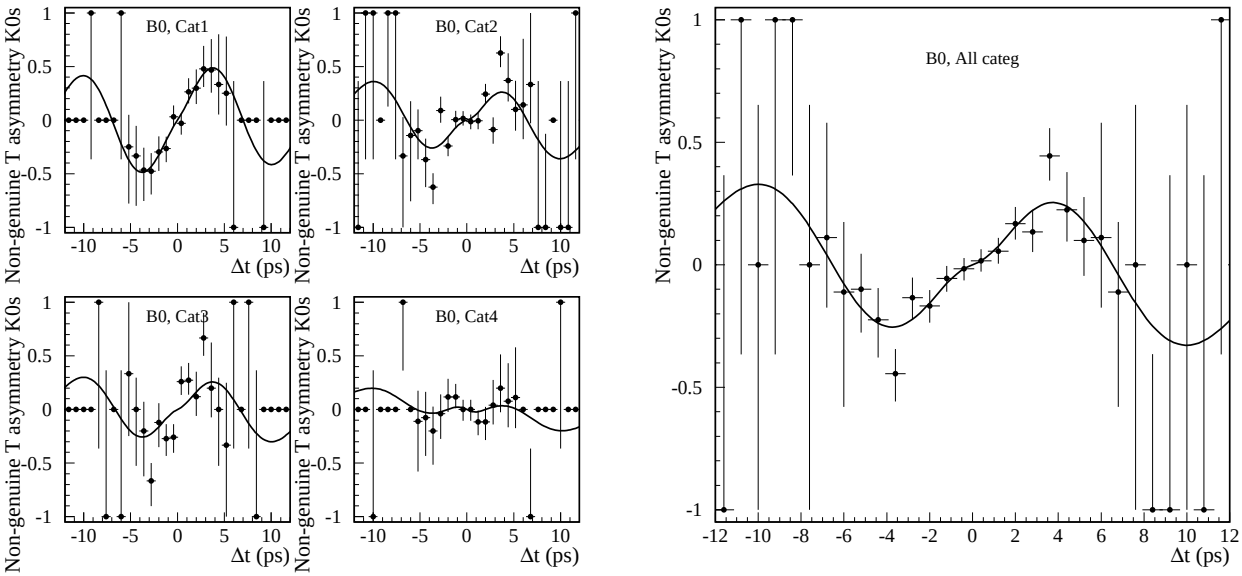

Figure 47: The non-genuine T asymmetry $A_{\Delta t, B_{CPK^0_S}, B^0}(\Delta t)$ as defined in equation (134) for each tagging category (left) and all categories together (right), for standard Monte Carlo (inclusive charmonium).

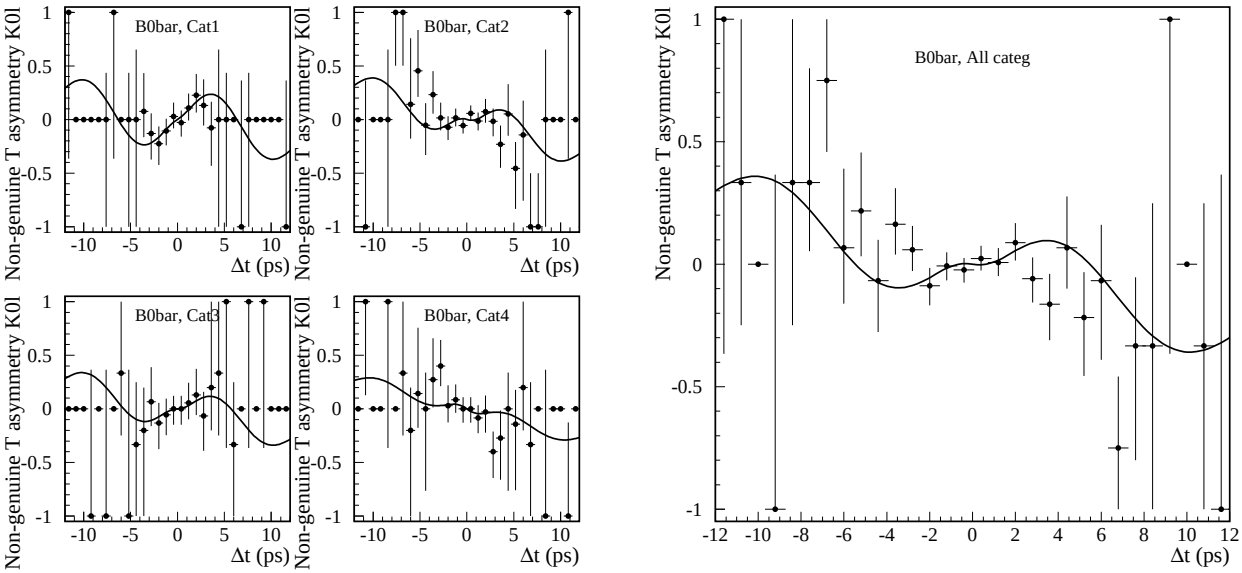

Figure 48: The non-genuine T asymmetry $A_{\Delta t, B_{CPK^0_L}, \bar{B}^0}(\Delta t)$ as defined in equation (134) for each tagging category (left) and all categories together (right), for standard Monte Carlo (inclusive charmonium).

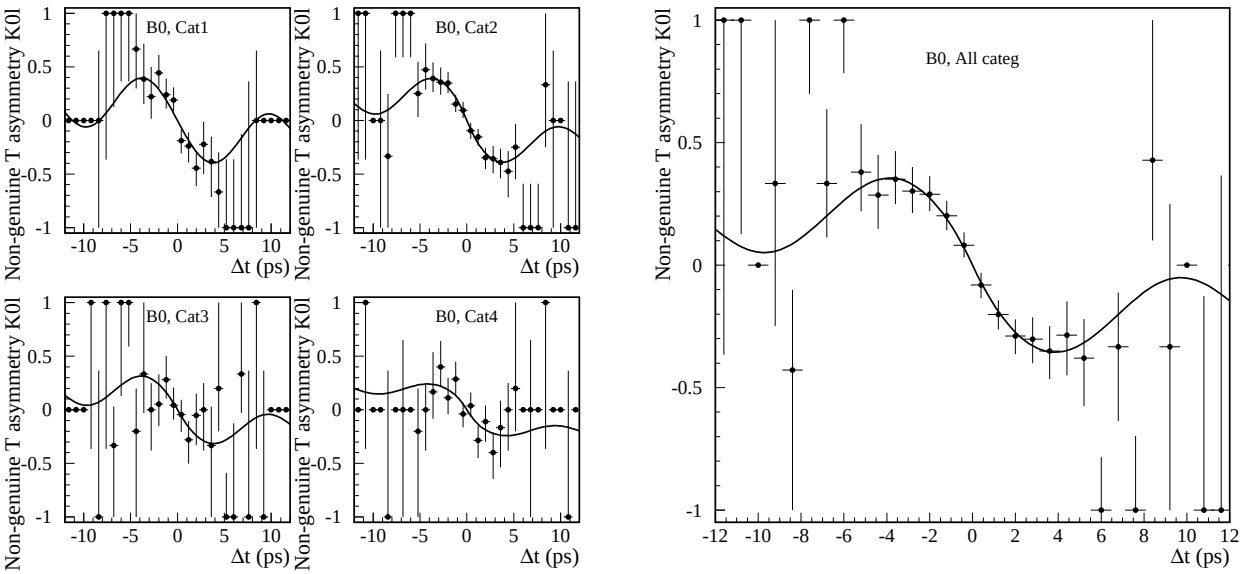

Figure 49: The non-genuine T asymmetry $A_{\Delta t, B_{CPK^0_L}, B^0}(\Delta t)$ as defined in equation (134) for each tagging category (left) and all categories together (right), for standard Monte Carlo (inclusive charmonium).

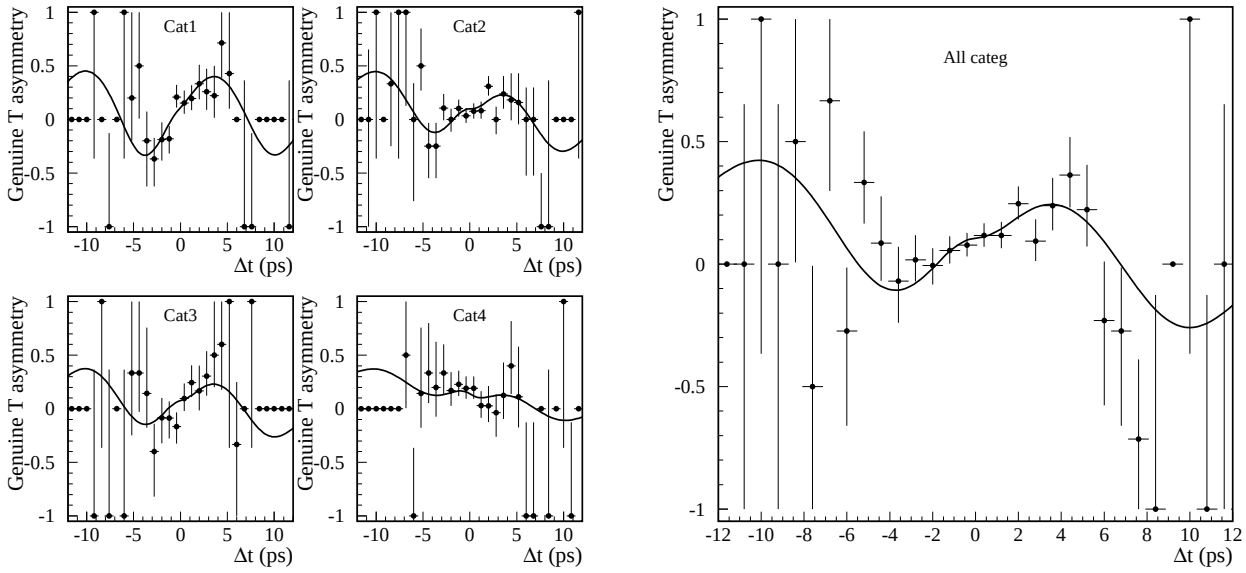

Figure 50: The genuine T asymmetry $A_T(\Delta t)$ as defined in equation (135) for each tagging category (left) and all categories together (right), for standard Monte Carlo (inclusive charmonium).

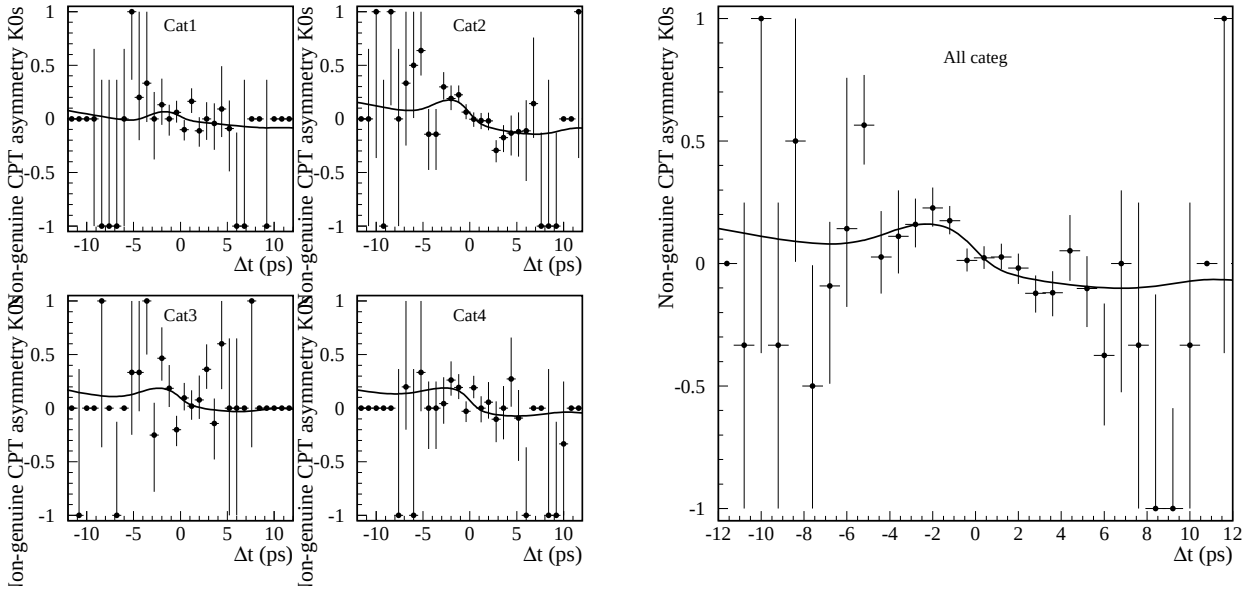

Figure 51: The non-genuine CPT asymmetry $A_{CP\Delta t,B_{CPK^0_S}}(\Delta t)$ as defined in equation (136) for each tagging category (left) and all categories together (right), for standard Monte Carlo (inclusive charmonium).

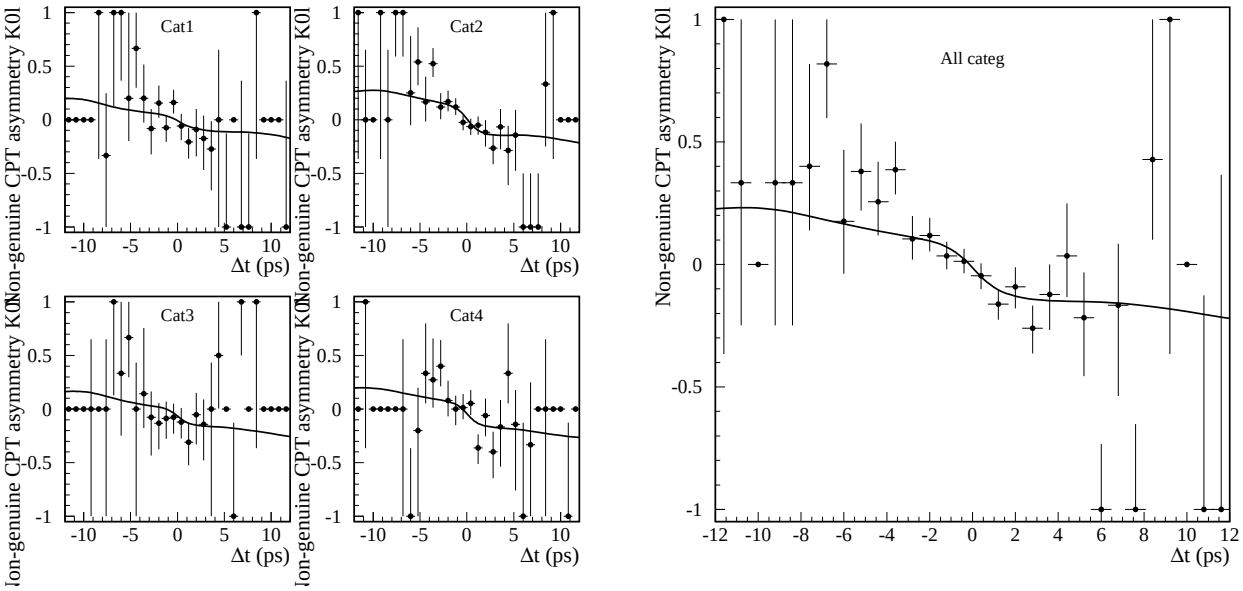

Figure 52: The non-genuine CPT asymmetry $A_{CP\Delta t,B_{CPK_L^0}}(\Delta t)$ as defined in equation (136) for each tagging category (left) and all categories together (right), for standard Monte Carlo (inclusive charmonium).

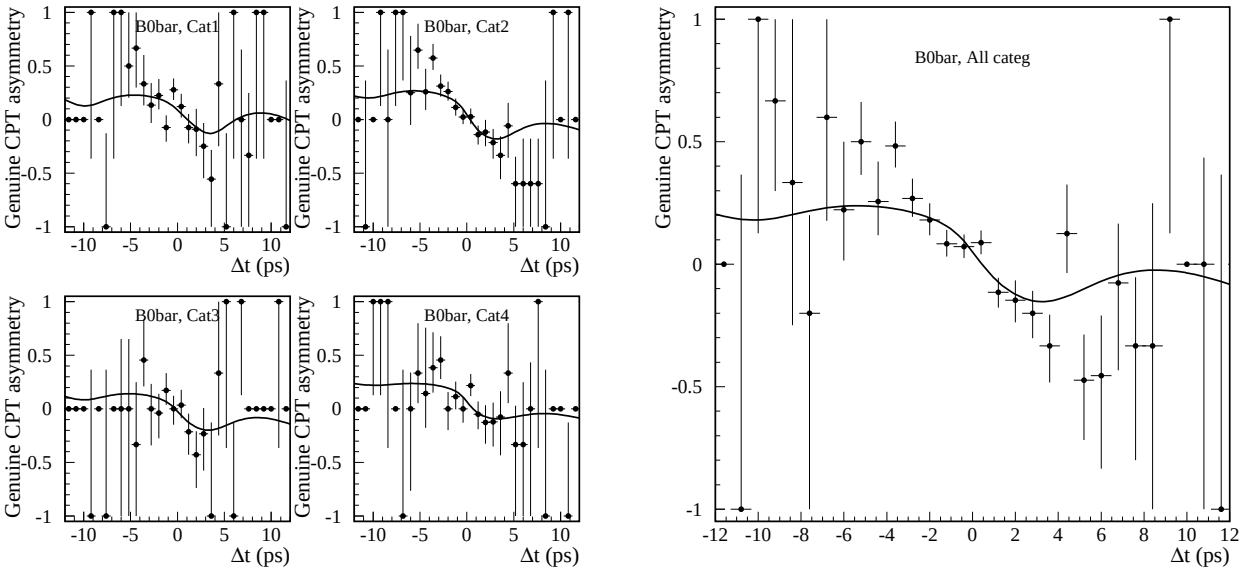

Figure 53: The genuine CPT asymmetry $A_{CPT,\bar{B}^0}(\Delta t)$ as defined in equation (137) for each tagging category (left) and all categories together (right), for standard Monte Carlo (inclusive charmonium).

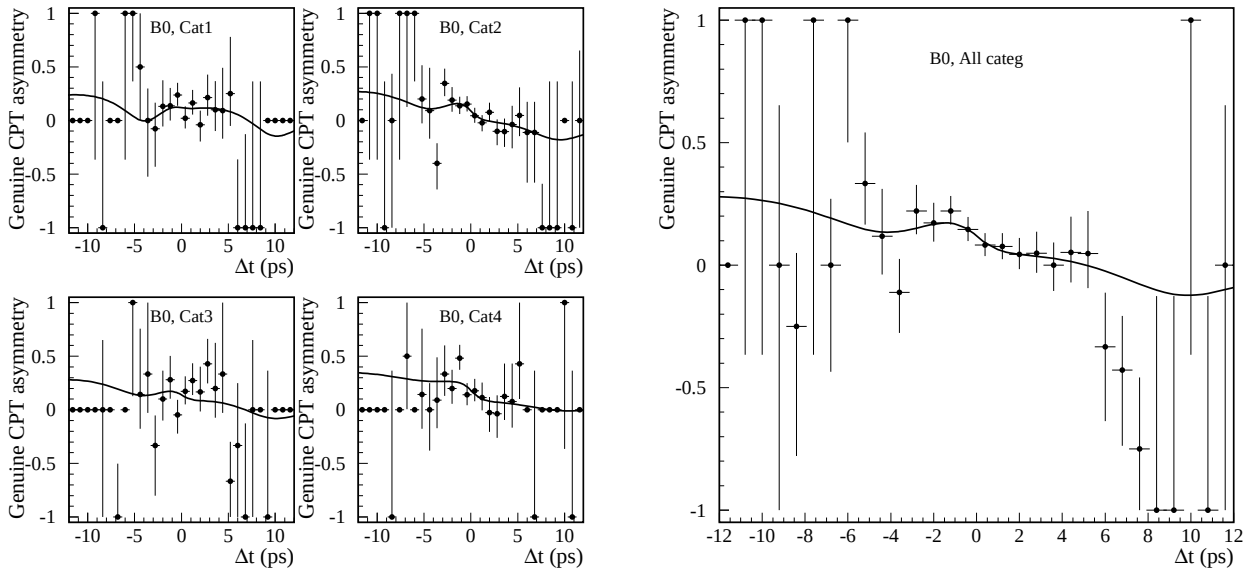

Figure 54: The genuine CPT asymmetry $A_{CPT,B^0}(\Delta t)$ as defined in equation (137) for each tagging category (left) and all categories together (right), for standard Monte Carlo (inclusive charmonium).

8.8 Results from dedicated full Monte Carlo

The nominal fits were also performed on the high statistics dedicated Monte Carlo described in section 3. As in the case of the standard Monte Carlo sample, we did not keep the relative fractions of B_{flav}, $B_{CPK_S^0}$ and $B_{CPK_L^0}$ events as observed in the data but we just used all the available statistics. Fits to Monte Carlo truth (perfect resolution, perfect tag) were first applied in order to check the correctness of the truth values in this dedicated Monte Carlo production. The results of these MC truth fits are given in table 41.

Parameter	Fit result
τ_B	1.542 ± 0.005
Δm	0.4748 ± 0.0018
$\Delta\Gamma/\Gamma$	0.205 ± 0.008
$\mid q/p \mid$	1.033 ± 0.004
$\frac{\mathrm{Im}\lambda_{CP}}{\mid\lambda_{CP}\mid}$	0.681 ± 0.009
$\frac{\mathrm{Re}\lambda_{CP}}{\mid\lambda_{CP}\mid}$Rez	-0.003 ± 0.006
Imz	0.005 ± 0.005

Table 41: Results from maximum likelihood fits to the MC truth information (perfect resolution, perfect tag) in the dedicated full Monte Carlo prodution.

The fit results corresponding to Analysis 1 and Analysis 2, for the *GG* and *GExp* resolution models, are given in tables 42–45. All peaking backgrounds in these fits were assumed zero.

8.9 Results from reweighted dedicated full Monte Carlo

The dedicated full Monte Carlo was also used to "generate" samples with CPT violation ($z \neq 0$) and DCKM effects ($\lambda_{tag}, \bar{\lambda}_{tag}, \lambda_{flav}, \bar{\lambda}_{flav} \neq 0$). This was done using reweighting techniques.

8.9.1 Strategy

The reweighting of the dedicated Monte Carlo events is performed using the truth values of Δt and the flavors of the two B mesons in the event. The flavor of the B mesons allows us to classify the B_{flav} and B_{CP} events according to 4 categories each: (B^0_{tag} B^0_{flav}, $\overline{B}^0_{tag}$ B^0_{flav}, B^0_{tag} $\overline{B}^0_{flav}$ and $\overline{B}^0_{tag}$ $\overline{B}^0_{flav}$) and (B^0_{tag} $\eta_{CP} = -1, \overline{B}^0_{tag}$ $\eta_{CP} = -1, B^0_{tag}$ $\eta_{CP} = +1, \overline{B}^0_{tag}$ $\eta_{CP} = +1$), respectively. For each event class, we then calculate the ratio of the new and original (standard events) PDF's. While doing this, special attention must be put to the fact that the new physics parameters change the time-integrated rates. As with this technique we only want to change the physics but not the detector effects, the two PDF's entering into the ratio must use a common normalization, i.e. the new PDF must not be renormalized with the new physics parameter values. In this way, the change in the number of events in each event category is purely due to physics. Figure 55 shows the PDF ratios (new/original), corresponding to the physics paramaters of the CPT reweighted configuration given in table 46.

Parameter	B^0 fit results (*GG* model)
Δm	0.4812 ± 0.0047
$\Delta\Gamma/\Gamma$	0.182 ± 0.015
$\mid q/p \mid$	1.0398 ± 0.0091
$\frac{\mathrm{Im}\lambda_{CP}}{\mid\lambda_{CP}\mid}$	0.703 ± 0.021
S_{core}	1.197 ± 0.044
δ_{core}^{lepton}	-0.131 ± 0.040
δ_{core}^{kaon}	-0.293 ± 0.027
δ_{core}^{NT1}	-0.172 ± 0.048
δ_{core}^{NT2}	-0.243 ± 0.035
f_{tail}	$(8.6 \pm 2.7) \cdot 10^{-2}$
S_{tail}	3.22 ± 0.32
δ_{tail}	-1.44 ± 0.36
$f_{outlier}$	$(2.00 \pm 0.65) \cdot 10^{-3}$
w_0^{lepton}	$(5.2 \pm 1.1) \cdot 10^{-2}$
w_0^{kaon}	$(6.37 \pm 0.94) \cdot 10^{-2}$
w_0^{NT1}	0.203 ± 0.020
w_0^{NT2}	0.343 ± 0.017
w_{slope}^{lepton}	$(0.8 \pm 2.0) \cdot 10^{-2}$
w_{slope}^{kaon}	0.162 ± 0.015
w_{slope}^{NT1}	$(1.3 \pm 3.3) \cdot 10^{-2}$
w_{slope}^{NT2}	$(-0.4 \pm 2.5) \cdot 10^{-2}$
Δw^{lepton}	$(-4.8 \pm 7.1) \cdot 10^{-3}$
Δw^{kaon}	$(-1.39 \pm 0.52) \cdot 10^{-2}$
Δw^{NT1}	$(0.7 \pm 1.1) \cdot 10^{-2}$
Δw^{NT2}	$(-2.02 \pm 0.85) \cdot 10^{-2}$

Parameter	B^0 fit results (*GG* model)
$\frac{\mathrm{Im}\lambda_{flav}}{\mid\lambda_{flav}\mid}$	-0.42 ± 0.50
$\frac{\mathrm{Im}\lambda_{flav}}{\mid\lambda_{flav}\mid}$	-0.68 ± 0.52
$\frac{\mathrm{Im}\lambda_{tag}}{\mid\lambda_{tag}\mid}$	0.14 ± 0.49
$\frac{\mathrm{Im}\lambda_{tag}}{\mid\lambda_{tag}\mid}$	0.51 ± 0.52
$f_{prompt,B_{flav}}^{lepton}$	0.402 ± 0.074
$f_{prompt,B_{flav}}^{kaon}$	0.368 ± 0.044
$f_{prompt,B_{flav}}^{NT1}$	0.351 ± 0.084
$f_{prompt,B_{flav}}^{NT2}$	0.510 ± 0.058
S_{back}	1.898 ± 0.089
δ_{back}	-0.246 ± 0.054
$f_{back,outlier}$	$(4.2 \pm 5.7) \cdot 10^{-3}$
$w_{0,prompt}^{lepton}$	$(0.00 \pm 0.24) \cdot 10^{-3}$
$w_{0,prompt}^{kaon}$	$(0.00 \pm 0.81) \cdot 10^{-3}$
$w_{0,prompt}^{NT1}$	0.05 ± 0.11
$w_{0,prompt}^{NT2}$	0.270 ± 0.053
$w_{0,non-prompt}^{lepton}$	0.402 ± 0.061
$w_{0,non-prompt}^{kaon}$	0.444 ± 0.034
$w_{0,non-prompt}^{NT1}$	0.484 ± 0.066
$w_{0,non-prompt}^{NT2}$	0.592 ± 0.052
$\tau_{non-prompt}$	1.753 ± 0.094
$f_{prompt,B_{CPK_S^0}}$	0.29 ± 0.15
$\tau_{non-prompt,B_{CPK_S^0}}$	1.99 ± 0.38

Table 42: Results from dedicated full Monte Carlo, Analysis 1 fit, *GG* resolution function.

8.9.2 Results from Monte Carlo truth fits

Fits to Monte Carlo truth (perfect resolution, perfect tag) were first applied in order to check that the generated values are correct. In the case of the DCKM reweighted sample, r_{tag}, $\bar{r}_{tag}$, $\frac{\mathrm{Im}\lambda_{tag}}{\mid\lambda_{tag}\mid}$, $\frac{\mathrm{Im}\bar{\lambda}_{tag}}{\mid\lambda_{tag}\mid}$, r_{flav}, $\bar{r}_{flav}$, $\frac{\mathrm{Im}\lambda_{flav}}{\mid\lambda_{flav}\mid}$ and $\frac{\mathrm{Im}\bar{\lambda}_{flav}}{\mid\lambda_{flav}\mid}$ were fixed to the generated values. The results of these fits are given in table 47.

8.9.3 Results from nominal fits

The fit results corresponding to the Analysis 2 fits from the CPT reweighted samples, for the *GG* and *GExp* resolution models, are given in tables 48 and 49. Tables 50 and 51 show the fit results, again for Analysis 2 and 1 respectively, from the DCKM reweighted samples. In all cases the fitted values are consistent with the generated ones.

Parameter	B^0 fit results (*GG* model)
Δm	0.4812 ± 0.0047
$\Delta\Gamma/\Gamma$	0.182 ± 0.015
$\mid q/p \mid$	1.0397 ± 0.0091
$\frac{\mathrm{Im}\lambda_{CP}}{\mid\lambda_{CP}\mid}$	0.703 ± 0.021
$\frac{\mathrm{Re}\lambda_{CP}}{\mid\lambda_{CP}\mid}\mathrm{Rez}$	$(0.4 \pm 1.5) \cdot 10^{-2}$
Imz	$(-0.3 \pm 1.6) \cdot 10^{-2}$
S_{core}	1.197 ± 0.044
δ_{core}^{lepton}	-0.131 ± 0.040
δ_{core}^{kaon}	-0.292 ± 0.027
δ_{core}^{NT1}	-0.172 ± 0.048
δ_{core}^{NT2}	-0.243 ± 0.035
f_{tail}	$(8.6 \pm 2.7) \cdot 10^{-2}$
S_{tail}	3.22 ± 0.32
δ_{tail}	-1.44 ± 0.36
$f_{outlier}$	$(1.99 \pm 0.65) \cdot 10^{-3}$
w_0^{lepton}	$(5.2 \pm 1.1) \cdot 10^{-2}$
w_0^{kaon}	$(6.37 \pm 0.94) \cdot 10^{-2}$
w_0^{NT1}	0.203 ± 0.020
w_0^{NT2}	0.343 ± 0.017
w_{slope}^{lepton}	$(0.8 \pm 2.0) \cdot 10^{-2}$
w_{slope}^{kaon}	0.162 ± 0.015
w_{slope}^{NT1}	$(1.3 \pm 3.3) \cdot 10^{-2}$
w_{slope}^{NT2}	$(-0.4 \pm 2.5) \cdot 10^{-2}$
Δw^{lepton}	$(-4.8 \pm 7.1) \cdot 10^{-3}$
Δw^{kaon}	$(-1.39 \pm 0.52) \cdot 10^{-2}$
Δw^{NT1}	$(0.7 \pm 1.1) \cdot 10^{-2}$
Δw^{NT2}	$(-2.02 \pm 0.85) \cdot 10^{-2}$

Parameter	B^0 fit results (*GG* model)
$\frac{\mathrm{Im}\lambda_{flav}}{\mid\lambda_{flav}\mid}$	-0.45 ± 0.59
$\frac{\mathrm{Im}\lambda_{flav}}{\mid\lambda_{flav}\mid}$	-0.65 ± 0.60
$\frac{\mathrm{Im}\lambda_{tag}}{\mid\lambda_{tag}\mid}$	0.10 ± 0.62
$\frac{\mathrm{Im}\lambda_{tag}}{\mid\lambda_{tag}\mid}$	0.54 ± 0.63
$f_{prompt,B_{flav}}^{lepton}$	0.402 ± 0.074
$f_{prompt,B_{flav}}^{kaon}$	0.368 ± 0.044
$f_{prompt,B_{flav}}^{NT1}$	0.351 ± 0.084
$f_{prompt,B_{flav}}^{NT2}$	0.510 ± 0.058
S_{back}	1.898 ± 0.089
δ_{back}	-0.246 ± 0.054
$f_{back,outlier}$	$(4.2 \pm 5.7) \cdot 10^{-3}$
$w_{0,prompt}^{lepton}$	$(0.00 \pm 0.24) \cdot 10^{-3}$
$w_{0,prompt}^{kaon}$	$(0.00 \pm 0.81) \cdot 10^{-3}$
$w_{0,prompt}^{NT1}$	0.05 ± 0.11
$w_{0,prompt}^{NT2}$	0.270 ± 0.053
$w_{0,non-prompt}^{lepton}$	0.402 ± 0.061
$w_{0,non-prompt}^{kaon}$	0.444 ± 0.034
$w_{0,non-prompt}^{NT1}$	0.484 ± 0.066
$w_{0,non-prompt}^{NT2}$	0.592 ± 0.052
$\tau_{non-prompt}$	1.753 ± 0.094
$f_{prompt,B_{CPK_S^0}}$	0.29 ± 0.15
$\tau_{non-prompt,B_{CPK_S^0}}$	1.99 ± 0.38

Table 43: Results from dedicated full Monte Carlo, Analysis 2 fit, *GG* resolution function.

8.10 Alternative tagging configuration

The nominal fits were also performed using the Moriond Tagger [20], for data and the standard full Monte Carlo (inclusive charmonium). The results and the comparison to the default Elba Tagger are summarized in tables 52, 53, 54, 55, 56 and 57.

8.11 Alternative vertexing configurations

Tables from 58 to 66 summarize the differences of the results for the physics parameters (Analysis 1 and Analysis 2) for different alternative vertexing configurations with respect to the nominal configuration. In order to avoid additional statistical uncertainties from events moving around only those common to the nominal and the modified configurations are used. The errors on the differences are estimated from the quadratic difference of the statistical Gaussian errors. The configurations are:

Parameter	B^0 fit results (*GExp* model)
Δm	0.4782 ± 0.0047
$\Delta\Gamma/\Gamma$	0.195 ± 0.015
$\mid q/p \mid$	1.0415 ± 0.0091
$\frac{\mathrm{Im}\lambda_{CP}}{\lvert\lambda_{CP}\rvert}$	0.707 ± 0.021
S	1.158 ± 0.027
τ_r^{lepton}	1.28 ± 0.28
τ_r^{kaon}	1.35 ± 0.11
τ_r^{NT1}	1.60 ± 0.33
τ_r^{NT2}	1.02 ± 0.27
f_{Exp}^{lepton}	0.191 ± 0.050
f_{Exp}^{kaon}	0.300 ± 0.028
f_{Exp}^{NT1}	0.181 ± 0.047
f_{Exp}^{NT2}	0.320 ± 0.086
$f_{outlier}$	$(2.34 \pm 0.67) \cdot 10^{-3}$
w_0^{lepton}	$(5.2 \pm 1.1) \cdot 10^{-2}$
w_0^{kaon}	$(6.36 \pm 0.94) \cdot 10^{-2}$
w_0^{NT1}	0.204 ± 0.019
w_0^{NT2}	0.343 ± 0.017
w_{slope}^{lepton}	$(1.1 \pm 2.0) \cdot 10^{-2}$
w_{slope}^{kaon}	0.163 ± 0.015
w_{slope}^{NT1}	$(1.3 \pm 3.3) \cdot 10^{-2}$
w_{slope}^{NT2}	$(-0.3 \pm 2.5) \cdot 10^{-2}$
Δw^{lepton}	$(-5.6 \pm 7.1) \cdot 10^{-3}$
Δw^{kaon}	$(-1.43 \pm 0.52) \cdot 10^{-2}$
Δw^{NT1}	$(0.7 \pm 1.1) \cdot 10^{-2}$
Δw^{NT2}	$(-2.05 \pm 0.85) \cdot 10^{-2}$

Parameter	B^0 fit results (*GExp* model)
$\frac{\mathrm{Im}\lambda_{flav}}{\lvert\lambda_{flav}\rvert}$	-0.50 ± 0.50
$\frac{\mathrm{Im}\lambda_{flav}}{\lvert\lambda_{flav}\rvert}$	-0.76 ± 0.52
$\frac{\mathrm{Im}\lambda_{tag}}{\lvert\lambda_{tag}\rvert}$	0.19 ± 0.49
$\frac{\mathrm{Im}\lambda_{tag}}{\lvert\lambda_{tag}\rvert}$	0.53 ± 0.52
$f_{prompt,B_{flav}}^{lepton}$	0.429 ± 0.080
$f_{prompt,B_{flav}}^{kaon}$	0.395 ± 0.047
$f_{prompt,B_{flav}}^{NT1}$	0.382 ± 0.090
$f_{prompt,B_{flav}}^{NT2}$	0.554 ± 0.062
S_{back}	1.824 ± 0.089
$\tau_{r,back}$	2.25 ± 0.61
$f_{back,outlier}$	$(3.3 \pm 5.2) \cdot 10^{-3}$
$w_{0,prompt}^{lepton}$	$(0.00 \pm 0.23) \cdot 10^{-3}$
$w_{0,prompt}^{kaon}$	$(0.0 \pm 1.1) \cdot 10^{-3}$
$w_{0,prompt}^{NT1}$	0.05 ± 0.11
$w_{0,prompt}^{NT2}$	0.264 ± 0.053
$w_{0,non-prompt}^{lepton}$	0.420 ± 0.069
$w_{0,non-prompt}^{kaon}$	0.464 ± 0.039
$w_{0,non-prompt}^{NT1}$	0.505 ± 0.073
$w_{0,non-prompt}^{NT2}$	0.631 ± 0.063
$\tau_{non-prompt}$	1.69 ± 0.10
$f_{prompt,B_{CPK_S^0}}$	0.34 ± 0.15
$\tau_{non-prompt,B_{CPK_S^0}}$	2.00 ± 0.40

Table 44: Results from dedicated full Monte Carlo, Analysis 1 fit, *GExp* resolution function.

- J/ψ mass constraint imposed for the *CP* vertex (table 58);
- use charmonium (J/ψ or $\psi(2S)$) vertex for the *CP* vertex (table 59);
- remove K_S^0 mass constraint (table 60);
- removing photons from the *CP* vertex (table 61);
- do not use the constraints from the beam (table 62);
- use only the constraint from the beam spot (table 63);
- remove the V^0 veto for the tag vertex (table 64);
- use the *average boost approximation* instead of the *average-τ_B approximation* for the $\Delta z \to \Delta t$ conversion [24] (table 65);
- use `FvtCluster` instead of the default `BtaSelFit` [24] (table 66).

Figures 56 and 57 show the same results in a graphical way.

Parameter	B^0 fit results (*GExp* model)
Δm	0.4782 ± 0.0047
$\Delta\Gamma/\Gamma$	0.195 ± 0.015
$\mid q/p \mid$	1.0414 ± 0.0091
$\frac{\mathrm{Im}\lambda_{CP}}{\mid\lambda_{CP}\mid}$	0.706 ± 0.021
$\frac{\mathrm{Re}\lambda_{CP}}{\mid\lambda_{CP}\mid}$Rez	$(0.3 \pm 1.5) \cdot 10^{-2}$
Imz	$(-0.3 \pm 1.6) \cdot 10^{-2}$
S	1.158 ± 0.027
τ_r^{lepton}	1.29 ± 0.28
τ_r^{kaon}	1.35 ± 0.11
τ_r^{NT1}	1.60 ± 0.33
τ_r^{NT2}	1.02 ± 0.27
f_{Exp}^{lepton}	0.190 ± 0.050
f_{Exp}^{kaon}	0.300 ± 0.028
f_{Exp}^{NT1}	0.181 ± 0.047
f_{Exp}^{NT2}	0.320 ± 0.087
$f_{outlier}$	$(2.34 \pm 0.67) \cdot 10^{-3}$
w_0^{lepton}	$(5.2 \pm 1.1) \cdot 10^{-2}$
w_0^{kaon}	$(6.36 \pm 0.94) \cdot 10^{-2}$
w_0^{NT1}	0.203 ± 0.019
w_0^{NT2}	0.343 ± 0.017
w_{slope}^{lepton}	$(1.1 \pm 2.0) \cdot 10^{-2}$
w_{slope}^{kaon}	0.163 ± 0.015
w_{slope}^{NT1}	$(1.3 \pm 3.3) \cdot 10^{-2}$
w_{slope}^{NT2}	$(-0.3 \pm 2.5) \cdot 10^{-2}$
Δw^{lepton}	$(-5.6 \pm 7.1) \cdot 10^{-3}$
Δw^{kaon}	$(-1.43 \pm 0.52) \cdot 10^{-2}$
Δw^{NT1}	$(0.7 \pm 1.1) \cdot 10^{-2}$
Δw^{NT2}	$(-2.05 \pm 0.85) \cdot 10^{-2}$

Parameter	B^0 fit results (*GExp* model)
$\frac{\mathrm{Im}\lambda_{flav}}{\mid\lambda_{flav}\mid}$	-0.54 ± 0.59
$\frac{\mathrm{Im}\lambda_{flav}}{\mid\lambda_{flav}\mid}$	-0.73 ± 0.60
$\frac{\mathrm{Im}\lambda_{tag}}{\mid\lambda_{tag}\mid}$	0.13 ± 0.62
$\frac{\mathrm{Im}\lambda_{tag}}{\mid\lambda_{tag}\mid}$	0.57 ± 0.63
$f_{prompt,B_{flav}}^{lepton}$	0.429 ± 0.080
$f_{prompt,B_{flav}}^{kaon}$	0.395 ± 0.047
$f_{prompt,B_{flav}}^{NT1}$	0.382 ± 0.090
$f_{prompt,B_{flav}}^{NT2}$	0.554 ± 0.062
S_{back}	1.823 ± 0.089
$\tau_{r,back}$	2.25 ± 0.59
$f_{back,outlier}$	$(3.3 \pm 5.2) \cdot 10^{-3}$
$w_{0,prompt}^{lepton}$	$(0.00 \pm 0.23) \cdot 10^{-3}$
$w_{0,prompt}^{kaon}$	$(0.0 \pm 1.1) \cdot 10^{-3}$
$w_{0,prompt}^{NT1}$	0.05 ± 0.11
$w_{0,prompt}^{NT2}$	0.264 ± 0.053
$w_{0,non-prompt}^{lepton}$	0.420 ± 0.069
$w_{0,non-prompt}^{kaon}$	0.464 ± 0.038
$w_{0,non-prompt}^{NT1}$	0.505 ± 0.073
$w_{0,non-prompt}^{NT2}$	0.631 ± 0.063
$\tau_{non-prompt}$	1.693 ± 0.098
$f_{prompt,B_{CPK_S^0}}$	0.34 ± 0.15
$\tau_{non-prompt,B_{CPK_S^0}}$	2.00 ± 0.40

Table 45: Results from dedicated full Monte Carlo, Analysis 2 fit, *GExp* resolution function.

Parameter	Original (dedicated MC)	CPT reweighted	DCKM reweighted
$\Delta\Gamma/\Gamma$	0.20	0.20	0.20
$\mid q/p \mid$	1.04	1.04	1.04
$\frac{\mathrm{Im}\lambda_{CP}}{\mid\lambda_{CP}\mid}$	0.70	0.70	0.70
Δm	0.472	0.472	0.472
$\frac{\mathrm{Re}\lambda_{CP}}{\mid\lambda_{CP}\mid}\mathrm{Re}z$	0.00	0.10	0.00
$\mathrm{Im}z$	0.00	0.02	0.00
$r_{tag}/\bar{r}_{tag}$	0.00	0.00	0.04
$\frac{\mathrm{Im}\lambda_{tag}}{\mid\lambda_{tag}\mid}$	0.00	0.00	-1.00
$\frac{\mathrm{Im}\lambda_{tag}}{\mid\lambda_{tag}\mid}$	0.00	0.00	+1.00
$r_{flav}/\bar{r}_{flav}$	0.00	0.00	0.04
$\frac{\mathrm{Im}\lambda_{flav}}{\mid\lambda_{flav}\mid}$	0.00	0.00	-1.00
$\frac{\mathrm{Im}\lambda_{flav}}{\mid\lambda_{flav}\mid}$	0.00	0.00	+1.00

Table 46: Physics parameter values of the dedicated and reweighted CPT and DCKM full Monte Carlo.

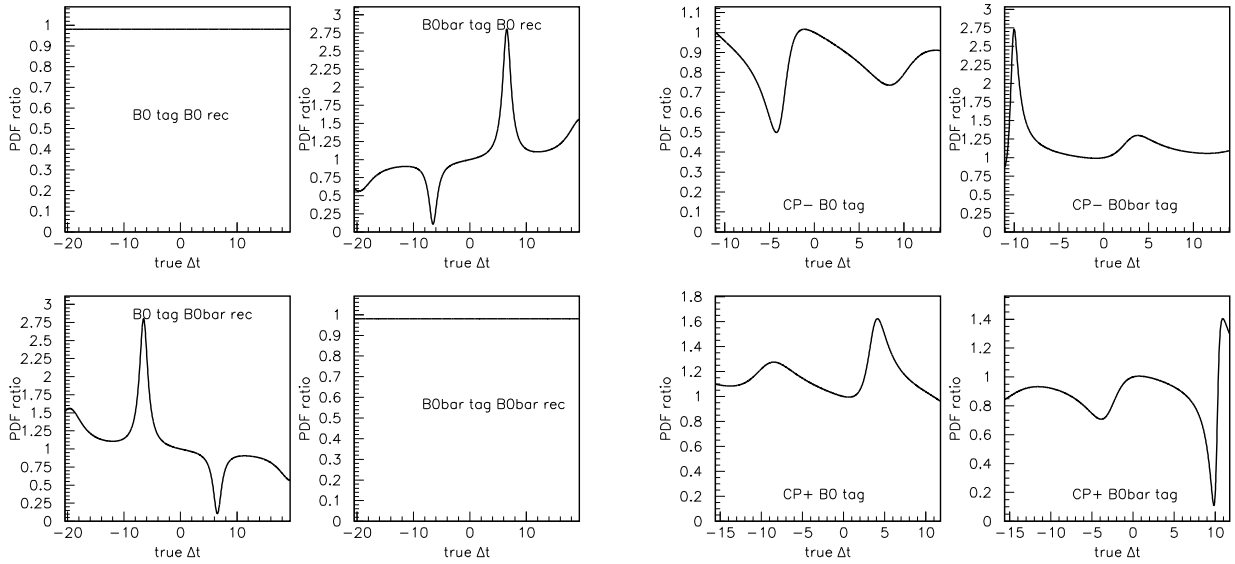

Figure 55: Reweighting functions for B_{flav} (left hand) and CP (right hand) events, corresponding to the CPT reweighted configuration with parameter values given in table 46.

Parameter	CPT reweighted	DCKM reweighted
τ_B	1.541 ± 0.008	1.538 ± 0.006
Δm	0.4755 ± 0.0032	0.4730 ± 0.0022
$\Delta\Gamma/\Gamma$	0.193 ± 0.012	0.214 ± 0.009
$\mid q/p \mid$	1.035 ± 0.007	1.035 ± 0.005
$\frac{\mathrm{Im}\lambda_{CP}}{\mid\lambda_{CP}\mid}$	0.678 ± 0.013	0.684 ± 0.010
$\frac{\mathrm{Re}\lambda_{CP}}{\mid\lambda_{CP}\mid}$Rez	0.106 ± 0.010	-0.004 ± 0.008
Imz	0.025 ± 0.007	0.005 ± 0.006

Table 47: Results from maximum likelihood fits to the MC truth information (perfect resolution, perfect tag) in the reweighted CPT and DCKM full Monte Carlo.

Parameter	B^0 fit results (*GG* model)
Δm	0.4840 ± 0.0082
$\Delta\Gamma/\Gamma$	0.172 ± 0.022
$\mid q/p \mid$	1.062 ± 0.015
$\frac{\mathrm{Im}\lambda_{CP}}{\mid\lambda_{CP}\mid}$	0.702 ± 0.032
$\frac{\mathrm{Re}\lambda_{CP}}{\mid\lambda_{CP}\mid}$Rez	0.106 ± 0.023
Imz	$(1.3 \pm 2.5) \cdot 10^{-2}$
S_{core}	1.041 ± 0.096
δ_{core}^{lepton}	-0.121 ± 0.071
δ_{core}^{kaon}	-0.262 ± 0.048
δ_{core}^{NT1}	$(-6.4 \pm 8.7) \cdot 10^{-2}$
δ_{core}^{NT2}	-0.291 ± 0.059
f_{tail}	0.180 ± 0.065
S_{tail}	2.77 ± 0.32
δ_{tail}	-0.97 ± 0.29
$f_{outlier}$	$(2.05 \pm 1.00) \cdot 10^{-3}$
w_0^{lepton}	$(5.3 \pm 1.8) \cdot 10^{-2}$
w_0^{kaon}	$(7.0 \pm 1.6) \cdot 10^{-2}$
w_0^{NT1}	0.172 ± 0.033
w_0^{NT2}	0.334 ± 0.028
w_{slope}^{lepton}	$(1.4 \pm 3.3) \cdot 10^{-2}$
w_{slope}^{kaon}	0.147 ± 0.026
w_{slope}^{NT1}	$(7.0 \pm 5.6) \cdot 10^{-2}$
w_{slope}^{NT2}	$(0.1 \pm 4.2) \cdot 10^{-2}$
Δw^{lepton}	$(-0.1 \pm 1.2) \cdot 10^{-2}$
Δw^{kaon}	$(-1.10 \pm 0.85) \cdot 10^{-2}$
Δw^{NT1}	$(0.1 \pm 1.9) \cdot 10^{-2}$
Δw^{NT2}	$(-2.2 \pm 1.4) \cdot 10^{-2}$

Parameter	B^0 fit results (*GG* model)
$\frac{\mathrm{Im}\lambda_{flav}}{\mid\lambda_{flav}\mid}$	-1.03 ± 0.96
$\frac{\mathrm{Im}\lambda_{flav}}{\mid\lambda_{flav}\mid}$	-1.7 ± 1.0
$\frac{\mathrm{Im}\lambda_{tag}}{\mid\lambda_{tag}\mid}$	0.03 ± 0.98
$\frac{\mathrm{Im}\lambda_{tag}}{\mid\lambda_{tag}\mid}$	-0.0 ± 1.0
$f_{prompt,B_{flav}}^{lepton}$	0.37 ± 0.13
$f_{prompt,B_{flav}}^{kaon}$	0.292 ± 0.083
$f_{prompt,B_{flav}}^{NT1}$	0.294 ± 0.095
$f_{prompt,B_{flav}}^{NT2}$	0.297 ± 0.095
S_{back}	1.72 ± 0.16
δ_{back}	-0.204 ± 0.090
$f_{back,outlier}$	$(0.00 \pm 0.20) \cdot 10^{-3}$
$w_{0,prompt}^{lepton}$	$(0.00 \pm 0.31) \cdot 10^{-3}$
$w_{0,prompt}^{kaon}$	$(0.0 \pm 2.2) \cdot 10^{-3}$
$w_{0,prompt}^{NT1}$	$(0.0 \pm 1.6) \cdot 10^{-3}$
$w_{0,prompt}^{NT2}$	0.03 ± 0.20
$w_{0,non-prompt}^{lepton}$	0.309 ± 0.085
$w_{0,non-prompt}^{kaon}$	0.395 ± 0.052
$w_{0,non-prompt}^{NT1}$	0.502 ± 0.083
$w_{0,non-prompt}^{NT2}$	0.625 ± 0.066
$\tau_{non-prompt}$	1.660 ± 0.098
$f_{prompt,B_{CPK_S^0}}$	$(0.00 \pm 0.73) \cdot 10^{-3}$
$\tau_{non-prompt,B_{CPK_S^0}}$	1.06 ± 0.19

Table 48: Results from CPT reweighted full Monte Carlo, Analysis 2 fit, *GG* resolution function.

Parameter	B^0 fit results (*GExp* model)
Δm	0.4790 ± 0.0081
$\Delta\Gamma/\Gamma$	0.181 ± 0.022
$\mid q/p \mid$	1.065 ± 0.015
$\frac{\mathrm{Im}\lambda_{CP}}{\mid\lambda_{CP}\mid}$	0.704 ± 0.032
$\frac{\mathrm{Re}\lambda_{CP}}{\mid\lambda_{CP}\mid}$Rez	0.109 ± 0.023
Imz	$(1.1 \pm 2.5) \cdot 10^{-2}$
S	1.130 ± 0.043
τ_r^{lepton}	1.31 ± 0.44
τ_r^{kaon}	1.33 ± 0.16
τ_r^{NT1}	1.70 ± 0.40
τ_r^{NT2}	1.66 ± 0.50
f_{Exp}^{lepton}	0.212 ± 0.082
f_{Exp}^{kaon}	0.305 ± 0.042
f_{Exp}^{NT1}	0.167 ± 0.056
f_{Exp}^{NT2}	0.237 ± 0.080
$f_{outlier}$	$(2.2 \pm 1.1) \cdot 10^{-3}$
w_0^{lepton}	$(5.4 \pm 1.8) \cdot 10^{-2}$
w_0^{kaon}	$(7.0 \pm 1.6) \cdot 10^{-2}$
w_0^{NT1}	0.173 ± 0.033
w_0^{NT2}	0.333 ± 0.028
w_{slope}^{lepton}	$(1.7 \pm 3.3) \cdot 10^{-2}$
w_{slope}^{kaon}	0.150 ± 0.025
w_{slope}^{NT1}	$(7.0 \pm 5.6) \cdot 10^{-2}$
w_{slope}^{NT2}	$(0.3 \pm 4.2) \cdot 10^{-2}$
Δw^{lepton}	$(-0.2 \pm 1.2) \cdot 10^{-2}$
Δw^{kaon}	$(-1.20 \pm 0.85) \cdot 10^{-2}$
Δw^{NT1}	$(0.1 \pm 1.8) \cdot 10^{-2}$
Δw^{NT2}	$(-2.2 \pm 1.4) \cdot 10^{-2}$

Parameter	B^0 fit results (*GExp* model)
$\frac{\mathrm{Im}\lambda_{flav}}{\mid\lambda_{flav}\mid}$	-1.11 ± 0.96
$\frac{\mathrm{Im}\lambda_{flav}}{\mid\lambda_{flav}\mid}$	-1.8 ± 1.0
$\frac{\mathrm{Im}\lambda_{tag}}{\mid\lambda_{tag}\mid}$	0.07 ± 0.97
$\frac{\mathrm{Im}\lambda_{tag}}{\mid\lambda_{tag}\mid}$	-0.0 ± 1.0
$f_{prompt,B_{flav}}^{lepton}$	0.38 ± 0.14
$f_{prompt,B_{flav}}^{kaon}$	0.301 ± 0.092
$f_{prompt,B_{flav}}^{NT1}$	0.32 ± 0.10
$f_{prompt,B_{flav}}^{NT2}$	0.32 ± 0.10
S_{back}	1.68 ± 0.17
$\tau_{r,back}$	2.1 ± 1.8
$f_{back,outlier}$	$(0.00 \pm 0.15) \cdot 10^{-3}$
$w_{0,prompt}^{lepton}$	$(0.00 \pm 0.30) \cdot 10^{-3}$
$w_{0,prompt}^{kaon}$	$(0.0 \pm 1.6) \cdot 10^{-3}$
$w_{0,prompt}^{NT1}$	$(0.0 \pm 1.6) \cdot 10^{-3}$
$w_{0,prompt}^{NT2}$	0.04 ± 0.20
$w_{0,non-prompt}^{lepton}$	0.316 ± 0.092
$w_{0,non-prompt}^{kaon}$	0.400 ± 0.058
$w_{0,non-prompt}^{NT1}$	0.523 ± 0.093
$w_{0,non-prompt}^{NT2}$	0.638 ± 0.074
$\tau_{non-prompt}$	1.60 ± 0.15
$f_{prompt,B_{CPK_S^0}}$	$(0.00 \pm 0.78) \cdot 10^{-3}$
$\tau_{non-prompt,B_{CPK_S^0}}$	1.02 ± 0.20

Table 49: Results from CPT reweighted full Monte Carlo, Analysis 2 fit, *GExp* resolution function.

Parameter	B^0 fit results (*GG* model)
Δm	0.4833 ± 0.0057
$\Delta\Gamma/\Gamma$	0.184 ± 0.017
$\mid q/p \mid$	1.030 ± 0.011
$\frac{\mathrm{Im}\lambda_{CP}}{\mid\lambda_{CP}\mid}$	0.700 ± 0.025
$\frac{\mathrm{Re}\lambda_{CP}}{\mid\lambda_{CP}\mid}\mathrm{Re}z$	$(-0.8 \pm 1.8) \cdot 10^{-2}$
$\mathrm{Im}z$	$(-4.8 \pm 4.9) \cdot 10^{-2}$
S_{core}	1.169 ± 0.055
δ_{core}^{lepton}	-0.145 ± 0.047
δ_{core}^{kaon}	-0.276 ± 0.032
δ_{core}^{NT1}	-0.179 ± 0.056
δ_{core}^{NT2}	-0.221 ± 0.041
f_{tail}	$(9.8 \pm 3.1) \cdot 10^{-2}$
S_{tail}	3.28 ± 0.35
δ_{tail}	-1.35 ± 0.36
$f_{outlier}$	$(1.86 \pm 0.77) \cdot 10^{-3}$
w_0^{lepton}	$(4.8 \pm 1.5) \cdot 10^{-2}$
w_0^{kaon}	$(6.3 \pm 1.3) \cdot 10^{-2}$
w_0^{NT1}	0.188 ± 0.024
w_0^{NT2}	0.344 ± 0.020
w_{slope}^{lepton}	$(3.0 \pm 2.5) \cdot 10^{-2}$
w_{slope}^{kaon}	0.170 ± 0.019
w_{slope}^{NT1}	$(4.5 \pm 4.0) \cdot 10^{-2}$
w_{slope}^{NT2}	$(-0.5 \pm 3.0) \cdot 10^{-2}$
Δw^{lepton}	$(-1.3 \pm 9.7) \cdot 10^{-3}$
Δw^{kaon}	$(-5.0 \pm 6.9) \cdot 10^{-3}$
Δw^{NT1}	$(-0.0 \pm 1.4) \cdot 10^{-2}$
Δw^{NT2}	$(-2.1 \pm 1.0) \cdot 10^{-2}$

Parameter	B^0 fit results (*GG* model)
$\frac{\mathrm{Im}\lambda_{flav}}{\mid\lambda_{flav}\mid}$	-1.62 ± 0.70
$\frac{\mathrm{Im}\lambda_{flav}}{\mid\lambda_{flav}\mid}$	1.63 ± 0.71
$\frac{\mathrm{Im}\lambda_{tag}}{\mid\lambda_{tag}\mid}$	-1.25 ± 0.66
$\frac{\mathrm{Im}\lambda_{tag}}{\mid\lambda_{tag}\mid}$	2.21 ± 0.66
$f_{prompt,B_{flav}}^{lepton}$	0.332 ± 0.093
$f_{prompt,B_{flav}}^{kaon}$	0.351 ± 0.053
$f_{prompt,B_{flav}}^{NT1}$	0.322 ± 0.090
$f_{prompt,B_{flav}}^{NT2}$	0.442 ± 0.071
S_{back}	1.89 ± 0.11
δ_{back}	-0.298 ± 0.066
$f_{back,outlier}$	$(3.5 \pm 6.8) \cdot 10^{-3}$
$w_{0,prompt}^{lepton}$	$(0.00 \pm 0.35) \cdot 10^{-3}$
$w_{0,prompt}^{kaon}$	$(0.00 \pm 0.71) \cdot 10^{-3}$
$w_{0,prompt}^{NT1}$	$(0.0 \pm 1.2) \cdot 10^{-3}$
$w_{0,prompt}^{NT2}$	0.04 ± 0.11
$w_{0,non-prompt}^{lepton}$	0.392 ± 0.069
$w_{0,non-prompt}^{kaon}$	0.436 ± 0.039
$w_{0,non-prompt}^{NT1}$	0.454 ± 0.070
$w_{0,non-prompt}^{NT2}$	0.752 ± 0.059
$\tau_{non-prompt}$	1.70 ± 0.11
$f_{prompt,B_{CPK_S^0}}$	0.51 ± 0.16
$\tau_{non-prompt,B_{CPK_S^0}}$	2.40 ± 0.67

Table 50: Results from DCKM reweighted full Monte Carlo, Analysis 2 fit, *GG* resolution function.

Parameter	B^0 fit results (*GG* model)
Δm	0.4833 ± 0.0057
$\Delta\Gamma/\Gamma$	0.184 ± 0.017
$\mid q/p \mid$	1.030 ± 0.011
$\frac{\mathrm{Im}\lambda_{CP}}{\mid\lambda_{CP}\mid}$	0.702 ± 0.025
S_{core}	1.170 ± 0.055
δ_{core}^{lepton}	-0.146 ± 0.047
δ_{core}^{kaon}	-0.277 ± 0.032
δ_{core}^{NT1}	-0.181 ± 0.056
δ_{core}^{NT2}	-0.222 ± 0.041
f_{tail}	$(9.7 \pm 3.1) \cdot 10^{-2}$
S_{tail}	3.29 ± 0.35
δ_{tail}	-1.37 ± 0.37
$f_{outlier}$	$(1.86 \pm 0.77) \cdot 10^{-3}$
w_0^{lepton}	$(4.3 \pm 1.3) \cdot 10^{-2}$
w_0^{kaon}	$(5.9 \pm 1.2) \cdot 10^{-2}$
w_0^{NT1}	0.185 ± 0.024
w_0^{NT2}	0.342 ± 0.021
w_{slope}^{lepton}	$(3.1 \pm 2.5) \cdot 10^{-2}$
w_{slope}^{kaon}	0.171 ± 0.019
w_{slope}^{NT1}	$(4.5 \pm 4.1) \cdot 10^{-2}$
w_{slope}^{NT2}	$(-0.5 \pm 3.1) \cdot 10^{-2}$
Δw^{lepton}	$(-3.1 \pm 9.1) \cdot 10^{-3}$
Δw^{kaon}	$(-6.2 \pm 6.5) \cdot 10^{-3}$
Δw^{NT1}	$(-0.2 \pm 1.4) \cdot 10^{-2}$
Δw^{NT2}	$(-2.2 \pm 1.0) \cdot 10^{-2}$

Parameter	B^0 fit results (*GG* model)
$\frac{\mathrm{Im}\lambda_{flav}}{\mid\lambda_{flav}\mid}$	-1.01 ± 0.38
$\frac{\mathrm{Im}\lambda_{flav}}{\mid\lambda_{flav}\mid}$	0.98 ± 0.39
$\frac{\mathrm{Im}\lambda_{tag}}{\mid\lambda_{tag}\mid}$	-0.65 ± 0.31
$\frac{\mathrm{Im}\lambda_{tag}}{\mid\lambda_{tag}\mid}$	1.59 ± 0.33
$f_{prompt,B_{flav}}^{lepton}$	0.332 ± 0.093
$f_{prompt,B_{flav}}^{kaon}$	0.352 ± 0.053
$f_{prompt,B_{flav}}^{NT1}$	0.322 ± 0.090
$f_{prompt,B_{flav}}^{NT2}$	0.442 ± 0.071
S_{back}	1.89 ± 0.11
δ_{back}	-0.298 ± 0.066
$f_{back,outlier}$	$(3.5 \pm 6.8) \cdot 10^{-3}$
$w_{0,prompt}^{lepton}$	$(0.00 \pm 0.35) \cdot 10^{-3}$
$w_{0,prompt}^{kaon}$	$(0.00 \pm 0.71) \cdot 10^{-3}$
$w_{0,prompt}^{NT1}$	$(0.0 \pm 1.2) \cdot 10^{-3}$
$w_{0,prompt}^{NT2}$	0.04 ± 0.11
$w_{0,non-prompt}^{lepton}$	0.392 ± 0.069
$w_{0,non-prompt}^{kaon}$	0.436 ± 0.039
$w_{0,non-prompt}^{NT1}$	0.454 ± 0.070
$w_{0,non-prompt}^{NT2}$	0.752 ± 0.059
$\tau_{non-prompt}$	1.71 ± 0.11
$f_{prompt,B_{CPK_S^0}}$	0.51 ± 0.15
$\tau_{non-prompt,B_{CPK_S^0}}$	2.40 ± 0.67

Table 51: Results from DCKM reweighted full Monte Carlo, Analysis 1 fit, *GG* resolution function.

Parameter	B^0 fit results (*GG* model)
Δm	0.5209 ± 0.0094
$\Delta\Gamma/\Gamma$	$(-1.4 \pm 5.2) \cdot 10^{-2}$
$\mid q/p \mid$	0.959 ± 0.018
$\frac{\mathrm{Im}\lambda_{CP}}{\mid\lambda_{CP}\mid}$	0.655 ± 0.078
$\frac{\mathrm{Re}\lambda_{CP}}{\mid\lambda_{CP}\mid}$Rez	$(-8.9 \pm 4.2) \cdot 10^{-2}$
Imz	-0.918 ± 0.035
S_{core}	1.270 ± 0.054
δ_{core}^{cat1}	$(2.5 \pm 7.8) \cdot 10^{-2}$
δ_{core}^{cat2}	-0.301 ± 0.059
δ_{core}^{cat3}	-0.323 ± 0.053
δ_{core}^{cat4}	-0.313 ± 0.053
f_{tail}	$(2.9 \pm 1.2) \cdot 10^{-2}$
S_{tail}	5.7 ± 1.2
δ_{tail}	-1.88 ± 0.88
$f_{outlier}$	$(0.3 \pm 1.4) \cdot 10^{-3}$
w_0^{cat1}	$(2.3 \pm 2.2) \cdot 10^{-2}$
w_0^{cat2}	$(2.1 \pm 2.5) \cdot 10^{-2}$
w_0^{cat3}	0.149 ± 0.029
w_0^{cat4}	0.257 ± 0.030
w_{slope}^{cat1}	$(0.0 \pm 4.1) \cdot 10^{-2}$
w_{slope}^{cat2}	0.145 ± 0.044
w_{slope}^{cat3}	0.106 ± 0.045
w_{slope}^{cat4}	$(8.0 \pm 4.5) \cdot 10^{-2}$
Δw^{cat1}	$(0.1 \pm 1.4) \cdot 10^{-2}$
Δw^{cat2}	$(-2.7 \pm 1.5) \cdot 10^{-2}$
Δw^{cat3}	$(-2.3 \pm 1.6) \cdot 10^{-2}$
Δw^{cat4}	$(-4.0 \pm 1.6) \cdot 10^{-2}$

Parameter	B^0 fit results (*GG* model)
$\frac{\mathrm{Im}\lambda_{flav}}{\mid\lambda_{flav}\mid}$	2.7 ± 1.3
$\frac{\mathrm{Im}\lambda_{flav}}{\mid\lambda_{flav}\mid}$	-0.2 ± 1.4
$\frac{\mathrm{Im}\lambda_{tag}}{\mid\lambda_{tag}\mid}$	2.0 ± 1.5
$\frac{\mathrm{Im}\lambda_{tag}}{\mid\lambda_{tag}\mid}$	-0.4 ± 1.5
$f_{prompt,B_{flav}}^{cat1}$	0.328 ± 0.069
$f_{prompt,B_{flav}}^{cat2}$	0.647 ± 0.029
$f_{prompt,B_{flav}}^{cat3}$	0.669 ± 0.026
$f_{prompt,B_{flav}}^{cat4}$	0.668 ± 0.025
S_{back}	1.390 ± 0.024
δ_{back}	$(-3.8 \pm 1.7) \cdot 10^{-2}$
$f_{back,outlier}$	$(1.11 \pm 0.22) \cdot 10^{-2}$
$w_{0,prompt}^{cat1}$	$(0.00 \pm 0.35) \cdot 10^{-3}$
$w_{0,prompt}^{cat2}$	0.182 ± 0.017
$w_{0,prompt}^{cat3}$	0.307 ± 0.014
$w_{0,prompt}^{cat4}$	0.420 ± 0.014
$w_{0,non-prompt}^{cat1}$	0.364 ± 0.050
$w_{0,non-prompt}^{cat2}$	0.355 ± 0.029
$w_{0,non-prompt}^{cat3}$	0.368 ± 0.026
$w_{0,non-prompt}^{cat4}$	0.453 ± 0.026
$\tau_{non-prompt}$	1.356 ± 0.060
$f_{prompt,B_{CPK_S^0}}$	0.632 ± 0.072
$\tau_{non-prompt,B_{CPK_S^0}}$	2.32 ± 0.48

Table 52: Analysis 2 fit results, *GG* resolution function, using Moriond tagger.

Parameter	Nominal fit (Elba tagger)	Moriond Tagger
Δm	0.523 ± 0.010	0.5209 ± 0.0094
$\Delta\Gamma/\Gamma$	$(-2.1 \pm 4.8) \cdot 10^{-2}$	$(-1.4 \pm 5.2) \cdot 10^{-2}$
$\mid q/p \mid$	0.945 ± 0.018	0.959 ± 0.018
$\frac{\mathrm{Im}\lambda_{CP}}{\mid\lambda_{CP}\mid}$	0.620 ± 0.083	0.655 ± 0.078
$\frac{\mathrm{Re}\lambda_{CP}}{\mid\lambda_{CP}\mid}$Rez	$(-6.4 \pm 4.6) \cdot 10^{-2}$	$(-8.9 \pm 4.2) \cdot 10^{-2}$
Imz	-0.918 ± 0.034	-0.918 ± 0.035

Table 53: Comparison of Analysis 2 fit results, *GG* resolution function, between the default Elba Tagger and the Moriond tagger.

Parameter	Nominal fit (Elba tagger)	Moriond Tagger
Δm	0.5220 ± 0.0098	0.5208 ± 0.0093
$\Delta\Gamma/\Gamma$	$(-0.8 \pm 4.9) \cdot 10^{-2}$	$(-0.6 \pm 5.1) \cdot 10^{-2}$
$\mid q/p \mid$	0.946 ± 0.018	0.960 ± 0.018
$\frac{\mathrm{Im}\lambda_{CP}}{\mid\lambda_{CP}\mid}$	0.612 ± 0.085	0.646 ± 0.080

Table 54: Comparison of Analysis 1 fit results, *GG* resolution function, between the default Elba Tagger and the Moriond tagger.

Parameter	B^0 fit results (*GG* model)
Δm	0.4812 ± 0.0059
$\Delta\Gamma/\Gamma$	$(2.8 \pm 2.8) \cdot 10^{-2}$
$\mid q/p \mid$	1.013 ± 0.012
$\frac{\mathrm{Im}\lambda_{CP}}{\mid\lambda_{CP}\mid}$	0.669 ± 0.046
$\frac{\mathrm{Re}\lambda_{CP}}{\mid\lambda_{CP}\mid}\mathrm{Rez}$	$(-1.1 \pm 3.2) \cdot 10^{-2}$
Imz	$(-0.6 \pm 2.1) \cdot 10^{-2}$
S_{core}	1.296 ± 0.047
δ_{core}^{cat1}	-0.121 ± 0.048
δ_{core}^{cat2}	-0.355 ± 0.038
δ_{core}^{cat3}	-0.349 ± 0.034
δ_{core}^{cat4}	-0.292 ± 0.034
f_{tail}	$(2.3 \pm 1.7) \cdot 10^{-2}$
S_{tail}	4.9 ± 1.4
δ_{tail}	-1.79 ± 0.98
$f_{outlier}$	$(1.29 \pm 0.98) \cdot 10^{-3}$
w_0^{cat1}	$(3.5 \pm 1.2) \cdot 10^{-2}$
w_0^{cat2}	$(2.2 \pm 1.4) \cdot 10^{-2}$
w_0^{cat3}	0.128 ± 0.017
w_0^{cat4}	0.262 ± 0.018
w_{slope}^{cat1}	$(-0.7 \pm 2.3) \cdot 10^{-2}$
w_{slope}^{cat2}	0.123 ± 0.026
w_{slope}^{cat3}	0.124 ± 0.026
w_{slope}^{cat4}	$(5.7 \pm 2.7) \cdot 10^{-2}$
Δw^{cat1}	$(-6.5 \pm 8.7) \cdot 10^{-3}$
Δw^{cat2}	$(-1.61 \pm 0.86) \cdot 10^{-2}$
Δw^{cat3}	$(-2.63 \pm 0.94) \cdot 10^{-2}$
Δw^{cat4}	$(-3.12 \pm 0.98) \cdot 10^{-2}$

Parameter	B^0 fit results (*GG* model)
$\frac{\mathrm{Im}\lambda_{flav}}{\mid\lambda_{flav}\mid}$	-0.28 ± 0.81
$\frac{\mathrm{Im}\lambda_{flav}}{\mid\lambda_{flav}\mid}$	-0.01 ± 0.84
$\frac{\mathrm{Im}\lambda_{tag}}{\mid\lambda_{tag}\mid}$	0.39 ± 0.90
$\frac{\mathrm{Im}\lambda_{tag}}{\mid\lambda_{tag}\mid}$	0.03 ± 0.93
$f_{prompt,B_{flav}}^{cat1}$	0.55 ± 0.12
$f_{prompt,B_{flav}}^{cat2}$	0.349 ± 0.077
$f_{prompt,B_{flav}}^{cat3}$	0.465 ± 0.080
$f_{prompt,B_{flav}}^{cat4}$	0.423 ± 0.079
S_{back}	1.85 ± 0.11
δ_{back}	$(-8.7 \pm 6.1) \cdot 10^{-2}$
$f_{back,outlier}$	$(6.8 \pm 6.6) \cdot 10^{-3}$
$w_{0,prompt}^{cat1}$	$(0.00 \pm 0.27) \cdot 10^{-3}$
$w_{0,prompt}^{cat2}$	$(0.00 \pm 0.33) \cdot 10^{-3}$
$w_{0,prompt}^{cat3}$	$(7.8 \pm 6.8) \cdot 10^{-2}$
$w_{0,prompt}^{cat4}$	0.265 ± 0.069
$w_{0,non-prompt}^{cat1}$	0.280 ± 0.091
$w_{0,non-prompt}^{cat2}$	0.375 ± 0.051
$w_{0,non-prompt}^{cat3}$	0.475 ± 0.054
$w_{0,non-prompt}^{cat4}$	0.472 ± 0.051
$\tau_{non-prompt}$	1.71 ± 0.14
$f_{prompt,B_{CPK_S^0}}$	0.35 ± 0.12
$\tau_{non-prompt,B_{CPK_S^0}}$	2.04 ± 0.32

Table 55: Analysis 2 fit results, for inclusive MC, *GG* resolution function, using Moriond tagger.

Parameter	Nominal fit (Elba tagger)	Moriond Tagger
Δm	0.4785 ± 0.0061	0.4812 ± 0.0059
$\Delta\Gamma/\Gamma$	$(3.6 \pm 3.0) \cdot 10^{-2}$	$(2.8 \pm 2.8) \cdot 10^{-2}$
$\mid q/p \mid$	1.009 ± 0.012	1.013 ± 0.012
$\frac{\mathrm{Im}\lambda_{CP}}{\mid\lambda_{CP}\mid}$	0.679 ± 0.048	0.669 ± 0.046
$\frac{\mathrm{Re}\lambda_{CP}}{\mid\lambda_{CP}\mid}$Rez	$(-0.1 \pm 3.4) \cdot 10^{-2}$	$(-1.1 \pm 3.2) \cdot 10^{-2}$
Imz	$(-0.8 \pm 2.1) \cdot 10^{-2}$	$(-0.6 \pm 2.1) \cdot 10^{-2}$

Table 56: Comparison of Analysis 2 fit results, *GG* resolution function, between the default Elba Tagger and the Moriond tagger, for the standard inclusive Monte Carlo.

Parameter	Nominal fit (Elba tagger)	Moriond Tagger
Δm	0.4784 ± 0.0061	0.4811 ± 0.0059
$\Delta\Gamma/\Gamma$	$(3.5 \pm 3.0) \cdot 10^{-2}$	$(2.9 \pm 2.8) \cdot 10^{-2}$
$\mid q/p \mid$	1.009 ± 0.012	1.013 ± 0.012
$\frac{\mathrm{Im}\lambda_{CP}}{\mid\lambda_{CP}\mid}$	0.681 ± 0.048	0.670 ± 0.046

Table 57: Comparison of Analysis 1 fit results, *GG* resolution function, between the default Elba Tagger and the Moriond tagger, for the standard inclusive Monte Carlo.

Parameter	Analysis 1	Analysis 2
Δm	$(0.6 \pm 1.2) \cdot 10^{-3}$	$(6.7 \pm 8.9) \cdot 10^{-4}$
$\Delta\Gamma/\Gamma$	$(1.0 \pm 1.7) \cdot 10^{-2}$	$(0.8 \pm 1.8) \cdot 10^{-2}$
$\mid q/p \mid$	$(-0.1 \pm 1.2) \cdot 10^{-3}$	$(-0.1 \pm 1.0) \cdot 10^{-3}$
$\frac{\mathrm{Im}\lambda_{CP}}{\mid\lambda_{CP}\mid}$	$(3.3 \pm 8.2) \cdot 10^{-3}$	$(3.9 \pm 7.9) \cdot 10^{-3}$
$\frac{\mathrm{Re}\lambda_{CP}}{\mid\lambda_{CP}\mid}$Rez	—	$(0.1 \pm 1.2) \cdot 10^{-2}$
Imz	—	$(-1.4 \pm 2.4) \cdot 10^{-3}$

Table 58: Differences between the standard fit and the one done imposing J/ψ mass constraint for the *CP* vertex (for technical reasons $B^0 \to J/\psi K_S^0$ ($\pi^0\pi^0$) is excluded from this comparison). The quadratic error difference is reported as well. Only common events are used here.

Parameter	Analysis 1	Analysis 2
Δm	$(0.3 \pm 1.3) \cdot 10^{-3}$	$(9.5 \pm 6.1) \cdot 10^{-4}$
$\Delta\Gamma/\Gamma$	$(0.2 \pm 1.7) \cdot 10^{-2}$	$(-0.1 \pm 1.1) \cdot 10^{-2}$
$\mid q/p \mid$	$(9.8 \pm 7.5) \cdot 10^{-4}$	$(7.3 \pm 6.9) \cdot 10^{-4}$
$\frac{\mathrm{Im}\lambda_{CP}}{\mid\lambda_{CP}\mid}$	$(-2.4 \pm 7.6) \cdot 10^{-3}$	$(-2.6 \pm 2.4) \cdot 10^{-3}$
$\frac{\mathrm{Re}\lambda_{CP}}{\mid\lambda_{CP}\mid}$Rez	—	$(1.17 \pm 0.58) \cdot 10^{-2}$
Imz	—	$(4.4 \pm 1.5) \cdot 10^{-3}$

Table 59: Differences between the standard fit and the one done using the charmonium vertex as *CP* vertex. The quadratic error difference is reported as well. Only common events are used here.

Parameter	Analysis 1	Analysis 2
Δm	$(0.6 \pm 5.4) \cdot 10^{-4}$	$(-0.6 \pm 6.6) \cdot 10^{-4}$
$\Delta\Gamma/\Gamma$	$(0.3 \pm 6.7) \cdot 10^{-3}$	$(0.4 \pm 7.8) \cdot 10^{-3}$
$\mid q/p \mid$	$(-1.1 \pm 6.5) \cdot 10^{-4}$	$(-0.9 \pm 6.4) \cdot 10^{-4}$
$\frac{\mathrm{Im}\lambda_{CP}}{\mid\lambda_{CP}\mid}$	$(4.1 \pm 4.7) \cdot 10^{-3}$	$(4.9 \pm 3.6) \cdot 10^{-3}$
$\frac{\mathrm{Re}\lambda_{CP}}{\mid\lambda_{CP}\mid}$Rez	—	$(-2.1 \pm 4.8) \cdot 10^{-3}$
Imz	—	$(0.8 \pm 1.4) \cdot 10^{-4}$

Table 60: Differences between the standard fit and the one done removing the K_S^0 mass constraint. The quadratic error difference is reported as well. Only common events are used here.

8.12 $B^0\overline{B}^0$ differences in reconstruction and tagging efficiencies

In this analysis, $B^0\overline{B}^0$ differences in reconstruction and tagging efficiencies, μ^α and ν^α, are extracted simultaneously with all the other parameters from the time-dependent extended maximum likelihood fit and using the time-integrated constraints described in section 2.

To check the feasibility of this technique, three toy Monte Carlo checks were performed.

The first test was based on more than 600 toy Monte Carlo experiments with equivalent luminosity of $\approx$ 60 fb^{-1}with the same physics parameter values as in the standard full Monte Carlo (table 6), and with $B^0\overline{B}^0$ reconstruction and tagging asymmetries similar to those found in the data. The samples were fitted with and

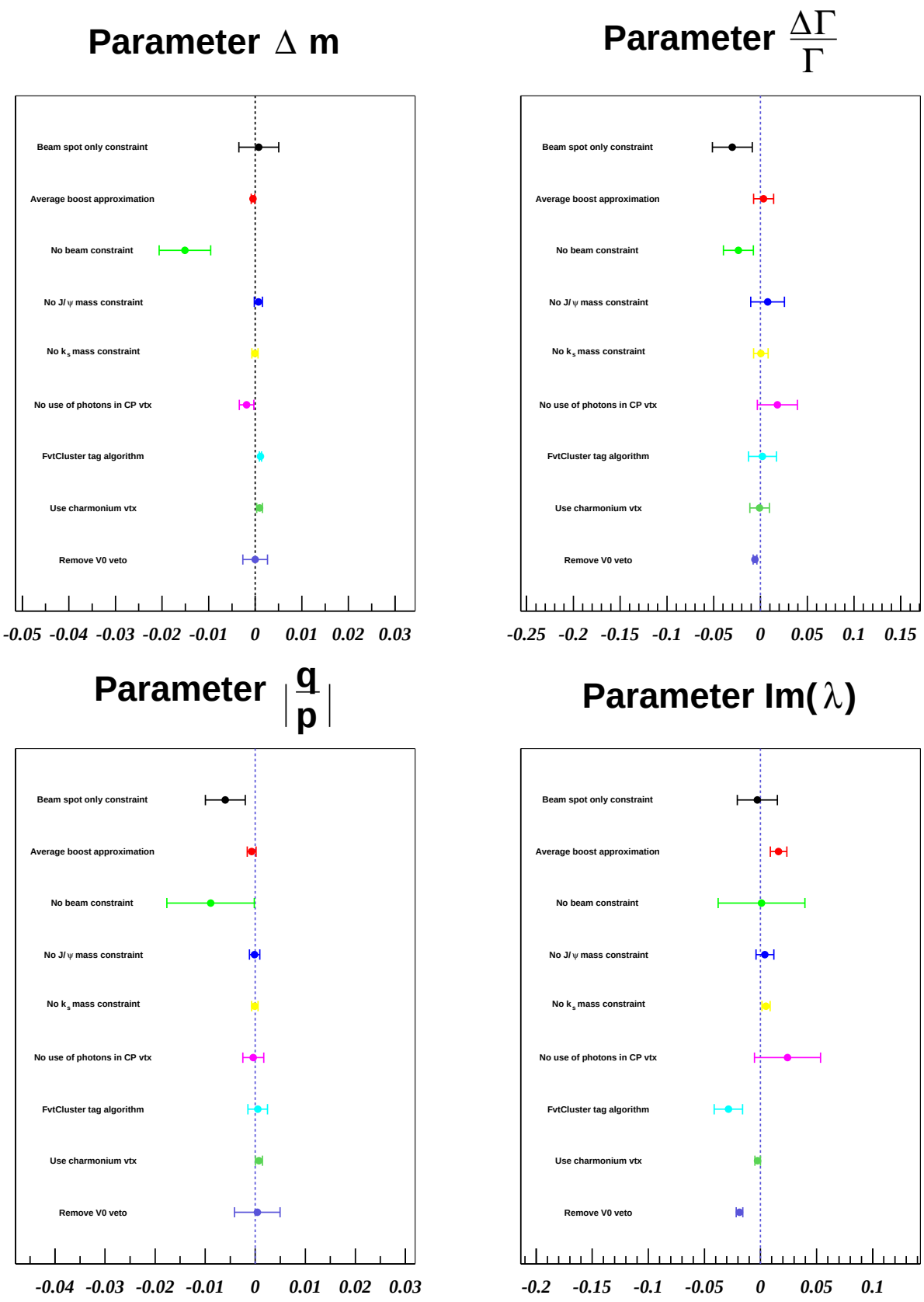

Figure 56: Graphical summary of the differences between the standard fit and the different vertexing configurations (explained in the text) from common events, for Δm, $\Delta\Gamma/\Gamma$, $|\,q/p\,|$ and $\frac{\mathrm{Im}\lambda_{CP}}{|\lambda_{CP}|}$ (Analysis 2).

Parameter	Analysis 1	Analysis 2
Δm	$(-9.2 \pm 5.5) \cdot 10^{-4}$	$(-1.9 \pm 1.5) \cdot 10^{-3}$
$\Delta\Gamma/\Gamma$	$(1.3 \pm 1.7) \cdot 10^{-2}$	$(1.8 \pm 2.1) \cdot 10^{-2}$
$\mid q/p \mid$	$(-1.2 \pm 2.2) \cdot 10^{-3}$	$(-0.4 \pm 2.1) \cdot 10^{-3}$
$\frac{\mathrm{Im}\lambda_{CP}}{\mid\lambda_{CP}\mid}$	$(2.4 \pm 2.9) \cdot 10^{-2}$	$(2.4 \pm 2.9) \cdot 10^{-2}$
$\frac{\mathrm{Re}\lambda_{CP}}{\mid\lambda_{CP}\mid}\mathrm{Re}z$	—	$(-2.1 \pm 1.7) \cdot 10^{-2}$
$\mathrm{Im}z$	—	$(-0.9 \pm 4.4) \cdot 10^{-3}$

Table 61: Differences between the standard fit and the one done removing the photons from the *CP* vertex. The quadratic error difference is reported as well. Only common events are used here.

Parameter	Analysis 1	Analysis 2
Δm	$(-1.46 \pm 0.55) \cdot 10^{-2}$	$(-1.51 \pm 0.55) \cdot 10^{-2}$
$\Delta\Gamma/\Gamma$	$(-2.1 \pm 1.1) \cdot 10^{-2}$	$(-2.4 \pm 1.6) \cdot 10^{-2}$
$\mid q/p \mid$	$(-8.7 \pm 8.7) \cdot 10^{-3}$	$(-8.9 \pm 8.7) \cdot 10^{-3}$
$\frac{\mathrm{Im}\lambda_{CP}}{\mid\lambda_{CP}\mid}$	$(-0.3 \pm 3.7) \cdot 10^{-2}$	$(0.1 \pm 3.9) \cdot 10^{-2}$
$\frac{\mathrm{Re}\lambda_{CP}}{\mid\lambda_{CP}\mid}\mathrm{Re}z$	—	$(-0.2 \pm 1.5) \cdot 10^{-2}$
$\mathrm{Im}z$	—	$(0.7 \pm 2.2) \cdot 10^{-2}$

Table 62: Differences between the standard fit and the one done removing the constraints from the beam. The quadratic error difference is reported as well. Only common events are used here.

Parameter	Analysis 1	Analysis 2
Δm	$(-1.0 \pm 3.0) \cdot 10^{-3}$	$(0.8 \pm 4.3) \cdot 10^{-3}$
$\Delta\Gamma/\Gamma$	$(-0.9 \pm 3.3) \cdot 10^{-2}$	$(-3.0 \pm 2.1) \cdot 10^{-2}$
$\mid q/p \mid$	$(-5.1 \pm 4.2) \cdot 10^{-3}$	$(-6.0 \pm 4.0) \cdot 10^{-3}$
$\frac{\mathrm{Im}\lambda_{CP}}{\mid\lambda_{CP}\mid}$	$(-0.9 \pm 1.7) \cdot 10^{-2}$	$(-0.3 \pm 1.8) \cdot 10^{-2}$
$\frac{\mathrm{Re}\lambda_{CP}}{\mid\lambda_{CP}\mid}\mathrm{Re}z$	—	$(2.4 \pm 1.4) \cdot 10^{-2}$
$\mathrm{Im}z$	—	$(0.5 \pm 1.2) \cdot 10^{-2}$

Table 63: Differences between the standard fit and the one done using only the beam spot constraint. The quadratic error difference is reported as well. Only common events are used here.

Parameter	Analysis 1	Analysis 2
Δm	$(-0.3 \pm 2.6) \cdot 10^{-3}$	$(-0.0 \pm 2.6) \cdot 10^{-3}$
$\Delta\Gamma/\Gamma$	$(-1.2 \pm 9.5) \cdot 10^{-3}$	$(-5.8 \pm 2.0) \cdot 10^{-3}$
$\mid q/p \mid$	$(0.7 \pm 4.5) \cdot 10^{-3}$	$(0.4 \pm 4.6) \cdot 10^{-3}$
$\frac{\mathrm{Im}\lambda_{CP}}{\mid\lambda_{CP}\mid}$	$(-1.7 \pm 1.3) \cdot 10^{-2}$	$(-1.87 \pm 0.30) \cdot 10^{-2}$
$\frac{\mathrm{Re}\lambda_{CP}}{\mid\lambda_{CP}\mid}\mathrm{Re}z$	—	$(0.5 \pm 1.6) \cdot 10^{-2}$
$\mathrm{Im}z$	—	$(-0.5 \pm 1.1) \cdot 10^{-2}$

Table 64: Differences between the standard fit and the one done removing the V^0 veto in the tag vertex reconstructions. The quadratic error difference is reported as well. Only common events are used here.

Parameter	Analysis 1	Analysis 2
Δm	$(-0.3 \pm 1.1) \cdot 10^{-3}$	$(-5.0 \pm 3.8) \cdot 10^{-4}$
$\Delta\Gamma/\Gamma$	$(0.2 \pm 1.1) \cdot 10^{-2}$	$(0.3 \pm 1.1) \cdot 10^{-2}$
$\mid q/p \mid$	$(-9.6 \pm 8.6) \cdot 10^{-4}$	$(-7.3 \pm 8.8) \cdot 10^{-4}$
$\frac{\mathrm{Im}\lambda_{CP}}{\lvert\lambda_{CP}\rvert}$	$(1.79 \pm 0.93) \cdot 10^{-2}$	$(1.61 \pm 0.74) \cdot 10^{-2}$
$\frac{\mathrm{Re}\lambda_{CP}}{\lvert\lambda_{CP}\rvert}\mathrm{Re}z$	—	$(-3.8 \pm 6.6) \cdot 10^{-3}$
$\mathrm{Im}z$	—	$(1.3 \pm 3.6) \cdot 10^{-3}$

Table 65: Differences between the standard fit and the one done using the *average boost approximation*. The quadratic error difference is reported as well. Only common events are used here.

Parameter	Analysis 1	Analysis 2
Δm	$(1.19 \pm 0.58) \cdot 10^{-3}$	$(1.11 \pm 0.22) \cdot 10^{-3}$
$\Delta\Gamma/\Gamma$	$(-0.2 \pm 1.3) \cdot 10^{-2}$	$(0.2 \pm 1.5) \cdot 10^{-2}$
$\mid q/p \mid$	$(0.5 \pm 2.0) \cdot 10^{-3}$	$(0.5 \pm 2.0) \cdot 10^{-3}$
$\frac{\mathrm{Im}\lambda_{CP}}{\lvert\lambda_{CP}\rvert}$	$(-2.9 \pm 1.0) \cdot 10^{-2}$	$(-2.9 \pm 1.3) \cdot 10^{-2}$
$\frac{\mathrm{Re}\lambda_{CP}}{\lvert\lambda_{CP}\rvert}\mathrm{Re}z$	—	$(5.9 \pm 5.8) \cdot 10^{-3}$
$\mathrm{Im}z$	—	$(-0.5 \pm 3.5) \cdot 10^{-3}$

Table 66: Differences between the standard fit and the one done using the alternative `FvtCluster` tag vertex algorithm. The quadratic error difference is reported as well. Only common events are used here.

without fitting for the charge asymmetries (detector asymmetries+possible CP violation in decay in the tagging and flavor B sides). It was found that the only physics parameter significantly affected was $\mid q/p \mid$, which error increased by about 30%, as expected due to the correlation between $\mid q/p \mid$ and the reconstructed and tagging efficiencies. At the end of the fitting procedure, the values of ν^{α} and μ^{α} were consistent with those generated. This exercise proves that with this approach were are translating the systematics induced by the possible detector charge asymmetries into a larger statistical error.

A second toy Monte Carlo was devoted to verify that this proceduce is able to disentangle the physics (mainly $\mid q/p \mid \neq 0$) and charge asymmetries. Here, we generated 200 toy Monte Carlo experiments with a large detector asymmetry ($\nu = 10\%$ and μ^{α} is 5%, 10%, 5% and 5% for the different tagging categories), as well as a large value of $\frac{\mathrm{Re}\varepsilon}{1+|\varepsilon|^2}(\mid q/p \mid)$, 0.05. The samples were then fitted using two different sets of starting values for ν^{α}, μ^{α}, $\frac{\mathrm{Re}\varepsilon}{1+|\varepsilon|^2}$ and $\Delta\Gamma/\Gamma$: i) the generated values, ii) all zero and $\Delta\Gamma/\Gamma$=0.1. Figure 58 shows the sample-by-sample comparison of the results of the fit for $\Delta\Gamma/\Gamma$ and $\frac{\mathrm{Re}\varepsilon}{1+|\varepsilon|^2}$ (the correlation and the differences). From this check we concluded that with this procedure we are able to disentangle the physics and charge asymmetries which would result in an asymmetry in the number of $B^0\bar{B}^0$ events, at the cost of a reasonable increase in the statistical error on $\mid q/p \mid$(previous test).

The third check was performed using the dedicated full Monte Carlo sample. Here, we rerun the B reconstruction, vertexing and tagging code after killing randomly and uniformly (no p, θ, ϕ dependencies) 5% of positive and negative tracks. This 5% is approximately the precision with which we have verified on the data that there are no statistically significant asymmetries (tables 27 and 28). Then, the standard fits were applied. The results from these fits, for the Analysis 1 and Analysis 2 fits, are shown in table 67. The variation with respect to the results with no killing (tables 42 and 43) are consistent with the statistical difference. These results were used to estimate a systematic uncertainty to account for any possible residual effect (see section

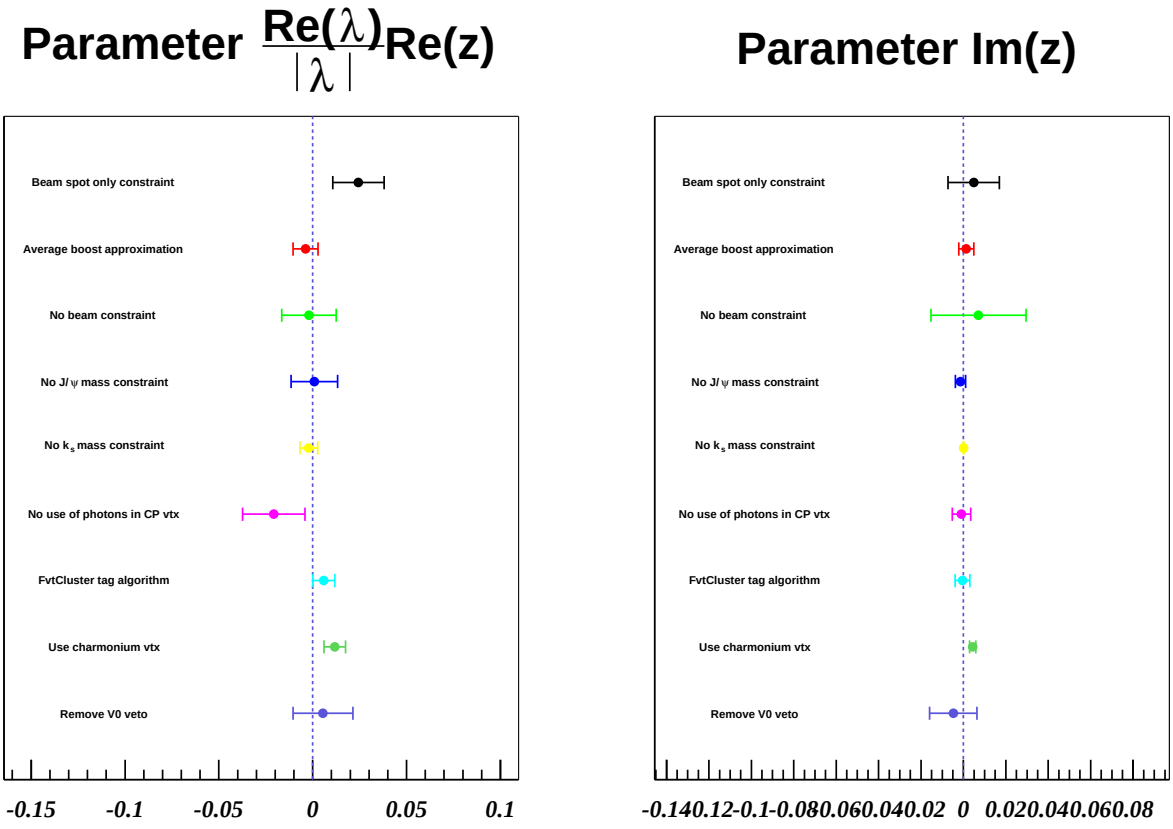

Figure 57: Graphical summary of the differences between the standard fit and the different vertexing configurations (explained in the text) from common events, for Rez$\frac{\mathrm{Re}\lambda_{CP}}{|\lambda_{CP}|}$ and Imz (Analysis 2).

9.9).

Parameter	An. 1 - positive	An. 1 - negative	An. 2 - positive	An. 2 - negative
Δm	0.4828 ± 0.0050	0.4817 ± 0.0051	0.4828 ± 0.0050	0.4816 ± 0.0051
$\Delta\Gamma/\Gamma$	0.182 ± 0.016	0.177 ± 0.016	0.182 ± 0.016	0.176 ± 0.016
$\mid q/p \mid$	1.0400 ± 0.0097	1.0330 ± 0.0097	1.0397 ± 0.0097	1.0329 ± 0.0097
$\frac{\mathrm{Im}\lambda_{CP}}{\lvert\lambda_{CP}\rvert}$	0.704 ± 0.022	0.705 ± 0.023	0.705 ± 0.022	0.702 ± 0.023
$\frac{\mathrm{Re}\lambda_{CP}}{\lvert\lambda_{CP}\rvert}$Rez	—	—	$(0.8 \pm 1.6) \cdot 10^{-2}$	$(0.5 \pm 1.7) \cdot 10^{-2}$
Imz	—	—	$(0.1 \pm 1.7) \cdot 10^{-2}$	$(-0.9 \pm 1.7) \cdot 10^{-2}$

Table 67: Results from dedicated full Monte Carlo, Analysis 2 fit, killing 5% of positive and negative tracks. *GG* resolution function is used.

Finally, as an alternative approach, one may extract ν^{α} and μ^{α} directly from the time-dependent analysis without applying the time-integrated constraints. In this case it was explicitely assumed a common ν^{α} value for all tagging categories. Given the large anti-correlation of $\mid q/p \mid$ with these parameters (about -95%), its error increases dramatically, as shown in table 68. All the other parameters remain basically unchanged.

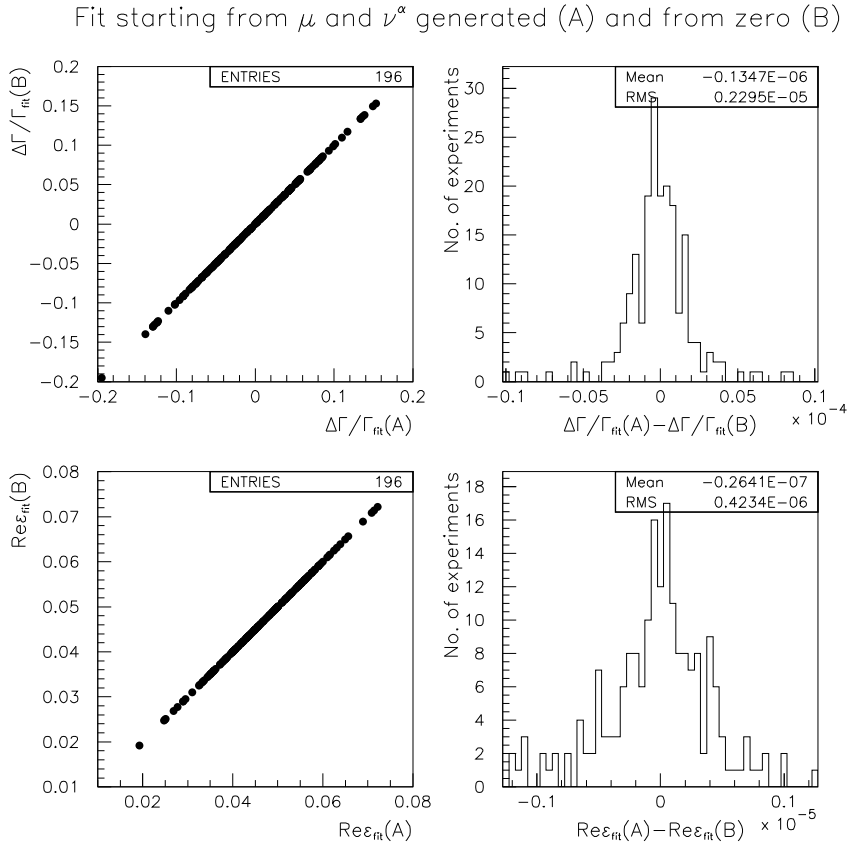

Figure 58: Comparison between the results obtained fitting the same 60 fb^{-1} samples generated with large $B^0\bar{B}^0$ differences in reconstruction and tagging efficiencies and large $\frac{\mathrm{Re}\epsilon}{1+|\epsilon|^2}$ ($\mid q/p \mid$), using different starting points for the corresponding parameters (see text for details). The upper left plot shows the correlation among the fitted values of $\Delta\Gamma/\Gamma$ from the two sets of starting points, while the upper right shows the distribution of the differnce between the two fitted parameters. The lower plots show the analogous for the $\frac{\mathrm{Re}\epsilon}{1+|\epsilon|^2}$ parameter.

Parameter	Analysis 1	Analysis 2
Δm	0.5221 ± 0.0098	0.523 ± 0.010
$\Delta\Gamma/\Gamma$	$(-0.9 \pm 4.9) \cdot 10^{-2}$	$(-2.2 \pm 4.8) \cdot 10^{-2}$
$\mid q/p \mid$	0.908 ± 0.056	0.905 ± 0.056
$\frac{\mathrm{Im}\lambda_{CP}}{\lvert\lambda_{CP}\rvert}$	0.612 ± 0.085	0.620 ± 0.082
$\frac{\mathrm{Re}\lambda_{CP}}{\lvert\lambda_{CP}\rvert}$Rez	—	$(-6.4 \pm 4.5) \cdot 10^{-2}$
Imz	—	-0.916 ± 0.034

Table 68: Results from fits to where μ^{α} and ν^{α} are extracted from the time-dependent analysis without time-integrated constraints. These results must be compared to those of tables 17 and 21. Note the dramatic increase in the $\mid q/p \mid$ error.

8.13 Results by run period

The fit was also performed for three different data taking periods: Run 1, Run 2a and Run 2b. The results are given in table 69.

Parameter	Run 1	Run 2a	Run 2b
Δm	0.504 ± 0.018	0.554 ± 0.022	0.524 ± 0.014
$\Delta\Gamma/\Gamma$	$(-5.0 \pm 7.5) \cdot 10^{-2}$	-0.06 ± 0.15	$(3.1 \pm 6.8) \cdot 10^{-2}$
$\mid q/p \mid$	0.965 ± 0.032	0.904 ± 0.039	0.946 ± 0.026
$\frac{\mathrm{Im}\lambda_{CP}}{\lvert\lambda_{CP}\rvert}$	0.50 ± 0.14	0.85 ± 0.17	0.64 ± 0.13

Parameter	Run 1	Run 2a	Run 2b
Δm	0.518 ± 0.021	0.554 ± 0.022	0.524 ± 0.014
$\Delta\Gamma/\Gamma$	$(-5.1 \pm 5.9) \cdot 10^{-2}$	-0.06 ± 0.17	$(2.8 \pm 7.0) \cdot 10^{-2}$
$\mid q/p \mid$	0.963 ± 0.033	0.903 ± 0.039	0.946 ± 0.026
$\frac{\mathrm{Im}\lambda_{CP}}{\lvert\lambda_{CP}\rvert}$	0.53 ± 0.13	0.86 ± 0.16	0.65 ± 0.13
$\frac{\mathrm{Re}\lambda_{CP}}{\lvert\lambda_{CP}\rvert}\mathrm{Re}z$	$(7.4 \pm 6.9) \cdot 10^{-2}$	-0.115 ± 0.035	-0.105 ± 0.063
$\mathrm{Im}z$	-0.892 ± 0.057	-0.906 ± 0.083	-0.936 ± 0.049

Table 69: Fit results by run period for Analysis 1 (up) and 2 (down).

8.14 Splitting of B_{flav} sample

As a cross-check of the DCKM effects in the reconstructed side (B_{flav} sample), the B_{flav} sample was splitted in two sub-samples: $B^0 \to \mathrm{D}^{(*)}\pi(\rho, \mathrm{a}_1)$ and $B^0 \to J/\psi K^{*0}$, the latter free of DCKM contributions in the reco'd side. The test was performed running the nominal fit separately for $B^0 \to \mathrm{D}^{(*)}\pi(\rho, \mathrm{a}_1)$ and $B^0 \to J/\psi K^{*0}$. $B_{CPK_S^0}$ and $B_{CPK_L^0}$ samples are unchanged with respect to nominal fit. When fitting the $B^0 \to J/\psi K^{*0}$ sample $\frac{\mathrm{Im}\lambda_{flav}}{\lvert\lambda_{flav}\rvert}$ and $\frac{\mathrm{Im}\bar{\lambda}_{flav}}{\lvert\lambda_{flav}\rvert}$ were fixed to zero. The complete fit results from both these fits are given in table 70.

Parameter	Standard B_{flav}	Using D^*X	Using $J/\psi K^*$
Δm	0.523 ± 0.010	0.522 ± 0.011	0.524 ± 0.028
$\Delta\Gamma/\Gamma$	$(-2.1 \pm 4.8) \cdot 10^{-2}$	$(-1.7 \pm 4.7) \cdot 10^{-2}$	$(-3.5 \pm 6.1) \cdot 10^{-2}$
$\mid q/p \mid$	0.945 ± 0.018	0.947 ± 0.019	0.916 ± 0.046
$\frac{\mathrm{Im}\lambda_{CP}}{\mid\lambda_{CP}\mid}$	0.620 ± 0.083	0.625 ± 0.082	0.589 ± 0.099
$\frac{\mathrm{Re}\lambda_{CP}}{\mid\lambda_{CP}\mid}\mathrm{Rez}$	$(-6.4 \pm 4.6) \cdot 10^{-2}$	$(-6.1 \pm 4.6) \cdot 10^{-2}$	$(2.2 \pm 6.7) \cdot 10^{-2}$
Imz	-0.918 ± 0.034	-0.910 ± 0.035	-1.002 ± 0.077
$\frac{\mathrm{Im}\lambda_{flav}}{\mid\lambda_{flav}\mid}$	1.7 ± 1.4	2.1 ± 1.5	3.5 ± 4.0
$\frac{\mathrm{Im}\lambda_{flav}}{\mid\lambda_{flav}\mid}$	-0.7 ± 1.4	-0.8 ± 1.5	4.7 ± 3.5
$\frac{\mathrm{Im}\lambda_{tag}}{\mid\lambda_{tag}\mid}$	1.7 ± 1.5	2.5 ± 1.6	1.0 ± 3.6
$\frac{\mathrm{Im}\lambda_{tag}}{\mid\lambda_{tag}\mid}$	-0.8 ± 1.6	-0.7 ± 1.6	5.7 ± 3.4
S_{core}	1.241 ± 0.059	1.235 ± 0.063	1.30 ± 0.11
δ_{core}^{lepton}	$(0.4 \pm 8.4) \cdot 10^{-2}$	$(5.0 \pm 8.4) \cdot 10^{-2}$	0.09 ± 0.18
δ_{core}^{kaon}	-0.302 ± 0.060	-0.282 ± 0.055	-0.387 ± 0.096
δ_{core}^{NT1}	-0.215 ± 0.093	-0.168 ± 0.092	-0.43 ± 0.21
δ_{core}^{NT2}	-0.263 ± 0.077	-0.236 ± 0.075	-0.31 ± 0.14
f_{tail}	$(3.8 \pm 1.8) \cdot 10^{-2}$	$(3.4 \pm 3.2) \cdot 10^{-2}$	$(1.9 \pm 1.4) \cdot 10^{-2}$
S_{tail}	4.3 ± 1.7	2.8 ± 1.6	7.8 ± 2.2
δ_{tail}	-2.7 ± 1.4	-4.2 ± 3.0	-1.5 ± 2.6
$f_{outlier}$	$(1.5 \pm 2.0) \cdot 10^{-3}$	$(2.6 \pm 1.6) \cdot 10^{-3}$	$(0.0 \pm 8.5) \cdot 10^{-5}$
w_0^{lepton}	$(9.3 \pm 2.4) \cdot 10^{-2}$	$(9.3 \pm 2.5) \cdot 10^{-2}$	0.103 ± 0.098
w_0^{kaon}	$(7.1 \pm 2.0) \cdot 10^{-2}$	$(7.9 \pm 2.2) \cdot 10^{-2}$	$(2.2 \pm 2.2) \cdot 10^{-2}$
w_0^{NT1}	0.184 ± 0.043	0.171 ± 0.045	0.25 ± 0.11
w_0^{NT2}	0.362 ± 0.037	0.353 ± 0.039	0.45 ± 0.10
w_{slope}^{lepton}	$(-3.5 \pm 4.3) \cdot 10^{-2}$	$(-3.2 \pm 4.4) \cdot 10^{-2}$	-0.06 ± 0.21
w_{slope}^{kaon}	0.167 ± 0.033	0.151 ± 0.035	0.30000 ± 0.00052
w_{slope}^{NT1}	$(4.2 \pm 7.3) \cdot 10^{-2}$	$(6.8 \pm 7.6) \cdot 10^{-2}$	-0.13 ± 0.19
w_{slope}^{NT2}	$(1.3 \pm 5.6) \cdot 10^{-2}$	$(2.8 \pm 5.9) \cdot 10^{-2}$	-0.16 ± 0.16
Δw^{lepton}	$(2.1 \pm 1.6) \cdot 10^{-2}$	$(2.0 \pm 1.7) \cdot 10^{-2}$	$(3.6 \pm 5.3) \cdot 10^{-2}$
Δw^{kaon}	$(-1.3 \pm 1.2) \cdot 10^{-2}$	$(-1.7 \pm 1.3) \cdot 10^{-2}$	$(0.3 \pm 3.1) \cdot 10^{-2}$
Δw^{NT1}	$(1.7 \pm 2.4) \cdot 10^{-2}$	$(1.7 \pm 2.5) \cdot 10^{-2}$	$(4.1 \pm 6.6) \cdot 10^{-2}$
Δw^{NT2}	$(-3.5 \pm 1.9) \cdot 10^{-2}$	$(-3.7 \pm 2.0) \cdot 10^{-2}$	$(2.8 \pm 4.6) \cdot 10^{-2}$
$f_{prompt,B_{flav}}^{lepton}$	0.384 ± 0.067	0.395 ± 0.069	0.23 ± 0.19
$f_{prompt,B_{flav}}^{kaon}$	0.643 ± 0.024	0.651 ± 0.024	0.108 ± 0.068
$f_{prompt,B_{flav}}^{NT1}$	0.615 ± 0.038	0.634 ± 0.038	$(0.0 \pm 4.4) \cdot 10^{-4}$
$f_{prompt,B_{flav}}^{NT2}$	0.701 ± 0.025	0.704 ± 0.025	0.64 ± 0.13
S_{back}	1.389 ± 0.023	1.393 ± 0.023	0.88 ± 0.13
δ_{back}	$(-3.8 \pm 1.7) \cdot 10^{-2}$	$(-4.0 \pm 1.7) \cdot 10^{-2}$	$(-2.9 \pm 8.6) \cdot 10^{-2}$
$f_{back,outlier}$	$(1.18 \pm 0.21) \cdot 10^{-2}$	$(1.16 \pm 0.21) \cdot 10^{-2}$	$(3.8 \pm 1.7) \cdot 10^{-2}$
$w_{0,prompt}^{lepton}$	0.143 ± 0.080	0.150 ± 0.078	$(0.0 \pm 1.7) \cdot 10^{-3}$
$w_{0,prompt}^{kaon}$	0.250 ± 0.011	0.247 ± 0.011	1.0000 ± 0.0020
$w_{0,prompt}^{NT1}$	0.339 ± 0.030	0.340 ± 0.029	1.0000 ± 0.0048
$w_{0,prompt}^{NT2}$	0.449 ± 0.015	0.447 ± 0.015	0.69 ± 0.15
$w_{0,non-prompt}^{lepton}$	0.399 ± 0.055	0.398 ± 0.057	0.39 ± 0.19
$w_{0,non-prompt}^{kaon}$	0.388 ± 0.020	0.394 ± 0.020	0.330 ± 0.067
$w_{0,non-prompt}^{NT1}$	0.448 ± 0.045	0.454 ± 0.047	0.37 ± 0.11
$w_{0,non-prompt}^{NT2}$	0.461 ± 0.032	0.466 ± 0.032	$(0.0 \pm 9.7) \cdot 10^{-4}$
$\tau_{non-prompt}$	1.319 ± 0.057	1.321 ± 0.058	1.43 ± 0.17
$f_{prompt,B_{CPK_S^0}}$	0.632 ± 0.070	0.635 ± 0.069	0.348 ± 0.094
$\tau_{non-prompt,B_{CPK_S^0}}$	2.30 ± 0.45	2.31 ± 0.46	1.36 ± 0.23

Table 70: Comparison of Analysis 2 fit results using $B^0 \to D^{(*)}\pi(\rho, a_1)$ or $B^0 \to J/\psi K^{*0}$ alone as B_{flav} sample. $\frac{\mathrm{Im}\lambda_{flav}}{\mid\lambda_{flav}\mid}$ and $\frac{\mathrm{Im}\bar{\lambda}_{flav}}{\mid\lambda_{flav}\mid}$ were fixed to zero for the latter.

8.15 Comparison of NAG, Minuit and RooFitTools results

Several checks were performed by comparing cptNagFit (NAG against Minuit) and RooFitTools [16]. These checks were done on both toy Monte Carlo and the data sample.

In the first check, we generated 60 fb^{-1} toy Monte Carlo experiments, signal events only, using the cptNagFit generator. Then we we performed fits to $\frac{\mathrm{Im}\lambda_{CP}}{|\lambda_{CP}|}$ only using the two packages. The physics parameter values used in this generation are those corresponding to the standard full Monte Carlo, shown in table 6. In this exercise, $B^0\bar{B}^0$ differences in tagging and reconstruction efficiencies and taggin/vertexing correlations were neglected. The correlation among the central values and reported errors for the two fitters are shown in figure 59(a). The errors reported by cptNagFit tend to be slightly smaller than RooFit. Figure 59(b) shows the corresponding differences, indicating that the spread of the central values is consistent with the small difference (calculated quadratically) in the reported errors.

As an additional check, we performed the fit with cptNagFit using NAG and Minuit libraries, fitting the same toy Monte Carlo experiments, but now now leaving all physics parameters free. Figure 60 shows the correlation of the results from the two libraries, for the converged fits. The NAG option is the one used by default in this analysis. From these Monte Carlo studies we observe that the rate of failed fits and the speed is signficantly better for NAG, the difference increasing as the number of free parameters increases. As an example, the CPU needed by NAG to perform a nonimal full fit on ≈ 60 fb^{-1} (signal+background) is on average less than half of what is needed by Minuit. In the case of the data fit (see below) Minuit takes more than twice CPU time than NAG.

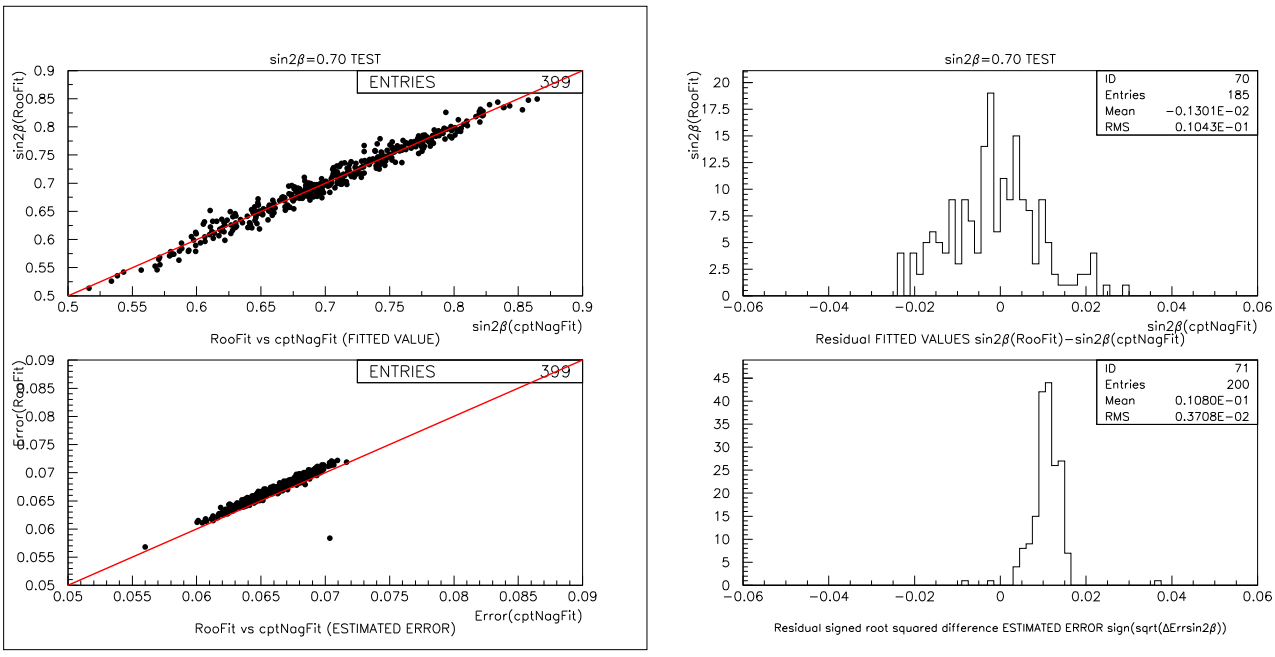

(a) (b)

Figure 59: (a) RooFit versus cptNagFit central values and errors for $\sin 2\beta$ only fits, from toy Monte Carlo samples with generated $\sin 2\beta = 0.70$); (b) residual distribution for the two considered quantities. The residual error distributions shows the signed root square difference between the squared errors of the two fitters. The sign is determined by the sign of the difference (b).

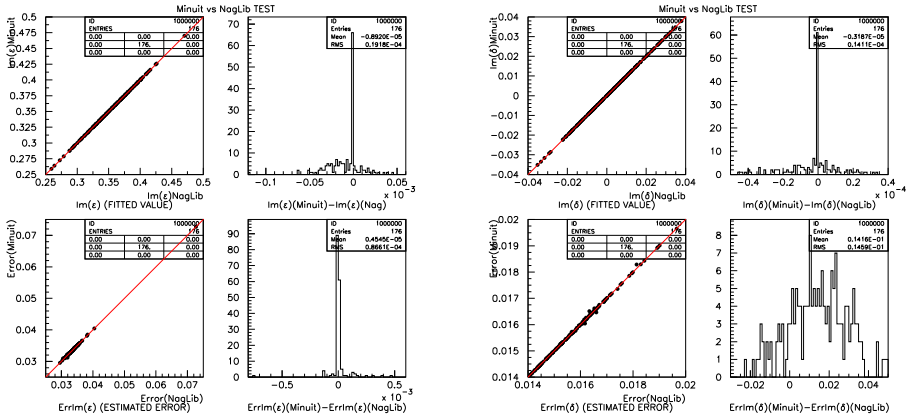

(a) (b)

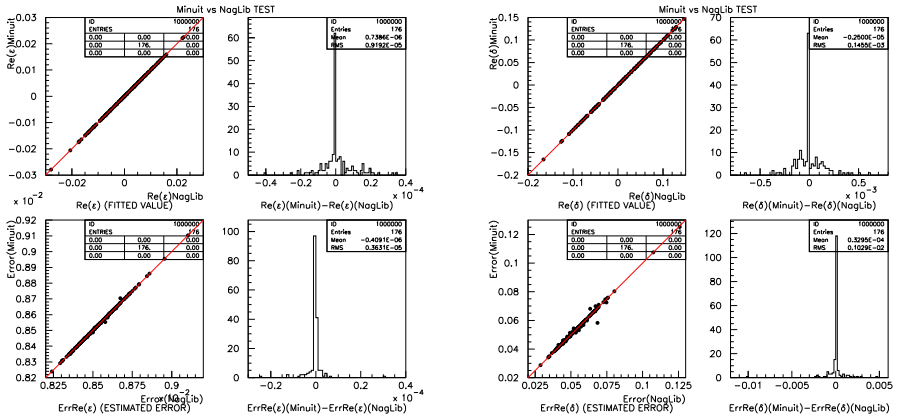

(c) (d)

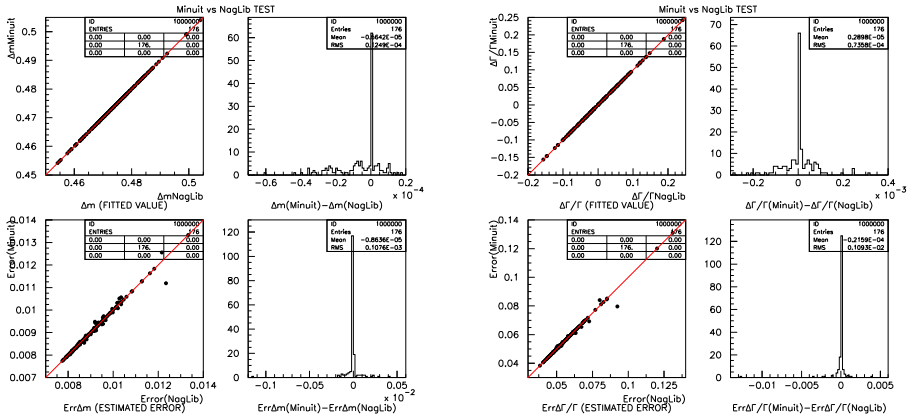

(e) (f)

Figure 60: `Minuit` versus `NAG`, and residual distribution for the physics parameters and their estimated errors: (a) $\frac{\mathrm{Im}\varepsilon}{1+|\varepsilon|^2}$, (b) $\frac{\mathrm{Im}\delta}{1+|\varepsilon|^2}$, (c) $\frac{\mathrm{Re}\varepsilon}{1+|\varepsilon|^2}$ (d) $\frac{\mathrm{Re}\delta}{1+|\varepsilon|^2}$, (e) Δm and (f) $\Delta\Gamma/\Gamma$.

The third test we performed was the comparison of results found with `cptNagFit` and `RootFitTools` for $\sin 2\beta$ only fits in data. In this check, the following simplications were made (in order to compare with the standard $\sin 2\beta$ analysis results, [8]): i) Δm, σ_{tail} and r_k ($k = tag, flav$) were fixed respectively to 0.472 ps^{-1}, 3.0 and 0 (therefore we did not fit for $\frac{\mathrm{Im}\lambda_{tag}}{|\lambda_{tag}|}$, $\frac{\mathrm{Im}\lambda_{tag}}{|\lambda_{tag}|}$, $\frac{\mathrm{Im}\lambda_{flav}}{|\lambda_{flav}|}$ and $\frac{\mathrm{Im}\lambda_{flav}}{|\lambda_{flav}|}$); ii) the tagging/vertexing correlations were neglected. The only differences between the `RootFitTools` and the `cptNagFit` fits were: i) `cptNagFit` fitted for the $B^0\bar{B}^0$ differences in reconstruction and tagging efficiencies ($\sin 2\beta$ is however insensitive to this); ii) the $\sigma_{\Delta t}$ cut was 1.4 ps for `cptNagFit` while it was 2.5 ps for `RootFitTools`. As the data sample we are using was already unblided (for $\sin 2\beta$) these fits were performed unblinded. Table 71 compares the fit results for the combined $B_{CPK^0_S}$ and $B_{CPK^0_L}$ fit. The corresponding values for $B_{CPK^0_S}$ and $B_{CPK^0_L}$ only fits are compared in tables 72 and 73 respectively.

Finally, the nominal fits for Analysis 1 and Analysis 2 were performed using `Minuit` instead of the default `NAG` option in `cptNagFit`. The results are reported in tables 74 and 75, for Analysis 1 and 2 respectively. The agreement with the nominal fits, tables 17 and 21, is excellent. This cross-check for data fits using two completely different minimization libraries was very important to verify the robustness of the final result.

8.16 Results from charged B's

As an additional control check, the nominal fit was applied to the charged B sample. As flavor sample in this case we used the charged B sample described in section 7.1.1, and as CP sample we used the charmonium B^+ sample, with the following modes: $B^+ \to J/\psi K^+$, $B^+ \to \psi(2S)K^+$, $B^+ \to \chi_{c1}\ K^+$ and $B^+ \to J/\psi K^{*+}(K^0_S\pi^+)$, with $J/\psi \to e^-e^-, \mu^+\mu^-$ and $\psi(2S) \to J/\psi e^-e^-, \mu^+\mu^-, J/\psi\pi^+\pi^-$; $\chi_{c1} \to J/\psi\gamma$ [8]. Due to the absence of mixing and CP violation in these samples, it was not possible to perform a simulatenous fit to all the parameters. The check was then performed by fixing Δm=0 and $\mid q/p \mid$=1 in the B_{flav} sample, and Δm=0.472 ps^{-1} and $\frac{\mathrm{Im}\lambda_{CP}}{|\lambda_{CP}|}$=0 in the B_{CP} samples, fitting only for $\Delta\Gamma/\Gamma$, Rez and Imz. The results are given in table 76. No statistically significant deviations from 0 are observed.

Figure 61 summarizes graphically the differences to the nominal fit in the data for the different cross-check configurations described in this section.

9 Systematic uncertainties

9.1 Signal probability of B_{flav} and $B_{CPK^0_S}$ samples

The event-by-event probability for B_{flav} and $B_{CPK^0_S}$ samples was fixed to the values obtained from the previous m_{ES} fits. We compared the fit results from the nominal fits to the values obtained by changing one sigma up and down all the m_{ES} distribution parameters, taking into account their correlations. This is performed simultaneously for all tagging categories, and independently for the B_{flav} and $B_{CPK^0_S}$ samples. The resulting variations of physical parameters, given in table 77, are taken as systematic uncertainty.

We adopted also an alternative approach assuming a flat signal probability distribution: the events belonging to the sideband region ($m_{ES}<5.27$ GeV/c^2) are assigned a signal probability of zero, while we assigned a signal probability equal to the purity of the corresponding sample to signal region events ($m_{ES}>5.27$ GeV/c^2). The differences among fitted physical parameters with respect to standard approach are given in table 78. Results are in all cases consistent. The change off the different parameters by varying up and down with the error of the sample purity the signal probability are reported in table 79.

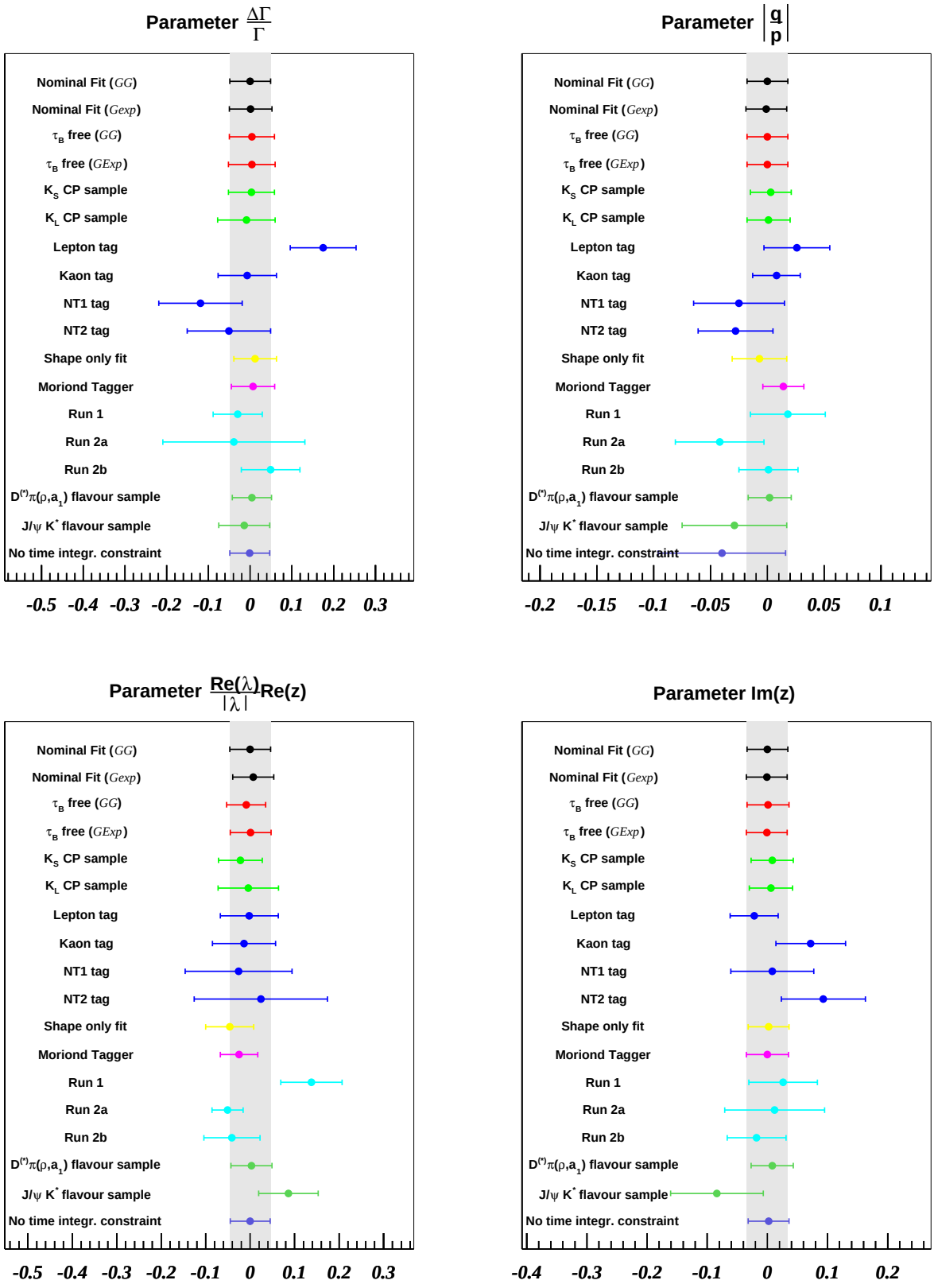

Figure 61: Graphical summary of the differences between the standard data fit and the different cross-check configurations described in this section for $\Delta\Gamma/\Gamma$, $|\,q/p\,|$, $\frac{\mathrm{Re}\lambda_{CP}}{|\lambda_{CP}|}$Rez and Imz (Analysis 2).

Parameter	cptNagFit	RooFit
$\frac{\mathrm{Im}\lambda_{CP}}{\lvert\lambda_{CP}\rvert}(\sin 2\beta)$	0.753 ± 0.089	0.753 ± 0.089
S_{core}	1.190 ± 0.056	1.167 ± 0.053
δ_{core}^{lepton}	$(1.0 \pm 7.3) \cdot 10^{-2}$	$(2.1 \pm 6.6) \cdot 10^{-2}$
δ_{core}^{kaon}	-0.279 ± 0.047	-0.229 ± 0.040
δ_{core}^{NT1}	-0.203 ± 0.087	-0.226 ± 0.079
δ_{core}^{NT2}	-0.240 ± 0.067	-0.190 ± 0.058
f_{tail}	$(2.9 \pm 2.0) \cdot 10^{-2}$	$(7.0 \pm 2.5) \cdot 10^{-2}$
δ_{tail}	-4.0 ± 1.8	-2.02 ± 0.72
$f_{outlier}$	$(3.1 \pm 1.5) \cdot 10^{-3}$	$(3.5 \pm 1.5) \cdot 10^{-3}$
w_0^{lepton}	$(8.67 \pm 0.91) \cdot 10^{-2}$	$(8.57 \pm 0.87) \cdot 10^{-2}$
w_0^{kaon}	0.1821 ± 0.0069	0.1823 ± 0.0065
w_0^{NT1}	0.218 ± 0.015	0.218 ± 0.014
w_0^{NT2}	0.375 ± 0.013	0.372 ± 0.012
Δw^{lepton}	$(1.9 \pm 1.6) \cdot 10^{-2}$	$(1.1 \pm 1.4) \cdot 10^{-2}$
Δw^{kaon}	$(-1.4 \pm 1.1) \cdot 10^{-2}$	$(-9.0 \pm 9.8) \cdot 10^{-3}$
Δw^{NT1}	$(1.4 \pm 2.3) \cdot 10^{-2}$	$(0.6 \pm 2.1) \cdot 10^{-2}$
Δw^{NT2}	$(-3.6 \pm 1.9) \cdot 10^{-2}$	$(-3.6 \pm 1.7) \cdot 10^{-2}$
Parameter	cptNagFit	RooFit
$f_{prompt,B_{flav}}^{lepton}$	0.383 ± 0.067	0.372 ± 0.067
$f_{prompt,B_{flav}}^{kaon}$	0.643 ± 0.024	0.633 ± 0.024
$f_{prompt,B_{flav}}^{NT1}$	0.615 ± 0.038	0.594 ± 0.039
$f_{prompt,B_{flav}}^{NT2}$	0.701 ± 0.025	0.702 ± 0.024
S_{back}	1.391 ± 0.023	1.390 ± 0.021
δ_{back}	$(-3.8 \pm 1.7) \cdot 10^{-2}$	$(-3.2 \pm 1.6) \cdot 10^{-2}$
$f_{back,outlier}$	$(1.18 \pm 0.21) \cdot 10^{-2}$	$(1.76 \pm 0.23) \cdot 10^{-2}$
$w_{0,prompt}^{lepton}$	0.132 ± 0.081	0.123 ± 0.085
$w_{0,prompt}^{kaon}$	0.248 ± 0.011	0.257 ± 0.012
$w_{0,prompt}^{NT1}$	0.337 ± 0.030	0.332 ± 0.031
$w_{0,prompt}^{NT2}$	0.448 ± 0.015	0.456 ± 0.015
$w_{0,non-prompt}^{lepton}$	0.407 ± 0.055	0.411 ± 0.054
$w_{0,non-prompt}^{kaon}$	0.393 ± 0.020	0.394 ± 0.020
$w_{0,non-prompt}^{NT1}$	0.452 ± 0.045	0.452 ± 0.043
$w_{0,non-prompt}^{NT2}$	0.463 ± 0.032	0.463 ± 0.032
$\tau_{non-prompt}$	1.322 ± 0.057	1.290 ± 0.054

Table 71: Comparison of `cptNagFit` and `RootFitTools` results for the $\sin 2\beta$ only fit. $\sin 2\beta$ is in this case unblinded.

We finally assigned as systematics the larger one sigma variation between the two methods.

In addition, we changed the m_{ES} endpoint in the m_{ES} fit (by default is fixed to 5.291 GeV/c^2) by ± 0.002 GeV/c^2. The change on the parameters is given in table 80.

Parameter	cptNagFit	RooFit
$\frac{\mathrm{Im}\lambda_{CP}}{\lvert\lambda_{CP}\rvert}(\sin 2\beta)$	0.755 ± 0.100	0.758 ± 0.100
S_{core}	1.188 ± 0.057	1.183 ± 0.054
δ_{core}^{lepton}	$(1.0 \pm 7.4) \cdot 10^{-2}$	$(2.2 \pm 6.9) \cdot 10^{-2}$
δ_{core}^{kaon}	-0.272 ± 0.047	-0.238 ± 0.041
δ_{core}^{NT1}	-0.213 ± 0.088	-0.220 ± 0.082
δ_{core}^{NT2}	-0.236 ± 0.069	-0.202 ± 0.061
f_{tail}	$(2.9 \pm 2.0) \cdot 10^{-2}$	$(5.6 \pm 2.5) \cdot 10^{-2}$
δ_{tail}	-4.1 ± 1.8	-2.5 ± 1.0
$f_{outlier}$	$(3.4 \pm 1.6) \cdot 10^{-3}$	$(3.7 \pm 1.6) \cdot 10^{-3}$
w_0^{lepton}	$(8.60 \pm 0.91) \cdot 10^{-2}$	$(8.62 \pm 0.90) \cdot 10^{-2}$
w_0^{kaon}	0.1814 ± 0.0069	0.1812 ± 0.0068
w_0^{NT1}	0.217 ± 0.015	0.220 ± 0.015
w_0^{NT2}	0.376 ± 0.013	0.372 ± 0.013
Δw^{lepton}	$(2.2 \pm 1.6) \cdot 10^{-2}$	$(0.9 \pm 1.5) \cdot 10^{-2}$
Δw^{kaon}	$(-0.8 \pm 1.1) \cdot 10^{-2}$	$(-0.7 \pm 1.0) \cdot 10^{-2}$
Δw^{NT1}	$(2.4 \pm 2.4) \cdot 10^{-2}$	$(1.8 \pm 2.3) \cdot 10^{-2}$
Δw^{NT2}	$(-3.6 \pm 1.9) \cdot 10^{-2}$	$(-4.1 \pm 1.9) \cdot 10^{-2}$
Parameter	cptNagFit	RooFit
$f_{prompt,B_{flav}}^{lepton}$	0.385 ± 0.067	0.384 ± 0.068
$f_{prompt,B_{flav}}^{kaon}$	0.645 ± 0.024	0.641 ± 0.024
$f_{prompt,B_{flav}}^{NT1}$	0.617 ± 0.038	0.612 ± 0.038
$f_{prompt,B_{flav}}^{NT2}$	0.703 ± 0.025	0.705 ± 0.024
S_{back}	1.393 ± 0.023	1.394 ± 0.021
δ_{back}	$(-3.8 \pm 1.7) \cdot 10^{-2}$	$(-3.4 \pm 1.6) \cdot 10^{-2}$
$f_{back,outlier}$	$(1.18 \pm 0.21) \cdot 10^{-2}$	$(1.74 \pm 0.23) \cdot 10^{-2}$
$w_{0,prompt}^{lepton}$	0.133 ± 0.080	0.132 ± 0.082
$w_{0,prompt}^{kaon}$	0.248 ± 0.011	0.254 ± 0.012
$w_{0,prompt}^{NT1}$	0.337 ± 0.030	0.333 ± 0.030
$w_{0,prompt}^{NT2}$	0.448 ± 0.015	0.453 ± 0.015
$w_{0,non-prompt}^{lepton}$	0.408 ± 0.055	0.410 ± 0.056
$w_{0,non-prompt}^{kaon}$	0.393 ± 0.020	0.399 ± 0.020
$w_{0,non-prompt}^{NT1}$	0.452 ± 0.045	0.457 ± 0.045
$w_{0,non-prompt}^{NT2}$	0.463 ± 0.032	0.468 ± 0.033
$\tau_{non-prompt}$	1.323 ± 0.057	1.292 ± 0.056

Table 72: Comparison of `cptNagFit` and `RootFitTools` results for the $\sin 2\beta$ only fit ($B_{CPK_S^0}$ only). $\sin 2\beta$ is in this case unblinded.

9.2 Resolution function

Two difference sources of systematics from the resolution function are considered.

The first one is due to its parameterization, for signal and combinatorial background. This is estimated from the difference between the (*GG* vs *GExp*) resolution models. The differences are reported in table 81.

Parameter	cptNagFit	RooFit
$\frac{\mathrm{Im}\lambda_{CP}}{\lvert\lambda_{CP}\rvert}(\sin 2\beta)$	0.74 ± 0.19	0.73 ± 0.19
S_{core}	1.177 ± 0.060	1.155 ± 0.058
δ_{core}^{lepton}	$(-1.1 \pm 7.5) \cdot 10^{-2}$	$(-0.2 \pm 7.0) \cdot 10^{-2}$
δ_{core}^{kaon}	-0.268 ± 0.048	-0.236 ± 0.043
δ_{core}^{NT1}	-0.188 ± 0.089	-0.201 ± 0.085
δ_{core}^{NT2}	-0.231 ± 0.069	-0.203 ± 0.063
f_{tail}	$(3.6 \pm 2.4) \cdot 10^{-2}$	$(8.0 \pm 2.6) \cdot 10^{-2}$
δ_{tail}	-3.6 ± 1.6	-1.80 ± 0.62
$f_{outlier}$	$(2.8 \pm 1.5) \cdot 10^{-3}$	$(2.7 \pm 1.5) \cdot 10^{-3}$
w_0^{lepton}	$(8.65 \pm 0.91) \cdot 10^{-2}$	$(8.65 \pm 0.91) \cdot 10^{-2}$
w_0^{kaon}	0.1822 ± 0.0069	0.1809 ± 0.0068
w_0^{NT1}	0.218 ± 0.015	0.220 ± 0.015
w_0^{NT2}	0.375 ± 0.013	0.372 ± 0.013
Δw^{lepton}	$(1.6 \pm 1.6) \cdot 10^{-2}$	$(0.6 \pm 1.5) \cdot 10^{-2}$
Δw^{kaon}	$(-1.6 \pm 1.1) \cdot 10^{-2}$	$(-1.2 \pm 1.1) \cdot 10^{-2}$
Δw^{NT1}	$(0.9 \pm 2.4) \cdot 10^{-2}$	$(0.5 \pm 2.3) \cdot 10^{-2}$
Δw^{NT2}	$(-4.4 \pm 2.0) \cdot 10^{-2}$	$(-4.4 \pm 1.9) \cdot 10^{-2}$
Parameter	cptNagFit	RooFit
$f_{prompt,B_{flav}}^{lepton}$	0.384 ± 0.067	0.388 ± 0.068
$f_{prompt,B_{flav}}^{kaon}$	0.644 ± 0.024	0.643 ± 0.024
$f_{prompt,B_{flav}}^{NT1}$	0.616 ± 0.038	0.614 ± 0.038
$f_{prompt,B_{flav}}^{NT2}$	0.702 ± 0.025	0.706 ± 0.024
S_{back}	1.391 ± 0.023	1.395 ± 0.021
δ_{back}	$(-3.6 \pm 1.7) \cdot 10^{-2}$	$(-3.2 \pm 1.6) \cdot 10^{-2}$
$f_{back,outlier}$	$(1.16 \pm 0.20) \cdot 10^{-2}$	$(1.64 \pm 0.23) \cdot 10^{-2}$
$w_{0,prompt}^{lepton}$	0.132 ± 0.080	0.134 ± 0.080
$w_{0,prompt}^{kaon}$	0.248 ± 0.011	0.254 ± 0.012
$w_{0,prompt}^{NT1}$	0.337 ± 0.030	0.333 ± 0.030
$w_{0,prompt}^{NT2}$	0.448 ± 0.015	0.453 ± 0.015
$w_{0,non-prompt}^{lepton}$	0.408 ± 0.055	0.411 ± 0.056
$w_{0,non-prompt}^{kaon}$	0.393 ± 0.020	0.400 ± 0.020
$w_{0,non-prompt}^{NT1}$	0.452 ± 0.045	0.457 ± 0.045
$w_{0,non-prompt}^{NT2}$	0.463 ± 0.032	0.468 ± 0.033
$\tau_{non-prompt}$	1.325 ± 0.057	1.304 ± 0.057

Table 73: Comparison of `cptNagFit` and `RootFitTools` results for the $\sin 2\beta$ only fit ($B_{CPK_L^0}$ only). $\sin 2\beta$ is in this case unblinded.

The second source contributing to the systematics from the resolution function is due to the parameters of the the outlier component (width and bias), fixed to 8.0 and 0.0 ps. The uncertainty was estimated in this case by assuming a flat outlier Gaussian (table 82). An additional contribution was estimated by varying ± 6 ps the width, and ± 5 ps the bias. The results from this variation are summarized in tables 83 and 84.

Parameter	B^0 fit results (*GG* model)
Δm	0.5218 ± 0.0097
$\Delta\Gamma/\Gamma$	$(-1.1 \pm 5.0) \cdot 10^{-2}$
$\mid q/p \mid$	0.946 ± 0.018
$\frac{\mathrm{Im}\lambda_{CP}}{\lvert\lambda_{CP}\rvert}$	0.611 ± 0.085
S_{core}	1.291 ± 0.045
δ_{core}^{lepton}	$(-1.7 \pm 7.1) \cdot 10^{-2}$
δ_{core}^{kaon}	-0.316 ± 0.040
δ_{core}^{NT1}	-0.233 ± 0.083
δ_{core}^{NT2}	-0.278 ± 0.061
f_{tail}	$(1.04 \pm 0.31) \cdot 10^{-2}$
S_{tail}	0.40 ± 0.67
δ_{tail}	-7.71 ± 0.62
$f_{outlier}$	$(2.9 \pm 1.4) \cdot 10^{-3}$
w_0^{lepton}	$(9.3 \pm 2.2) \cdot 10^{-2}$
w_0^{kaon}	$(7.2 \pm 2.0) \cdot 10^{-2}$
w_0^{NT1}	0.182 ± 0.040
w_0^{NT2}	0.362 ± 0.037
w_{slope}^{lepton}	$(-3.3 \pm 3.9) \cdot 10^{-2}$
w_{slope}^{kaon}	0.164 ± 0.032
w_{slope}^{NT1}	$(4.6 \pm 6.8) \cdot 10^{-2}$
w_{slope}^{NT2}	$(1.3 \pm 5.5) \cdot 10^{-2}$
Δw^{lepton}	$(2.2 \pm 1.6) \cdot 10^{-2}$
Δw^{kaon}	$(-1.2 \pm 1.2) \cdot 10^{-2}$
Δw^{NT1}	$(1.8 \pm 2.4) \cdot 10^{-2}$
Δw^{NT2}	$(-3.4 \pm 1.9) \cdot 10^{-2}$

Parameter	B^0 fit results (*GG* model)
$\frac{\mathrm{Im}\lambda_{flav}}{\lvert\lambda_{flav}\rvert}$	0.7 ± 1.2
$\frac{\mathrm{Im}\lambda_{flav}}{\lvert\lambda_{flav}\rvert}$	0.5 ± 1.2
$\frac{\mathrm{Im}\lambda_{tag}}{\lvert\lambda_{tag}\rvert}$	0.5 ± 1.3
$\frac{\mathrm{Im}\lambda_{tag}}{\lvert\lambda_{tag}\rvert}$	0.6 ± 1.3
$f_{prompt,B_{flav}}^{lepton}$	0.383 ± 0.067
$f_{prompt,B_{flav}}^{kaon}$	0.643 ± 0.024
$f_{prompt,B_{flav}}^{NT1}$	0.615 ± 0.038
$f_{prompt,B_{flav}}^{NT2}$	0.701 ± 0.025
S_{back}	1.388 ± 0.023
δ_{back}	$(-3.8 \pm 1.6) \cdot 10^{-2}$
$f_{back,outlier}$	$(1.18 \pm 0.21) \cdot 10^{-2}$
$w_{0,prompt}^{lepton}$	0.143 ± 0.079
$w_{0,prompt}^{kaon}$	0.250 ± 0.011
$w_{0,prompt}^{NT1}$	0.339 ± 0.030
$w_{0,prompt}^{NT2}$	0.449 ± 0.015
$w_{0,non-prompt}^{lepton}$	0.398 ± 0.055
$w_{0,non-prompt}^{kaon}$	0.387 ± 0.020
$w_{0,non-prompt}^{NT1}$	0.448 ± 0.045
$w_{0,non-prompt}^{NT2}$	0.461 ± 0.032
$\tau_{non-prompt}$	1.320 ± 0.056
$f_{prompt,B_{CPK_S^0}}$	0.632 ± 0.069
$\tau_{non-prompt,B_{CPK_S^0}}$	2.30 ± 0.45

Table 74: Analysis 1 results from `Minuit`, *GG* resolution model.

9.3 Beam spot

The beam spot position and width are used in the vertexing algorithm of the tagging B [24]. For this reason is important to determine the systematic contribution coming from the determination of its parameters. We performed Analysis 1 and 2 data fits moving the beam spot by 20 and 40 μm in the y direction (the one along which is best determined the width) and increasing the width by the same amount (separately). Since the sample composition of the reconstructed events can differ when the beam spots parameters are changed, we used the events common to the two samples to perform a fit in the standard configuration and in the one where we introduced the systematic effect. The differences among the fitted values are reported in tables 85 and 86. The largest differences are used to assign the systematic error.

9.4 Absolute z scale and boost uncertainty

The uncertainty in the scale of the Δz measurement has been estimated to be about $\pm 0.3\%$ [25]. As this estimate corresponds to the beampipe, the uncertainty has been conservatively increased by a factor 2 to account for possible mistakes in the extrapolation to the beamspot. On the other hand, the boost is known with a relative precision of $\pm 0.1\%$ [27]. The effect of the uncertainty on the absolute z scale and boost can then be evaluated scaling the measured Δt and its error by 0.6% in the data sample. The effect on the physical parameters is shown in table 88.

Parameter	B^0 fit results (*GG* model)
Δm	0.523 ± 0.010
$\Delta\Gamma/\Gamma$	$(-2.4 \pm 4.9) \cdot 10^{-2}$
$\mid q/p \mid$	0.945 ± 0.018
$\frac{\mathrm{Im}\lambda_{CP}}{\mid\lambda_{CP}\mid}$	0.618 ± 0.083
$\frac{\mathrm{Re}\lambda_{CP}}{\mid\lambda_{CP}\mid}\mathrm{Rez}$	$(-6.0 \pm 4.7) \cdot 10^{-2}$
Imz	-0.918 ± 0.034
S_{core}	1.291 ± 0.045
δ_{core}^{lepton}	$(-1.9 \pm 7.1) \cdot 10^{-2}$
δ_{core}^{kaon}	-0.316 ± 0.040
δ_{core}^{NT1}	-0.233 ± 0.083
δ_{core}^{NT2}	-0.278 ± 0.061
f_{tail}	$(1.03 \pm 0.30) \cdot 10^{-2}$
S_{tail}	0.38 ± 0.67
δ_{tail}	-7.71 ± 0.62
$f_{outlier}$	$(2.9 \pm 1.4) \cdot 10^{-3}$
w_0^{lepton}	$(9.3 \pm 2.2) \cdot 10^{-2}$
w_0^{kaon}	$(7.2 \pm 2.0) \cdot 10^{-2}$
w_0^{NT1}	0.182 ± 0.040
w_0^{NT2}	0.362 ± 0.037
w_{slope}^{lepton}	$(-3.4 \pm 3.9) \cdot 10^{-2}$
w_{slope}^{kaon}	0.165 ± 0.032
w_{slope}^{NT1}	$(4.6 \pm 6.8) \cdot 10^{-2}$
w_{slope}^{NT2}	$(1.3 \pm 5.5) \cdot 10^{-2}$
Δw^{lepton}	$(2.1 \pm 1.6) \cdot 10^{-2}$
Δw^{kaon}	$(-1.3 \pm 1.2) \cdot 10^{-2}$
Δw^{NT1}	$(1.7 \pm 2.4) \cdot 10^{-2}$
Δw^{NT2}	$(-3.4 \pm 1.9) \cdot 10^{-2}$

Parameter	B^0 fit results (*GG* model)
$\frac{\mathrm{Im}\lambda_{flav}}{\mid\lambda_{flav}\mid}$	1.7 ± 1.4
$\frac{\mathrm{Im}\lambda_{flav}}{\mid\lambda_{flav}\mid}$	-0.6 ± 1.4
$\frac{\mathrm{Im}\lambda_{tag}}{\mid\lambda_{tag}\mid}$	1.7 ± 1.5
$\frac{\mathrm{Im}\lambda_{tag}}{\mid\lambda_{tag}\mid}$	-0.7 ± 1.6
$f_{prompt,B_{flav}}^{lepton}$	0.383 ± 0.067
$f_{prompt,B_{flav}}^{kaon}$	0.643 ± 0.024
$f_{prompt,B_{flav}}^{NT1}$	0.615 ± 0.038
$f_{prompt,B_{flav}}^{NT2}$	0.701 ± 0.025
S_{back}	1.388 ± 0.023
δ_{back}	$(-3.8 \pm 1.6) \cdot 10^{-2}$
$f_{back,outlier}$	$(1.18 \pm 0.21) \cdot 10^{-2}$
$w_{0,prompt}^{lepton}$	0.143 ± 0.079
$w_{0,prompt}^{kaon}$	0.250 ± 0.011
$w_{0,prompt}^{NT1}$	0.339 ± 0.030
$w_{0,prompt}^{NT2}$	0.449 ± 0.015
$w_{0,non-prompt}^{lepton}$	0.398 ± 0.055
$w_{0,non-prompt}^{kaon}$	0.387 ± 0.020
$w_{0,non-prompt}^{NT1}$	0.448 ± 0.045
$w_{0,non-prompt}^{NT2}$	0.461 ± 0.032
$\tau_{non-prompt}$	1.320 ± 0.056
$f_{prompt,B_{CPK_S^0}}$	0.632 ± 0.069
$\tau_{non-prompt,B_{CPK_S^0}}$	2.30 ± 0.45

Table 75: Analysis 2 results from `Minuit`, *GG* resolution model.

9.5 SVT misalignment

In table 87 are reported the differences among the fitted values of the same Monte Carlo sample with perfect and `diffEL` alignments. `diffEL` (difference between the E and L alignment sets) is considered an extreme and unrealistic representation of the real misalignment. Conservatively, we use it to estimate the systematic error from the SVT internal misalignment [8].

9.6 Average B^0 lifetime

The average B^0 lifetime was varied by ± 0.032 ps [22]. The effect on the physical parameters is reported in table 89.

9.7 B^+ lifetime

The B^+ lifetime (used in the peaking background of the B_{flav} sample) was varied by ± 0.031 ps [22]. The effect of the variation can be found in table 90. Let us note that there is no effect propagated via the B^+ mistags

Parameter	B^+ fit results (GG model)
$\Delta\Gamma/\Gamma$	$(-3.1 \pm 2.4) \cdot 10^{-2}$
$\frac{\mathrm{Re}\lambda_{CP}}{\lvert\lambda_{CP}\rvert}$Rez	$(0.4 \pm 3.9) \cdot 10^{-2}$
Imz	$(-4.6 \pm 4.3) \cdot 10^{-2}$
S_{core}	1.13 ± 0.40
δ_{core}^{lepton}	-0.15 ± 0.22
δ_{core}^{kaon}	-0.21 ± 0.18
δ_{core}^{NT1}	-0.12 ± 0.26
δ_{core}^{NT2}	-0.25 ± 0.17
f_{tail}	0.15 ± 0.71
S_{tail}	2.0 ± 2.3
δ_{tail}	-0.48 ± 0.83
$f_{outlier}$	$(0.1 \pm 1.1) \cdot 10^{-3}$
w_0^{lepton}	$(4.7 \pm 1.4) \cdot 10^{-2}$
w_0^{kaon}	$(3.9 \pm 1.3) \cdot 10^{-2}$
w_0^{NT1}	$(9.4 \pm 3.1) \cdot 10^{-2}$
w_0^{NT2}	0.318 ± 0.030
w_{slope}^{lepton}	$(-1.1 \pm 2.5) \cdot 10^{-2}$
w_{slope}^{kaon}	0.140 ± 0.022
w_{slope}^{NT1}	0.169 ± 0.057
w_{slope}^{NT2}	$(5.0 \pm 4.7) \cdot 10^{-2}$
Δw^{lepton}	$(2.3 \pm 9.1) \cdot 10^{-3}$
Δw^{kaon}	$(1.0 \pm 8.0) \cdot 10^{-3}$
Δw^{NT1}	$(2.3 \pm 2.1) \cdot 10^{-2}$
Δw^{NT2}	$(-2.1 \pm 1.9) \cdot 10^{-2}$

Parameter	B^+ fit results (GG model)
$f_{prompt,B_{flav}}^{lepton}$	0.236 ± 0.081
$f_{prompt,B_{flav}}^{kaon}$	0.679 ± 0.024
$f_{prompt,B_{flav}}^{NT1}$	0.725 ± 0.036
$f_{prompt,B_{flav}}^{NT2}$	0.753 ± 0.026
S_{back}	1.400 ± 0.023
δ_{back}	$(-4.0 \pm 1.8) \cdot 10^{-2}$
$f_{back,outlier}$	$(1.21 \pm 0.23) \cdot 10^{-2}$
$w_{0,prompt}^{lepton}$	0.26 ± 0.12
$w_{0,prompt}^{kaon}$	0.1634 ± 0.0098
$w_{0,prompt}^{NT1}$	0.280 ± 0.028
$w_{0,prompt}^{NT2}$	0.399 ± 0.017
$w_{0,non-prompt}^{lepton}$	0.128 ± 0.038
$w_{0,non-prompt}^{kaon}$	0.231 ± 0.019
$w_{0,non-prompt}^{NT1}$	0.431 ± 0.063
$w_{0,non-prompt}^{NT2}$	0.391 ± 0.042
$\tau_{non-prompt}$	1.344 ± 0.066

Table 76: Results from the fit to the B^+ control sample.

Parameter	Analysis 1	Analysis 2
$\Delta\Gamma/\Gamma$	$^{-6.7\cdot10^{-4}}_{+6.6\cdot10^{-4}}$	$^{-5.3\cdot10^{-4}}_{+4.8\cdot10^{-4}}$
$\lvert q/p \rvert$	$^{-2.0\cdot10^{-4}}_{+2.1\cdot10^{-4}}$	$^{-1.8\cdot10^{-4}}_{+2.0\cdot10^{-4}}$
$\frac{\mathrm{Re}\lambda_{CP}}{\lvert\lambda_{CP}\rvert}$Rez	—	$^{+1.2\cdot10^{-3}}_{-1.0\cdot10^{-3}}$
Imz	—	$^{+2.3\cdot10^{-4}}_{-2.6\cdot10^{-4}}$

Parameter	Analysis 1	Analysis 2
$\Delta\Gamma/\Gamma$	$^{+1.2\cdot10^{-3}}_{-10.0\cdot10^{-4}}$	$^{+8.7\cdot10^{-4}}_{-7.0\cdot10^{-4}}$
$\lvert q/p \rvert$	$^{-1.7\cdot10^{-4}}_{+1.8\cdot10^{-4}}$	$^{-2.5\cdot10^{-4}}_{+2.5\cdot10^{-4}}$
$\frac{\mathrm{Re}\lambda_{CP}}{\lvert\lambda_{CP}\rvert}$Rez	—	$^{+9.7\cdot10^{-4}}_{-1.0\cdot10^{-3}}$
Imz	—	$^{+3.7\cdot10^{-4}}_{-3.6\cdot10^{-4}}$

Table 77: Signal probability systematics, $B_{CPK_S^0}$(left) and B_{flav}(right) sample.

since in the charged B sample fit used to extract the mistag parameters the B^+ lifetime was left free.

Parameter	Analysis 1	Analysis 2
$\Delta\Gamma/\Gamma$	$(0.1 \pm 4.9) \cdot 10^{-2}$	$(0.4 \pm 4.8) \cdot 10^{-2}$
$\mid q/p \mid$	$(-0.1 \pm 1.8) \cdot 10^{-2}$	$(-0.1 \pm 1.8) \cdot 10^{-2}$
$\frac{\mathrm{Re}\lambda_{CP}}{\mid\lambda_{CP}\mid}$Rez	—	$(-0.1 \pm 4.6) \cdot 10^{-2}$
Imz	—	$(0.8 \pm 3.4) \cdot 10^{-2}$

Parameter	Analysis 1	Analysis 2
$\Delta\Gamma/\Gamma$	$(0.5 \pm 4.9) \cdot 10^{-2}$	$(0.4 \pm 4.8) \cdot 10^{-2}$
$\mid q/p \mid$	$(0.0 \pm 1.8) \cdot 10^{-2}$	$(0.0 \pm 1.8) \cdot 10^{-2}$
$\frac{\mathrm{Re}\lambda_{CP}}{\mid\lambda_{CP}\mid}$Rez	—	$(0.6 \pm 4.6) \cdot 10^{-2}$
Imz	—	$(-0.0 \pm 3.4) \cdot 10^{-2}$

Table 78: Differences of the parameters using signal probability flat distribution instead of standard ARGUS, for $B_{CPK^0_S}$(top) and B_{flav}(bottom) sample. The errors are the quadratic statistical differences among the two measurements.

Parameter	Analysis 1	Analysis 2
$\Delta\Gamma/\Gamma$	$^{-8.0\cdot10^{-4}}_{+8.4\cdot10^{-4}}$	$^{-6.6\cdot10^{-4}}_{+6.9\cdot10^{-4}}$
$\mid q/p \mid$	$^{+8.7\cdot10^{-5}}_{-9.2\cdot10^{-5}}$	$^{+1.1\cdot10^{-4}}_{-1.2\cdot10^{-4}}$
$\frac{\mathrm{Re}\lambda_{CP}}{\mid\lambda_{CP}\mid}$Rez	—	$^{+1.2\cdot10^{-3}}_{-1.2\cdot10^{-3}}$
Imz	—	$^{-4.4\cdot10^{-4}}_{+4.3\cdot10^{-4}}$

Parameter	Analysis 1	Analysis 2
$\Delta\Gamma/\Gamma$	$^{+9.5\cdot10^{-4}}_{-8.9\cdot10^{-4}}$	$^{+8.2\cdot10^{-4}}_{-8.2\cdot10^{-4}}$
$\mid q/p \mid$	$^{-1.2\cdot10^{-4}}_{+1.2\cdot10^{-4}}$	$^{-2.0\cdot10^{-4}}_{+1.9\cdot10^{-4}}$
$\frac{\mathrm{Re}\lambda_{CP}}{\mid\lambda_{CP}\mid}$Rez	—	$^{+2.5\cdot10^{-4}}_{-9.3\cdot10^{-5}}$
Imz	—	$^{+2.6\cdot10^{-4}}_{-3.2\cdot10^{-4}}$

Table 79: Signal probability systematics using signal probability flat distribution, for $B_{CPK^0_S}$(left) and B_{flav}(right) sample.

Parameter	Analysis 1	Analysis 2
$\Delta\Gamma/\Gamma$	$^{-1.3\cdot10^{-4}}_{-3.1\cdot10^{-4}}$	$^{-1.8\cdot10^{-4}}_{+8.4\cdot10^{-5}}$
$\mid q/p \mid$	$^{-1.6\cdot10^{-4}}_{-7.6\cdot10^{-3}}$	$^{-1.6\cdot10^{-4}}_{-7.5\cdot10^{-3}}$
$\frac{\mathrm{Re}\lambda_{CP}}{\mid\lambda_{CP}\mid}$Rez	—	$^{+3.9\cdot10^{-4}}_{+7.6\cdot10^{-4}}$
Imz	—	$^{-1.8\cdot10^{-4}}_{+2.0\cdot10^{-3}}$

Table 80: m_{ES} endpoint systematics.

9.8 B^+ mistags

Change by $\pm\sigma$ the B^+ mistags (only the average mistag at $\sigma_{\Delta t} = 0$; the slope and $B^0\overline{B}^0$ differences were not varied). All the mistags were moved simultaneously one σ up and down. The variation of the physics parameters is given in table 91.

Parameter	Analysis 1	Analysis 2
$\Delta\Gamma/\Gamma$	$+5.3\cdot10^{-3}$	$+7.4\cdot10^{-4}$
$\mid q/p \mid$	$+1.8\cdot10^{-4}$	$-1.9\cdot10^{-4}$
$\frac{\mathrm{Re}\lambda_{CP}}{\mid\lambda_{CP}\mid}$Rez	—	$+6.1\cdot10^{-3}$
Imz	—	$-1.4\cdot10^{-3}$

Table 81: Resolution function parameterization systematics.

Parameter	Analysis 1	Analysis 2
$\Delta\Gamma/\Gamma$	$+1.1\cdot10^{-3}$	$+6.8\cdot10^{-4}$
$\mid q/p \mid$	$-1.8\cdot10^{-4}$	$-2.0\cdot10^{-4}$
$\frac{\mathrm{Re}\lambda_{CP}}{\mid\lambda_{CP}\mid}$Rez	—	$-2.5\cdot10^{-3}$
Imz	—	$+1.4\cdot10^{-3}$

Table 82: Systematic shift fixing $\sigma_{outlier}$ to a very large value (20 ps).

Parameter	Analysis 1	Analysis 2
$\Delta\Gamma/\Gamma$	$+1.2\cdot10^{-3}$ $+1.7\cdot10^{-3}$	$+6.1\cdot10^{-4}$ $-6.5\cdot10^{-3}$
$\mid q/p \mid$	$-7.4\cdot10^{-5}$ $-5.0\cdot10^{-5}$	$-9.7\cdot10^{-5}$ $-1.4\cdot10^{-3}$
$\frac{\mathrm{Re}\lambda_{CP}}{\mid\lambda_{CP}\mid}$Rez	—	$-1.6\cdot10^{-3}$ $+1.1\cdot10^{-2}$
Imz	—	$+8.9\cdot10^{-4}$ $+8.7\cdot10^{-5}$

Table 83: Systematic shift corresponding to the variation of $\sigma_{outlier}$ of +4/-2 ps around the value fixed in the standard fit (9 ps).

Parameter	Analysis 1	Analysis 2
$\Delta\Gamma/\Gamma$	$-4.6\cdot10^{-4}$ $+9.2\cdot10^{-4}$	$+6.6\cdot10^{-4}$ $+2.7\cdot10^{-4}$
$\mid q/p \mid$	$-4.4\cdot10^{-5}$ $-3.5\cdot10^{-4}$	$-1.8\cdot10^{-6}$ $-3.9\cdot10^{-4}$
$\frac{\mathrm{Re}\lambda_{CP}}{\mid\lambda_{CP}\mid}$Rez	—	$+1.3\cdot10^{-4}$ $-2.4\cdot10^{-3}$
Imz	—	$+3.2\cdot10^{-4}$ $+1.5\cdot10^{-3}$

Table 84: Systematic shift corresponding to the variation of $\delta_{outlier}$ of ±5 ps around zero (standard fit).

Parameter	Analysis 1	Analysis 2
$\Delta\Gamma/\Gamma$	$+1.3\cdot10^{-3}$	$+2.7\cdot10^{-3}$
$\mid q/p \mid$	$+1.5\cdot10^{-3}$	$+1.6\cdot10^{-3}$
$\frac{\mathrm{Re}\lambda_{CP}}{\mid\lambda_{CP}\mid}$Rez	—	$+6.5\cdot10^{-4}$
Imz	—	$-1.1\cdot10^{-3}$

Parameter	Analysis 1	Analysis 2
$\Delta\Gamma/\Gamma$	$+1.1\cdot10^{-3}$	$+2.2\cdot10^{-3}$
$\mid q/p \mid$	$-6.4\cdot10^{-5}$	$-3.4\cdot10^{-4}$
$\frac{\mathrm{Re}\lambda_{CP}}{\mid\lambda_{CP}\mid}$Rez	—	$+5.6\cdot10^{-3}$
Imz	—	$+7.6\cdot10^{-4}$

Table 85: Variation of the fitted physical parameters, when the beam spot position is moved of 20 μm (left table) and 40 μm (right table) in the positive y direction.

Parameter	Analysis 1	Analysis 2
$\Delta\Gamma/\Gamma$	$-1.1\cdot10^{-4}$	$-1.0\cdot10^{-4}$
$\mid q/p \mid$	$+1.8\cdot10^{-4}$	$+1.8\cdot10^{-4}$
$\frac{\mathrm{Re}\lambda_{CP}}{\mid\lambda_{CP}\mid}$Rez	—	$+2.9\cdot10^{-4}$
Imz	—	$+6.2\cdot10^{-5}$

Parameter	Analysis 1	Analysis 2
$\Delta\Gamma/\Gamma$	$-1.1\cdot10^{-4}$	$-1.0\cdot10^{-4}$
$\mid q/p \mid$	$+1.8\cdot10^{-4}$	$+1.8\cdot10^{-4}$
$\frac{\mathrm{Re}\lambda_{CP}}{\mid\lambda_{CP}\mid}$Rez	—	$+2.9\cdot10^{-4}$
Imz	—	$+6.2\cdot10^{-5}$

Table 86: Variation of the fitted physical parameters, when the beam spot width is expanded of 20 μm (left table) and 40 μm (right table) in the y direction.

9.9 $B^0\overline{B}^0$ differences in reconstruction and tagging efficiencies

Time-integrated charge asymmetries induced by a difference in the detector response for positive and negative tracks and any possible direct CP violation in the decay of flavor eigenstate B mesons (tagging B's and reconstructed B's in the flavor eigenstate sample) are included in the PDF and extracted together with the other parameters from the time-dependent analysis. By this reason no significant systematic effects are expected from

Parameter	Analysis 1	Analysis 2
$\Delta\Gamma/\Gamma$	$-2.5\cdot10^{-3}$	$-6.0\cdot10^{-3}$
$\mid q/p \mid$	$-9.4\cdot10^{-3}$	$-1.2\cdot10^{-2}$
$\frac{\mathrm{Re}\lambda_{CP}}{\mid\lambda_{CP}\mid}$Rez	—	$+6.5\cdot10^{-3}$
Imz	—	$-1.6\cdot10^{-2}$

Table 87: Systematic contribution coming from SVT alignment. The values reported are the differences among perfect and `diffEL` alignments using the same MC sample. UPDATED.

Parameter	Analysis 1	Analysis 2
$\Delta\Gamma/\Gamma$	$^{+2.0\cdot10^{-3}}_{-4.0\cdot10^{-3}}$	$^{+1.3\cdot10^{-3}}_{-3.1\cdot10^{-3}}$
$\mid q/p \mid$	$^{-3.6\cdot10^{-4}}_{-3.1\cdot10^{-5}}$	$^{-3.9\cdot10^{-4}}_{-7.6\cdot10^{-6}}$
$\frac{\mathrm{Re}\lambda_{CP}}{\mid\lambda_{CP}\mid}$Rez	—	$^{-6.4\cdot10^{-5}}_{+5.6\cdot10^{-3}}$
Imz	—	$^{-3.8\cdot10^{-4}}_{-2.2\cdot10^{-4}}$

Table 88: Variation of the physics parameters by scaling the measured Δt and its error by 0.6% in the data sample.

Parameter	Analysis 1	Analysis 2
$\Delta\Gamma/\Gamma$	$^{-6.2\cdot10^{-3}}_{+4.5\cdot10^{-3}}$	$^{-5.1\cdot10^{-3}}_{+4.1\cdot10^{-3}}$
$\mid q/p \mid$	$^{-3.4\cdot10^{-4}}_{+6.9\cdot10^{-4}}$	$^{-4.8\cdot10^{-4}}_{+8.0\cdot10^{-4}}$
$\frac{\mathrm{Re}\lambda_{CP}}{\mid\lambda_{CP}\mid}$Rez	—	$^{+1.3\cdot10^{-2}}_{-9.7\cdot10^{-3}}$
Imz	—	$^{-5.7\cdot10^{-4}}_{+6.7\cdot10^{-4}}$

Table 89: Systematics from the variation of the average B^0 lifetime by ±0.032 ps.

Parameter	Analysis 1	Analysis 2
$\Delta\Gamma/\Gamma$	$^{+7.6\cdot10^{-5}}_{-7.5\cdot10^{-5}}$	$^{+2.0\cdot10^{-4}}_{-2.0\cdot10^{-4}}$
$\mid q/p \mid$	$^{+2.0\cdot10^{-5}}_{-2.0\cdot10^{-5}}$	$^{+3.0\cdot10^{-5}}_{-2.8\cdot10^{-5}}$
$\frac{\mathrm{Re}\lambda_{CP}}{\mid\lambda_{CP}\mid}$Rez	—	$^{-2.8\cdot10^{-4}}_{+2.8\cdot10^{-4}}$
Imz	—	$^{-7.1\cdot10^{-5}}_{+7.2\cdot10^{-5}}$

Table 90: Systematics the the variation of the B^+ lifetime by ±0.031 ps.

this source. However, in order to account for any possible and residual effect, we used the half difference between the results given in table 67, which were obtained by fitting the dedicated full Monte Carlo sample after a 5% killing of positive and negative tracks (5% is approximately the precision with which we have verified in the data that there are no charge asymmetries). The final systematics from this soure is given in table 92.

9.10 CP violation in the decay

We changed by $\pm10\%$ the ratio of conjugate decay amplitudes for CP eigenstates, $r_{CP,CP}$. The impact on the physics parameters is given in tables 93. No systematics is assigned to possible direct CP violation effects in the tagging and flavor eigenstate B samples since these effects are included in the PDF and are part of the charge asymetries, parameters ν and μ^{α}, equations (100) and (99).

Parameter	Analysis 1	Analysis 2
$\Delta\Gamma/\Gamma$	$^{+7.4\cdot10^{-6}}_{-7.4\cdot10^{-6}}$	$^{-1.0\cdot10^{-4}}_{+1.0\cdot10^{-4}}$
$\mid q/p \mid$	$^{-4.0\cdot10^{-7}}_{+3.0\cdot10^{-7}}$	$^{-1.1\cdot10^{-5}}_{+1.1\cdot10^{-5}}$
$\frac{\mathrm{Re}\lambda_{CP}}{\lvert\lambda_{CP}\rvert}$Rez	—	$^{+4.4\cdot10^{-4}}_{-4.4\cdot10^{-4}}$
Imz	—	$^{+1.4\cdot10^{-5}}_{-1.5\cdot10^{-5}}$

Table 91: Systematic uncertainties due to the variation of one σ variation of the B^+ mistag rates. Central values are varied simultaneously for all the tagging categories in the same direction.

Parameter	Analysis 1	Analysis 2
$\Delta\Gamma/\Gamma$	$-2.6\cdot10^{-3}$	$-2.6\cdot10^{-3}$
$\mid q/p \mid$	$-3.5\cdot10^{-3}$	$-3.4\cdot10^{-3}$
$\frac{\mathrm{Re}\lambda_{CP}}{\lvert\lambda_{CP}\rvert}$Rez	—	$-1.5\cdot10^{-3}$
Imz	—	$-5.1\cdot10^{-3}$

Table 92: Systematics from residual charge asymmetries.

Parameter	Analysis 1	Analysis 2
$\Delta\Gamma/\Gamma$	$^{+1.9\cdot10^{-3}}_{-1.6\cdot10^{-3}}$	$^{+2.1\cdot10^{-3}}_{-1.9\cdot10^{-3}}$
$\mid q/p \mid$	$^{-5.7\cdot10^{-3}}_{+6.3\cdot10^{-3}}$	$^{-5.7\cdot10^{-3}}_{+6.4\cdot10^{-3}}$
$\frac{\mathrm{Re}\lambda_{CP}}{\lvert\lambda_{CP}\rvert}$Rez	—	$^{-7.5\cdot10^{-4}}_{+5.6\cdot10^{-4}}$
Imz	—	$^{-3.0\cdot10^{-3}}_{+1.5\cdot10^{-3}}$

Table 93: Variation in the physics parameters due to a $\pm10\%$ direct CP violation in the CP eigenstate sample ($r_{CP,CP}$ parameter).

9.11 Doubly-CKM-Suppressed decays

Systematics from Doubly-CKM-Suppressed decays arise due to uncertainties in $r_{tag}\frac{\mathrm{Re}\lambda_{tag}}{|\lambda_{tag}|}$, $\bar{r}_{tag}\frac{\mathrm{Re}\bar{\lambda}_{tag}}{|\lambda_{tag}|}$, $r_{flav}\frac{\mathrm{Re}\lambda_{flav}}{|\lambda_{flav}|}$ and $\bar{r}_{tag}\frac{\mathrm{Re}\bar{\lambda}_{flav}}{|\lambda_{flav}|}$. Uncertainties from r_k and $\bar{r}_k$ via the DCKM cosine terms are taken into account via the rescaling of $\frac{\mathrm{Im}\lambda_{tag}}{|\lambda_{tag}|}$, $\frac{\mathrm{Im}\bar{\lambda}_{tag}}{|\lambda_{tag}|}$, $\frac{\mathrm{Im}\lambda_{flav}}{|\lambda_{flav}|}$ and $\frac{\mathrm{Im}\bar{\lambda}_{flav}}{|\lambda_{flav}|}$, as discussed in section 2.8. As the DCKM effects are dominated by the tagging side, the systematics was factorized and evaluated separately in the tagging and reconstructed sides by generating toy Monte Carlo samples with all possible values of the DCKM phase which give different values of the cosines, for B^0 and $\bar{B}^0$ independently (9 combinations). The generation used a single channel since, as discussed in 2.8 and proved in A.3, this corresponds to the worse situation. We assume the central value of r_{tag} and r_{flav} to be 0.02, estimated assuming that the amplitudes are dominated by the Standard Model $b \to c$

and $b \to c$ transitions for the favored and suppressed decays, respectively (see figure 1), and taking the values of the CKM matrix elements from [23]. To account for potential additional diagrams (due to new physics), factorization and $B^0\bar{B}^0$ differences, we assign an uncertainty of 100%, which gives a maximum value of 0.04. This is the value used in the generation. The samples were then fitted with the nominal fit and including all the experimental effects except backgrounds. From about 110 times the data statistics the largest offsets for all the physical parameters together with their statistical uncertainties are reported in tables 94 and 95, for Analysis 2 (CPT/T/CP/$\Delta\Gamma$) and Analysis 1 (T/CP/$\Delta\Gamma$), respectively. The largest between the most significant bias and its statistical uncertainty is used to assign the systematics from Doubly-CKM-Suppressed decays, as given in table 96. Tagging and reconstructed effects are added in quadrature.

	Δm	$\Delta\Gamma/\Gamma$	$\mid q/p \mid$
Tagging side	0.0029 ± 0.0007	0.008 ± 0.004	0.0063 ± 0.0014
Reconstructed side	0.0024 ± 0.0007	0.011 ± 0.004	0.0050 ± 0.0013
	$\frac{\mathrm{Re}\lambda_{CP}}{\lvert\lambda_{CP}\rvert}\mathrm{Rez}$	$\frac{\mathrm{Im}\lambda_{CP}}{\lvert\lambda_{CP}\rvert}$	Imz
Tagging side	0.027 ± 0.004	0.008 ± 0.005	0.005 ± 0.003
Reconstructed side	0.011 ± 0.004	0.012 ± 0.006	0.007 ± 0.004

Table 94: Largest variation of the CPT/T/CP/oscillation parameters from the DCKM systematics scanning (Analysis 2). Estimated from ≈ 110 times the data statistics.

	Δm	$\Delta\Gamma/\Gamma$	$\mid q/p \mid$	$\frac{\mathrm{Im}\lambda_{CP}}{\lvert\lambda_{CP}\rvert}$
Tagging side	0.0008 ± 0.0007	0.006 ± 0.005	0.0062 ± 0.0012	0.022 ± 0.006
Reconstructed side	0.0009 ± 0.0005	0.004 ± 0.003	0.0052 ± 0.0011	0.005 ± 0.006

Table 95: Largest variation of the T/CP/oscillation parameters from the DCKM systematics scanning (Analysis 1). Estimated from ≈ 110 times the data statistics.

9.12 PDF asymptotic normalization

The PDF in the nominal fit was normalized asymptotically. The effect from this assumption was evaluated by normalizing in the finite range defined by the Δt cuts ($[-20, 20]$ ps), according to equation (104). The effect on the different parameters is summarized in table 97.

Parameter	Analysis 1	Analysis 2
$\Delta\Gamma/\Gamma$	0.0072	0.0136
$\mid q/p \mid$	0.0081	0.0080
$\frac{\mathrm{Re}\lambda_{CP}}{\lvert\lambda_{CP}\rvert}\mathrm{Rez}$	–	0.0292
Imz	–	0.0086

Table 96: Systematics from Doubly-CKM-Suppressed decays.

Parameter	Analysis 1	Analysis 2
$\Delta\Gamma/\Gamma$	$-3.0\cdot10^{-3}$	$-2.3\cdot10^{-3}$
$\mid q/p \mid$	$+1.6\cdot10^{-4}$	$+1.5\cdot10^{-4}$
$\frac{\mathrm{Re}\lambda_{CP}}{\mid\lambda_{CP}\mid}$Rez	—	$+2.2\cdot10^{-3}$
Imz	—	$-3.4\cdot10^{-4}$

Table 97: Systematic contribution from the usage of PDF asymptotic normalization.

9.13 Likelihood fit

The precision on which we have verified from toy Monte Carlo (section 7.6) that the fitting procedure provides an unbiassed estimation of all the physics parameters is assigned as systematic error due to the fitting procedure. More specifically, we take as systematic error due to this source the largest between the observed bias (mean value of the residual distributions) and its statistical error due to the limited amount of toy Monte Carlo experiments. The values can be found in table 98.

Parameter	Analysis 1	Analysis 2
$\Delta\Gamma/\Gamma$	$3.6\cdot10^{-3}$	$3.0\cdot10^{-3}$
$\mid q/p \mid$	$2.8\cdot10^{-3}$	$7.6\cdot10^{-4}$
$\frac{\mathrm{Re}\lambda_{CP}}{\mid\lambda_{CP}\mid}$Rez	—	$1.4\cdot10^{-2}$
Imz	—	$1.5\cdot10^{-3}$

Table 98: Likelihood fit systematics from fitting procedure.

Another source of uncertainty contributing to the likelihood fit systematics is the assumption of universality of the Δt resolution and mistags. More specifically: i) Δt resolution and mistags for B_{flav} and B_{CP} events are the same; ii) the resolution function is the same for right and wrong tags. To evaluate this contribution we split the complete exclusive Monte Carlo sample into data-sized samples, keeping the relative sizes of signal B_{flav}, $B_{CPK_S^0}$ and $B_{CPK_L^0}$ samples as observed in the data. The dedicated Monte Carlo was also used after reweighting it to the values of the standard sample. The nominal fit (signal only) was then applied to the samples. The small combinatorial backgrounds in these exclusive samples was neglected (a check was also performed to verify it by selecting only events in the signal region, $m_{ES} > 5.25$ GeV/c^2). The total available statistics after applying this procedure was 6 times the B_{flav} sample and 34 times the $B_{CPK_S^0}$ and $B_{CPK_L^0}$. To take profit of the much larger B_{CP} statistics, we performed the fit for all possible combinations of B_{CP} and B_{flav} samples (6 fits). For B_{CP} dominated measurements ($\Delta\Gamma/\Gamma$, $\frac{\mathrm{Re}\lambda_{CP}}{\mid\lambda_{CP}\mid}$Rez), we evaluated the mean bias from the 6×34 fits, and the error from the combination of 34 fits (6) with the largest RMS. For B_{flav} dominated measurements ($\mid q/p \mid$, Imz), the mean bias and RMS was estimated from 6 random B_{CP} samples (as expected, no sizeable changes were observed by selecting a different set of B_{CP} samples). The results obtained with this procedure are reported in table 99. We assigned as systematics the largest between the mean residual and its uncertainty, as given in table 100. No corrections were applied to the central values extracted from the data. Let us note that this procedure also takes into account other possible missing or not accurate enough assumptions reproduced by the *BABAR* Monte Carlo.

Parameter	Analysis 1	Analysis 2
$\Delta\Gamma/\Gamma$	0.0137 ± 0.0081	0.0135 ± 0.0078
$\mid q/p \mid$	0.0127 ± 0.0081	0.0127 ± 0.0079
$\frac{\mathrm{Re}\lambda_{CP}}{\mid\lambda_{CP}\mid}$Rez	—	-0.0027 ± 0.0122
Imz	—	-0.0129 ± 0.0093

Table 99: Mean residuals with error from the data-sized full Monte Carlo fits.

Parameter	Analysis 1	Analysis 2
$\Delta\Gamma/\Gamma$	0.0137	0.0135
$\mid q/p \mid$	0.0127	0.0127
$\frac{\mathrm{Re}\lambda_{CP}}{\mid\lambda_{CP}\mid}$Rez	—	0.0122
Imz	—	0.0129

Table 100: Likelihood fit systematics from common mistags and Δt resolution.

9.14 Peaking background fractions

The effect due to the uncertainty on the amount of charged B background that peaks in the m_{ES} B_{flav} distribution was estimated by changing the fraction of peaking background, f^{α}_{peak}, by $\pm 0.6\%$. In the case of the $B_{CPK^0_S}$ sample, it was changed by $\pm 1.0\%$. The impact on the physics parameters is given in tables 101.

Parameter	Analysis 1	Analysis 2
$\Delta\Gamma/\Gamma$	$^{-2.6\cdot10^{-4}}_{+2.4\cdot10^{-4}}$	$^{+6.8\cdot10^{-4}}_{-8.5\cdot10^{-4}}$
$\mid q/p \mid$	$^{+6.8\cdot10^{-6}}_{-9.0\cdot10^{-6}}$	$^{+7.0\cdot10^{-5}}_{-7.8\cdot10^{-5}}$
$\frac{\mathrm{Re}\lambda_{CP}}{\mid\lambda_{CP}\mid}$Rez	—	$^{-3.3\cdot10^{-3}}_{+3.8\cdot10^{-3}}$
Imz	—	$^{+6.5\cdot10^{-5}}_{-8.0\cdot10^{-5}}$

Parameter	Analysis 1	Analysis 2
$\Delta\Gamma/\Gamma$	$^{-6.0\cdot10^{-5}}_{+5.7\cdot10^{-5}}$	$^{-9.1\cdot10^{-5}}_{+8.7\cdot10^{-5}}$
$\mid q/p \mid$	$^{-2.9\cdot10^{-5}}_{+2.9\cdot10^{-5}}$	$^{-7.7\cdot10^{-6}}_{+1.2\cdot10^{-5}}$
$\frac{\mathrm{Re}\lambda_{CP}}{\mid\lambda_{CP}\mid}$Rez	—	$^{-5.5\cdot10^{-4}}_{+5.1\cdot10^{-4}}$
Imz	—	$^{-2.9\cdot10^{-4}}_{+2.8\cdot10^{-4}}$

Table 101: Peaking background systematics (left: B_{flav} sample; right: $B_{CPK^0_S}$ sample).

9.15 CP content in $B_{CPK^0_S}$ peaking background

The nominal fit assumes that the effective η_{CP} of the peaking background for the $B_{CPK^0_S}$ sample is zero. The resolution function, mistags and physics parameters are assumed to be the same as for the signal. We varied the the effective η_{CP} between $+1$ and -1, and we assigned as systematic error from this source the difference to the nominal fit. The results are given in table 102.

Parameter	Analysis 1	Analysis 2
$\Delta\Gamma/\Gamma$	$-9.2\cdot10^{-5}$ $+8.1\cdot10^{-5}$	$-1.5\cdot10^{-4}$ $+1.3\cdot10^{-4}$
$\mid q/p \mid$	$-4.4\cdot10^{-5}$ $+4.3\cdot10^{-5}$	$-1.5\cdot10^{-5}$ $+1.8\cdot10^{-5}$
$\frac{\mathrm{Re}\lambda_{CP}}{\lvert\lambda_{CP}\rvert}$Rez	—	$-7.6\cdot10^{-4}$ $+7.6\cdot10^{-4}$
Imz	—	$-3.6\cdot10^{-4}$ $+4.2\cdot10^{-4}$

Table 102: Systematics due to the CP content of the peaking background component in the $B_{CPK^0_S}$ sample.

9.16 Δt structure in combinatorial background

Another source of systematic uncertainty originates from the assumption that the temporal structure of the combinatorial background in the side band region is a good description of the one in the signal region. We varied the lower edge of m_{ES} distribution from 5.20 GeV/c^2 to 5.27 GeV/c^2, simultaneously for the B_{flav} and $B_{CPK^0_S}$ samples. The variations of the fitted parameters with respect to the nominal fit are shown in figure 62.

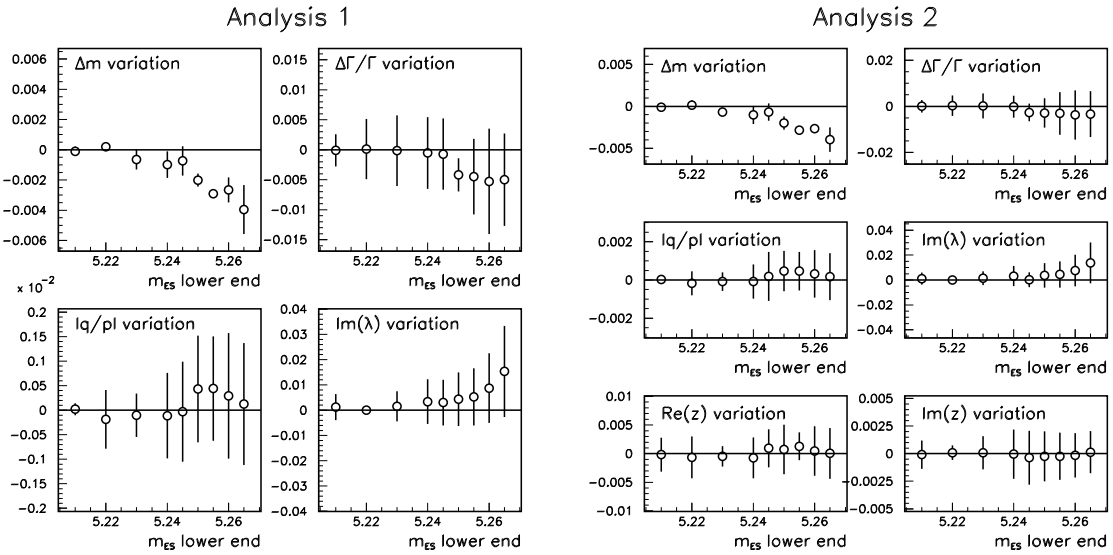

Figure 62: Variation of the fitted physical parameters for Analysis 1 and 2 with respect to the nominal fit for different values of the lower edge of the m_{ES} distribution (nominal value is 5.2 GeV/c^2).

We also split the sideband region in seven equal slices each 10 MeV/c^2 wide, simultaneously for the B_{flav} and $B_{CPK^0_S}$ samples, and used each of these ranges, in a standard fit. The results are shown in figure 63, where we indicated also the extrapolation to signal region. We estimate as systematic uncertainty the quadratic sum of the extrapolation and the error on it. Results are reported in table 103.

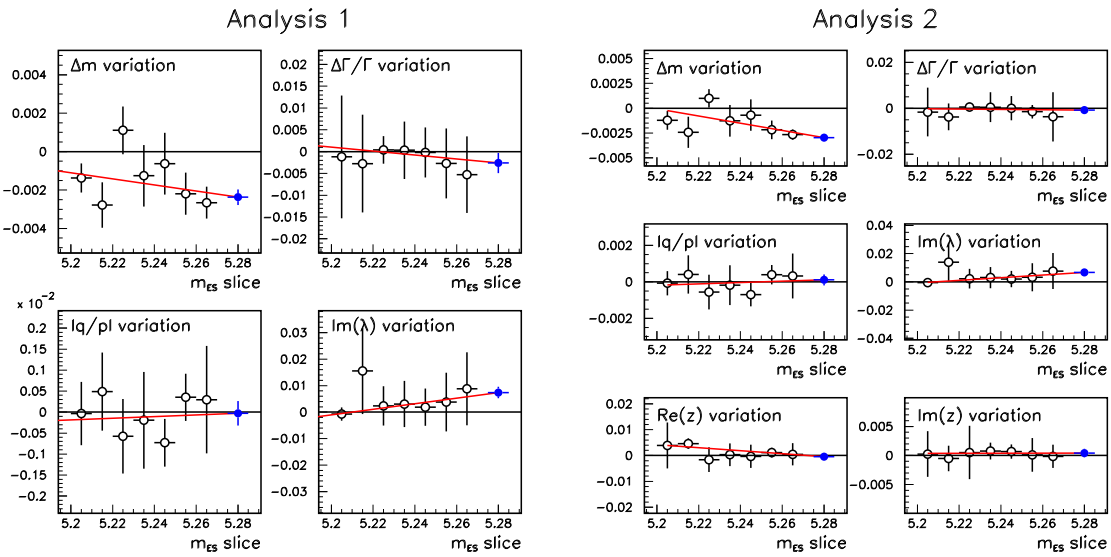

Figure 63: Variation of the fitted physical parameters for Analysis 1 and 2 with respect to the nominal fit using different "slices" of events in the m_{ES} sideband region. The extrapolation to the signal region (blue solid circle) from a linear fit is indicated as well.

Parameter	Analysis 1	Analysis 2
$0\ \Delta\Gamma/\Gamma$	$2.4 \cdot 10^{-3}$	$1.7 \cdot 10^{-3}$
$\mid q/p \mid$	$7.7 \cdot 10^{-3}$	$6.9 \cdot 10^{-3}$
$\frac{\mathrm{Re}\lambda_{CP}}{\lvert\lambda_{CP}\rvert}$Rez	—	$1.3 \cdot 10^{-3}$
Imz	—	$8.6 \cdot 10^{-4}$

Table 103: Systematic error due to the assumption of a common temporal structure for sideband and signal events in the m_{ES} distribution. See text and figure 63 for details.

9.17 $\Delta\Gamma$/CPT/T/CP/Mixing content in B_{flav} and $B_{CPK^0_S}$ combinatorial backgrounds

The nominal fit assumes that there is no $\Delta\Gamma$, T/CP/CPT and mixing structure in the combinatorial background for the B_{flav} and $B_{CPK^0_S}$ samples. To evaluate the effect from this assumption we repeated the fit but now assumming non-zero $\Delta\Gamma$, T/CP and mixing effects. This check was performed by introducing in the PDF an independent set of physics parameters to those of the signal. We still assumed no CPT structure since the fit allowing also for CPT effects did not work, due to the almost complete absence of mixing and CP violation in the background (similar problems as when trying to fit all the parameters in the B^+ control sample). Precisely because of this any effect on the CPT parameter z is expected to be completely negligile (this is a consequence of the fact that CPT violation cannot be observed in absence of CP violation). We assumed maximal mixing by fixing Δm in the combinatorial background to 0.489 ps^{-1} [22]. The differences with respect to the nominal fit are assigned as systematic uncertainty from this source, and are shown in table 104. In order to evaluate this systematics we assumed $\eta_{CP} = -1$ for the $B_{CPK^0_S}$ sample (taking $\eta_{CP} = +1$ would just change the sign of the background $\Delta\Gamma$ and T/CP/CPT T/CP/CPT parameters).

Parameter	Analysis 1	Analysis 2
$\Delta\Gamma/\Gamma$	$+4.4\cdot10^{-3}$	$+3.3\cdot10^{-3}$
$\mid q/p \mid$	$+2.5\cdot10^{-3}$	$+2.5\cdot10^{-3}$
$\frac{\mathrm{Re}\lambda_{CP}}{\mid\lambda_{CP}\mid}$Rez	—	$+2.8\cdot10^{-3}$
Imz	—	$-4.9\cdot10^{-4}$

Table 104: Systematics due to the ΔΓ/CPT/T/CP/Mixing content of the combinatorial background components in the B_{flav} and $B_{CPK^0_S}$ samples.

9.18 Charm content

Change fraction of charm content in tagging side. Expected to be negligible since it is mostly parameterized in the bias of the resoltion function and the correlation of $\sigma_\Delta t$ with the mistag fractions. To be done.

9.19 $J/\psi K^0_L$ specific systematics

The $B_{CPK^0_L}$ specific systematics is evaluated as detailed in [18]. In the following all the sources of systematics are listed and their contribution reported. For a summary of the different contributions, see tables 117 and 118.

9.19.1 CP content of background

The CP eigenvalue of most of the components in the fit is known. The cases where it is not known:

- $B^0\to J/\psi K^{*0}$, $K^{*0}\to K^0_L\pi^0$: Change the nominal value (-0.68) by ±0.07. The effect of the variation is shown in table 105;
- non-itemized inclusive J/ψ background: change the nominal net CP ($+0.19$ in the EMC and $+0.21$ in the IFR) from 0.15 to 0.33. The effect of this variation is shown in table 106;
- non-J/ψ background: the same procedure as described in section 9.17 was used here, varying the net CP (nominal is 0) by ±1. The effect of the variation can be found in table 107;

9.19.2 Prompt fraction and lifetime of non-J/ψ background

The fraction of the prompt component and the lifetime of the non-prompt of the non-J/ψ background were varied according with the errors from the external fit to the sideband events, ±0.12 and ±0.3, respectively. The effects of these variations are reported in tables 108 and 109.

9.19.3 IFR K^0_L angular resolution

The same prescription as in [18] has been used to estimate the systematics due to the difference between data and Monte Carlo in the K^0_L angular resolution (2.5 MeV ΔE smearing). The effect on the parameters is reported in table 110.

Parameter	Analysis 1	Analysis 2
$\Delta\Gamma/\Gamma$	$^{+2.3\cdot10^{-5}}_{-2.3\cdot10^{-5}}$	$^{+5.1\cdot10^{-5}}_{-5.9\cdot10^{-5}}$
$\mid q/p \mid$	$^{-2.0\cdot10^{-5}}_{+2.0\cdot10^{-5}}$	$^{-2.3\cdot10^{-5}}_{+2.5\cdot10^{-5}}$
$\frac{\mathrm{Re}\lambda_{CP}}{\mid\lambda_{CP}\mid}\mathrm{Re}z$	—	$^{+2.2\cdot10^{-4}}_{-2.1\cdot10^{-4}}$
$\mathrm{Im}z$	—	$^{-2.7\cdot10^{-4}}_{+2.7\cdot10^{-4}}$

Table 105: $J/\psi K_L^0$ specific systematics: assumed CP eigenvalue of the $B^0\to J/\psi K^{*0}$, $K^{*0}\to K_L^0\pi^0$ background.

Parameter	Analysis 1	Analysis 2
$\Delta\Gamma/\Gamma$	$^{+2.1\cdot10^{-5}}_{-1.7\cdot10^{-5}}$	$^{+7.8\cdot10^{-5}}_{-4.7\cdot10^{-5}}$
$\mid q/p \mid$	$^{-4.7\cdot10^{-5}}_{+2.5\cdot10^{-5}}$	$^{-5.2\cdot10^{-5}}_{+2.7\cdot10^{-5}}$
$\frac{\mathrm{Re}\lambda_{CP}}{\mid\lambda_{CP}\mid}\mathrm{Re}z$	—	$^{+6.0\cdot10^{-4}}_{-2.5\cdot10^{-4}}$
$\mathrm{Im}z$	—	$^{-6.7\cdot10^{-4}}_{+2.7\cdot10^{-4}}$

Table 106: $J/\psi K_L^0$ specific systematics: assumed net CP eigenvalue of the non-itemized inclusive J/ψ background.

Parameter	Analysis 1	Analysis 2
$\Delta\Gamma/\Gamma$	$+4.6\cdot10^{-4}$	$-3.1\cdot10^{-4}$
$\mid q/p \mid$	$+2.6\cdot10^{-3}$	$+2.5\cdot10^{-3}$
$\frac{\mathrm{Re}\lambda_{CP}}{\mid\lambda_{CP}\mid}\mathrm{Re}z$	—	$+3.8\cdot10^{-3}$
$\mathrm{Im}z$	—	$+1.3\cdot10^{-3}$

Table 107: $J/\psi K_L^0$ specific systematics: assumed net CP eigenvalue of the non-J/ψ background. UPDATED.

Parameter	Analysis 1	Analysis 2
$\Delta\Gamma/\Gamma$	$^{-2.2\cdot10^{-4}}_{+2.1\cdot10^{-4}}$	$^{-2.9\cdot10^{-4}}_{+2.8\cdot10^{-4}}$
$\mid q/p \mid$	$^{-9.6\cdot10^{-5}}_{+9.6\cdot10^{-5}}$	$^{-1.2\cdot10^{-4}}_{+1.2\cdot10^{-4}}$
$\frac{\mathrm{Re}\lambda_{CP}}{\mid\lambda_{CP}\mid}\mathrm{Re}z$	—	$^{+1.6\cdot10^{-4}}_{-1.4\cdot10^{-4}}$
$\mathrm{Im}z$	—	$^{-1.1\cdot10^{-4}}_{+1.0\cdot10^{-4}}$

Table 108: $J/\psi K_L^0$ specific systematics: prompt fraction of non-J/ψ background.

Parameter	Analysis 1	Analysis 2
$\Delta\Gamma/\Gamma$	$^{+4.7\cdot10^{-4}}_{-4.2\cdot10^{-4}}$	$^{+4.9\cdot10^{-4}}_{-4.6\cdot10^{-4}}$
$\mid q/p \mid$	$^{+5.9\cdot10^{-5}}_{-6.2\cdot10^{-5}}$	$^{+6.7\cdot10^{-5}}_{-7.1\cdot10^{-5}}$
$\frac{\mathrm{Re}\lambda_{CP}}{\lvert\lambda_{CP}\rvert}$Rez	—	$^{-1.9\cdot10^{-4}}_{+2.0\cdot10^{-4}}$
Imz	—	$^{-4.2\cdot10^{-5}}_{+2.8\cdot10^{-5}}$

Table 109: $J/\psi K_L^0$ specific systematics: lifetime of non-J/ψ background.

Parameter	Analysis 1	Analysis 2
$\Delta\Gamma/\Gamma$	$-3.1\cdot10^{-3}$	$-3.0\cdot10^{-3}$
$\mid q/p \mid$	$+2.0\cdot10^{-6}$	$+6.5\cdot10^{-5}$
$\frac{\mathrm{Re}\lambda_{CP}}{\lvert\lambda_{CP}\rvert}$Rez	—	$-9.7\cdot10^{-5}$
Imz	—	$+1.8\cdot10^{-3}$

Table 110: $J/\psi K_L^0$ specific systematics: K_L^0 angular resolution.

9.19.4 Shape of ΔE distributions

The ΔE distributions used to help to discriminate between signal and background are taken from Monte Carlo. To have good agreement with the data, the Monte Carlo was shifted by -0.5 MeV and smeared by 0.85 MeV. The sensitivity to the uncertainties on the ΔE shape were evaluated by applying an additional shift of ±0.25 MeV and an additional smearing of 0.45 MeV. The impact of the physics parameters is shown in tables 111 and 112.

Parameter	Analysis 1	Analysis 2
$\Delta\Gamma/\Gamma$	$^{-7.7\cdot10^{-4}}_{+4.3\cdot10^{-4}}$	$^{-7.8\cdot10^{-4}}_{+4.2\cdot10^{-4}}$
$\mid q/p \mid$	$^{-3.4\cdot10^{-5}}_{-1.9\cdot10^{-4}}$	$^{-3.8\cdot10^{-5}}_{-2.0\cdot10^{-4}}$
$\frac{\mathrm{Re}\lambda_{CP}}{\lvert\lambda_{CP}\rvert}$Rez	—	$^{+6.8\cdot10^{-4}}_{-2.0\cdot10^{-5}}$
Imz	—	$^{+1.5\cdot10^{-4}}_{+6.3\cdot10^{-5}}$

Table 111: $J/\psi K_L^0$ specific systematics: ΔE shape (ΔE shift).

9.19.5 Measured sample composition from ΔE fit

The relative amount of signal, inclusive J/ψ background, and non J/ψ background is determined from a three component fit of the ΔE spectrum, which is described in reference [17]. The fitted fractions for IFR and EMC samples are variated randomly accordingly to the covariance matrix from the ΔE fit and the global

Parameter	Analysis 1	Analysis 2
$\Delta\Gamma/\Gamma$	$-6.5\cdot10^{-4}$	$-6.9\cdot10^{-4}$
$\mid q/p \mid$	$-1.5\cdot10^{-4}$	$-1.5\cdot10^{-4}$
$\frac{\mathrm{Re}\lambda_{CP}}{\mid\lambda_{CP}\mid}$Rez	—	$+6.4\cdot10^{-4}$
Imz	—	$+1.7\cdot10^{-4}$

Table 112: $J/\psi K_L^0$ specific systematics: ΔE shape (additional ΔE smearing).

fit is performed for each of the configurations. In figure 64 we report the distributions of the fitted values for 100 random configurations. The width of a gaussian fit to these distributions are quoted as the systematic contribution for each variable.

Parameter	Analysis 1	Analysis 2
$\Delta\Gamma/\Gamma$	$5.9\cdot10^{-3}$	$6.9\cdot10^{-4}$
$\mid q/p \mid$	$1.3\cdot10^{-4}$	$1.6\cdot10^{-4}$
$\frac{\mathrm{Re}\lambda_{CP}}{\mid\lambda_{CP}\mid}$Rez	—	$1.4\cdot10^{-3}$
Imz	—	$7.6\cdot10^{-3}$

Table 113: $J/\psi K_L^0$ specific systematics: uncertainties from the variation of the sample composition. .

9.19.6 Branching fractions

One of the inputs of the sample composition fit are the branching fractions of the various $J/\psi X$ modes. We varied these numbers by either their measured errors or conservative estimates. After each variation the ΔE fit for the sample composition is recomputed. The difference among the results of the subsequent global fit and the nominal case are taken as the sytematic error.

There is a known problem in the SP4 generation of $J/\psi K_S^0$, with K_S^0 decaying in two neutral pion, since each π^0 decays twice in the detector. We took in account of this effect varying the corresponding branching fractionb varying it upward of a larger value (50% instead of 10%). This approach is the same as in [18].

Parameter	Analysis 1	Analysis 2
$\Delta\Gamma/\Gamma$	$^{+6.4\cdot10^{-6}}_{-4.8\cdot10^{-6}}$	$^{+8.0\cdot10^{-6}}_{-8.2\cdot10^{-6}}$
$\mid q/p \mid$	$^{+1.1\cdot10^{-6}}_{-7.0\cdot10^{-7}}$	$^{+1.6\cdot10^{-6}}_{+1.8\cdot10^{-6}}$
$\frac{\mathrm{Re}\lambda_{CP}}{\mid\lambda_{CP}\mid}$Rez	—	$^{-2.4\cdot10^{-5}}_{+6.2\cdot10^{-6}}$
Imz	—	$^{+5.4\cdot10^{-6}}_{-7.8\cdot10^{-6}}$

Parameter	Analysis 1	Analysis 2
$\Delta\Gamma/\Gamma$	$^{+9.2\cdot10^{-5}}_{-1.3\cdot10^{-5}}$	$^{+7.8\cdot10^{-5}}_{-1.0\cdot10^{-5}}$
$\mid q/p \mid$	$^{+1.6\cdot10^{-5}}_{-2.1\cdot10^{-6}}$	$^{+1.9\cdot10^{-5}}_{-2.3\cdot10^{-6}}$
$\frac{\mathrm{Re}\lambda_{CP}}{\mid\lambda_{CP}\mid}$Rez	—	$^{-2.3\cdot10^{-4}}_{+3.5\cdot10^{-5}}$
Imz	—	$^{+1.9\cdot10^{-4}}_{-3.1\cdot10^{-5}}$

Table 114: $J/\psi K_L^0$ specific systematics: $\pm10\%$ variation of $B\to J/\psi K^*$ branching fraction (left); $-10\%/+50\%$ variation of $B^0\to J/\psi K_S^0$ branching fraction (right).

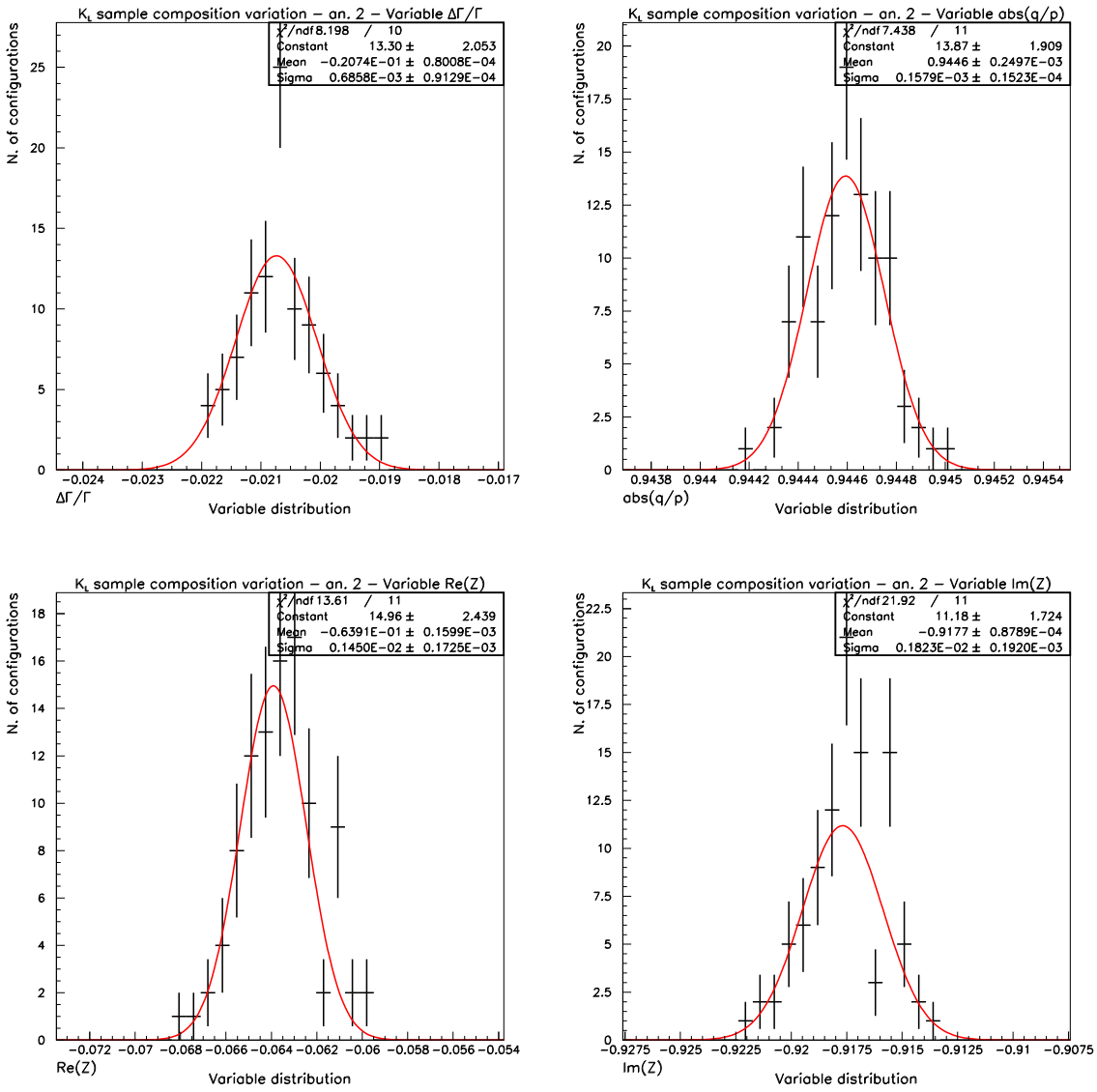

Figure 64: Distribution of the (BLIND) fitted parameters from Analysis 2 varying the sample composition extracted from ΔE fit. The widths of the fitted gaussians are taken as the systematic uncertainties.

10 Summary of results

In 56 fb^{-1}, we measure $\Delta\Gamma/\Gamma$ and test the T/CPT asymmetries. The parameter results and checks for the two analyses are:

- Analysis 1 results (blind):

$$\Delta\Gamma/\Gamma = -0.008^{+0.048}_{-0.049}(\text{stat}) \pm 0.021(\text{syst})$$
$$|\, q/p \,| = 0.946 \pm 0.018(\text{stat}) \pm 0.023(\text{syst})$$

Parameter	Analysis 1	Analysis 2
$\Delta\Gamma/\Gamma$	$+3.0\cdot10^{-6}$ $+1.6\cdot10^{-6}$	$+5.8\cdot10^{-6}$ $-1.9\cdot10^{-6}$
$\mid q/p \mid$	$-1.6\cdot10^{-6}$ $+1.9\cdot10^{-6}$	$-3.0\cdot10^{-7}$ $+2.2\cdot10^{-6}$
$\frac{\mathrm{Re}\lambda_{CP}}{\mid\lambda_{CP}\mid}\mathrm{Re}z$	—	$-2.1\cdot10^{-6}$ $-7.2\cdot10^{-6}$
$\mathrm{Im}z$	—	$-1.7\cdot10^{-5}$ $+4.2\cdot10^{-6}$

Parameter	Analysis 1	Analysis 2
$\Delta\Gamma/\Gamma$	$+9.8\cdot10^{-6}$ $+2.5\cdot10^{-6}$	$-2.0\cdot10^{-7}$ $+1.5\cdot10^{-5}$
$\mid q/p \mid$	$+6.3\cdot10^{-6}$ $-4.6\cdot10^{-6}$	$+8.6\cdot10^{-6}$ $-5.8\cdot10^{-6}$
$\frac{\mathrm{Re}\lambda_{CP}}{\mid\lambda_{CP}\mid}\mathrm{Re}z$	—	$-8.9\cdot10^{-5}$ $+6.4\cdot10^{-5}$
$\mathrm{Im}z$	—	$+8.5\cdot10^{-5}$ $-8.8\cdot10^{-5}$

Table 115: $J/\psi K_L^0$ specific systematics: $\pm50\%$ variation of $B\to J/\psi K_L\pi$ branching fraction (left); $\pm50\%$ variation of $B^0\to\chi_c K_L$ branching fraction (right).

Parameter	Analysis 1	Analysis 2
$\Delta\Gamma/\Gamma$	$+6.4\cdot10^{-6}$ $-4.8\cdot10^{-6}$	$+8.0\cdot10^{-6}$ $-8.2\cdot10^{-6}$
$\mid q/p \mid$	$+1.1\cdot10^{-6}$ $-7.0\cdot10^{-7}$	$+1.6\cdot10^{-6}$ $+1.8\cdot10^{-6}$
$\frac{\mathrm{Re}\lambda_{CP}}{\mid\lambda_{CP}\mid}\mathrm{Re}z$	—	$-2.4\cdot10^{-5}$ $+6.2\cdot10^{-6}$
$\mathrm{Im}z$	—	$+5.4\cdot10^{-6}$ $-7.8\cdot10^{-6}$

Table 116: $J/\psi K_L^0$ specific systematics: $\pm50\%$ variation of $B\to J/\psi X$ residual branching fraction.

- Analysis 1 checks (Δm, τ_B are unblind, $\frac{\mathrm{Im}\lambda_{CP}}{\mid\lambda_{CP}\mid}$ blind):

$$\Delta m = 0.5220 \pm 0.0098(\mathrm{stat})$$
$$\frac{\mathrm{Im}\lambda_{CP}}{\mid\lambda_{CP}\mid} = 0.612^{+0.085}_{-0.086}(\mathrm{stat})$$
$$\tau_B = 1.515 \pm 0.022(\mathrm{stat})$$

- Analysis 2 results (blind):

$$\Delta\Gamma/\Gamma = -0.021^{+0.048}_{-0.047}(\mathrm{stat}) \pm 0.023(\mathrm{syst})$$
$$\mid q/p \mid = 0.946 \pm 0.018(\mathrm{stat}) \pm 0.023(\mathrm{syst})$$
$$\frac{\mathrm{Re}\lambda_{CP}}{\mid\lambda_{CP}\mid}\mathrm{Re}z = -0.064^{+0.074}_{-0.047}(\mathrm{stat}) \pm 0.041(\mathrm{syst})$$
$$\mathrm{Im}z = -0.918 \pm 0.034(\mathrm{stat}) \pm 0.025(\mathrm{syst})$$

- Analysis 2 checks (Δm, τ_B are unblind, $\frac{\mathrm{Im}\lambda_{CP}}{\mid\lambda_{CP}\mid}$ blind):

$$\Delta m = 0.523 \pm^{+0.017}_{-0.010}(\mathrm{stat})$$
$$\frac{\mathrm{Im}\lambda_{CP}}{\mid\lambda_{CP}\mid} = 0.620 \pm^{+0.081}_{-0.084}(\mathrm{stat})$$

Systematics	$\Delta\Gamma/\Gamma$	$\mid q/p \mid$
CP of K^* bkg	$2.3 \cdot 10^{-5}$	$2.0 \cdot 10^{-5}$
CP of non itemized J/ψ bkg	$2.1 \cdot 10^{-5}$	$7.8 \cdot 10^{-5}$
CP non-J/ψ bkg	$4.6 \cdot 10^{-4}$	$2.6 \cdot 10^{-3}$
prompt fraction of non-J/ψ bkg	$2.2 \cdot 10^{-4}$	$9.6 \cdot 10^{-5}$
lifetime of non-J/ψ bkg	$4.7 \cdot 10^{-4}$	$6.2 \cdot 10^{-5}$
angular resolution	$3.1 \cdot 10^{-3}$	$2.0 \cdot 10^{-6}$
ΔE shape (shift)	$7.7 \cdot 10^{-4}$	$1.9 \cdot 10^{-4}$
ΔE shape (additional smearing)	$6.5 \cdot 10^{-4}$	$1.5 \cdot 10^{-4}$
Measured sample composition	$5.9 \cdot 10^{-3}$	$1.3 \cdot 10^{-4}$
Branching fraction: $J/\psi K^*$	$6.4 \cdot 10^{-6}$	$1.1 \cdot 10^{-6}$
Branching fraction: $J/\psi K_S$	$9.2 \cdot 10^{-5}$	$7.8 \cdot 10^{-5}$
Branching fraction: $J/\psi K_L \pi$	$3.0 \cdot 10^{-6}$	$5.8 \cdot 10^{-6}$
Branching fraction: $\chi_c K_L$	$9.8 \cdot 10^{-6}$	$6.3 \cdot 10^{-6}$
Branching fraction: $J/\psi X$ other	$6.4 \cdot 10^{-6}$	$1.1 \cdot 10^{-6}$
Total	**0.0068**	**0.0026**

Table 117: Analysis 1 K_L^0 specific systematics summary.

$$\tau_B = 1.517 \pm 0.022(\text{stat})$$

The break-down of the error for the two analyses are given in tables 119 and 120.

To first order in the CPT parameter δ and the T violation in mixing parameter Reε, we can alternatively provide the above results in the $\{\varepsilon, \delta\}$ formalism, using the relations shown in section 2.3:

- Analysis 1 results (blind):

$$\frac{\text{Re}\varepsilon}{1+\mid \varepsilon \mid^2} = 0.028 \pm 0.008(\text{stat}) \pm 0.010(\text{syst})$$

- Analysis 1 checks (blind):

$$\frac{\text{Im}\varepsilon}{1+\mid \varepsilon \mid^2} = -0.306 \pm 0.043(\text{stat})$$

- Analysis 2 results (blind):

$$\frac{\text{Re}\varepsilon}{1+\mid \varepsilon \mid^2} = 0.028 \pm 0.008(\text{stat}) \pm 0.010(\text{syst})$$

$$\frac{1-\mid \varepsilon \mid^2}{1+\mid \varepsilon \mid^2}\frac{\text{Re}\delta}{1+\mid \varepsilon \mid^2} = -0.064^{+0.074}_{-0.047}(\text{stat}) \pm 0.041(\text{syst})$$

$$\frac{\text{Im}\delta}{1+\mid \varepsilon \mid^2} - 0.918 \pm 0.034(\text{stat}) \pm 0.025(\text{syst})$$

Systematics	$\Delta\Gamma/\Gamma$	$\mid q/p \mid$	$\frac{\mathrm{Re}\lambda_{CP}}{\mid\lambda_{CP}\mid}$Rez	Imz
CP of K^* bkg	$5.9\cdot10^{-5}$	$2.5\cdot10^{-5}$	$2.2\cdot10^{-4}$	$2.7\cdot10^{-4}$
CP of non itemized J/ψ bkg	$7.8\cdot10^{-5}$	$5.2\cdot10^{-5}$	$6.0\cdot10^{-4}$	$6.7\cdot10^{-4}$
CP non-J/ψ bkg	$7.6\cdot10^{-4}$	$1.3\cdot10^{-3}$	$3.0\cdot10^{-3}$	$2.9\cdot10^{-4}$
prompt fraction of non-J/ψ bkg	$3.1\cdot10^{-4}$	$2.5\cdot10^{-3}$	$3.8\cdot10^{-3}$	$1.3\cdot10^{-3}$
lifetime of non-J/ψ bkg	$2.9\cdot10^{-4}$	$1.2\cdot10^{-4}$	$1.6\cdot10^{-4}$	$1.1\cdot10^{-4}$
angular resolution	$3.0\cdot10^{-3}$	$6.5\cdot10^{-5}$	$9.7\cdot10^{-5}$	$1.8\cdot10^{-3}$
ΔE shape (shift)	$7.8\cdot10^{-4}$	$2.0\cdot10^{-4}$	$6.8\cdot10^{-4}$	$1.5\cdot10^{-4}$
ΔE shape (additional smearing)	$6.9\cdot10^{-4}$	$1.5\cdot10^{-4}$	$6.4\cdot10^{-4}$	$1.7\cdot10^{-4}$
Measured sample composition	$6.9\cdot10^{-4}$	$1.6\cdot10^{-4}$	$1.4\cdot10^{-3}$	$7.6\cdot10^{-3}$
Branching fraction: $J/\psi K^*$	$8.2\cdot10^{-6}$	$1.8\cdot10^{-6}$	$2.4\cdot10^{-5}$	$7.8\cdot10^{-6}$
Branching fraction: $J/\psi K_S$	$7.8\cdot10^{-5}$	$1.9\cdot10^{-5}$	$2.3\cdot10^{-4}$	$1.9\cdot10^{-4}$
Branching fraction: $J/\psi K_L\pi$	$5.8\cdot10^{-6}$	$2.2\cdot10^{-6}$	$7.2\cdot10^{-6}$	$1.7\cdot10^{-5}$
Branching fraction: $\chi_c K_L$	$1.5\cdot10^{-5}$	$8.6\cdot10^{-5}$	$8.9\cdot10^{-5}$	$8.8\cdot10^{-5}$
Branching fraction: $J/\psi X$ other	$8.2\cdot10^{-6}$	$1.8\cdot10^{-6}$	$2.4\cdot10^{-5}$	$7.8\cdot10^{-6}$
Total	**0.0034**	**0.0028**	**0.0052**	**0.0080**

Table 118: Analysis 2 K_L^0 specific systematics summary.

- Analysis 2 checks (blind):

$$\frac{\mathrm{Im}\varepsilon}{1+\mid\varepsilon\mid^2} = -0.310^{+0.041}_{-0.042}(\mathrm{stat})$$

Discuss the results and show the main asymmetries (those candidate to be included in the paper) in a nice format. Will make a discussion about what is seen there.

Acknowledgments

We want to thank David Kirkby and Bob Cahn for their unvaluable help to make this analysis possible, and Gerhard Raven for his advice in many issues. We are indeed grateful to the $\sin 2\beta$ AWG for providing the data sample. Thanks to Bryam Dahmes for his help with the $J/\psi K_L^0$ systematics.

Systematics	$\Delta\Gamma/\Gamma$	$\mid q/p \mid$
Signal probability (B_{flav})	$1.2 \cdot 10^{-3}$	$1.8 \cdot 10^{-4}$
Signal probability ($B_{CPK^0_S}$)	$8.4 \cdot 10^{-4}$	$2.1 \cdot 10^{-4}$
m_{ES} endpoint	$3.1 \cdot 10^{-4}$	$7.6 \cdot 10^{-3}$
Resolut. function param.	$5.3 \cdot 10^{-3}$	$1.8 \cdot 10^{-5}$
$\sigma_{outlier}$ variation	$1.7 \cdot 10^{-3}$	$7.4 \cdot 10^{-5}$
$\sigma_{outlier}$ very large	$1.1 \cdot 10^{-3}$	$2.3 \cdot 10^{-4}$
$\delta_{outlier}$ variation	$9.2 \cdot 10^{-4}$	$3.5 \cdot 10^{-4}$
Beam spot position	$1.3 \cdot 10^{-3}$	$1.5 \cdot 10^{-3}$
Beam spot expansion	$1.1 \cdot 10^{-4}$	$1.8 \cdot 10^{-4}$
SVT alignment	$2.5 \cdot 10^{-3}$	$9.4 \cdot 10^{-3}$
z scale and boost	$4.0 \cdot 10^{-3}$	$3.6 \cdot 10^{-4}$
Average B^0 lifetime	$6.2 \cdot 10^{-3}$	$6.9 \cdot 10^{-4}$
Average B^+ lifetime	$7.6 \cdot 10^{-5}$	$2.0 \cdot 10^{-5}$
B^+ mistag rates	$7.4 \cdot 10^{-6}$	$4.0 \cdot 10^{-7}$
Residual charge asymmetry	$2.6 \cdot 10^{-3}$	$3.5 \cdot 10^{-3}$
Direct CP violation	$1.9 \cdot 10^{-3}$	$6.3 \cdot 10^{-3}$
Doubly CKM suppressed decays systematics	$7.2 \cdot 10^{-3}$	$8.1 \cdot 10^{-3}$
PDF asymptotic normalization	$3.0 \cdot 10^{-3}$	$1.6 \cdot 10^{-4}$
Fitting procedure	$3.6 \cdot 10^{-3}$	$2.8 \cdot 10^{-3}$
Common mistag and Δt res.	$1.4 \cdot 10^{-2}$	$1.3 \cdot 10^{-2}$
Fraction of peaking bg (B_{flav})	$2.6 \cdot 10^{-4}$	$9.0 \cdot 10^{-6}$
Fraction of peaking bg ($B_{CPK^0_S}$)	$6.0 \cdot 10^{-5}$	$2.9 \cdot 10^{-5}$
CP content of peaking bg	$3.0 \cdot 10^{-3}$	$1.9 \cdot 10^{-4}$
Δt structure in combinatorial background	$2.4 \cdot 10^{-3}$	$7.7 \cdot 10^{-3}$
$\Delta\Gamma$/CP/T/Mixing content in combinatorial bkg	$4.4 \cdot 10^{-3}$	$2.5 \cdot 10^{-3}$
Charm content	$. \cdot 10^{-}$	$. \cdot 10^{-}$
K^0_L specific systematics	$6.8 \cdot 10^{-3}$	$2.6 \cdot 10^{-3}$
Total	**0.021**	**0.023**

Table 119: Analysis 1 systematics break-down.

Systematics	$\Delta\Gamma/\Gamma$	$\mid q/p \mid$	$\frac{\mathrm{Re}\lambda_{CP}}{\mid\lambda_{CP}\mid}$Rez	Imz
Signal probability (B_{flav})	$8.7\cdot10^{-4}$	$2.5\cdot10^{-4}$	$1.0\cdot10^{-3}$	$3.7\cdot10^{-4}$
Signal probability ($B_{CPK^0_S}$)	$6.9\cdot10^{-4}$	$2.0\cdot10^{-4}$	$1.2\cdot10^{-3}$	$4.4\cdot10^{-4}$
m_{ES} endpoint	$1.8\cdot10^{-4}$	$7.5\cdot10^{-3}$	$7.6\cdot10^{-4}$	$2.0\cdot10^{-3}$
Resolut. function param.	$7.4\cdot10^{-4}$	$1.9\cdot10^{-4}$	$6.1\cdot10^{-3}$	$1.4\cdot10^{-3}$
$\sigma_{outlier}$ variation	$6.5\cdot10^{-3}$	$1.4\cdot10^{-3}$	$1.1\cdot10^{-2}$	$8.9\cdot10^{-4}$
$\sigma_{outlier}$ very large	$6.8\cdot10^{-4}$	$2.0\cdot10^{-4}$	$2.5\cdot10^{-3}$	$1.4\cdot10^{-3}$
$\delta_{outlier}$ variation	$6.6\cdot10^{-4}$	$3.9\cdot10^{-4}$	$2.4\cdot10^{-3}$	$1.5\cdot10^{-3}$
beam spot position	$2.7\cdot10^{-3}$	$1.6\cdot10^{-3}$	$5.6\cdot10^{-3}$	$1.1\cdot10^{-3}$
beam spot expansion	$1.0\cdot10^{-4}$	$1.8\cdot10^{-4}$	$2.9\cdot10^{-4}$	$6.2\cdot10^{-4}$
SVT alignment	$6.0\cdot10^{-3}$	$1.2\cdot10^{-2}$	$6.5\cdot10^{-3}$	$1.6\cdot10^{-2}$
z scale and boost	$3.1\cdot10^{-3}$	$3.9\cdot10^{-4}$	$5.6\cdot10^{-3}$	$3.8\cdot10^{-4}$
Average B^0 lifetime	$5.1\cdot10^{-3}$	$8.0\cdot10^{-4}$	$1.3\cdot10^{-2}$	$6.7\cdot10^{-4}$
Average B^+ lifetime	$7.6\cdot10^{-5}$	$3.0\cdot10^{-5}$	$2.8\cdot10^{-4}$	$7.2\cdot10^{-5}$
B^+ mistag rates	$1.0\cdot10^{-4}$	$1.1\cdot10^{-5}$	$4.4\cdot10^{-4}$	$1.5\cdot10^{-5}$
Residual charge asymmetry	$2.6\cdot10^{-3}$	$3.4\cdot10^{-3}$	$1.5\cdot10^{-3}$	$5.1\cdot10^{-3}$
Direct CP violation	$2.1\cdot10^{-3}$	$6.4\cdot10^{-3}$	$7.5\cdot10^{-4}$	$3.0\cdot10^{-3}$
Doubly CKM suppressed decays systematics	$1.4\cdot10^{-2}$	$8.0\cdot10^{-3}$	$2.9\cdot10^{-2}$	$8.6\cdot10^{-3}$
PDF asympotic normalization	$2.3\cdot10^{-3}$	$1.5\cdot10^{-4}$	$2.2\cdot10^{-3}$	$3.4\cdot10^{-4}$
Fitting procedure	$3.0\cdot10^{-3}$	$7.6\cdot10^{-4}$	$1.4\cdot10^{-2}$	$1.5\cdot10^{-3}$
Common mistag and Δt res.	$1.3\cdot10^{-2}$	$1.3\cdot10^{-2}$	$1.2\cdot10^{-2}$	$1.3\cdot10^{-2}$
Fraction of peaking bg (B_{flav})	$8.5\cdot10^{-4}$	$7.8\cdot10^{-5}$	$3.8\cdot10^{-3}$	$8.0\cdot10^{-5}$
Fraction of peaking bg ($B_{CPK^0_S}$)	$9.1\cdot10^{-5}$	$1.2\cdot10^{-5}$	$5.5\cdot10^{-4}$	$2.9\cdot10^{-4}$
CP content of peaking bg	$1.5\cdot10^{-4}$	$1.8\cdot10^{-5}$	$7.6\cdot10^{-4}$	$4.2\cdot10^{-4}$
Δt structure in combinatorial background	$1.7\cdot10^{-3}$	$6.9\cdot10^{-3}$	$1.3\cdot10^{-3}$	$8.6\cdot10^{-4}$
$\Delta\Gamma$/CP/T/Mixing content in combinatorial bkg	$3.3\cdot10^{-3}$	$2.5\cdot10^{-3}$	$2.8\cdot10^{-3}$	$4.9\cdot10^{-4}$
Charm content	$.\cdot10^{-}$	$.\cdot10^{-}$	$.\cdot10^{-}$	$.\cdot10^{-}$
K^0_L specific systematics	$3.4\cdot10^{-3}$	$2.8\cdot10^{-3}$	$5.2\cdot10^{-3}$	$8.0\cdot10^{-3}$
Total	**0.023**	**0.023**	**0.041**	**0.025**

Table 120: Analysis 2 systematics break-down.

A Doubly-CKM-Suppressed Decays Toy Monte Carlo studies

A.1 Sensitivity studies

We investigated the numerical sensitivity of the CPT/T/CPT/Mixing parameters to DCKM effects using toy Monte Carlo. For these studies, the samples were generated with the values of the phases that maximize and minimize the PDF (this occurrs at the physical region boundaries of the sines and cosines of the phases). In the most general case without model asumptions we have a total of 16 possible combinations for each B meson, reconstructed and tagging (4 possible angles for each B^0 and $\bar{B}^0$: 0, $\pi/2$, π, $3\pi/2$). In practice, the matrix of combinations is "antisymmetric" under B^0 and $\bar{B}^0$ interchange, which gives a total of 10 different combinations. In order to reduce futher the number of combinations and simplify as much as possible this study, we assumed $\theta = \phi_{strong} + \phi_{weak}$, $\bar{\theta} = \phi_{strong} - \phi_{weak}$, with $\phi_{weak} = 2\beta + \gamma = 1.85$, which reduces to 4 combinations. This assumption will be released for the systematic error evaluation in the final analysis. The rates r_{flav}, $\bar{r}_{flav}$, r_{tag} and $\bar{r}_{tag}$ were generated to be 0.05. One single effective channel contributing to the reconstructed (flavor sample) and tagging (common for the flavor and CP samples) sides was assumed here. The samples consisted of about 100 experiments with an statistics equivalent to about 60 fb^{-1} each, with perfect Δt resolution but mistags as those observed in the data. The relative populations of flavor and CP events was kept the same as observed in the data. Tagging-vertexing correlations and $B^0\bar{B}^0$ differences in reconstruction and tagging efficiencies were neglected here. We assumed no direct CP violation effects, $r_{CP,CP} = r_{CP,flav} = r_{CP,tag} = 1$. The CP phase θ_{CP} was generated to be 0.86 rad (which corresponds to $\frac{\mathrm{Im}\lambda_{CP}}{|\lambda_{CP}|}$=0.75). z and $\mid q/p \mid$ were assumed to be 0 and 1, respectively.

We first analyzed the effects in the tagging side. The mean residuals obtained when fitting the samples neglecting the DCKM effects in both, tagging and reconstructed sides (**fit configuration 1**), but generating DCKM effects in the tagging side only, are summarized in table 121. To evaluate the significance of the offsets, these values should be compared to the RMS reported in the same table. The statiscal error on the offsets are about 10 times smaller than the reported RMS. We observe a large impact on Imz, a non-negligible effect on $\frac{\mathrm{Re}\lambda_{CP}}{|\lambda_{CP}|}$Rez and to a less extend on $\frac{\mathrm{Im}\lambda_{CP}}{|\lambda_{CP}|}$. The effects for all the other parameters are negligible[5].

θ_{tag}	Δm	$\Delta\Gamma/\Gamma$	$\mid q/p \mid$	$\frac{\mathrm{Re}\lambda_{CP}}{\lvert\lambda_{CP}\rvert}$Rez	$\frac{\mathrm{Im}\lambda_{CP}}{\lvert\lambda_{CP}\rvert}$	Imz
0	0.0020	-0.0032	0.0011	-0.0263	-0.0032	0.0175
$\pi/2$	0.0016	0.0019	-0.0001	-0.0098	0.0033	-0.0615
π	0.0014	0.0066	0.0005	0.0253	-0.0050	-0.0186
$3\pi/2$	0.0020	-0.0025	0.0005	0.0008	0.0185	0.0614
RMS	0.0078	0.052	0.013	0.056	0.068	0.013

Table 121: Mean residuals and RMS for fit configuration 1, tagging side phase scan.

When the same samples are fitted letting free $\frac{\mathrm{Im}\lambda_{tag}}{|\lambda_{tag}|}$ and $\frac{\mathrm{Im}\bar{\lambda}_{tag}}{|\lambda_{tag}|}$, with $r_{tag} = \bar{r}_{tag}$ fixed to 0.05 and $\frac{\mathrm{Re}\lambda_{tag}}{|\lambda_{tag}|} = \frac{\mathrm{Re}\bar{\lambda}_{tag}}{|\lambda_{tag}|} = 0$[6] (**fit configuration 2**), we obtain the mean residuals and RMS listed in table 122. The large effect on Imz has disappeared here, at the price of an increase in its statistical error (from 0.013 to 0.019). The effect on $\frac{\mathrm{Im}\lambda_{CP}}{|\lambda_{CP}|}$ seems to be also reduced. The mean biases and statistical reach of all the other parameters remain

[5] The Δm mean residual should be compared to the mean residual when no DCKM effects are generated, about 0.0022. This small bias is known to be due to the simultaneous extraction of Δm with the CPT parameters. When CPT is assumed to be a good symmetry this small effect goes away.

[6] r_{flav}, $\bar{r}_{flav}$, $\frac{\mathrm{Re}\lambda_{flav}}{|\lambda_{flav}|}$, $\frac{\mathrm{Re}\bar{\lambda}_{flav}}{|\lambda_{flav}|}$, $\frac{\mathrm{Im}\lambda_{flav}}{|\lambda_{flav}|}$ and $\frac{\mathrm{Im}\bar{\lambda}_{flav}}{|\lambda_{flav}|}$ are all fixed to zero.

basically unchanged. The RMS for $\frac{\mathrm{Im}\lambda_{tag}}{|\lambda_{tag}|}$ and $\frac{\mathrm{Im}\bar{\lambda}_{tag}}{|\lambda_{tag}|}$ is 0.32.

θ_{tag}	Δm	$\Delta\Gamma/\Gamma$	$\mid q/p \mid$	$\frac{\mathrm{Re}\lambda_{CP}}{\lvert\lambda_{CP}\rvert}$Rez	$\frac{\mathrm{Im}\lambda_{CP}}{\lvert\lambda_{CP}\rvert}$	Imz
0	0.0018	0.0014	0.0013	-0.0253	-0.0074	-0.0009
$\pi/2$	0.0021	0.0025	-0.0003	-0.0080	0.0079	-0.0017
π	0.0017	0.0068	-0.0002	0.0252	0.0022	0.0020
$3\pi/2$	0.0019	-0.0076	0.0007	-0.0002	0.0092	0.0032
RMS	0.0078	0.054	0.013	0.056	0.069	0.019

Table 122: Mean residuals and RMS for fit configuration 2, tagging side phase scan.

The same samples were also fitted with $\frac{\mathrm{Im}\lambda_{tag}}{|\lambda_{tag}|}$, $\frac{\mathrm{Im}\bar{\lambda}_{tag}}{|\lambda_{tag}|}$, $\frac{\mathrm{Re}\lambda_{tag}}{|\lambda_{tag}|}$ and $\frac{\mathrm{Re}\bar{\lambda}_{tag}}{|\lambda_{tag}|}$ free and $r_{tag} = \bar{r}_{tag}$ fixed to 0.05 (**fit configuration 3**). The mean residuals and RMS obtained are those summarized in table 123. The situation for $\frac{\mathrm{Re}\lambda_{CP}}{|\lambda_{CP}|}$Rez is now slightly better, at the price of an increase of its statistical precision. The $\mid q/p \mid$ and $\frac{\mathrm{Im}\lambda_{CP}}{|\lambda_{CP}|}$ RMS' are also slightly poorer. The RMS for $\frac{\mathrm{Im}\lambda_{tag}}{|\lambda_{tag}|}$ and $\frac{\mathrm{Im}\bar{\lambda}_{tag}}{|\lambda_{tag}|}$ is 0.32 as before, while it is 2.1 for $\frac{\mathrm{Re}\lambda_{tag}}{|\lambda_{tag}|}$ and $\frac{\mathrm{Re}\bar{\lambda}_{tag}}{|\lambda_{tag}|}$. We observe that the sensitivity to the real parts in the tagging side is poor.

θ_{tag}	Δm	$\Delta\Gamma/\Gamma$	$\mid q/p \mid$	$\frac{\mathrm{Re}\lambda_{CP}}{\lvert\lambda_{CP}\rvert}$Rez	$\frac{\mathrm{Im}\lambda_{CP}}{\lvert\lambda_{CP}\rvert}$	Imz
0	0.0010	0.0013	0.0025	0.0093	-0.0121	-0.0005
$\pi/2$	0.0017	0.0055	-0.0003	0.0031	0.0005	-0.0016
π	0.0004	0.0089	-0.0003	0.0016	0.0058	-0.0034
$3\pi/2$	0.0019	-0.0051	-0.0014	-0.0098	0.0090	0.0030
RMS	0.0077	0.054	0.017	0.065	0.070	0.019

Table 123: Mean residuals and RMS for fit configuration 3, tagging side phase scan.

Results from tables 121, 122 and 123 confirm some of the expectations discussed in the previous section: i) Rez(Imz) is mainly correlated with the DCKM real(imaginary) parts, ii) the effects on Δm and $\Delta\Gamma$ are small, iii) the effect on $\frac{\mathrm{Im}\lambda_{CP}}{|\lambda_{CP}|}$ is rather small, and comes mainly from the DCKM imaginary parts.

The above studies have been repeated but now generating the DCKM effects in the reconstructed side only (flavor sample). The mean residuals and RMS obtained when fitting with **configuration 1** are summarized in table 124. We observe again a large offset on Imz but significantly smaller than in the previous case where the DCKM effects were generated in the tagging side. No significant effects are observed in all the other parameters. Comparing these results with those equivalent in the tagging side (table 121) we conclude that the tagging side gives the largest systematic effect to the determination of the CPT/CP/T/oscillation parameters. The effect on Imz goes away if $\frac{\mathrm{Im}\lambda_{flav}}{|\lambda_{flav}|}$, $\frac{\mathrm{Im}\bar{\lambda}_{flav}}{|\lambda_{flav}|}$ are also fitted, with $r_{flav} = \bar{r}_{flav}$ fixed to 0.05 (**fit configuration 4**) (and all the other DCKM related parameters fixed to zero), as reported in table 125. The RMS for $\frac{\mathrm{Im}\lambda_{flav}}{|\lambda_{flav}|}$ and $\frac{\mathrm{Im}\bar{\lambda}_{flav}}{|\lambda_{flav}|}$ is 0.32, as in the case of the tagging side. When $\frac{\mathrm{Re}\lambda_{flav}}{|\lambda_{flav}|}$ and $\frac{\mathrm{Re}\bar{\lambda}_{flav}}{|\lambda_{flav}|}$ were considered as additional free parameters in the fit most of them failed, due to the extremelly poor sensitivity to these parameters (RMS ~ 10).

From these sensitivity studies we verified numerically the features anticipated from the analytical study described in section 2.2.6 concluding that the optimal trade-off between statistical precision and systematic uncertainties due to Doubly-CKM-Suppressed decays requires the introduction of 4 additional fit parameters

θ_{flav}	Δm	$\Delta\Gamma/\Gamma$	$\mid q/p \mid$	$\frac{Re\lambda_{CP}}{\mid\lambda_{CP}\mid}$Rez	$\frac{Im\lambda_{CP}}{\mid\lambda_{CP}\mid}$	Imz
0	0.0021	0.0052	0.0001	0.0027	0.0050	0.0051
$\pi/2$	0.0040	0.0006	0.0001	-0.0094	-0.0145	-0.0178
π	0.0031	-0.0056	-0.0011	0.0031	-0.0019	-0.0049
$3\pi/2$	0.0012	-0.0032	0.0014	-0.0001	0.0153	0.0202
RMS	0.0078	0.054	0.013	0.056	0.069	0.013

Table 124: Mean residuals and RMS for fit configuration 1, reconstructed (flavor sample) side phase scan.

θ_{flav}	Δm	$\Delta\Gamma/\Gamma$	$\mid q/p \mid$	$\frac{Re\lambda_{CP}}{\mid\lambda_{CP}\mid}$Rez	$\frac{Im\lambda_{CP}}{\mid\lambda_{CP}\mid}$	Imz
0	0.0024	0.0046	-0.0003	0.0007	-0.0059	-0.0008
$\pi/2$	0.0037	-0.0028	0.0008	-0.0056	-0.0100	0.0003
π	0.0029	-0.0060	-0.0011	0.0030	-0.0027	0.0005
$3\pi/2$	0.0012	0.0015	0.0008	-0.0016	0.0118	-0.0009
RMS	0.0080	0.053	0.013	0.056	0.069	0.014

Table 125: Mean residuals and RMS for fit configuration 4, reconstructed (flavor sample) side phase scan.

(in addition to the 6 CPT/T/CP and oscillation parameters), the sines of the DCKM phases, 2 for the tagging side and 2 for the reconstructed (flavor sample) B (**reference fit configuration**). It was verified for different DCKM phase configurations that this fitting configuration provides unbiassed estimates for all the parameters, and the quadratic errors reported by the fit give a good estimation of the statistical reach, within 10%. Table 126 summarizes the results obtained for a particular DCKM configuration where all phases were generated to be $\pi/2$, with $r_{tag} = \bar{r}_{tag} = r_{flav} = \bar{r}_{flav} = 0.05$. The residual and quadratic error distributions are shown in figure 65. Table 127 summarizes the largest average correlation coefficients among the physics parameters and any DCKM parameter.

	Δm	$\Delta\Gamma/\Gamma$	$\mid q/p \mid$	$\frac{Re\lambda_{CP}}{\mid\lambda_{CP}\mid}$Rez	$\frac{Im\lambda_{CP}}{\mid\lambda_{CP}\mid}$	Imz
Mean residual	0.0025	0.0039	-0.0015	-0.0052	0.0101	0.0002
Error mean residual	0.0005	0.0031	0.0010	0.0031	0.0045	0.0017
RMS	0.008	0.052	0.016	0.052	0.071	0.028
Average quadratic error	0.008	0.049	0.017	0.050	0.068	0.029

Table 126: Mean residuals, RMS and average quadratic error from the reference fit configuration. The DCKM phases were taken for this particular exercise to be $\pi/2$, with $r_{tag} = \bar{r}_{tag} = r_{flav} = \bar{r}_{flav} = 0.05$.

A.2 Effects from mistags

The feature described in the second paragraph of section 2.8 was verified fitting a common set of toy Monte Carlo experiments fixing $r_{tag} = \bar{r}_{tag}$ to 0.05 and 0.10 (the samples were generated with 0.05). Figure 66 shows the perfect one-to-one correlation (up to numerical differences) among the fitted results for all the CPT/T/CP/oscillation parameters. In this exercise the real and imaginary parts in the tagging side were left free, while only the imaginary parts in the reconstructed (flavor sample) side were considered as free parameters (real parts were fixed to zero). For the same experiments/fits, figure 67 shows the rescaling of the mistag fractions and the DCKM parameters in the tagging side.

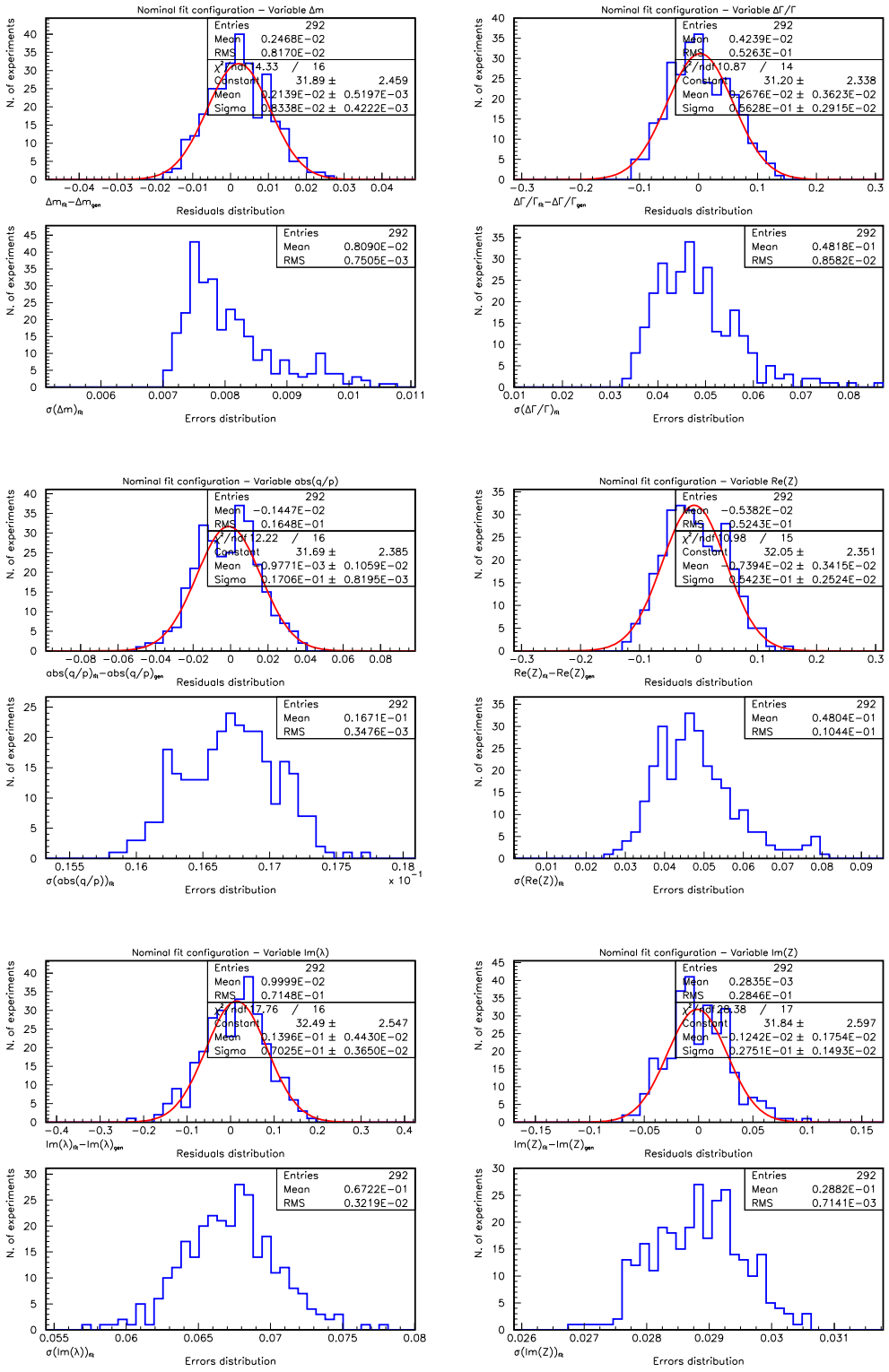

Figure 65: The residual and error (quadratic) distributions for the CPT/CPT/T/oscillation parameters from the reference fit configuration. The DCKM phases were taken for this particular exercise to be $\pi/2$, with $r_{tag} = \overline{r}_{tag} = r_{flav} = \overline{r}_{flav} = 0.05$.

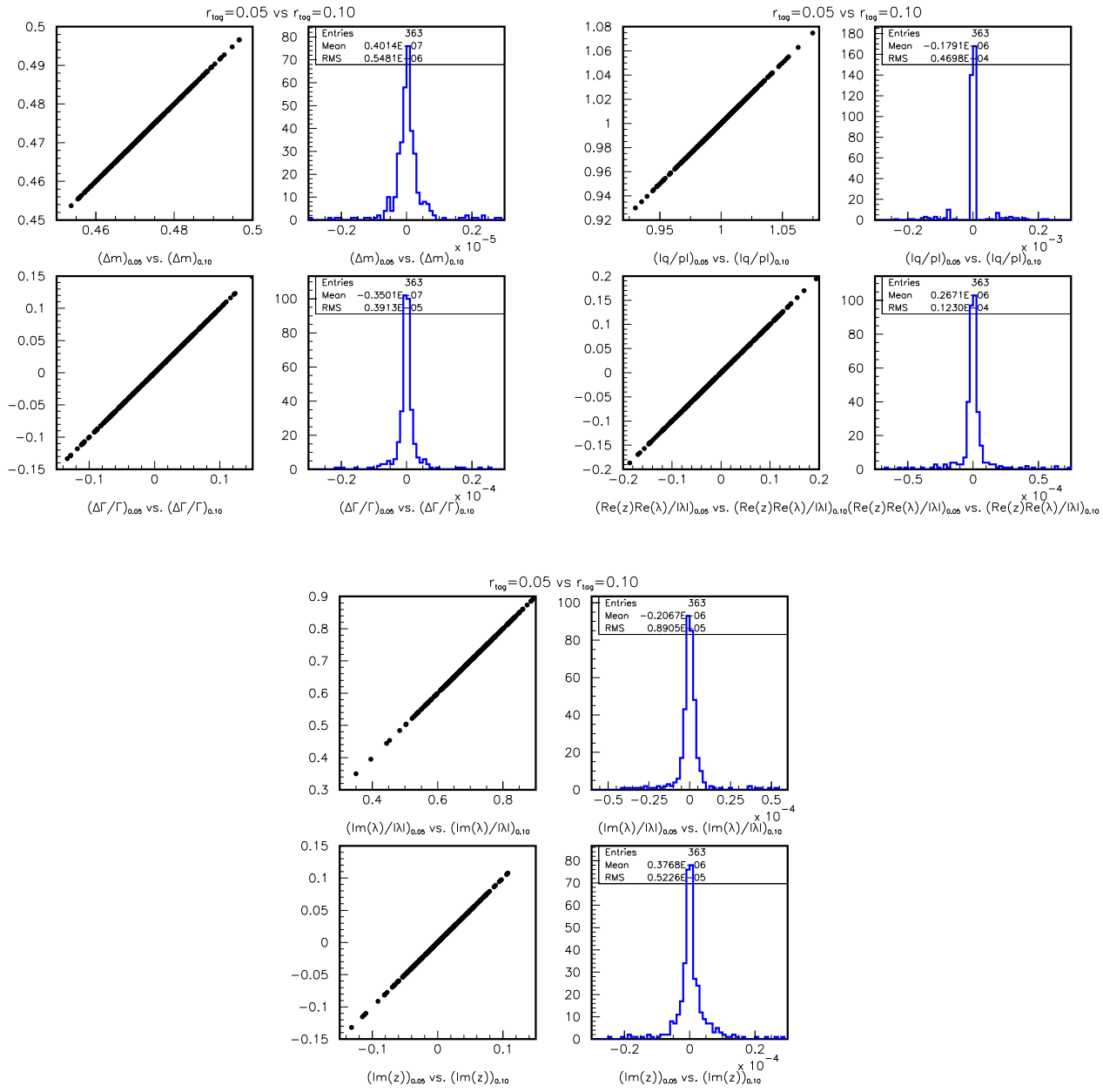

Figure 66: Experiment-by-experiment comparison (scatter and difference) of the fitted results for all the CPT/T/CP/oscillation parameters when the same toy Monte Carlo samples are fitted with different values of $r_{tag} = \overline{r}_{tag}$ (0.05 and 0.10).

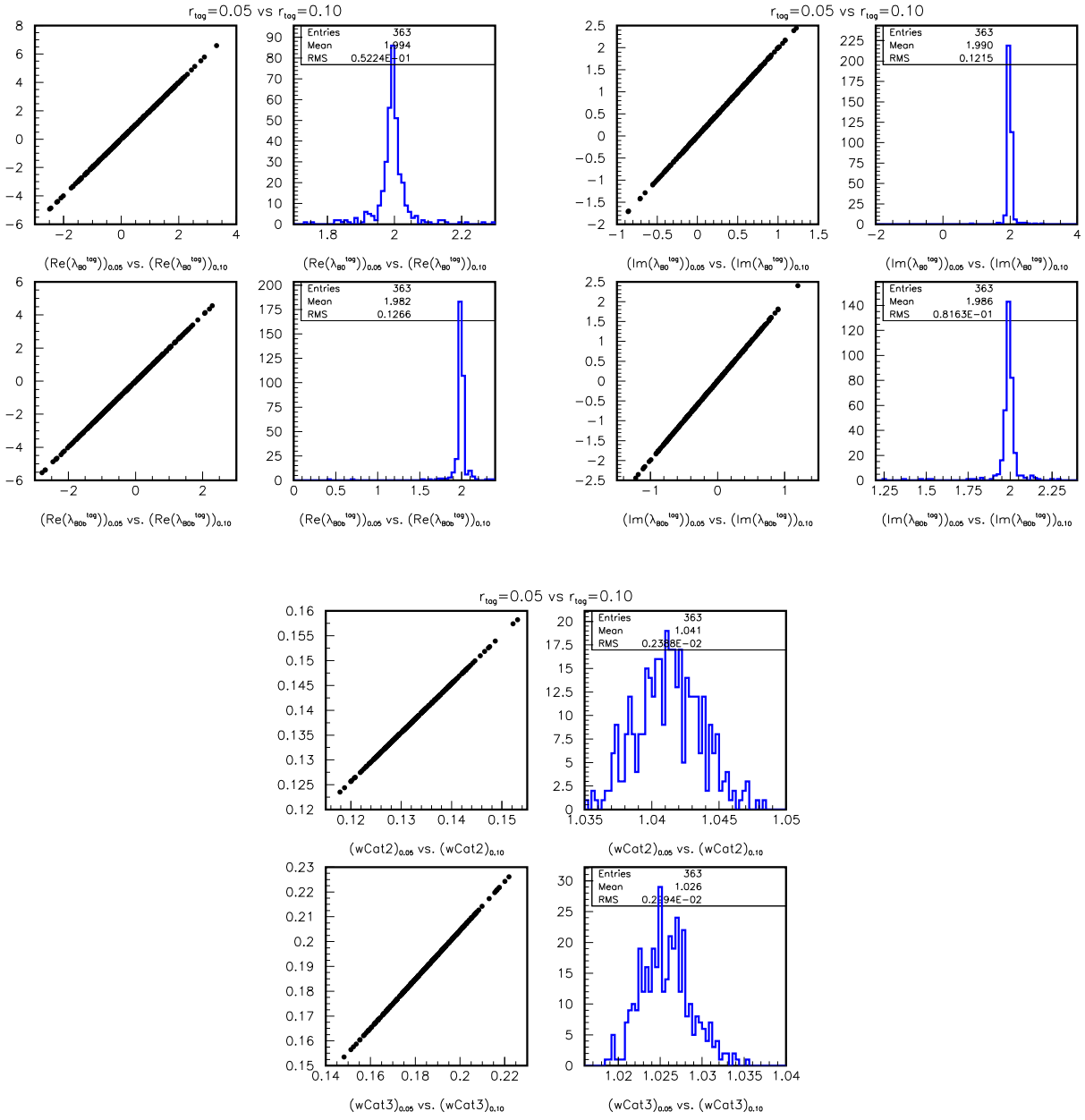

Figure 67: Experiment-by-experiment comparison (scatter and ratio) of the fitted results for the mistag fractions (Kaon and NT1 tagging categories) and the DCKM parameters when the same toy Monte Carlo samples are fitted with different values of $r_{tag} = \overline{r}_{tag}$ (0.05 and 0.10).

Parameter	Parameter	Average correlation coefficient
Imz	$\frac{\mathrm{Im}\lambda_{flav}}{\lvert\lambda_{flav}\rvert}$	50
	$\frac{\mathrm{Im}\lambda_{flav}}{\lvert\lambda_{flav}\rvert}$	-55
	$\frac{\mathrm{Im}\lambda_{tag}}{\lvert\lambda_{tag}\rvert}$	53
	$\frac{\mathrm{Im}\lambda_{tag}}{\lvert\lambda_{tag}\rvert}$	-58
$\frac{\mathrm{Im}\lambda_{flav}}{\lvert\lambda_{flav}\rvert}$	$\frac{\mathrm{Im}\lambda_{tag}}{\lvert\lambda_{tag}\rvert}$	72
	$\frac{\mathrm{Im}\lambda_{tag}}{\lvert\lambda_{tag}\rvert}$	10
$\frac{\mathrm{Im}\bar{\lambda}_{flav}}{\lvert\lambda_{flav}\rvert}$	$\frac{\mathrm{Im}\lambda_{tag}}{\lvert\bar{\lambda}_{tag}\rvert}$	10
	$\frac{\mathrm{Im}\lambda_{tag}}{\lvert\lambda_{tag}\rvert}$	76
$\frac{\mathrm{Im}\lambda_{tag}}{\lvert\lambda_{tag}\rvert}$	$\frac{\mathrm{Im}\lambda_{tag}}{\lvert\lambda_{tag}\rvert}$	19

Table 127: Largest ($>= 10\%$) correlations between the CPT/T/CP/oscillation parameters and the DCKM parameters, for the reference fit configuration. The DCKM phases were taken for this particular exercise to be $\pi/2$, with $r_{tag} = \bar{r}_{tag} = r_{flav} = \bar{r}_{flav} = 0.05$.

A.3 Multiple final states

In order to check that DCKM effects from semi-inclusive channels are always smaller than those from a single channel (third paragraph of section 2.8), we generated two different sets of toy Monte Carlo samples (about 200 experiments each), similarly as described in section A.1. In the first set each sample was split into two same-sized sub-samples with phases $\theta^a_{tag}/\theta^b_{tag} = 0, \pi/2, \pi, 3\pi/2$, with $\theta_{weak} = 1.85$ fixed. In the second set only one single channel was considered. To enhance the effect we want to investigate, r was generated to be 0.1 in the tagging side. No DCKM effects in the reconstructed side (flavor sample) were generated for this study. Each sample was then fitted with the standard, single channel approach, and then we compared the results for the two-channel and single-channel samples. The mean residuals of the fit results are shown in tables 128 and 129, for the two and single channel case. From the comparison of these two tables we conclude that the biases in the two-channel case are about the average of the biases from the samples generated with a single channel. The worse case (largest bias) in the case of a single channel is always larger than any of the two-channels configurations.

θ^a_{tag} / θ^b_{tag}	Δm	$\Delta\Gamma/\Gamma$	$\lvert q/p \rvert$	$\frac{\mathrm{Re}\lambda_{CP}}{\lvert\lambda_{CP}\rvert}$ Rez	$\frac{\mathrm{Im}\lambda_{CP}}{\lvert\lambda_{CP}\rvert}$	Imz
0 / $\frac{\pi}{2}$	$(2.67 \pm 0.55) \cdot 10^{-3}$	$(-4.8 \pm 3.7) \cdot 10^{-3}$	$(-1.4 \pm 1.3) \cdot 10^{-3}$	$(-4.27 \pm 0.37) \cdot 10^{-2}$	$(3.7 \pm 4.9) \cdot 10^{-3}$	$(0.9 \pm 1.4) \cdot 10^{-3}$
0 / π	$(2.94 \pm 0.59) \cdot 10^{-3}$	$(2.7 \pm 3.6) \cdot 10^{-3}$	$(-1.3 \pm 1.3) \cdot 10^{-3}$	$(-5.6 \pm 4.5) \cdot 10^{-3}$	$(5.7 \pm 4.8) \cdot 10^{-3}$	$(0.8 \pm 1.5) \cdot 10^{-3}$
0 / $\frac{3}{2}\pi$	$(1.86 \pm 0.56) \cdot 10^{-3}$	$(2.7 \pm 3.8) \cdot 10^{-3}$	$(-1.2 \pm 1.3) \cdot 10^{-3}$	$(-1.87 \pm 0.40) \cdot 10^{-2}$	$(-5.0 \pm 4.7) \cdot 10^{-3}$	$(-0.2 \pm 1.5) \cdot 10^{-3}$
$\frac{\pi}{2}$ / π	$(1.53 \pm 0.53) \cdot 10^{-3}$	$(4.2 \pm 4.2) \cdot 10^{-3}$	$(-2.8 \pm 1.3) \cdot 10^{-3}$	$(1.34 \pm 0.40) \cdot 10^{-2}$	$(0.9 \pm 4.1) \cdot 10^{-3}$	$(1.4 \pm 1.2) \cdot 10^{-3}$
$\frac{\pi}{2}$ / $\frac{3}{2}\pi$	$(2.49 \pm 0.57) \cdot 10^{-3}$	$(0.4 \pm 4.2) \cdot 10^{-3}$	$(-2.3 \pm 1.3) \cdot 10^{-3}$	$(0.8 \pm 4.1) \cdot 10^{-3}$	$(8.7 \pm 5.3) \cdot 10^{-3}$	$(-0.6 \pm 1.3) \cdot 10^{-3}$
π / $\frac{3}{2}\pi$	$(2.62 \pm 0.55) \cdot 10^{-3}$	$(4.4 \pm 4.0) \cdot 10^{-3}$	$(-0.9 \pm 1.3) \cdot 10^{-3}$	$(3.03 \pm 0.38) \cdot 10^{-2}$	$(3.8 \pm 5.3) \cdot 10^{-3}$	$(-1.8 \pm 1.3) \cdot 10^{-3}$

Table 128: Mean residuals with error from about 200 toy Monte Carlo experiments generated with two channels in the tagging side (r_{tag} was generated to be 0.1).

θ_{tag}	Δm	$\Delta\Gamma/\Gamma$	$\mid q/p \mid$	$\frac{\mathrm{Re}\lambda_{CP}}{\mid\lambda_{CP}\mid}$Rez	$\frac{\mathrm{Im}\lambda_{CP}}{\mid\lambda_{CP}\mid}$	Imz
0	$(3.62\pm0.60)\cdot10^{-3}$	$(-5.7\pm4.0)\cdot10^{-3}$	$(-0.7\pm1.3)\cdot10^{-3}$	$(-4.87\pm0.35)\cdot10^{-2}$	$(2.3\pm5.3)\cdot10^{-3}$	$(-1.0\pm1.4)\cdot10^{-3}$
$\frac{\pi}{2}$	$(1.66\pm0.61)\cdot10^{-3}$	$(1.4\pm3.9)\cdot10^{-3}$	$(-1.9\pm1.2)\cdot10^{-3}$	$(-1.98\pm0.38)\cdot10^{-2}$	$(6.5\pm4.6)\cdot10^{-3}$	$(0.0\pm1.4)\cdot10^{-3}$
π	$(2.83\pm0.59)\cdot10^{-3}$	$(-2.8\pm3.7)\cdot10^{-3}$	$(-4.5\pm1.3)\cdot10^{-3}$	$(5.27\pm0.34)\cdot10^{-2}$	$(3.2\pm4.7)\cdot10^{-3}$	$(1.1\pm1.4)\cdot10^{-3}$
$\frac{3}{2}\pi$	$(2.03\pm0.57)\cdot10^{-3}$	$(-2.5\pm3.7)\cdot10^{-3}$	$(-2.5\pm1.2)\cdot10^{-3}$	$(1.32\pm0.41)\cdot10^{-2}$	$(-1.2\pm4.8)\cdot10^{-3}$	$(-0.3\pm1.4)\cdot10^{-3}$

Table 129: Mean residuals with error from about 200 toy Monte Carlo experiments generated with one single channel in the tagging side (r_{tag} was generated to be 0.1).

B Time-integrated constraints for the extraction of the $B^0\overline{B}^0$ reconstruction and tagging efficiency differences

As it was originally proposed in [14], the differences in tagging and reconstruction efficiencies can be determined using time-integrated data. The method proposed counts the numbers of events with the various tagging categories and the events that are untagged in the high statistics B_{flav} sample, and then they are extrapolated to the B_{CP} samples. This method does not spoil the statistical precision while the associated systematic uncertainties will be under control.

Integrating over $-\infty < \Delta t < +\infty$ equation (97) for the most general case, we obtain:

$$\begin{aligned}
H^{\alpha}_{B^0_{tag}B^0_{flav}} &= (1+\nu)\Big\{(1+\mu^{\alpha})T^{\alpha}(1-w^{\alpha}-\Delta w^{\alpha}/2)H_{B^0_{tag}B^0_{flav}} + \\
&\quad (1-\mu^{\alpha})T^{\alpha}(w^{\alpha}-\Delta w^{\alpha}/2)H_{\overline{B}^0_{tag}B^0_{flav}}\Big\} \\
H^{\alpha}_{B^0_{tag}\overline{B}^0_{flav}} &= (1-\nu)\Big\{(1+\mu^{\alpha})T^{\alpha}(1-w^{\alpha}-\Delta w^{\alpha}/2)H_{B^0_{tag}\overline{B}^0_{flav}} + \\
&\quad (1-\mu^{\alpha})T^{\alpha}(w^{\alpha}-\Delta w^{\alpha}/2)H_{\overline{B}^0_{tag}\overline{B}^0_{flav}}\Big\} \\
H^{\alpha}_{\overline{B}^0_{tag}B^0_{flav}} &= (1+\nu)\Big\{(1-\mu^{\alpha})T^{\alpha}(1-w^{\alpha}+\Delta w^{\alpha}/2)H_{\overline{B}^0_{tag}B^0_{flav}} + \\
&\quad (1+\mu^{\alpha})T^{\alpha}(w^{\alpha}+\Delta w^{\alpha}/2)H_{B^0_{tag}B^0_{flav}}\Big\} \\
H^{\alpha}_{\overline{B}^0_{tag}\overline{B}^0_{flav}} &= (1-\nu)\Big\{(1-\mu^{\alpha})T^{\alpha}(1-w^{\alpha}+\Delta w^{\alpha}/2)H_{\overline{B}^0_{tag}\overline{B}^0_{flav}} + \\
&\quad (1+\mu^{\alpha})T^{\alpha}(w^{\alpha}+\Delta w^{\alpha}/2)H_{B^0_{tag}\overline{B}^0_{flav}}\Big\} \\
H^{\alpha}_{no\ tag B^0_{flav}} &= (1+\nu)\Big\{[1-T^{\alpha}(1+\mu^{\alpha})]\,H_{B^0_{tag}B^0_{flav}} + \\
&\quad [1-T^{\alpha}(1-\mu^{\alpha})]\,H_{\overline{B}^0_{tag}B^0_{flav}}\Big\} \\
H^{\alpha}_{no\ tag \overline{B}^0_{flav}} &= (1-\nu)\Big\{[1-T^{\alpha}(1+\mu^{\alpha})]\,H_{B^0_{tag}\overline{B}^0_{flav}} + \\
&\quad [1-T^{\alpha}(1-\mu^{\alpha})]\,H_{\overline{B}^0_{tag}\overline{B}^0_{flav}}\Big\}
\end{aligned} \tag{138}$$

where ν, μ^{α} and T^{α} where defined in equations (93), (94), (95) and (96); and $H_{k_1k_2} = \int_{-\infty}^{+\infty} h_{k_1k_2}(\Delta t)d\Delta t$, where $h_{k_1k_2}(\Delta t)$ was given in equation (53). Only Δt odd terms of (53) are relevant (the even terms cancel out). The above expressions have been normalized for a reconstruction efficiency $R = 1$.

We form now combinations of the above quantities:

$$\begin{aligned}
H^{\alpha}_{any\ tag B^0_{flav}} &= H^{\alpha}_{B^0_{tag}B^0_{flav}} + H^{\alpha}_{\overline{B}^0_{tag}B^0_{flav}} = \\
&\quad (1+\nu)T^{\alpha}\left[(1+\mu^{\alpha})H_{B^0_{tag}B^0_{flav}} + (1-\mu^{\alpha})H_{\overline{B}^0_{tag}B^0_{flav}}\right]
\end{aligned} \tag{139}$$

$$H^{\alpha}_{any\ tag\overline{B}^0_{flav}} = H^{\alpha}_{B^0_{tag}\overline{B}^0_{flav}} + H^{\alpha}_{\overline{B}^0_{tag}\overline{B}^0_{flav}} = (1-\nu)T^{\alpha}\left[(1+\mu^{\alpha})H_{B^0_{tag}\overline{B}^0_{flav}} + (1-\mu^{\alpha})H_{\overline{B}^0_{tag}\overline{B}^0_{flav}}\right] \quad (140)$$

$$H^{\alpha}_{B^0_{flav}} = H^{\alpha}_{no\ tagB^0_{flav}} + H^{\alpha}_{any\ tagB^0_{flav}} = (1+\nu)\left[H_{B^0_{tag}B^0_{flav}} + H_{\overline{B}^0_{tag}B^0_{flav}}\right] \quad (141)$$

$$H^{\alpha}_{\overline{B}^0_{flav}} = H^{\alpha}_{no\ tag\overline{B}^0_{flav}} + H^{\alpha}_{any\ tag\overline{B}^0_{flav}} = (1-\nu)\left[H_{B^0_{tag}\overline{B}^0_{flav}} + H_{\overline{B}^0_{tag}\overline{B}^0_{flav}}\right] \quad (142)$$

or equivalently,

$$x = (1+\nu)T^{\alpha}[(1+\mu^{\alpha})a + (1-\mu^{\alpha})b] \quad (143)$$

$$y = (1-\nu)T^{\alpha}[(1+\mu^{\alpha})c + (1-\mu^{\alpha})d] \quad (144)$$

$$z+x = (1+\nu)(a+b) \quad (145)$$

$$w+y = (1-\nu)(c+d) \quad (146)$$

where

$$a = H_{B^0_{tag}B^0_{flav}}\ ,\ b = H_{\overline{B}^0_{tag}B^0_{flav}}\ ,\ c = H_{B^0_{tag}\overline{B}^0_{flav}}\ ,\ d = H_{\overline{B}^0_{tag}\overline{B}^0_{flav}}$$

$$x = H^{\alpha}_{any\ tagB^0_{flav}}\ ,\ y = H^{\alpha}_{any\ tag\overline{B}^0_{flav}}\ ,\ z = H^{\alpha}_{no\ tagB^0_{flav}}\ ,\ w = H^{\alpha}_{no\ tag\overline{B}^0_{flav}}\ .$$

Equations (143), (144), (145) and (146) can be worked out to obtain ν, μ^{α} and T^{α}:

$$\nu = \frac{1}{2}\frac{(z+x)(c+d) - (w+y)(a+b)}{(a+b)(c+d)} \quad (147)$$

$$\mu^{\alpha} = \frac{x(1-\nu)(c+d) - y(1+\nu)(a+b)}{y(1+\nu)(a-b) - x(1-\nu)(c-d)} \quad (148)$$

$$T^{\alpha} = \frac{1}{1-(\nu)^2}\frac{x(c-d)(1-\nu) - y(a-b)(1+\nu)}{2(bc-da)} \quad (149)$$

These expressions are also valid when the Δt resolution is considered. Let us note the reuse of events in the evaluation of ν, μ^{α} and T^{α}: for each tagging category it is required the number of tagged events in that category together with the excluded events (events tagged by other categories plus the untagged events).

References

[1] R.F. Streater and A.S. Wightman, *PCT, Spin and Statistics, and All That*, Benjamin, New York, 1964.

[2] M.B. Gavela et al., *Mod. Phys. Lett.* **A9** (1994) 795.

[3] I.I. Bigi, A.I. Sanda, *CP Violation*, Cambridge University Press, 2000.

[4] M. Kobayashi and A. I. Sanda, *Phys. Rev. Lett.* **69** (1992) 3139; Z. Xing, *Phys. Rev.* **D50** (1994) 2957; D. Colladay and V. A. Kostelecký, *Phys. Lett.* **B344** (1995) 259; V. A. Kostelecký and R. Van Kooten, *Phys. Rev.* **D54** (1996) 5585; P. Colangello and G. Corcella, *Eur. Phys. J.* **C1** (1998) 515.

[5] S.W. Hawking, *Phys. Rev.* **D14** (1975) 2460; *Commun. Math. Phys.* **87** 395 (1982); V.V. Barmin et al., *Nucl. Phys.* **B247** (1985) 293.

[6] B. Aubert et al., The BaBar Collaboration, Observation of CP Violation in the B^0 meson system, *Phys. Rev. Lett.* **87** 091801 (2001).

[7] A.S. Dighe et al., Measurement of the Lifetime Difference of B_d^0 Mesons: possible and Worthwhile?, *Nucl. Phys.* **B624** (2002) 377-404.

[8] *BABAR* Analysis Document # 356, Supporting document for the Moriond, 2002 $\sin 2\beta$ analysis.

[9] *BABAR* Analysis Document # 188, A general model for Neutral B decay time distributions.

[10] The *BABAR* Physics Book, Ed. P.F. Harrison and H.R. Quinn, SLAC-R-504 (1998).

[11] *BABAR* Analysis Document # 385, A study of indirect violation of CPT/CP and CP/T using fully reconstructed CP and flavor eigenstates.

[12] For a comparison of different formalisms, see for instance V. A. Kostelecký, *Phys. Rev.* **D64** 076001 (2001).

[13] M. C. Bañuls, J. Bernabéu, *Phys. Lett.* **B423** (1998) 151; *Phys. Lett.* **B464** (1999) 117; *JHEP* **9906:032** (1999); *Nucl. Phys.* **B590** (2000) 19.

[14] R. Cahn, Determining efficiency differences from time-integrated data, $\sin 2\beta$ HNs #183, or `http://www.slac.stanford.edu/~cahn/internal/differing_efficiencies.ps`

[15] R. Cahn, Some Things about $\Delta\Gamma$, `http://www.slac.stanford.edu/~cahn/internal/delta_Gamma.ps`

[16] *BABAR* Analysis Document # 18, A User's Guide to the RootFitTools Package for Unbinned Maximum Likelihood Fitting.

[17] *BABAR* Analysis Document # 56, Analysis of $B^0 \to J/\psi K_L^0$ decays.

[18] *BABAR* Analysis Document # 358, Aspects of the winter 2002 $\sin 2\beta$ measurement specific to the decay mode $B^0 \to J/\psi K_L^0$.

[19] *BABAR* Analysis Document # 119, B Tagging in BaBar: Status for the 2001 $\sin 2\beta$ Publications.

[20] *BABAR* Analysis Document # 317, BTagger-A Multivariate Tagging Algorithm with Categories Based on the Physics of the Btag Decay.

[21] *BABAR* Analysis Document # 125, Measurement of $B^0\bar{B}^0$ mixing with fully reconstructed hadronic B decays.

[22] Particle Data Group, D.E. Groom *et al.*, Eur. Phys. Jour. C **15**, 1 (2000).

[23] Particle Data Group, K. Hagiwara *et al., Phys. Rev.* **D66** 010001 (2002).

[24] *BABAR* Analysis Document # 102, The BaBar Vertexing.

[25] *BABAR* Analysis Document # 106, Study of Material Interactions with Gamma Conversions and Protons.

[26] *BABAR* Analysis Document # 144, Measurements of the charged and neutral B meson lifetimes using fully reconstructed B decays.

[27] *BABAR* Analysis Document # 14, Measuring the PEP-II Boost.

[28] NAG software, `http://wwwinfo.cern.ch/asd/nag/`

[29] F. James, MINUIT reference manual, CERN program library.
`http://wwwinfo.cern.ch/asdoc/Welcome.html`

[30] *BABAR* Analysis Document # 349, Correlation between mistag of kaon tag and calculated error on Δt.

[31] *BABAR* Analysis Document # 254, Vertexing supporting document for Summer 2001 Conferences.

[32] Bob Cahn, Dealing with lambda for Doubly Cabibbo-Suppressed Decays,
`http://babar-hn.slac.stanford.edu:5090/HyperNews/get/pubboard08/83/1/4.html`